OPTIMIZED CUMULUS PARAMETERIZATION IN WRF MODEL FOR SIMULATION OF EXTREME RAINFALL OVER EAST AFRICA

BY

GEORGE OTIENO OCHIENG

Reg No.I80/98628/2015

DEPARTMENT OF METEOROLOGY

UNIVERSITY OF NAIROBI

A Thesis submitted in fulfillment of the requirements for the degree of Doctor of Philosophy (Ph.D.) in Meteorology

Department of Meteorology University of Nairobi, Kenya

November 2018

DECLARATION

I declare that this PhD thesis is my original work and has not been submitted elsewhere for examination, award of a degree or publication. Where other people's work or my own work has been used, this has properly been acknowledged and referenced in accordance with the University of Nairobi's requirements.

Signature…….……Date…….

Mr. George Otieno Ochieng
Department of Meteorology
University of Nairobi

This Thesis has been submitted for examination with our approval as University Supervisors:

Signature Date

Dr. Joseph Mutemi…….…….……..
Department of Meteorology
University of Nairobi

Dr. Franklin Opijah…….…….…….
Department of Meteorology
University of Nairobi

Prof. Laban Ogallo…….…….…….
Department of Meteorology
University of Nairobi

DEDICATION

To my lovely wife, **Juliet** for her understanding, patience and words of encouragement during the period of the study. To my beloved parents, **Magnus** and **Monica** for instilling in me a sense of hard work, responsibility, discipline and commitment in life. To my siblings **Gaudensia, Seline**, **Jose, Peter** for complementing my quest for knowledge.

ACKNOWLEDGEMENTS

Thanks to the Almighty God for seeing me through my university education this far and successful completion of this doctorate studies. I would like to thank my supervisor's Dr Mutemi, Dr Opijah and Prof Ogallo from the Department of Meteorology for their continuous guidance, constructive criticisms, encouragement and their tireless review of the thesis. I am deeply indebted to Prof Jaiho-Oh of Pukyong National University, South Korea for offering me attachment at his laboratory and exposed me to the computing world; this enabled me to carry out the research work; without which it would have been impossible to complete the thesis in good time. Special thanks to Dr Benjamin Pohl for manuscript review and publications of the same as well. To the Director of ICPAC, Dr. Guleid Artan for supporting my research and provision of a conducive environment to complete the work. I am equally indebted to my fellow colleagues; Dr Hussein, Dr Zewdu, Dr Sabiiti, Dr Omondi and Dr Maslin for their availability in consultation and academic support. To my friends and colleagues in South Korea; Jiwon, Sumin, Sinil, Kyungmin and Jihan for technical and computing resource support. To my beloved wife Juliet, I am grateful for the patience, moral support and understanding when I was away in South Korea, carrying out experiment of my research as well as taking the utmost care of the family.

ABSTRACT

The use of numerical climate models for accurate simulation of weather and climate information is very crucial for optimum planning and management of weather related activities. The current study applied the Weather Research and Forecasting (WRF) model as the primary research tool in simulating the extreme rainfall characteristics over East Africa (EA) region.

The study focused on the customization of the WRF model through the simulations and evaluation of Kain-Fritsch (KF), Kain-Fritsch with a moisture-advection based trigger function (KFT), Grell Dévényi (GRELL) and Betts Miller Janjic (BML) cumulus parameterization schemes (CPSs) to identify which scheme improves simulation of the various rainfall characteristics for the wettest and driest years over the EA region. For higher skill and accuracy in the model simulations and proper customization of WRF model over the region, three adjustable parameters from the cumulus schemes namely the sub-grid scale cloud–radiation coupling, adjustment time scale (ATS) and entrainment based on the lifting condensation level (LCL) were identified and tested.

The main rainfall characteristics analyzed included the number of rainy days (NRD), intensity of rainy days (IRD) and the frequency of rainfall intensity (FRI) during the core rainfall seasons of March-April-May (MAM) and October-November-December (OND). The model evaluation was done using daily Climate Hazards Group Infrared Precipitation with Station data (CHIRPS) and ERA-Interim reanalysis.

The evaluation/ error analysis metrics adopted in the study were root mean square error (RMSE), mean bias error, spatial correlation (SC), coefficient of variation (CV), Taylor diagram and box and whisker plots. The atmospheric dynamics calculated included the convergence and divergence analyses, vertically inter-grated moisture fluxes (VIMF) and vertical velocity.

Generally, the cumulus schemes succeeded in reproducing the observed rainfall features associated with large scale systems like the Inter-tropical convergence zone (ITCZ). The GRELL scheme favored drier rainfall conditions over the eastern parts of the region. The KF and KFT schemes generated wetter rainfall conditions mainly confined to the western parts of the region.

The analyses of observed NRD showed that the western and eastern parts of the region were characterized by more and fewer NRD respectively. These were fairly reproduced by the KF, KFT and GRELL CPSs. The BML scheme alternated the areas under wet or dry rainfall biases.

The Indian Ocean, Congo Basin and eastern parts of the region experienced persistent rainfall biases. More NRD over the western parts of the equatorial region were mostly related to light rainfall intensity (1-10mm/day). The biases associated with the heavy rainfall (>20mm/day) events were in most cases very low in the KF and GRELL cumulus schemes. The schemes simulated too many rainy days under the light rainfall category over the western and eastern parts of the region, the heavy rainfall events were quite well reproduced over the same locations by the KF scheme.

The simulations of vertically inter-grated moisture flux (VIMF), vertical velocity circulations and upper level (200hPa) divergence/convergence showed a steady easterly moisture transport characterized by the development of anti-cyclonic flow over the northern part of Madagascar and along EA coasts were fairly simulated by the KF and GRELL schemes. The moisture convergence biases were found to be larger continentally as well as over parts of the nearby Indian Ocean, corroborating the observed larger rainfall biases noted over parts of East Africa region.

In conclusion, the study has provided a unique way of isolating the deficiencies and limitations of four cumulus parameterization schemes used in the WRF model in simulating extreme rainfall. A robust analyses and evaluation of suite of model simulations resulted to the identification of the modified Kain-Fritsch scheme (KF-new) as the most suitable for application in WRF model in order to improve simulations of key rainfall characteristics of East Africa rainfall. By adopting a more robust user relevant metrics makes the findings more relevant contributing useful knowledge that can lead to improved numerical weather prediction (NWP) tools/systems over EA region.

The tuning and testing of the specific adjustable parameters within the cumulus schemes led to the identification of the best cumulus scheme that can be used to improve the predictability of rainfall characteristics over the region. This contributes to the new knowledge and understanding of how choice and use of specific cumulus parameterization schemes in WRF model can influence the predictability and prediction of East Africa rainfall. The information from this study is an important contribution to the previous and ongoing research aimed at appropriately customizing numerical weather prediction models and climate modelling systems to skillfully/accurately predict and project climate and weather changes over the East Africa region.

TABLE OF CONTENTS

LIST OF FIGURES

LIST OF TABLES

LIST OF ACRONYMS AND ABBREVIATIONS

ABL	Atmospheric Boundary Layer
AEJ	African Easterly Jets
AGCM	Atmospheric General Circulation Models
AKT	Anthes Kuo Trigger
AKT	Anthes Kuo Trigger
ATS	Adjustment Timescale
BLFC	Boundary Layer Forcing Check
BML	Betts Miller Janjic
CAM	NCAR Community Atmosphere Model
CAPE	Convective Available Potential Energy
CCM4	Fourth Version of Coupled Climate Model
CEA	Coastal East Africa
CFS	Climate Forecasts System
CMIP5	Coupled Model Inter-comparison Project version Five
COF	Climate Outlook Forum
CPS	Cumulus Parameterization Scheme
CRCE	Cloud Radiation Coupling Effect
DJF	December-January-February
EA	East Africa
EAC	East Africa Community
ECMWF	European Center for Medium Range Weather Forecast
EEA	Equatorial East Africa
ENSO	El Niño Southern Oscillation
FRI	Frequency of Rainfall Intensity
GCMs	General Circulation Models
GDP	Gross Domestic Product
GFDL	Geophysical Fluid Dynamics Laboratory
GHA	Greater Horn of Africa
GPCs	Global Producing Centers
GRELL	Grell Devenyi
HSS	Heidke Skill Score

ICPAC	IGAD Climate Prediction and Application Center
ICTP	International Centre for Theoretical Physics
IOD	Indian Ocean Dipole
IPCC	Inter-governmental Panel on Climate Change
IRI	International Research Institute
ITCZ	Inter-Tropical Convergence Zone
KF	Kain-Fritsch
KF-new	Kain-Fritsch new
KF-old	Kain-Fritsch old
KFT	Kain-Fritsch with modified advection scheme
LBCs	Lateral Boundary Conditions
LCL	Lifting Condensation Level
LDT	Lifting Depth Trigger
LFC	Level of Free Convection
LVB	Lake Victoria Basin
LVB	Lake Victoria Basin
LW	Long Wave
MAM	March-April-May
MDG	Millennium Development Goal
MJO	Madden Julian Oscillation
MOS	Model Output Statistics
MP	Microphysics
NAT	Negative Area Trigger
NEA	Near Equatorial Africa
NMHS	National Meteorological and Hydrological Services
NRD	Number of Rainy Days
NWP	Numerical Weather Prediction
OGCM	Ocean General Circulation Model
OLR	Outgoing Longwave Radiation
OND	October-November-December
PBL	Planetary Boundary Layer
PRECIS	Providing REgional Climates for Impacts Studies
RCM	Regional Climate Model

RCOF	Regional Climate Outlook Forum
RegCM4	Regional Climate Model Fourth Version
RRTM	Rapid Radiative Transfer Model
SE	South Easterlies
SEA	Southern East Africa
SSTs	Sea Surface Temperatures
SW	Short Wave
TCs	Tropical Cyclones
TEJ	Tropical Easterly Jet
UNISDR	United Nations International Strategy for Disaster Reduction
USA	United State of America
USAID	United States Agency for International Development
WMO	World Meteorological Organization
WRF	Weather Research and Forecasting

CHAPTER ONE

1. Background of the Study

This chapter gives the introduction together with the background information required for this study. It also gives the specific objectives and statement of the problem under investigation. Most socio-economic development activities within the countries of the East Africa (EA) are negatively impacted by extreme weather and climate events, with rainfall related hazards being the major drivers of the regional disasters.

The understanding of rainfall patterns and characteristics in terms of rainfall amount, the associated intensities and their frequencies (FRI) is therefore fundamental for disaster risk reduction and building resilience to climate smart socio-economic development that effectively addresses the challenges associated with the risks of climate variability and change.

Furthermore, improved and better knowledge on the intra-seasonal rainfall characteristics is very useful for planning purposes to sectors like agriculture, hydrology, and for urban planning. Within the African continent, one of the impacts of a changing climate will be the alteration of regional rainfall characteristics including rainfall amount and their frequencies, onset, cessation and duration (Pohl *et al.,* 2017). Amongst the rainfall characteristics, the number of rainy days together with their intensities greatly impacts on the quality of the Agricultural activities within the East Africa region.

Related studies over the EA region are scarce and limited despite their relative importance to the economy. A study by Sun *et al.* (2006) on the seasonal rainfall characteristics found that the seasonal mean rainfall variability both in space and time is a product of the variability in the individual rainfall characteristics. The correct formulation and strategies in the numerical forecasting tools would provide better understanding of the various rainfall characteristics (Cristiano *et al.,* 2017; Kim *et al.,* 2018).

Furthermore, over the EA region, the complexity in the terrain, undulating topography and the interactions of the Inter-tropical convergence zone (ITCZ) together with the local circulations present complex climate systems that the current RCMs are not able to fully represent. The complexity of the regional climate details coupled with the huge computational demand to study detailed rainfall characteristics partly has hampered the continuity in the provision of accurate and

reliable rainfall forecasts over the region (Von *et al.,* 2000; Cretat *et al.,* 2015). The rainfall predictability therefore must consider known processes that majorly drive the rainfall including the interactions between the large-scale and local scale systems (Ogallo, 1989; Okoola, 1999; Mistry and Conway, 2003; Anyah *et al.,* 2006; Kim *et al.,* 2012).

Over the tropics and particularly Equatorial East Africa (EEA) region, the rainfall processes are majorly convective in nature due to strong solar insolation (Davies *et al.,* 2009; Pohl *et al.,* 2011). The understanding of the convective processes and their representation at sub grid-scale within RCMs is a step geared towards improving the seasonal rainfall forecasts, reducing risks and shocks associated with too extreme climate conditions.

Several studies including Anyah and Semazzi (2006); Segele *et al.*(2009); Pohl *et al.* (2011); Zaroug *et al.* (2014); Sun *et al.*(2014); Opijah *et al.* (2014); Ngaina, (2015); Ogwang *et al.*(2015a, b); Argent *et al.*(2015); Ntwali *et al.*(2016) and Kerandi *et al.* (2017) have used RCMs to evaluate rainfall characteristics. These studies reported that the RCMs succeed in most cases in reproducing the rainfall gradient due to the large-scale systems like the ITCZ. The model inconsistencies in simulating orography induced rainfall has also been reported in some of these studies. These studies found systemic model deficiencies (biases) in rainfall and temperature simulations.

A robust climate modelling aimed at identifying the strength and weakness of the model physics for climate simulations and forecasting clearly lacked in these regional studies. The current study therefore aimed at identifying the best cumulus scheme that provide skillful rainfall simulations for the specified rainfall characteristics during wet and dry rainfall years over the EA region.

1.1 Statement of the Problem

The East Africa region is characterized by extreme episodic rainfall that negatively impacts the economy of the region annually. These extreme rainfall at daily-seasonal timescale are driven by amongst others local scale dynamics like convective processes that are not quite well understood in the NWP models. There are very little research efforts using dynamical tools geared towards addressing such limitations in understanding. This implies that there is no clear information on the extent to which a particular RCM can be applied for full maximization of its climate information. Furthermore, there is no clear sub grid-scale information over the region that details the extent to which convective schemes could be modified to bring in scale awareness for improving high-resolution rainfall characteristics.

Lack of new conceptual approach to better improve methodology and implementation of essential mechanisms and processes has limited the creation of new knowledge and science advancement in the NWP processes. The application of regional climate models (RCMs) with broader range of physical parameterization schemes broaden the maximization and understanding of the challenges associated with the NWP for reduction of sector specific climate related risks.

In many of the previous modeling studies, the treatment of cumulus parameterization schemes in NWP have not been subjected to extensive evaluation. Such comprehensive tests are critical since most RCMs are developed and tested over mid-latitude regions and therefore not accustomed to the unique convective rainfall characteristics over the tropics. This, implies that the NWP models should be uniquely customized to improve on the simulations of different rainfall characteristics. The current study contributed towards filling this gap.

1.2 Objective of the Study

The overall objective of the study was to investigate how four cumulus parameterization schemes simulate specific rainfall characteristics during wet and dry years. The specific objectives used to achieve the main objective were to:

i. Determine the skill of four cumulus parameterization schemes in simulating intra-seasonal rainfall characteristics
ii. Establish the skill of the cumulus schemes in simulating the atmospheric circulations and dynamics
iii. Determine the specific adjustable parameters within the cumulus schemes that can be customized to improve rainfall simulations

1.3 Research Questions

The various research questions that the study aimed to address were as follows:

i. What are the significant differences in using different cumulus parameterization schemes in WRF model simulations of salient rainfall characteristics over East Africa?
ii. How well can the WRF model simulate key East Africa rainfall formation processes during wet and dry rainfall seasons?
iii. Are there some adjustable parameters in the WRF model cumulus parameterization schemes that are sensitive to the simulations of wet and dry conditions over East Africa?

1.4 Justification for the Study

Agriculture forms the backbone of the economy of the region that mainly depends on seasonal rainfall. The high variability of seasonal rainfall associated with climate extremes affects agriculture. Therefore, knowledge about the quality of the seasonal forecasts would provide early warning information to farmers and other users of climate information for preparedness to alleviate the devastating impacts associated with the climate extremes.

This provision of early warning information has been made possible by use of dynamical models in prediction. Over the EA region, rainfall is mostly convective in nature. This implies that the identification and documentation of robust model physical schemes relevant for the region is very important. The use of high-resolution RCM model in the region in the recent past has continued to encourage more detailed analyses of the African Regional Climate Outlook Forums (RCOFs) using improved datasets and methodologies. Few studies over the region using NWP tools to model rainfall processes include (Okeyo 1987; Mukabana and Piekle 1996; Pohl *et al.,* 2011; Kerandi *et al.,* 2017). There is still no consensus on suitable configurations of model physics that will be accurate in successfully reproducing observed regional climate characteristics.

Many studies on physical parameterization schemes outside the region, highlights the importance of the cumulus schemes in determining the rainfall variability; despite being least studied and documented over the East Africa region (Cretat and Pohl 2012; Cook and Vizy 2013). The research and documentation of a set of model physical configurations suitable for studying specific extreme rainfall conditions is therefore undisputable. This necessitates the demand to study the intra-seasonal rainfall characteristics over the EA region and to conduct further sensitivity experiments with RCMs like WRF due to relatively high uncertainties associated with the model physics.

Several efforts have been made by research institutions like Inter-Governmental Authority on Development Climate Prediction and Applications Center (ICPAC), National Meteorological and Hydrological Services (NMHSs), regional universities and other institutions to improve the prediction and early warning systems of the regional climate, but limitations still exist in the forecasts. These limitations offer a potential challenge in providing timely high-quality forecasts. The ability to fully maximize the use of the available climate information in reducing sector specific climate related risks in support of disaster risk reduction and sustainable development is also hampered.

1.5 The Study and Analysis Domains

The East Africa (EA) region was the study domain for the current study. The EA region consists of five countries Kenya, Burundi, Rwanda, Tanzania and Uganda, bounded by the latitudes 6 °N and 12 °S and longitudes 28 °E and 45 °E. Figure 1 shows the topography of the EA study region. The region is bordered by complex topographical features that include the Ethiopian highlands to the Northeast and East African highlands to the southwest. Some of the East Africa high mountains and top highlands include Kenya (5199 metres), Kilimanjaro (5895 metres), Elgon (4321 metres), Aberdare Ranges (3999 metres) and the Mau escarpment (3098 metres), (Otieno and Anyah 2013 b). The chains of the complex mountains provide stable sources for some of the major rivers within the region (Nicholson 2014). The Lake Victoria basin, Indian Ocean and the western and eastern highlands forms key unique physical features of the region. The rainfall driving systems are complex and vary across time latitude and longitude within the region. This provides unique rainfall regimes over the region (Mutemi *et al.,* 2007).

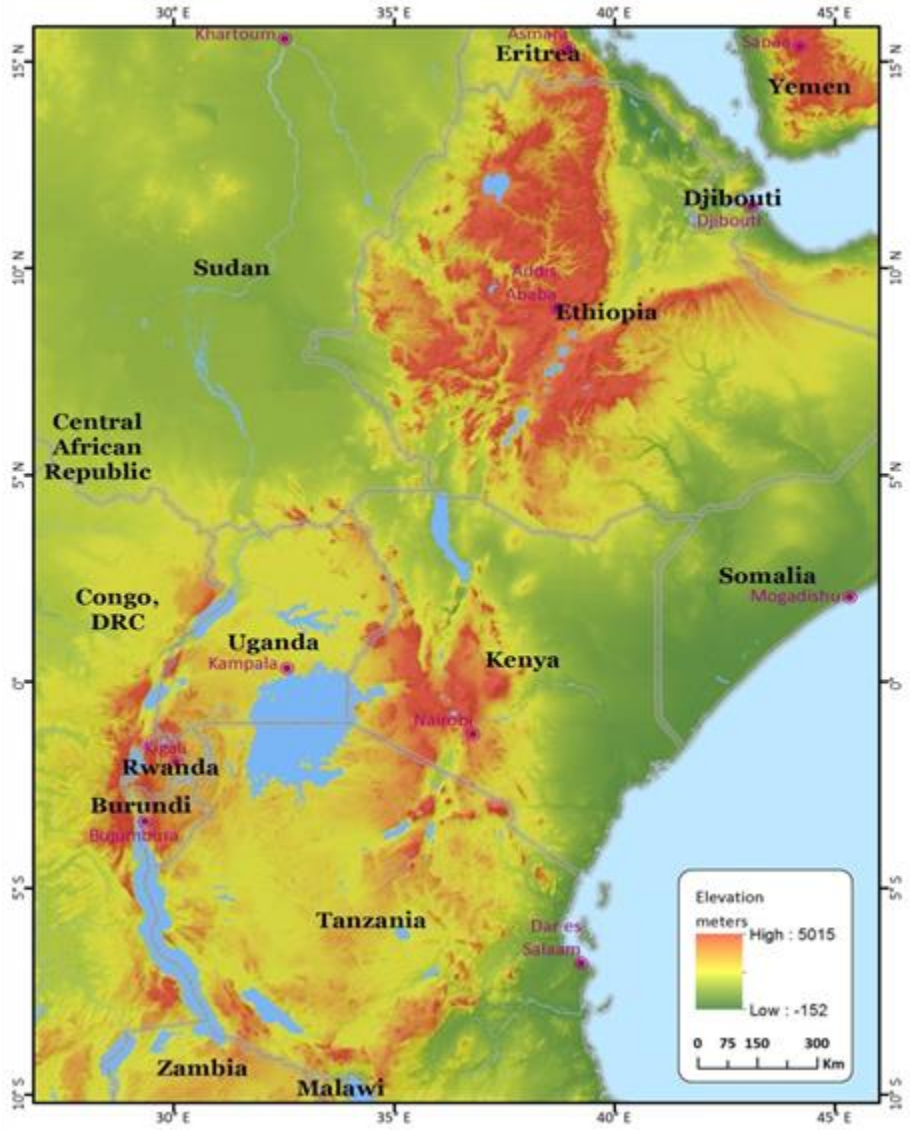

Figure 1: A topography map of covering part of East Africa and Greater Horn regions (*source:* Himeidan and Kweka 2012)

To provide a more objective understanding of the rainfall characteristics and their distributions, homogeneous zones with their representative stations developed by Omondi *et al.* (2013) was used. To lower the variability associated with the meteorological datasets from the individual stations, it more scientific to cluster rainfall stations into homogeneous climate zones. This aids in critical understanding of the mechanisms associated with climate variability. The process also reduces the number of variables which describe the regional climate variability (Ogallo 1988; Indeje 2000; Mutemi 2003; Nyakwada 2009). Figure 2 shows the homogeneous zones and their representative stations developed by Omondi *et al. (*2013) spread across the study domain for both the MAM and OND rainfall seasons.

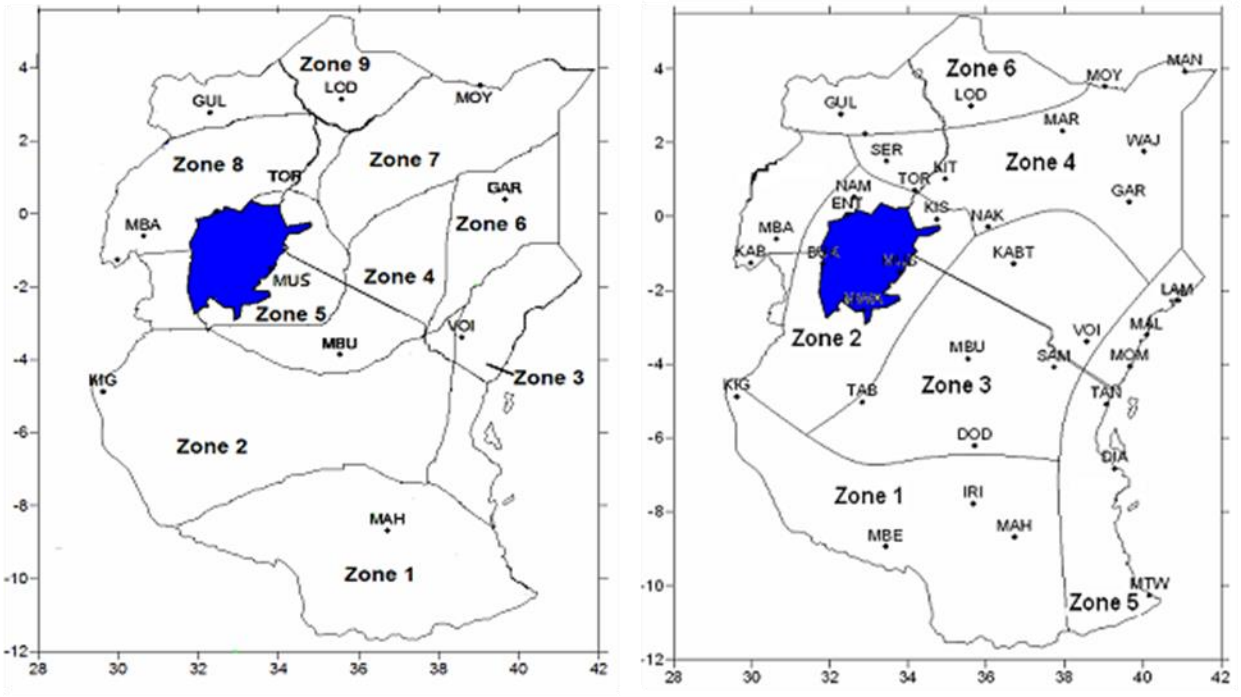

Figure 2: Homogeneous zones for East Africa during MAM (left panel) and OND (right panel) (*source:* Omondi *et al.*, 2013)

It is on this basis that the current study developed the analysis sub-domains for the study. Figure 3 shows the analysis domain used for computations of annual cycles and various rainfall statistics. The zones were developed based on their representations on the homogenous zones and uniform rainfall characteristics. For the uniformity and for purposes of providing fair comparison of the CPSs, the same sub-domains were used for both the seasons. These zones were closely linked to those earlier developed Ogallo (1989), Indeje (2000) and Anyah and Semmazzi (2007).

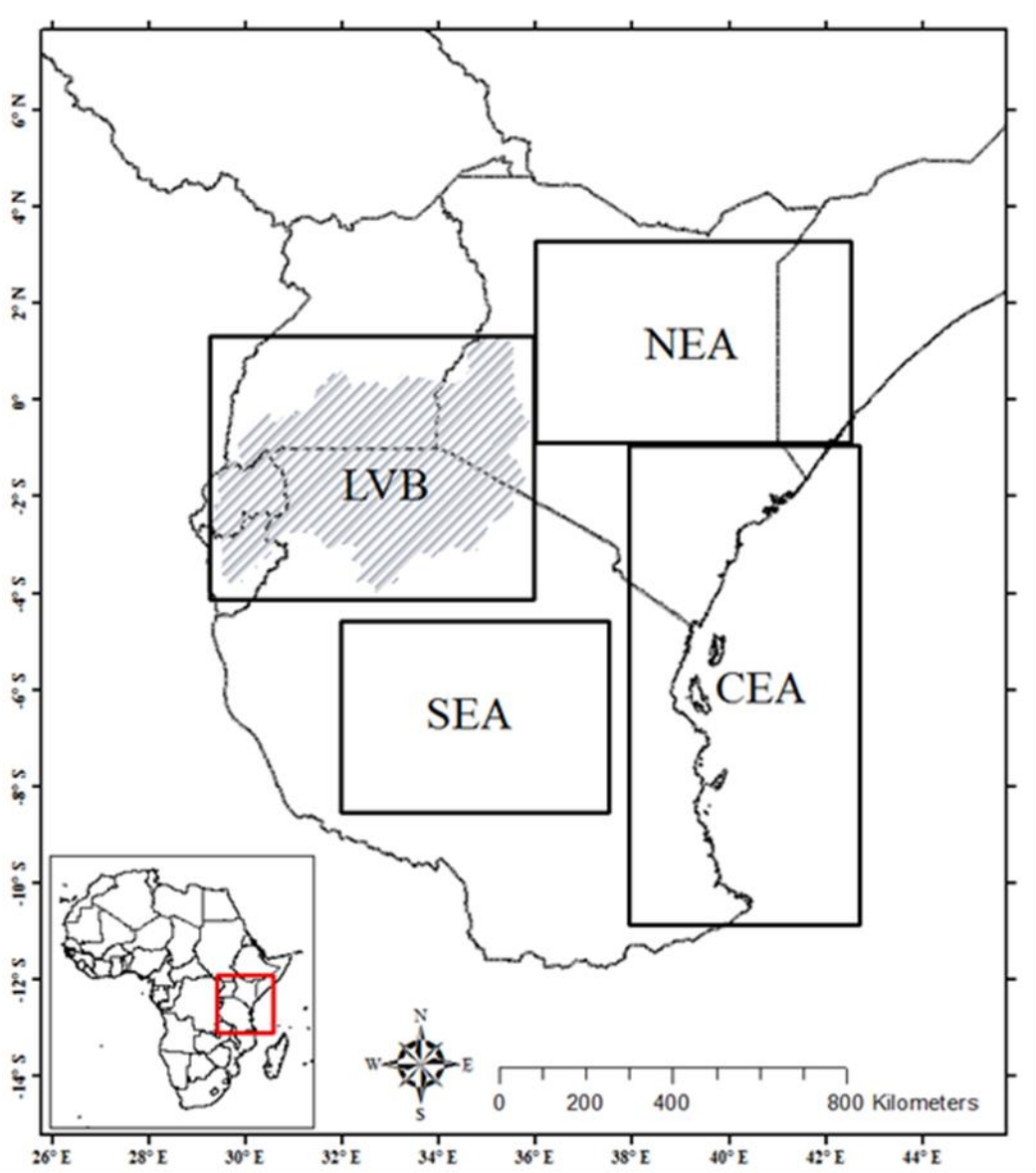

Figure 3: Study Area with four Sub-domains SEA, NEA, LVB and CEA utilized for analysis in this study during MAM and OND seasons. The shaded area shows the extent covered by the Lake Victoria basin

The four sub-domains were; Near Equatorial Africa (NEA), Southern East Africa (SEA), Coastal East Africa (CEA) and Lake Victoria Basin (LVB) utilized for analysis. The NEA sub-domain rainfall pattern is basically driven by the ITCZ, ENSO, IOD and local scale interactions. The rainfall pattern over the region is linked with the strength of the jets in the upper tropical Indian Ocean, surface westerly winds that reinforce the easterly oceanic temperature gradient and form part of the equatorial zonal-vertical circulation cell (Anyah *et al.*,2006; Endris *et al.*,2013; Gudoshava 2016).

Over both NEA and SEA sub-domains, the land-sea breezes, land use, moisture flux, monsoon winds, and Congo air mass are key local and large-scale systems driving rainfall over the sub-domains (Cook and Vizy 2013; Ogwang *et al.*, 2015a). The regional topography over these sub-mains also contributes significantly to the formation of local perturbations through coupling with the vertical components of wind speeds. This promotes the formation and development of clouds, precipitation and thunderstorms (Indeje *et al.*, 2000; Oettli and Camberlin 2005; Ogwang *et al.*, 2014).

Furthermore, over the SEA sub-domain, the complex topography characterized by mountains and water bodies in the western parts of Tanzania modulates rainfall pattern significantly. The complex rainfall systems influence the seasonal interactions within the ITCZ and the perturbations in the global circulations and changes in local circulation systems (Luhunga and Djolov 2017). The seasonal movement of the ITCZ causes both NEA and SEA domains to experience either unimodal or bimodal rainfall regimes. Areas like southern, southwestern, central and western parts of the SEA region experience uni-modal type of rainfall.

The interactions of the land-sea breezes, moisture flux from Congo and the inland lakes, and monsoonal winds play crucial role in modulating the internal climate dynamics over the LVB and CEA sub-domains (Godushava 2016). The upslope (katabatic) and downslope (anabatic) winds over the inland mountains and the coastal highlands plays key role in regulating the temperatures over these sub-domains (Anyah *et al.*, 2006).

There are four main rainfall seasons that characterize these sub-domains. The MAM and OND rainfall seasons are basically experienced within the NEA and LVB sub-domains. The southern parts of Tanzania region besides MAM season, experiences also the November-December-January-February (NDJF), similar to the CEA sub-domains (Nicholson 2014). These rainy seasons are majorly associated with the progression of the ITCZ across the region. The presence of the water bodies generates land/sea and land/lake breezes because of the water and land temperature contrasts due to the differential diurnal heating/cooling (Nikulin *et al.*, 2012).

These domains were considered based on the unique rainfall seasons MAM and OND they experience and the rainfall mechanisms whose interplay modulates the weather and the atmospheric circulations (Mutemi *et al.*, 2007; Anyah and Qiu, 2012; Otieno *et al.*, 2018).

CHAPTER TWO

2 Literature Review

In this chapter, a detailed review of the seasonal rainfall variability and rainfall characteristics, and its impacts on regional economy, definition of wet and dry years, regional climate modeling efforts and the current modeling framework are highlighted.

2.1 The East Africa Extreme Rainfall

Many studies over the region have been undertaken that linked East Africa (EA) seasonal rainfall anomalies with El Niño and La Niña years. The seasonal migration of the ITCZ, the El Niño Southern Oscillation Index (ENSO) and the associated remote teleconnections have been linked to the deficient or excess rainfall over East Africa region (Endris *et al.,* 2013). The linkages of EA rainfall with ENSO have been found to be stronger during the October-November-December (OND) than March-April-May (MAM) season. In most cases, the excess/deficient rainfall have resulted into flooding and drought (Indeje and Semazzi 2000; Bowden and Semazzi 2007; Owiti *et al.,* 2008; Shongwe *et al.,* 2011).

The ENSO (Ogallo 1988; Indeje and Semazzi 2000; Segele *et al.,* 2009; Diro *et al.,* 2012) and the IOD (Saji *et al.,* 1999; Ummenhofer *et al.,* 2009) are suggested to be the dominant drivers of the rainfall variability over EA region. Similar studies over the region have characterized the years based on these indices (Behera *et al.,* 2005; Harou *et al.,* 2006; Endris *et al.,* 2013; Zaroug *et al.,* 2014; Ogwang *et al.,* 2015b; Endris *et al.,* 2017).

The East Africa extreme rainfall, are also linked to the atmospheric circulation and the shifts in the ITCZ. For example, a study by Uhe *et al*.(2018) found that the interactions of the atmospheric circulations and the observed patterns of SST variability drives some of the recent drying trends for MAM seasonal rainfall. This has also been reported by Rowell *et al.* (2015) who confirmed that the evolving patterns of anomalous SSTs is primarily one of the causes of the decline in East Africa long rainfall. Furthermore, Hoell *et al*. (2017) explained that the interaction of internal variability and anthropogenic forcing potentially enhances the drying trend compared to internal variability acting alone. This eventually results to the observed rainfall variabilities causing early and late transitions between wet and dry periods (Souverijns *et al.,* 2016).

The Madden Julian Oscillation (MJO) which is a tropical fluctuation of the weather systems greatly modulates the intra-seasonal rainfall characteristics. It is an eastward progression of cloud

band near the equatorial region. The EA rainfall responds through this MJO forcing in a unidirectional way, allowing seasonal rectification and interannual modulation by seasonal MJO amplitude. The impact of MJO coupled with Quasi Biennial Oscillation (QBO) accounts for between 30–60% of the annual rainfall variability (Vellinga and Milton 2018).

According to Pohl and Camberlin (2006), the major phases of the MJO that leads to wet spells over the highland parts of the western region are associated with the development of large-scale convection in the Africa/Indian Ocean region. However, over the eastern parts of the coastal region, the MJO phases leading to wet spells are often associated with suppressed deep convection in the Africa/Indian Ocean region. The out of the phase MJO causes the deficiency in the East Africa rainfall. A study by Hogan *et al*. (2015) postulated of a robust seasonal rainfall dependency on the MJO transitional phases. The evolution of the phases has the effect of either enhancing or suppressing tropical convections over the inland highlands and the coastal lowlands.

2.2 Seasonal Rainfall Characteristics and Regional Economic Impact

The growing demand for accurate climate forecasts at local scales relevant to end-users is a clear manifestation that rainfall forecasting still needs more research. Over the EA region, sectors like Agriculture, Energy, Power, Transport, and Wind amongst others heavily depend on rainfall (Njau 2010; Gitau 2011; Kipkogei *et al.,* 2017). A study by Owiti and Zhu (2012) reported that seasonal rainfall patterns characterized by delayed onset, depressed rainfall amounts impacts negatively on the rainfall dependent economy making the region more vulnerable to the extreme climate events.

Study by Mwangi *et al.* (2014) reported that the greatest percentage of the gross domestic product (GDP) of the region is driven by rain-fed economic activities. The 1997 flooding and 2011 drought experienced over most parts of the EA region and neighboring countries of the Horn of Africa were the worst on record (Lyon and DeWitt 2012). Yang *et al.* (2014) used the climate models from Coupled Model Inter-comparison Project phase five (CMIP5) to study EA rainfall, and reported distinct biases differing in magnitude between the long and short rainfall seasons.

Through proper customization, credible climate information can be derived from climate models. This supports better understanding of underlying climate processes involved. The climate forecasting tools over the region should be able to represent the highly variable nature and the complexity of the regional climate systems. There is significant progress made since the first generation of global circulation models in modeling the physical processes of the climate systems.

The model errors and inaccurate climate forecasts still pose threat to socio-economic needs of the society (Diro *et al.*, 2012).

One of the major issues in the regional climate modelling is the gap between the synoptic-scale state variables drifting away from the small scale forcing. The utilization of advanced climate model physics helps in bridging this gap and their interaction together over a given region (Chen *et al.*, 2010; Miguez-Macho *et al.*, 2004). Therefore, accurate and reliable climate information and services becomes very crucial to the rain dependent economy and their future sustainability.

2.3 Modeling the Seasonal Rainfall Characteristics

The regional climate models (RCMs) are potent tools for studying the intra-seasonal rainfall characteristics. This is due to their relatively higher resolution than global models capable of resolving the local scale processes to much higher accuracy (Cretat *et al.*, 2012). Furthermore, RCMs are found to provide plausible solutions for regional climate details than general circulation models (GCMs), (Hudson and Jones 2002). A realistic regional climate information must take into consideration regional and global details. The dynamical downscaling of global systems by RCMs is used to bridge this gap.

According to studies by Sun *et al.* (2006) and Pohl *et al.* (2017), the eminent impact of climate change would be severe on the intra-seasonal rainfall characteristics over the African continent. A study by Jones and Hudson (2002) used RCM to study present and future climate over South Africa. The study found that the hydrological cycle was strongly simulated compared to the projected increase in rainfall intensity, magnitude of the moisture fluxes and soil moisture. The rainfall biases were found to be associated with the decrease in both the NRD and their intensity. The study further found that the projected climate over EA region was wetter, due to an increase in rainfall intensity rather than a change in the number of rain-days.

Some of the regional RCM based studies on research mode focusing on rainfall at annual, seasonal, monthly and daily time scales with little attention on the rainfall characteristics include (Dai *et al.*, 2004; Nicholson 2014; Kipkogei *et al.*, 2016; Nicholson 2017). Attempts to investigate such rainfall characteristics over the region include Camberlin and Okoola (2003), Kijazi and Reason (2005), Gitau *et al.* (2013, 2015) and Dunning *et al.* (2017). These studies reported that seasonal rainfall depends more strongly on the onset than cessation dates. The onset and cessation dates being independent of NRD and IRD. Earlier studies by Chen *et al.* (1996), Dai and Deser (1999),

Dai (2006) and Camberlin *et al.* (2009), reported that the unreasonable simulations rainfall patterns and amounts generated by most regional climate models (RCMs) partly stem from incorrect combinations of rainfall frequency and intensity.

Earlier research by Mapande and Reason (2005), Pohl and Camberlin (2006a, b) and Okoola *et al.* (2008) investigated the relationship between the wet spells and the associated atmospheric dynamics. Over the western Tanzania region, during wet years, the onset was found to begin earlier and ends late during the OND season. The number of moderate wet spells, although not necessarily more intense, were recorded in dry years. The extended wet spells were found to be associated with anomalous westerly flow at 850 hPa over Equatorial Africa. During the OND seasons, wet spells were associated with weak westerlies along the coast over the equatorial Indian Ocean (Okoola *et al.,* 2008). Studies focusing on the rainfall characteristics such as NRD, FRI and the intensity of wet and dry spells (Moron *et al.,* 2013) have pointed out that the predictability of wet days is much better than mean rainfall intensity with short rains better predicted than the long rains.

For any successful downscaling of the rainfall characteristics over the region, proper customization and evaluation of the model is paramount. The downscaling provides critical information on the model strengths and weaknesses for a specific region would be (Small *et al.,* 1999; Bergant *et al.,* 2007). This involves customization of model physics and dynamics to optimize the model performance (Kain 2004; Ratna *et al.,* 2013; Zheng *et al.,* 2016). The consideration of the size and location of the simulation's domain (Seth and Giorgi 1998; Leduc and Laprise 2009; Davis *et al.,* 2009; Rauscher *et al.,* 2010), the lateral boundary conditions (Diaconescu *et al.,* 2007; Sylla *et al.,* 2009), the resolution and the model physics (e.g. Flaounas *et al.,* 2011; Pohl *et al.,* 2011; Crétat *et al.,* 2012) are key ingredients that can radically modify the simulated climate and thus the quality of the simulation.

The evaluation of the CPSs in regions that convective rainfall is prevalent cannot be over-emphasized. It is a fundamental step to a successful utilization of regional climate information (Stensurd 2007). Over the EA and West Africa regions, the convective rainfall is frequent and therefore the evaluation of CPSs applied to specific region is inevitable. This helps in reducing the errors due to sub-grid scale processes (Giorgi and Marinucci 1996; Small *et al.,* 1999; Giorgi and Means1999; Pal *et al.,* 2007). Furthermore, the application and customization of different

convection schemes greatly influences the skill of rainfall simulations (Giorgi and Shields 1999; Segele *et al.,* 2009).

Evaluating RCMs over smaller regions with unique climate systems provide clear information on the model strengths and weaknesses. For example, Anyah and Semazi (2006), Mariotti *et al.* (2011) and Giorgi *et al.* (2012) applied WRF and RegCM4 models over LVB to assess the model performance in simulating lake temperature and precipitation. Besides the model biases found in these studies, large-scale moisture transported via the prevailing easterly trades were found to enhance Lake Basin precipitation considerably. The studies also successfully reproduced the general rainfall patterns associated with large-scale systems like the ITCZ.

The statistical and dynamical modeling of East Africa rainfall have not been devoted to the intra-seasonal rainfall characteristics. The advent of the dynamical downscaling was meant to supplement the limitations and challenges in the statistical downscaling (Ininda 2008 and Moufouma-Okia and Jones 2015). The dynamical downscaling involves the use of a regional climate model driven by GCM output to provide detailed climate information with higher accuracy (Tang *et al.,* 2016). The information required by the RCM from GCM as a boundary conditions include winds, humidity, surface temperature and pressure at different atmospheric levels, but does not include prognostic variables like rainfall that is simulated by the RCM.

Efforts to improve the regional climate forecasts have been quite tremendous with downscaling being used as the main strategy. The climate downscaling is supposed to bridge the gap between the large driving fields from the global models and the regional climate information from regional climate models. A single climate model may not completely provide full climate information (local and synoptic details). Studies by Otieno (2013), Otieno *et al.* (2014) and Kipkogei *et al.* (2016) used global models over the region for climate simulations. All their studies converged to a conclusion that regional climate details can only be achieved through a downscaling process.

Previously, Anyah and Qiu (2012) and Endris *et al.* (2013) studied the long-term climate variability of the region using CMIP3 models for precipitation and temperature. The study found a consistent mismatch in rainfall peak and dislocation of moisture bearing systems like the ITCZ during the OND and MAM seasons. The rainfall peaks tended to shift while the changes in temperature and variability were relatively average.

The unrealistic representations of regional climate details by the GCMs have been attributed to a number of factors such as; low horizontal resolution; model internal inconsistency in the physics and dynamic formulations (Kim *et al.,* 2012). And over the region, the regional complex terrain and undulating topography, the interaction of large-scale and local scale systems that forms major rainfall seasons, makes global models inadequate for regional studies. On the other hand, RCMs alone will not provide global signals needed for regional climate variability.

Although the dynamical technique is computationally expensive, it is the most preferred option for regional climate modeling (Giorgi and Mearns 1999; Brown *et al.,* 2008). Otieno and Anyah (2013a) and Korecha (2014) pointed out that over the EA region, downscaling of the GCM models has the potential to improve regional climate forecasting. These findings were also consistent with results from study by over Greater Horn of Africa (Otieno 2013).

The use of regional models to downscale seasonal climate in Africa is capable of providing climate information with useful local detail, including realistic extreme events (Sylla *et al.,* 2009). Denis *et al.* (2002) and Liu *et al.* (2012) summarized the sources of errors emanating from dynamical downscaling. The errors arise from mathematical formulation and strategy, spatial resolution differences between the driving data and the nested model, spin-up time, the frequency of updating the lateral boundary conditions (LBCs), physical parameterization inconsistencies, horizontal and vertical interpolation errors in domain size, quality of the driving data.

Several studies over the EA region have concentrated on the short and medium range weather forecasting (Omondi 2010; Gitau 2011; Gichira 201; Sagero 2012; Koech 2014; Kipkogei *et al.,* 2016) and reported good simulations of regional circulation patterns but biases were inherent in the forecasts especially over the lake and mountainous region. Batte and Deque (2010) pointed out that the stabilization of the model skill increases when the model is run in climate mode than at weather mode due to adjustment in the boundary fields from lower boundary conditions. Their findings were later corroborated by Nicholson (2014) who found that the predictability of rainfall is achieved with correct lead time of up to two months.

The low confidence in the climate models hinder their use for climate projection and attribution to the disaster and risk reduction. The study by Otieno and Anyah (2013a, b) assessed the skill of the global models from coupled model Inter-comparison project five (CMIP5) in climate projections

over the Greater Horn of Africa (GHA). The correct location of rainfall bearing systems was the strength of the simulation. The moisture from the Congo region, lakes and highlands regions was not properly simulated. The reason was attributed to physical inconsistencies and poorly controlled evolution of the large-scale systems in the model. The study recommended proper nudging of synoptic systems to minimize the contamination of the simulated solutions (Denis *et al.*, 2002).

Diro *et al.* (2012) used the third version of regional climate model (RegCM3) to downscale precipitation over EA using the European Center for Medium Range Weather Forecast (ECMWF) model. The study found the skill improvements in forecasts especially in reproducing the spatial and temporal patterns of rainfall and temperature. The ECMWF models could not simulate well the regional climate processes over mountainous regions. The inconsistency in the physics and parameterization schemes between the 'parent' and 'daughter' models contributed to the error.

The consistency in the representation of climate physical processes between the RCMs and GCMs is important in any regional climate simulations; with coupled models preferred due to their ability to simulate the land-ocean-Atmosphere feedback processes (Ratman *et al.*, 2013). Nyakwada *et al.* (2009) and Omondi (2010) used the atmospheric general circulation models (AGCMs) to simulate regional climate information over EA region. The results revealed the potency in using such GCMs for simulations but more diagnostic and accurate simulation strategies were required. Paeth *et al.* 2005) pointed out that downscaling has the ability to increase the resolution of the local climate details. However, the simulation of mesoscale and synoptic scale systems is still a challenge for the GCMs, especially over the tropics.

One of the major achievements for the region in seasonal forecasting for the past 15 years has been the issuance of consensus forecasts over the GHA region. The forecasts are a hybrid of statistical and dynamical products; with dynamical products derived from the global producing centers which are downscaled by the WRF model. Studies by Marengo *et al.* (2003) and Otieno (2013, 2014) assessed the skill of the individual models from the global centers to simulate regional rainfall characteristics over GHA region. The studies showed higher skill in simulating rainfall over the EA region using the dynamical approach than the statistical models. The models however, showed biases in representing large-scale processes like the African Easterly Jets (AEJ) and Tropical Easterly Jet (TEJ), which are major drivers of regional rainfall over the Sahel region.

Studies by Endris *et al.* (2013) used the climate model products from Coordinated Regional Downscaling Experiment (CORDEX) to assess the changes in extreme temperature. The study found that the models are able to reproduce realistic climate information but are weak in capturing the dominant teleconnections around these areas are suppressed by the interactions between large-scale and local scale forcing.

Studies by Otieno and Anyah (2012) found a constant decrease in precipitation and increase in temperature attributed to westerly winds anomaly circulation from the Congo region. Good simulation was reported over the equatorial sector than the northern and southern parts of the EA region. Similar studies by Davis *et al.* (2009), Otieno (2013), Yang *et al.* (2014), and Otieno *et al.* (2014) revealed that GCMs tend to displace the moisture during the peak time and overestimate the precipitation in some locations.

Extensive downscaling studies over the region have basically concentrated on using the RegCM4 model (Anyah and Semazzi 2006; Dennis *et al.,* 2009; Diro *et al.,* 2012; Otieno and Anyah 2012; Ogwang *et al.,* 2014; Ogwang *et al.,* 2015b; Segele *et al.,* 2015). Despite appreciable skill being reported, the clear understanding and quantification of local scale dynamics and its representations in RCM over EA region have remained a daunting task. Secondly, the studies have not been furthered to an extent of investigating the deficiencies arising from the model and under/over estimation of rainfall patterns.

These studies focused very little on the rainfall characteristics and their representations in the numerical weather prediction (NWP) models. Using a regional model that is highly customizable for regional studies and with different physics options and parameterization schemes partly helps to address the uncertainties in rainfall forecasts. A regional model, WRF is currently being used for research and operational studies at different resolutions which has millions of physics and schemes customizable for any domain (Pohl *et al.,* 2011; Cretat *et al.,* 2015; Pohl *et al.,* 2017).

The knowledge and information of the rainfall characteristics would therefore be useful for planning purposes in sectors like agriculture, hydrology and urban planning. A detailed analysis of the rainfall characteristics is a pointer to the underlying mechanism and the associated rainfall drivers (Salih *et al.,* 2018). The assessment of rainfall characteristics can provide insights into the fluctuations of forcing and the mechanisms that give rise to natural hazards, such as droughts and

floods and understanding of rainfall variability (Tennnant and Hewitson 2002). Such knowledge reveals model deficiencies and limitations to the climate modelers and developers. The current study is the latest effort in attaining higher forecasts skill through the provision of the best cumulus scheme over the EA region.

2.3.1 Cumulus Parameterization Schemes

The cumulus parameterization is the technique used in Numerical Weather Prediction (NWP) models to account for the effects of convective clouds and other moist processes that occur at relatively small-scale resolutions in the NWP models. Rainfall simulations and forecasting over the region have been found to be very sensitive to the cumulus parameterization schemes used in any RCM (Okeyo1987; Pohl *et al.,* 2011; Gudoshava 2016).

The cloud processes are very important aspects of NWP since they directly impact the timing, location, and intensity of precipitation. In many NWP models, the fractional cloudiness can influence atmospheric radiation budgets as well as the dynamics and thermodynamics of the atmosphere. The quantification of the coupling effect between the cloud and radiation processes in the atmosphere still remains a challenge since they occur at very high resolution with grid scales less than a kilometer. The effect of these processes can only be accounted for in the NWP through approximations/parameterization (Alaparty *et al.,* 2012; Zheng *et al.,* 2016).

The rate at which cloud forms and turn into precipitation within a column of air depends on several environmental factors. These include amongst others convective available potential energy (CAPE), lifting condensation level (LCL), entrainment and detrainment rates based on LCL, adjustment time scale (ATS), cloud radiation coupling effect (CRCE) and vertical velocity rate. The understanding of these factors and how they influence convective activities is very crucial for NWP over the East Africa region. The current study isolated these variables for discussions since the understanding of how they affect convection is fundamental to the success of the current study.

2.3.2 Convective Available Potential Energy

The convective available potential energy (CAPE) determines the rate at which clouds form and later yield into precipitation in the atmosphere. CAPE is the amount of energy required to lift a parcel of air up to LCL point. It provides the maximum vertical velocity for convective up draughts. When a parcel of air rises within a vertical layer adiabatically, the CAPE can be calculated when it reaches the level of neutral buoyancy (equilibrium level) from the starting

height. The parcel of air continues to rise moist-adiabatically, until it reaches the level of free convection (LFC), where the air parcel can rise freely.

The CAPE aids in the formation of deep convection that commonly causes rain especially over the tropics. For any convective clouds to form, the value of CAPE must remain positive (positive energy, CAPE>0), (Stensrud 2007). Large CAPE values imply sustained convective activities.

2.3.3 Adjustment Time Scale

The study by Fritsch and Chappell (1980) introduced the adjustment time scale (ATS) in the NWP models. The ATS is the time over which CAPE is reduced to stabilize the atmosphere. In most numerical models, the ATS (τ) is assigned a constant value (Perkey 1986). The estimation of the constant can be based on the mean tropospheric horizontal wind speed and grid resolution.

The idea of assigning ATS a constant value in numerical models was later challenged by Stensrud (2007), citing the limitation it poses at high resolution grids or where there are strong winds. Bullock *et al.* (2015), found out that the magnitude of the ATS is one of the parameters that cause wet biases in simulated precipitation amounts at higher grid resolutions (Keil *et al.,* 2014).

To make cumulus schemes seamless across all the grid resolution, the magnitude of ATS should increase with increased grid resolution such that the atmospheric stability restoration is gradually taken over by the resolved convective processes. Most of the NWP parameters are tied to grid spacing of around 25 km (Kain 2004). The ATS expressed in Equation 1.2 follows Zheng *et al.* (2016) and Bechtold *et al.,* (2008) definitions.

$$\tau = \frac{h}{w}\left[1 + \ln\left(\frac{25}{Dx}\right)\right] \qquad 1.2$$

In Equation 1.2, τ is the adjustment time scale over which the atmosphere is stabilized, *h* is cloud depth (m), *w* is cloud-averaged vertical velocity (m/s) and *Dx* is the horizontal grid spacing (km). For a high resolution, longer timescales are associated with better simulations. Higher skill and accuracy in simulations is obtained when τ .is set to medium timescale.

If ATS is only a few hours shorter than the timescale of the large-scale flow, CAPE will be removed as fast as it is created. Similarly, if ATS is longer than 12 hours, convection is generated too slowly to remove CAPE. This occurs alongside local factors controlling the rate of CAPE removal. Globally, the ATS concept has been applied with success in examining rainfall biases

and in studying severe precipitation events in the Mediterranean using re-analysis dataset (Done *et al.,* 2006; Molini *et al.,* 2011; Done *et al.,* 2012; Keil *et al.,* 2014).

2.3.4 Cloud- Radiation Coupling Effect

The convective systems and associated cloudiness directly influence the regional and local atmospheric radiation budgets, as well as atmospheric dynamics and thermodynamics, through feedback processes. Most of the NWP models at sub grid-scale do not consider cloud–radiation feedback processes in their algorithm. There is inaccurate representations of radiation-cloud feedback processes in the current NWP. This according to Stephens (2005), is due to the complexity in representing the governing equations and the associated errors in the parameterization of the small scale processes.

Studies by Pohl and Cretat (2014) and Herwehe *et al.* (2014) reported that lack of such cloud-radiation feedback mechanisms results into biases in both regional weather and climate simulations. Alaparty *et al.* (2012) introduced a subgrid-scale cumulus cloudiness formulation in the Kain Fritsch (KF) cumulus scheme and the rapid radiative transfer model (RRTM). The inclusion of subgrid-scale cloud–radiation interactions were found to have realistic longwave and shortwave radiation variability, leading to the improvement of several meteorological parameters for both weather and climate time scales.

Most of the current RCMs do not consider some of these tunable parameters in their closure schemes. The current study considered these parameters in the CPSs to assess their impact to the rainfall simulations. The WRF-ARW version 3.9 was the primary tool applied for research in the current study. The model flexibility in customization coupled with numerous physics differing in their closure schemes, was the basis for its choice in the study.

2.3.5 Regional Research Studies with WRF Model

The convective schemes are of primary importance for rainfall especially in regions receiving predominantly convective rainfall, such as tropical regions. Owing to the importance of convective processes for rainfall formation over the EA region, the current study used the four cumulus schemes namely the Grell Devenyi (GRELL), Betts Miller Janjic (BML), Kain-Fritsch (KF) and Kain-Fritsch with moisture advection (KFT) to assess their robustness in reproducing the rainfall characteristics over the EA region. The choice of these schemes was based on the previous studies

that found better results associated with some of them albeit their individual strengths and weakness (Pohl *et al.,* 201; Ogwang *et al.,* 2015a, b).

Ngaina (2015) used the KF scheme to study the effects of aerosol-cloud-precipitation interactions for weather modification in East Africa. The study found appreciable skill of WRF model for weather modification. The observed biases in the simulations weakened the skill of WRF model in reproducing the key rainfall characteristics over the EA region. In studying the seasonal and inter-annual variability of hydro-meteorological services, Kerandi *et al.* (2017) found good skill in using WRF model to reproduce the annual cycle and inter-annual variability.

A study by Cretat *et al.* (2012) tested three cumulus schemes namely; Kain-Fritsch, Grell Devenyi and Bettts Miller Janjic to assess their sensitivity in simulating seasonal climate and the associated uncertainties over South Africa. The study found out that, WRF simulates accurately seasonal large-scale rainfall characteristics. The rainfall biases were found to depend on the set of physical configurations applied. The Kain-Fritsch scheme was found to be associated with large wet biases; the Betts Miller Janjic was associated with under-estimation of rainfall, while biases in the Grell Devenyi were relatively lower. In a similar study, Ratna *et al.* (2013) found that, cumulus schemes control most of seasonal rainfall distribution, as well as their amounts. This was consistent by earlier studies by (Wang and Seaman 1997; Pohl *et al.,* 2011).

For a better representation of local scale details and processes in the NWP, Mukabana and Piekle (1996) found out that the large-scale monsoonal winds and the mesoscale circulations are key parameters to be considered in the NWP. Furthermore, the study found that high resolution RCM are capable of minimizing the model rainfall biases over the equatorial regime to a certain degree of accuracy. One of the major strength of the Kain-Fritsch and Grell Devenyi schemes is the ability to capture the rainfall extremes with reasonable accuracy; despite their characteristic nature of the wet and dry biases associated with them (Huang and Gao 2017). Other studies by Cretat *et al.* (2012; 2015) found that, in most cases the schemes are not able to accurately simulate the rainfall processes associated with the convergence zones like the ITCZ, and South Indian Convergence Zone (SICZ) for South Africa region.

CHAPTER THREE

3 Theoretical Framework

This chapter presents key physics and the dynamical attributes of WRF-ARW model used in the study. Also presented in the section is the modeling framework and the experimental design for the study.

3.1 Weather Research and Forecasting Model

The main research tool was the Weather Research and Forecasting (WRF-ARW) model applied in research mode. The WRF model is a non-hydrostatic model widely used for research and real-time forecasting. The model is largely preferred by the modeling community for NWP since it is offers large spectrum of capabilities for extensive range of applications to the scientific community (Cretat *et al.,* 2012; Ratna *et al.,* 2013). The ARW dynamic component incorporates both the compressible, non-hydrostatic Euler equations. The Euler equations are based on a terrain-following mass conservation vertical coordinate (Skamarock *et al.,* 2005; Skamarock 2008). The main physics in the WRF model are categorized as microphysics processes (MP), cumulus parameterization schemes (CPS), planetary boundary layer (PBL), land-surface model, and radiation.

3.1.1 The Microphysics Processes

In numerical models, the precipitation mainly has two components, the convective and non-convective components. The micro-physics (MP) is responsible for the non-convective part of the precipitation. Based on the physical laws of thermodynamics in numerical weather models, the MP depletes the moisture within a given air column. The MP scheme is responsible for the generation, growth and dissipation rate of the cloud particles. Furthermore, the simulated water vapor, clouds and precipitation processes are governed by these schemes. The options for the MP differ in the number of phase changes of water and the number of interactions between clouds and precipitation particles. The sedimentation, collision, condensation-evaporation, aerosol activation, and collision-coalescence are the key microphysical processes.

The aerosol size distribution assumes a single mode lognormal size distribution. The activation occurs when the ambient super saturation exceeds the critical super saturation for the given particle size (Petters and Kreidenweis 2007). There are various MP schemes in the WRF model including Kessler (1969); Lin (1983), WRF single moment 3 and 5 class and Eta (Ferrier 1994), WRF single

Scheme 6 Class, Goddard, Thompson, Milbrandt-Yau Double Moment and Morrison double moment (Jankov *et al*.,2011).

3.1.2 Radiation Scheme

The atmospheric and surface heat budgets form part of the radiation scheme in the numerical models. The energy budgets are derived from both longwave (LW) and shortwave (SW) components of the radiation spectrum. The infra-red and the gases emitted or absorbed by the surface form part of the longwave radiation. The shortwave radiation includes visible and ultra-violet wavelengths. The upward flux is the reflection due to surface albedo. In the WRF model, there are several parameterized radiation schemes for both LW and SW.

The interactions between radiation and cloud is key to the modulation of regional rainfall characteristics. Some examples of the radiative schemes applicable in WRF model include rapid radiative transfer model global (RRTMG), rapid radiative transfer model (RRTM), the geophysical fluid dynamics laboratory (GFDL) both for LW and SW schemes, NCAR community atmosphere model (CAM) schemes for both SW and LW, Dudhia SW, Goddard SW. A detailed description of these radiative schemes can be accessed in Skamarock (2008).

3.1.3 Cumulus Scheme

The convective part of the precipitation is determined by the cumulus schemes and their effects within a grid cell for both deep and shallow clouds. They describe the vertical fluxes due to unresolved updrafts and downdrafts as well as the entrainment and detrainment processes within a cloud cell. The cumulus schemes also provide the convective component of rainfall caused by convective eddies that are parameterized in the numerical models. There are various cumulus parameterized schemes developed for the WRF model. These include the Kain-Fritsch scheme, herein referred to as (KF) developed after (Kain 2004), Betts-Miller-Janjic scheme herein referred to as (BML) and developed after Betts (1986), Grell-Devenyi scheme known as (GRELL) and developed after Grell (1993).

Other schemes developed for WRF model are the Tiedtke scheme, Grell-Freitas (GF) scheme with improved Grell Devenyi scheme that tries to smooth the transition to cloud-resolving scales (Arakawa 2004). The old Kain-Fritsch scheme assumes a deep convection using mass flux approach with downdrafts and CAPE removal time scale. A summary of the theory behind some of these schemes are briefly discussed in the next sub-sections.

3.1.3.1 Kain Fritsch

The Kain Fritsch scheme (KF) is one of the examples of low-level control schemes. It is based on a mass flux parameterization and uses the Lagrangian parcel method, which can generally be grouped into three parts; the convective trigger function, the mass flux formulation, and the closure assumptions (Kain and Fritsch 1990, 1993; Stensurd 2007). The earlier version of the KF scheme was based on a simple cloud model with moist updrafts and downdrafts. The KF scheme has undergone rapid changes in its updraft/downdraft formulation and a closure assumption (Kain 2004; Zheng *et al.,* 2016).

The basic theory behind the scheme considers how an air parcel is able to overcome the convective inhibition factors and activate the CAPE. The trigger function in the scheme adjusts the parcel buoyancy at the LCL level. Shallow convection is only permitted in the absence of non-buoyant parcel assuming the turbulent kinetic energy for mass flux rather than CAPE is available. Within a grid column of air, the convection is triggered when the parcel overcomes negative buoyancy.

3.1.3.2 Betts-Miller Janjic

The Betts-Miller-Janjic scheme also referred to as BML is an example of deep layer control convective schemes (Betts 1986; Betts and Miller 1986). The deep convection profiles and the relaxation time are variable and depend on the cloud efficiency, a non-dimensional parameter that characterizes the convective regime (Janjic 1994). The cloud efficiency depends on the heat changes on the precipitation, and mean temperature of the cloud. The shallow convection moisture profile is derived from the requirement that the entropy change be small and positive (Janjic 1994). The scheme uses transformed set of thermodynamic variables, based upon the concept of saturation points.

In the scheme, the amount of CAPE is assumed to depend on the size of the environment that supplies it. For active convection to form, the height at which the cloud forms (cloud base) and the cloud top (the highest model level where the parcel is still buoyant), usually just below the equilibrium level must be determined. If the parcel is not afloat at any level, convection will not be activated at that level.

The difference between the cloud base and cloud top is therefore used to determine whether convection forms or not. For example, if the difference between the cloud base and cloud top is less than 200 hPa, the deep convection scheme aborts and instead a shallow convection scheme is

used (Stensurd 2007). The scheme structure favors activation in cases with significant amounts of moisture at low and mid-levels and positive CAPE. As a result of the deep-layer control, large CAPE values in the lower layers are not a sufficient condition for atmospheric convection to be activated in this scheme. The scheme rearranges the thermal and moisture structures to conform to the new state established by deep convection (Betts 1986)**.** The precipitation is expressed by Equation 2.3.

$$\Pr = \int_{pb}^{pt} \frac{q_R - q}{\tau} \frac{dp}{g} \quad \ldots\ldots\ldots\ldots\ldots\ldots\ldots\ldots\ldots\ldots\ldots\ldots \quad (2.3)$$

In Equation 2.3, q is the model's specific humidity, q_R is the reference-profile specific humidity, τ is the timescale over which the adjustment occurs, and *pt and pb* are the pressures at the cloud top and bottom, respectively and dp/g is the acceleration due to gravity. The scheme parameterizes the effects of shallow convection.

3.1.3.3 Grell Devenyi

The Grell Devenyi scheme (GRELL), Grell (1993), consider clouds as two steady-state circulations: an up-down draughts. No direct mixing occurs between the cloudy air and the environmental air except at the top and bottom of the circulations. The mass flux is constant with height and no entrainment or detrainment occurs along the cloud edges. The originating levels of the updraft and downdraft are given by the levels of maximum and minimum moist static energy, respectively. The scheme is activated when a lifted parcel attains moist convection. Condensation in the updraft is calculated by lifting a saturated parcel. The downdraft mass flux depends on the updraft mass flux.

Heating and moistening in the Grell scheme are determined both by the mass fluxes and the detrainment at the cloud top and bottom. Grell and Devenyi (2002) introduced an ensemble cumulus scheme in which effectively multiple cumulus schemes and variants are run within each grid box and then the results are averaged to give the feedback to the model. The schemes use mass-flux type schemes, but with differing updraft and downdraft entrainment and detrainment parameters, and precipitation efficiencies. The CAPE, low-level vertical velocity and or moisture convergence are key parameters for determining the dynamic controls and closure schemes.

The convective precipitation is proportional to the integral of the moisture advected by updraft. The total amount of cloud water due to condensation is removed by rainfall leaving no residual. This scheme allows subsidence to the nearby areas or within the grid-point if resolution is greater than 10 km. Some of the regional studies applying GRELL, KF and BML CPSs include (Pohl *et al.,* 2011; Argent *et al.,* 2014; Kerandi *et al.,* 2017).

3.1.4 Planetary Boundary Layer

The planetary boundary layer (PBL) is the lowest layer of the atmosphere where most processes are directly influenced by the earth's surface. The vertical subgrid-scale fluxes due to eddy transports in the atmosphere occur within the PBL. The PBL plays a crucial role in determining the surface and upper level processes (Deardorff 1972). The PBL schemes determine the flux profiles within the well-mixed boundary layer and the stable layer, and thus provide atmospheric tendencies of temperature, moisture (including clouds), and horizontal momentum in the entire atmospheric column. The land surface fluxes and the turbulence that occurs in the PBL are crucial factors in the evolution of the atmosphere because their impact might propagate to the whole atmospheric column.

An appropriate description of the turbulence permits heat distribution, moisture and momentum all over the atmosphere. Some of the processes like turbulence occur within the PBL and resolved such processes within the NWP. Since the surface influences the PBL and considering that the variety of surfaces on the earth is huge, resolving the turbulence adequately in a broad range of conditions is undoubtedly a challenge. A challenge associated with the description of the PBL is in its closure assumptions with non-linear characteristics of turbulence.

3.1.5 Land Surface Scheme

The land-surface models (LSMs) handle the initialization of the state of the ground and account for the surface forcing in the atmosphere. They provide the fluxes that determine the lower boundary condition for PBL schemes by describing the ground temperature, the soil moisture and temperature profiles, the canopy effects and the snow cover. The use of an appropriate sophisticated model that updates these variables is crucial from a climate point of view.

3.1.6 The Convective Trigger Function

For any convective process, a trigger mechanism is required. A trigger function is a set of criteria in a scheme that determines when, where and if the scheme is to be activated. The convection

initiation process occurs in small scales that cannot be explicitly represented in grid spacing of greater than 1km within the current NWP. Therefore, trigger functions aid in this through parameterized functions.

The triggering convection simply put is the onset of convection which evolves through its life cycle. The function activates the CPSs if it detects the potential for deep convection. The principle behind convective trigger function is based on the identification of convectively unstable layer within the PBL. The primary differences between various trigger functions lies on the identification of the source layer of convection and how it realizes the convective instability for cloud development.

Three factors believed to determine the convective instability of the boundary layer are; grid-scale vertical velocity (Kain and Fritsch 1992; Donner 1993; Bechtold et *al.,* 2001), boundary layer moisture convergence (Kuo 1974; Tiedtke 1989), and CAPE (Arakawa and Schubert 1974; Zhang and McFarlane 1995). The treatment of the trigger functions in climate models is not well defined. This has been found to cause too much wet biases in the current NWP models (Dai 2006).

There are many trigger functions based on different model assumptions. For example, trigger function based upon Fritsch Chapel Trigger (FCT), trigger function based on column integrated moisture convergence called Anthes Kuo Trigger (AKT), trigger function based upon the amount of convective inhibition called negative area trigger (NAT), trigger function based upon the depth between the LCL of a parcel and its level of free convection called lifting depth trigger (LDT), and trigger function that determines the boundary layer called boundary layer forcing check (BLFC). Summary and detailed descriptions of these functions can be found in (Kain and Fritsch 1992; Nguyen *et al.,* 2008).

The current study was carried into two main phases. The first phase involved subjecting the four CPSs to robust analyses to identify the best scheme that can simulate the various rainfall characteristics during extreme years. The second phase involved the identification of specific adjustable parameters within the cumulus schemes that need to be customized in order to improve and optimize the WRF model simulations for extreme rainfall over the East Africa region. The flow work was presented in a conceptual framework. Figure 4 illustrates the workflow and the various concepts involved at every stage of the work.

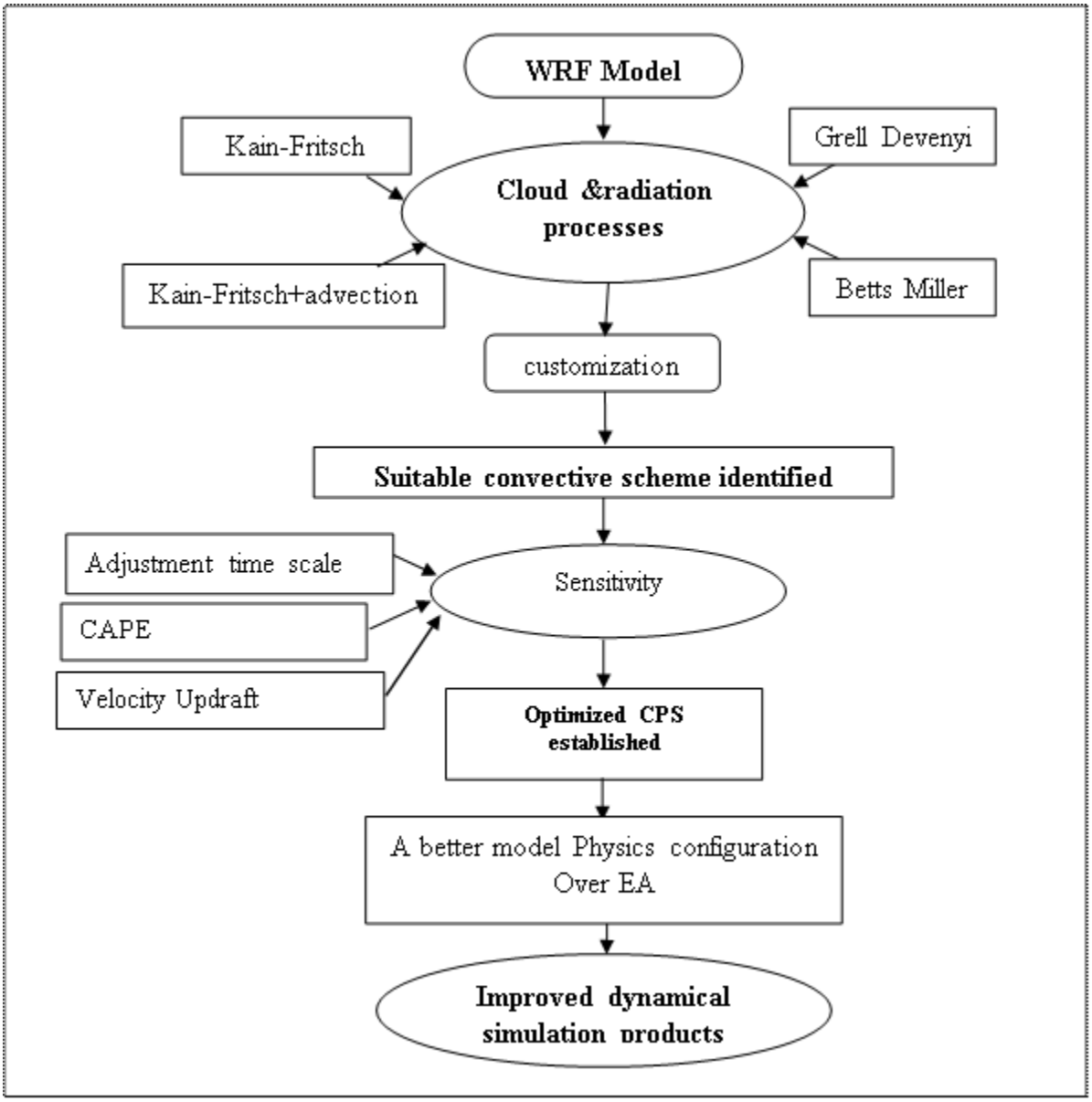

Figure 4: Conceptual framework of the study. The main elements of the framework were WRF-ARW model, cumulus parameters and adjustable parameters.

CHAPTER FOUR

4 Data and Methodology

This Chapter describes the data and their sources, methodologies, model and experimental procedure.

4.1 Data

The data used in the study included observed monthly point station datasets for rainfall obtained from ICPAC for some of the representative stations within the EA region, gridded datasets and simulated model output. The detailed descriptions of the individual datasets are in subsequent sections. The gridded datasets spanning from 1981 to 2016 were used for model validation as described in sub-sections 4.1.1.

4.1.1 Description of Data used in the Study

4.1.1.1 The *Insitu*-Data Observations

The *in-situ* data from few selected stations based on the homogeneous zones described earlier in this work (section 1.4) was used to validate the gridded observational dataset. The *in-situ* data from National Meteorological and Hydro Meteorological Services (NMHS) were obtained from the IGAD Climate Prediction and Applications Center (ICPAC). The gridded datasets were applied for analyses due to sparse network of stations within EA region and or lack of daily station data for some critical stations within EA contributed to using gridded dataset.

The three gridded datasets used included the Global Precipitation Climatology Project (GPCP), the Climate Research Unit (CRU) monthly dataset, and the Climate Hazards Group Infrared Precipitation with Station data (CHIRPS). The details of these datasets were briefly presented in subsequent sections.

4.1.1.2 The Global Precipitation Climatology Project

The Global Precipitation Climatology Project (GPCP) dataset resolution was at 2.5° by 2.5°. The GPCP rainfall estimate is a merged product of satellites and the station observations (Huffman *et al.,* 2009). Several studies over the EA region have used the GPCP data to represent the observed data in evaluating the performance of the climate models (Shreck and Semmazi 2004; Bowden

and Semazzi 2007, Temesgen 2011; Endris *et al.*, 2013; Yang *et al.*, 2014). Detailed information about the data can be accessed from Adler *et al.* (2003).

4.1.1.3 Climate Research Unit

The monthly data from the Climate Research Unit (CRU) were used in this study. CRU is a gridded observed rainfall dataset obtained from the University of East Anglia. The CRU datasets have been interpolated at different regular spacing. For example, the datasets are available at regular spacing of 0.5°, 1.5°, 2.0° and 2.5°. For this study, the datasets at 0.5 ° regular spacing was used since its resolution is nearly similar to the model simulations (0.36 °). The datasets contain five climatic parameters namely; precipitation, surface temperature, diurnal temperature range (DTR), cloud cover and vapor pressure.

In this study only, the rainfall was used for model evaluation. The CRU monthly datasets are derived from satellite data, model estimates and rain gauge data from ground stations. The final merged product is generated by combining the satellite and reanalysis data. It contains precipitation distributions with full global coverage and improved quality compared to the individual data sources. The comparisons of the CRU with other data sources revealed remarkable agreements over the global land areas and over tropical and subtropical oceanic areas. Studies within EA that have used CRU include but not limited to Omondi *et al.*, (2009) and Kerandi *et al.* (2017).

4.1.1.4 Climate Hazards Group Infrared Precipitation with Station

The observed gridded data was provided by the Climate Hazards Group Infrared Precipitation with Station (CHIRPS) data. The CHIRPS data is a blend of actual station data with satellite estimates (Funk *et al.*, 2015). The first part is obtained by calculating the percentage of time during the pentad that the Infra-red observations indicate cold cloud tops (<235° K), and converting that value into millimeters of precipitation by means of previously determined local regression with tropical rainfall measuring mission (TRMM) version 3B42 precipitation pentads. In the second part of the process, stations are blended with the CHIRPS data to produce the final product.

The main data sources used in the creation of CHIRPS are monthly precipitation climatology. The climatology is temporally disaggregated at each grid cell location into 72 pentads (6-pentads per month) long-term average accumulated values, quasi-global geostationary, infrared satellite observations from NOAA and Climate Prediction Center (CPC). For each grid location in the

CHIRPs domain, the five nearest station observations are used to calculate an adjustment ratio for the CHIRPs value. Each station is assigned a weight proportional to the square of their expected correlation.

The CHIRPS datasets are available at high resolution (0.05°, 0.25°). The interpolation is applied using rain gauge data with satellite estimates to supplement on the areas with no station network. The dataset has a longitudinal extent from 50°S to 50°N and runs from 1981 to present. CHIRPS were developed to deliver reliable, up to date, and more complete datasets. Both monthly and daily time series of the datasets are available. This study used daily resolution time series for model evaluation and skill assessment. Before using CHIRPS for analysis, it was validated with station data to check for its consistency with the climatology (Shukla *et al.,* 2014; Funk *et al.,* 2015; Appelhans and Nauss 2016). Studies by Dunning *et al.* (2016, 2017) and Kipkogei *et al.* (2017) have successfully used this new dataset for model evaluation and found robust skill.

4.1.1.5 The Atmospheric Variables

The daily data for atmospheric variables from ERA-Interim reanalysis (0.75° x 0.75 °) were used for model evaluation of atmospheric variables. The atmospheric fields (u and v wind vectors, specific humidity, and vertical pressure velocity (omega)) were drawn from the ECMWF center. The ERA-interim reanalysis has rigorously been used as a signature for atmospheric circulations (Pohl *et al.,* 2006, 2011; Endris *et al.,* 2013; Kerandi *et al.,* 2017).

4.2 Setting up WRF-ARW Model Domain

Before any regional downscaling experiment is conducted, the choice of the domain size, setting up of the domain size, choice of Lateral Boundary Conditions (LBCs) and grid spacing are very important aspects of dynamical downscaling to be considered (Xue *et al.,* 2007). The extent and domain size must be such that it satisfies the selection criteria of an optimal model domain to produce realistic regional climate simulations. Figure 5 shows simulation domain following recommendation by Davies *et al.* (2009) and Anyah *et al.* (2006) but with few modifications constraining the model domain over Congo airmass, Indian Ocean and Arabian highland which greatly impacts rainfall over the domain (Segele *et al.,* 2015). The domain enclosed moisture sources i.e Congo region, Indian ocean and inland water bodies like Lake Victoria that are key in moisture source of the region.

The third version of WRF-ARW model was configured over the simulation domain. The domain was the most probable compromise to constrain the development of synoptic, mesoscale flows and the perturbations due to variations in circulations between the RCM and GCM. This criterion and choice of domain has been extensively used by Girogi and Shields (1999), Omondi (2010), and Otieno and Anyah (2012) for simulation experimental studies.

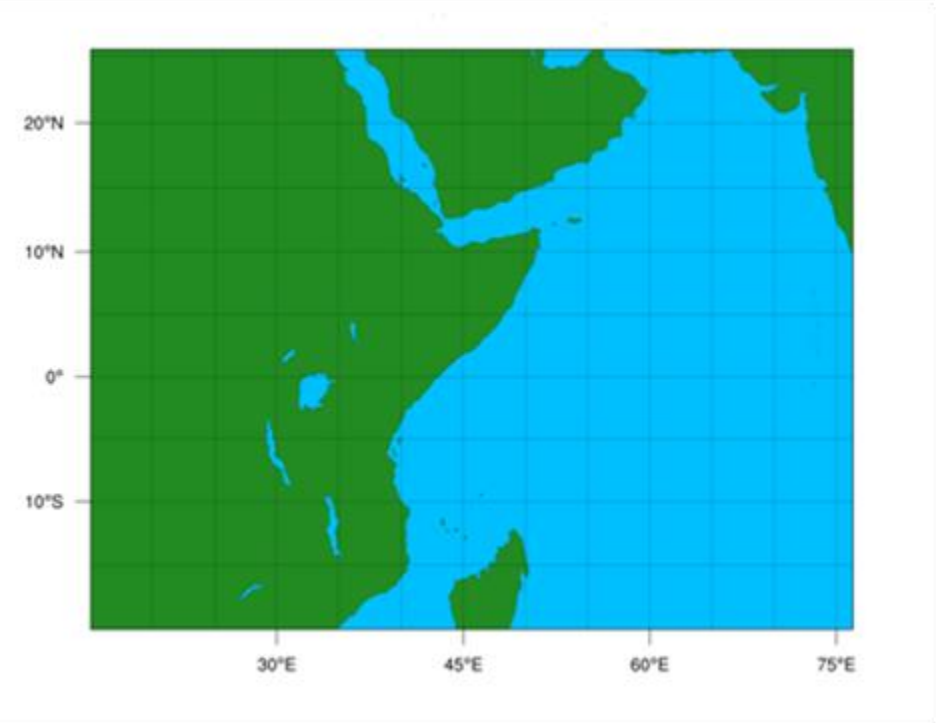

Figure 5: Model simulation domain centered over 15^0 W -75^0 E and 25^0 S-25^0 N

4.2.1 The 'Perfect' Boundary Simulation

The ERA-Interim reanalysis from European Centre for Medium-Range Weather Forecasts (ECMWF) was used to provide initial and lateral boundary conditions for the WRF model while sea surface temperature (SST) from NOAA was used to provide lower boundary forcing, updated every six hour. The lateral boundary forcing fields included geopotential height, air temperature, specific humidity and horizontal winds. The initial state conditions included surface pressure, sea level pressure, 2-m-height moisture, 2-m-height temperature, 10-m-height horizontal winds, soil moisture, soil temperature and skin temperature. The topographical information at 10-minute horizontal resolution was obtained from United State Geological Survey (USGS). The ERA-Interim from ECMWF centre (Dee *et al.,* 2011) was used for large scale forcing fields. The data is available from 1979 to current date at 6-hourly Integration timestamp.

4.2.2 Experimental Design

Four different simulations were performed for the widespread wettest and driest years using four cumulus schemes in the WRF model configured at 0.3° resolution (~36 km). A number of past numerical experiments have been centered on this resolution with good simulation being reported. For example, Wang and Seaman (1997) evaluated four different CPSs at nearly 36 km over Peninsula. Kerandi *et al.* (2017) evaluated WRF model over Kenya for hydrological studies at between 25-50 km. Studies by Pohl *et al.* (2011) and Pohl and Cretat (2014) evaluated WRF model over East Africa for atmospheric water and diurnal cycles at 60km, 36km and 12km horizontal resolutions respectively. Studies Cretat *et al.* (2012) and Cretat and Pohl (2012) used horizontal resolution of 35km over South Africa to evaluate WRF model for model internal variability. The current study used delineated wettest and driest years in its numerical integrations.

The simulations were carried out over the domain 0 ° - 75 ° E and 20 °S – 27 °N (190 by 145 grid points) using a single nest domain. The integrations were initialized on the 1st day of the month preceding the season. The integration time-step was 3 minutes and model output data archived every 6 hours from the first day of the simulation. The simulations were conducted for each of the four months of the selected dry and wet years. A total of sixteen (16) months integration were carried out for all the selected wet and dry years. The first month of the simulations were used as spin-up to let the model adjust to atmospheric initial conditions.

Four CPSs were applied together with PBL from Yonsei University Hong *et al.* (2006), MP of WRF Single Moment 6-class 6 (WSM6) (Hong and Lim 2006) and RRTMG for SW and LW radiations (Mlawer *et al.,* 1997). The four CPSs were selected on the basis of their widespread use in numerical models and the representativeness of different closure assumptions. The cumulus schemes applied were the KF, KFT, GRELL and BML from WRFV-ARW. Table 1 gives a summary of the physics and experimental design used for the simulations.

Table 1: The Experimental Design and Summary and convective Schemes

Experiment	Abbreviation	Convection	Radiation	PBL	MP
1	**KF**	Kain-Fritsch	RRTMG (Short and Longwave)	Yonsei University scheme	WRF Single-Moment 6-class scheme
2	**KFT**	Kain-Fritsch+Trigger Function	RRTMG (Short and Longwave)	Yonsei University scheme	WRF Single-Moment 6-class scheme
3	**GRELL**	Grell Schemes	RRTMG (Short and Longwave)	Yonsei University scheme	WRF Single-Moment 6-class scheme
4	**BML**	Betts Miller	RRTMG (Short and Longwave)	Yonsei University scheme	WRF Single-Moment 6-class scheme
5	**KF-new**	Kain-Fritsch	RRTMG (Short and Longwave)	Yonsei University scheme	WRF Single-Moment 6-class scheme

The land surface information was provided by the 4-layer NOAH land surface model (Chen and Dudhia 2001). Surface data derived from United States Geological Survey (USGS) database, which describes a 24-category land-use index based on climatological averages. The effects of the nearby lakes were activated since there is a unique climate developed by the lake system.

4.3 Methodology

The various methods employed to achieve the four specific objectives were; standardized rainfall index (SRI), principal component analysis (PCA) and Composite Analysis to delineate wet and dry years. For model evaluation, root mean square error (RMSE), correlation(R) and coefficient of variation (CV) was applied. Also used were Taylor and Box and Whisker diagrams for model ranking and distribution.

4.3.1 The Delineation of East Africa Extreme Rainfall

The methods applied here to delineate the observed extreme wet and dry rainfall events during the period of study included the standardized rainfall index (SRI), principal component analysis (PCA) and composite analysis.

4.3.1.1 Standardized Rainfall Index

This study focused on the wet and dry rainfall years during the March-April-May (MAM) and October-November-December (OND). The wet and dry years were first defined based on standardized rainfall index as had been used previously (Ogallo 1989; Okoola 1999; Camberlin *et al.,* 2009). Several past studies within the region have converted the data into comparable indices before any analysis including Ogallo (1989); Okoola (1999); Mutai and Neil (2000); Philippon *et al.* (2002); Ogallo *et al.* (2008); Owiti *et al. (*2008); Gitau (2011), and Mwangi *et al.* (2014).

4.3.1.2 The Varimax Principal Component Analysis

The varimax rotation of the principal component analysis (PCA) is a statistical method for filtering the modes of variability within a meteorological dataset based on diagonalization of the auto-covariance or auto-correlation matrix of a data set (Wilks 1995, 2006; Omondi *et al.*, 2012). The principal components (PCs) are rendered more robust by taking linear combinations of the leading empirical orthogonal functions (EOFs) and projecting them back on the input data matrix to obtain the PCs. This is referred to as the rotated (R) EOFs.

It is a widely used technique to extract the dominant modes of climate variability. It improves the physical interpretation of the PCA modes and helps to derive more localized components (Richman, 1986). The method assumes that the EOFs are weighted by the square roots of their respective eigen values. By rotating the EOFs, the large loadings are made larger while smaller loadings are made smaller.

Over the EA region, the varimax PCA technique has been widely used to map similarities in temporal and spatial patterns. Such studies include Ogallo (1980), Okoola (1999), Dommenget (2007), Nyakwada (2009), Omondi (2010), Omondi *et al.* (2013), Otieno and Anyah (2013b), have employed the time mode (T-mode) and temporal mode (S-mode) characteristics. The S-mode clusters regions with similar temporal patterns of climate while T-mode clusters together years with similar spatial characteristics.

In this study both S and T-mode characteristics of the varimax rotated patterns were used to show if all the wet and dry years are mapped within similar orthogonal functions. Thus T-mode EOFs solutions were used to determine if all the years clustered together as wet and dry years shared some commonality features.

4.3.1.3 The Scree Kaiser's criterion

The primary objective of the PCA method is to minimize the dimensionality of a dataset without losing crucial information. The critical question to ask is what determines the number of factor(s) to retain for rotation. The scree, Kaiser's criterion and sampling errors tests by North *et al*. (1982); Richman (1986) and Ntale *et al*. (2003) is used to determine how many modes to be retained for rotation. It is based on the cumulative variance that explains the highest variability in the dataset. Adding more factors, beyond this point will yield no better results and hence is referred to as the cut-off point (Costello *et al.*, 2005). Due to its wide-spread use in the atmospheric science field, the current study adopted this technique to determine how many factors to be retained for rotation.

4.3.1.4 Composite Analyses

Composite analysis involves averaging selected variables based on a given criteria to provide understanding of specific characteristics of the variables. The results of the composite analysis help to make inferences of associated patterns with a particular event (Okoola 1999; Koech 2014). The current study developed composites to provide understanding and general patterns of wet and dry events. This involved computing the average rainfall value from SRI at the specific grid points for the wet and dry cases. The averages of the meteorological variables and circulation parameters were also computed for these cases in order to identify dominant meteorological systems during extreme wet /dry years, as well as to understand how various model convective schemes are influenced by the circulation systems during the wet and dry conditions. Some studies over the region including Nicholson and Kim (1997), Okoola (1999) and Bowden and Semazzi (2007) isolated wet and dry years and their circulations patterns. These studies found that dry and wet rainfall composites follow a west-east rainfall gradient.

4.3.2 The Determination of the skill of four cumulus parameterization schemes in simulating intra-seasonal rainfall characteristics

The first specific objective aimed at assessing the skill of the model in providing information on sub-seasonal rainfall characteristics during MAM and OND seasons. The key rainfall characteristics analysed were number of rainy days (NRD), intensity of rainy days (IRD), and frequency of rainy days (FRI). A threshold for defining these various seasonal characteristics was first set and presented in Table 2. Some of the past studies that have adopted similar methods include Kijazi and Reason (2005, 2009). The WRF model evaluation was done using the coefficient of variation (CV), correlation analysis, RMSE and mean error bias.

Table 2: The summary of the Rainfall properties adopted for the study during MAM and OND Rainfall seasons over the EA region

	Rainfall Characteristics	**Definition**
1	Mean Rainfall	The total amount of rainfall received per time (mm/day) over a given place
2	Number of Rainy days (NRD)	Any day that records at least 1mm/day within a rainy season
3	Intensity of Rainy Days (IRD)	Average rainfall amount recorded for any rainy day based on 3 different thresholds. (i) Light between 1-10mm/day (ii) Moderate between 10-20mm/day (iii) Heavy above 20mm/day
4	Frequency of rainfall intensities (FRI)	The frequency of the rainfall intensities is defined based on (Dai 2006).

The frequency was calculated as a percentage of the number of rainy days under each of the rainfall intensities divided by all the number of rainy days within a season using Equation 3.4.

$$FRI = \frac{IRD}{NRD} \times 100\% \quad \text{..... (3.4)}$$

In Equation 3.4, FRI is the rainfall frequency for each category, IRD is the intensity of rainfall under each category, and NRD is the total number rainy days within a given season.

4.3.2.1 The Mean Bias Error

The mean bias error (MBE) measure is a statistical technique that assesses the model performance with respect to the observations. It highlights the model tendency to underestimate or overestimate meteorological quantities. The closer the model biases tends to zero, the more skillful the simulations become. A value below or above zero indicates a tendency to under or over forecast climate parameters respectively. The MBE measure was used to simulate how each of the model schemes represents the observed rainfall climatology using Equation 4.4.

$$MBE = \frac{1}{n}\sum_{1}^{n}\left(M_i - O_i\right) \quad (4.4)$$

In Equation 4.4, M_i and O_i are the model simulated and observed values respectively. The measure of bias shows the error between the models and observations. It is important to test the significance of the error calculated. The RMSE was used as a test measure for the error between the models and observation.

4.3.2.2 Root Mean Square Error

The root mean square error (RMSE) measures magnitude of the absolute error between the model and observations outputs. For each of the composites, the error between the model simulation and the observations was computed. The RMSE serves to aggregate the errors into a single measure of predictive capability. The errors were calculated and evaluated for each of the composites using Equation 5.4.

$$RMSE = \sqrt{\frac{\sum_{i=1}^{n}(O_i - M_i)^2}{n}} \qquad (5.4)$$

In Equation 5.4, O_i are rainfall observations, M_i is simulated model output, and n is the number of observations. For a perfect model, the RMSE should be as small as possible and almost tending to zero value for the verification period. Indeje and Semazzi (2000), Mutemi *et al.* (2007), Gitau *et al.* (2013) have applied the RMSE method in their studies.

4.3.2.3 Correlation Analysis

One of the simple but efficient statistical method to establish the linear relationship between model simulations and observations is the use of correlation analysis. The correlation coefficients range from negative one to positive one (-1 to 1). For a stronger relationship between any two variables, the correlation coefficients should be closer to positive one. An inverse relationship between the model and observation is indicated by negative correlation coefficients. The study calculated both temporal and spatial correlation coefficients between simulated rainfall and observed rainfall.

4.3.2.4 Coefficient of Variability

The coefficient of variability (CV) measures the deviation of the model from its mean observations. It is used to compare variability in the datasets when their mean is different. It is computed as the standard deviation divided by the arithmetic mean. In this study, CV was used to assess the variability associated with the calculated biases and the NRD and IRD. The equation 6.4a is an expression for standard deviation.

$$\sigma_x = \sqrt{\frac{1}{n}\sum_{1}^{n}\left(x_i - \bar{x}\right)^2} \qquad (6.4a)$$

The mean for the data series was expressed in Equation 6.4b.

$$\bar{x} = \frac{1}{n}\sum_{i=1}^{n} x_i \qquad (6.4b)$$

The CV was computed by dividing the standard deviation (6.4a) by the mean values (6.4b). Studies in the region like Anyah and Qiu (2012) and Kisaka (2015) have used the method for model evaluation.

4.3.2.5 Taylor Diagram

The skill of the WRF model using the four schemes in simulating East Africa rainfall was assessed. The statistics were summarized in a Taylor diagram (Taylor *et al*, 2012). The Taylor diagram compares model performance in terms of their correlation coefficients, mean square difference and standard deviations. The statistical significance of relative differences and the degree to which observational errors and inherent variability limits the expected agreement between simulated and observed behaviors.

4.3.3 The Establishment of the skill of the cumulus schemes in simulating the atmospheric circulations and dynamics

The second specific objective examined how the various CPSs simulated the dominant atmospheric circulation patterns and dynamics during the wettest/driest cases. The dynamical quantities analyzed were vertical velocity (omega), Vertically Integrated Moisture Flux (VIMF), convergence/divergences and CAPE.

4.3.3.1 Vertically Integrated Moisture Flux

The vertically integrated moisture flux (VIMF) is a dynamical quantity in the conservation of the water vapor equation and was first calculated in the 1950s and 1960s as a vertically integrated quantity to predict rainfall associated with synoptic-scale systems. A scale analysis shows that surface moisture flux (MF) Convergence/Divergence (MFC/MFD) is directly proportional to the horizontal mass convergence/Divergence field, allowing MFC/MFD to be highly effective in highlighting mesoscale boundaries between different air masses near the earth's surface that can be resolved by surface data and appropriate grid spacing in gridded analyses and numerical models. However, the effectiveness of boundaries in generating deep moist convection is influenced by many factors, including the depth of the vertical circulation along the boundary and the presence

of convective available potential energy (CAPE) and convective inhibition (CIN) near the boundary. The atmospheric water budget equation 7.4 was used to express and compute VIMF.

$$\partial PW/\partial t + MFD = \overline{E} - \overline{P} \qquad (7.4)$$

In Equation 7.4, E is evaporation from the surface; MFD is the vertically integrated moisture divergence between the surface and top of the atmosphere, and $\partial PW/\partial t$ is the temporal variation of precipitable water within air column. This term becomes negligible at seasonal timescales. This study focused on the capability of the various convective schemes to simulate rainfall and VIMF (Schneider *et al.,* 2006; Trenberth *et al.,* 2011; Newman *et al.,* 2012; Berhane and Zaitchik 2014).

4.3.3.2 Vertical Velocity in Pressure Coordinates

The vertical velocity (omega, ω) is a well-established measure of the large-scale vertical motion used to diagnose tropical circulation (Donner 1993; Bony *et al.,* 2004; Schwendike *et al.,* 2014; Oueslati and Bellon 2015). The omega analyses aids at understanding whether common precipitation biases are associated with vertical velocity motion properties. The negative (positive) values of ω are associated with upward (downward) motion. The current study used this technique to understand how rainfall biases are associated with the vertical uplift or sinking of motion during wet and dry years.

4.3.4 The Determination of the specific Adjustable parameters within the cumulus schemes that can be customized to improve rainfall simulations

The third objective aimed at obtaining higher skill and accuracy from the best CPS identified in Objectives 1 and 2. This was achieved through the CPS variable parameters identified based on recent interventions by scientists and their ability to bear greatest response to any adjusted parameter (Lin *et al.,* 2013; Zheng *et al.,* 2016). Once the saturation point (LCL) has been reached, the atmosphere regains its stability for new convective process to begin. This time is dictated by the adjustment time scale (ATS). The ATS is the time required for CAPE to be reduced from the environment once the saturation point has been achieved.

In the current NWP, the ATS has a set default range of 800-3600 seconds implies that it takes about between 30-60 minutes for stability of the atmosphere to be regained once the convection

occurred. Assigning such ATS ranges result to model hyper-activity giving too much rainfall. The current study had ATS range set to 800-18000 seconds, to lower the hyper-activity of the model (Bullock *et al.,* 2015). Previous study by Zheng et *al.* (2016) found out that the ATS is one of the adjusted parameters with the greatest impact to the quality of simulated rainfall in the NWP.

Another factor that modulates the quality of rainfall simulations is the cloud-radiation coupling. The absence of a mechanism to initiate the coupling effect in the regional climate models is one of the causes of model biases. The problem in NWP was first reported by Krishnamurti (1986). Alaparty *et al.* (2012) first introduced and tested this in WRF model. The interaction of cloud-radiation reduces the passivity in the cloud, lowers the surface heating that causes too much precipitation. The study reported that the interaction of cloud –radiation physics leads to a more realistic simulation of attenuation of downward surface shortwave radiation. The reduced surface shortwave radiation moderates the surface forcing for convection and results in a notable reduction in precipitation biases. This study applied the moisture-based advection scheme in the KF scheme.

Lastly, the entrainment based on lifting condensation level (LCL). It is based on varying the entrainment constant parameter that controls the magnitude of entrainment in a cloud cell. It is assumed to have a uniform value $\alpha = 0.03$ (Tokioka *et al.,* 1988). By varying the Tokioka Parameter (TP), the hyperactivity of subgrid-scale convection scheme can be regulated and biases reduced (Lin *et al.,* 2013). Increasing the TP results to a decrease in the sub-grid scale precipitation hence an increase in the grid-scale precipitation. As a result, this adjustment in the TP provides rainfall simulations with minimal rainfall biases.

This study used the TP value at 0.03. The study hypothesized that by varying any of these parameters in the model, the simulations would be improved and hence the forecasts. These factors impact greatly on dynamic cloud processes including cloud formation and growth. Their effects are greatest on cloud timing, location, and intensity of precipitation. This study varied these three variables in the Kain-Fritsch scheme and their combined response analyzed. It is important to note that the study did not analyze the individual response of each of these parameters due to computational constraints.

To achieve the optimum configurations, several sensitivity experiments were conducted but only the three parameters listed here showed better skill response to each rainfall characteristics. The study therefore concentrated only on these parameters for more detailed and extensive sensitivity

experiments. Each simulation was analyzed to test the response of the WRF model to the mean seasonal rainfall for a period 10 days. Once the optimal level for the respective parameters were achieved, a full year simulation using all the adjusted parameters were done. The analyses however, were based on the combined effect of the three parameters. The detailed descriptions of these parameters are provided under the literature review section as well as Zheng *et al.* (2016). The methods used for evaluating the model performance were already discussed in sub-sections (4.2.2).

CHAPTER FIVE

5 Results and Discussion

This chapter presents the results and discussion obtained with the various methods that were used to investigate the three specific objectives. The results for the identification of the best scheme that simulate the various rainfall characteristics are presented first. This was followed by the results from the identification of specific adjustable parameters within the cumulus schemes to improve and optimize the WRF model simulations of extreme rainfall over the East Africa region.

5.1 The Determination of the best Dataset for WRF model evaluation

The rainfall stations within homogenous zones were correlated with CRU, GPCP and CHIRPS datasets. Only the station (s) that had higher correlation values in each zone were presented for analysis. The homogeneous representative stations were Bujumbura, Dagoretti, Entebbe, Lodwar, Iringa and Mwanza. Tables 3 and 4 show the results of the correlation between station rainfall data with CRU, GPCP and CHIRPS datasets. The CHIRPS data had the highest correlation coefficients with the station data at all stations during both MAM (Table 3) and OND (Table 4) seasons. The highest correlation between CHIRPS and station data was 0.97 over Lodwar during OND season; this represented R-square of 94%. This was an indication of CHIRPS data accounting for as high as 94% of the variance of the station's rainfall data. This is important since CHIRPS data forms a critical component of most data that was used in many parts of this study.

Table 3: The correlation coefficients between Station Rainfall Data and GPCP, CRU and CHIRPS datasets for selected stations. The years were from 1981-2016 over EA region during the MAM season

Stations	CHIRPS	CRU	GPCP
Bujumbura	0.52	0.13	0.18
Dagoreti	0.74	0.51	0.13
Mwanza	0.94	0.75	0.20
Iringa	0.78	0.58	0.13
Lodwar	0.93	0.65	-0.47
Entebbe	0.91	0.45	0.38

Table 4: The correlation Coefficients between GPCP, CRU, CHIRPS and Station dataset for some selected stations from 1981-2016 over EEA region during OND season.

Station	CHIRPS	CRU	GPCP
Bujumbura	0.72	0.47	0.02
Dagoreti	0.78	0.51	0.40
Mwanza	0.22	0.16	0.25
Iringa	0.94	0.63	0.41
Lodwar	0.97	0.25	0.31
Entebbe	0.94	0.59	0.30

The sample plotted time series of station rainfall, CRU, GPCP and CHIRPS data were given in Figure 6. The similarity in the patterns of positive and negative anomalies for the station rainfall and CHIRPS are quite evident. Therefore, all subsequent results in the study used CHIRPS as the observed data for the analyses. Throughout the analyses, the WRF model results were first interpolated into the CHIRPS grids for fair comparison with the observation. The regional studies like Funk *et al.* (2010; 2015), and Dunning *et al.* (2016) have used CHIRPS in the analyses over East Africa. The next section presents the results for the characterization of extreme wet and dry years over the East Africa region.

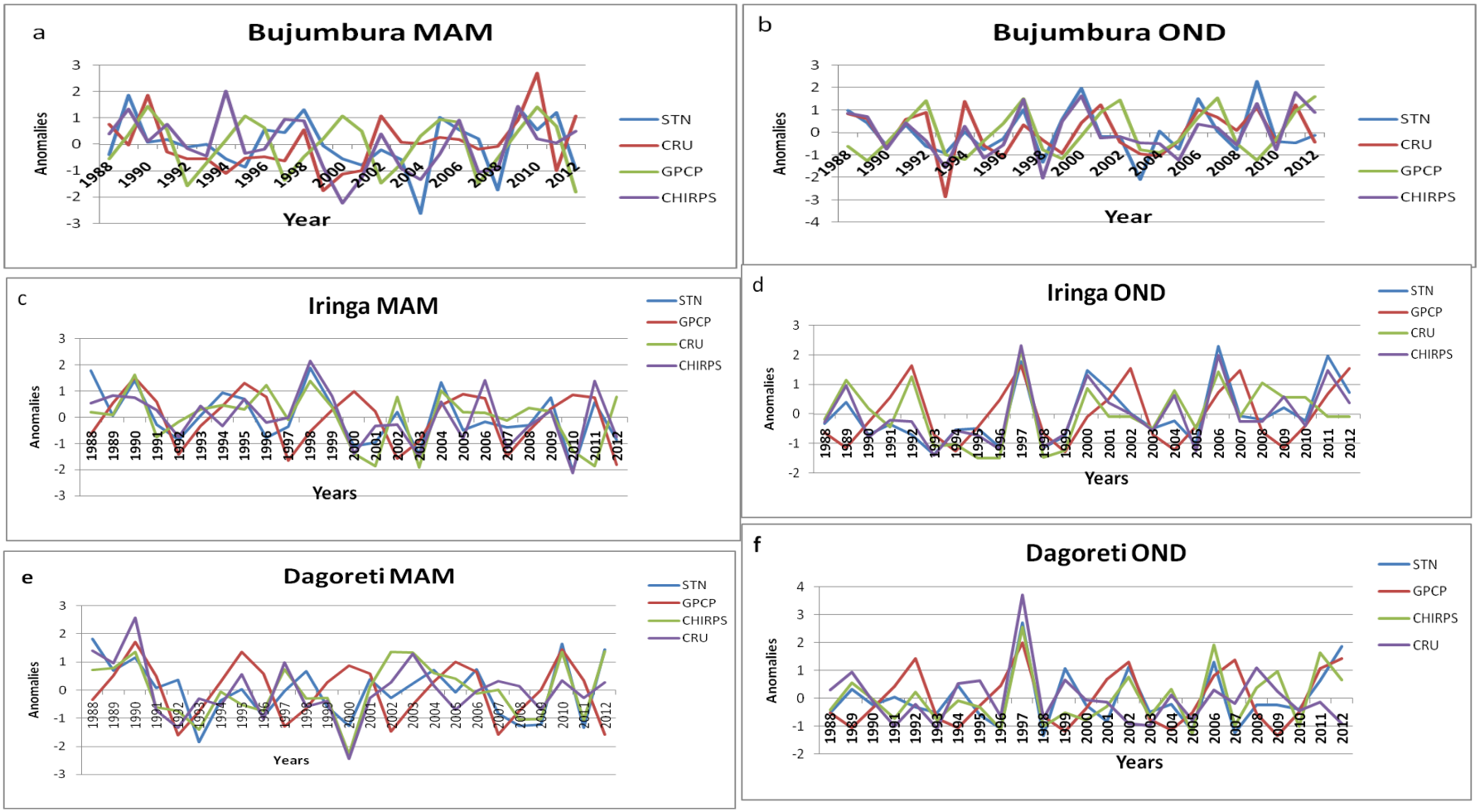

Figure 6: Inter-annual variability of standardized rainfall anomaly from CRU, CHIRPS, GPCP and station observations during MAM (left panel) and OND (right panel) over, Bujumbura, Iringa, and Dagoreti stations.

5.2 The Delineation of East Africa Extreme Rainfall years

In this section, the results from the three methods used to delineate wet and dry years were independently presented and compared. The methods applied included standardized rainfall index (SRI), principal component analysis (PCA) and composite analysis.

5.2.1 Standardized Rainfall Index

Figure 7 shows the time series for standardized rainfall Index (SRI) from CHIRPS datasets. An index threshold of 0.5 / (-0.5) was used for any wet/ (dry) year respectively. The major wet years isolated during MAM season were 1987,1988,1989,1990,1991,1992, 1998, 2003, 2007, 2010, 2012 and 2015, while the major MAM dry season years were 1984, 1993,1996, 2000, 2006, 2008, 2009. The wet years delineated for OND season were 1982, 1987, 1991, 1997, 2002, 2004, 2006, 2009, and 2015 and for dry cases the years were 1983, 1984, 1988, 1995, 1999, 2007, 2010, and 2013. Most of these dry and wet years have been isolated in some past studies including Okoola (1999), Nyakwada (2009), Owiti *et al.* (2008) and Philipon *et al.* (2015), among others. Many of these extremes also occurred during major ENSO years. The Indian Ocean Dipole (IOD) indices were also strong in some of these years.

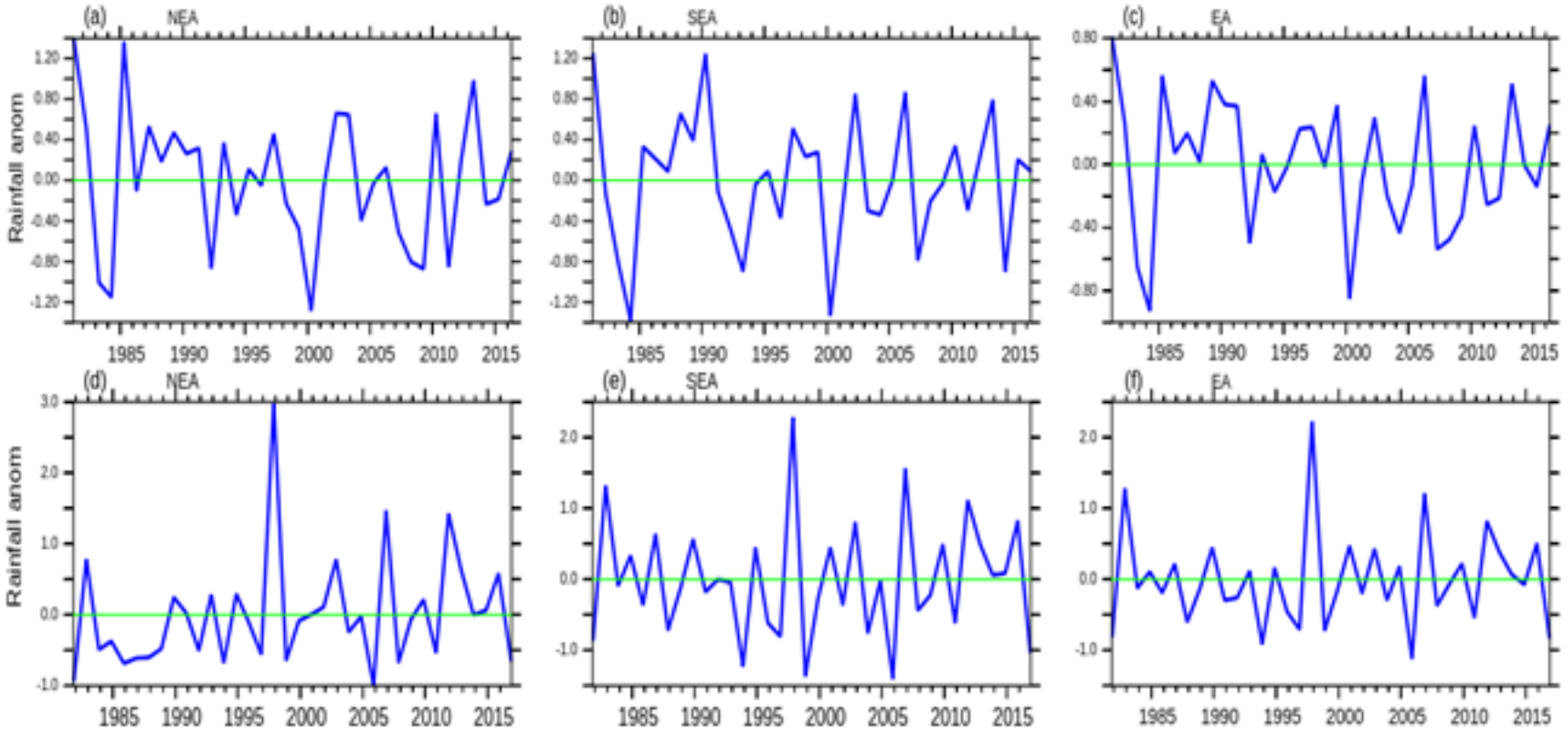

Figure 7: The Inter-annual variability of mean Rainfall (mm) from CHIRPS during MAM (top panel) and OND (bottom panel) seasons over NEA, SEA and EA sub-domains for the period 1981-2016.

5.2.2 Varimax PCA Analysis

In this study, both S and T-modes characteristics of the varimax rotations were used to delineate the major spatial and temporal rainfall characteristics for the MAM and OND seasons. The results for scree test were first presented.

5.2.2.1 Scree Test Method

The selection of the PCA modes for rotation was done using Scree test. Figure 8 shows the results for the scree test during the MAM and OND seasons. The first four modes accounted for 32.3% and 66.4% of total MAM and OND rainfall variance respectively. Therefore, only these four modes were subjected to rotation by varimax.

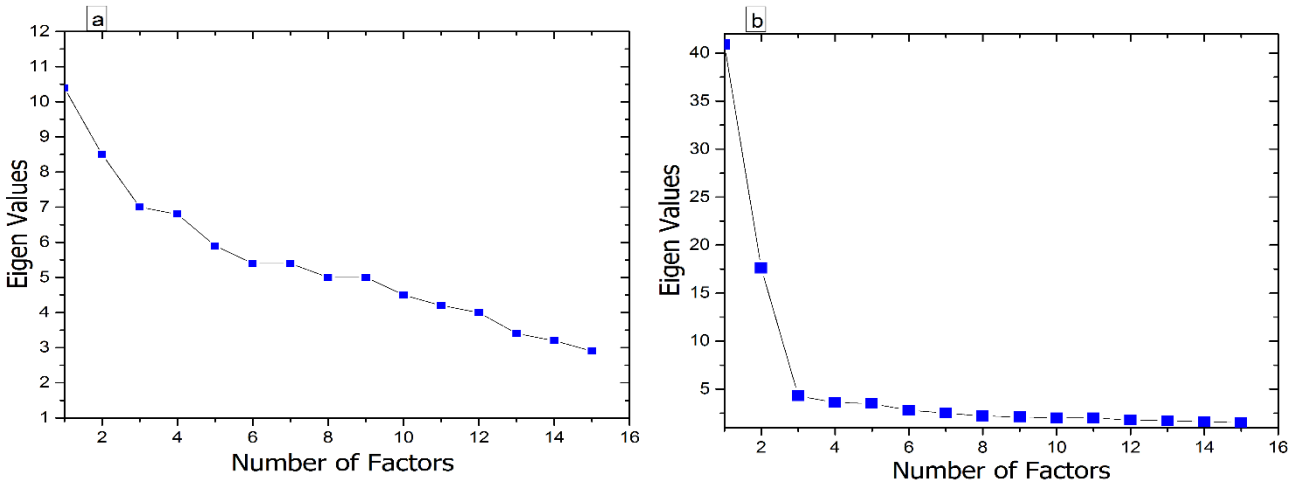

Figure 8: The Scree's test selection of dominant principal components for rotation during (a) MAM (b) OND rainfall seasons over Equatorial East Africa.

5.2.3 Varimax PCA Analysis

Figure 9a shows the first four varimax rotated PCA modes during MAM season. From the varimax rotation, the four modes accounted for over 43% (72%) of the total variance during the MAM (OND) seasons. The first PCA mode accounted for 16.5% of the spatial rainfall variance during MAM season. The PCA modes had negative loadings over most of the region, with few locations having small positive loadings over the southern sector of the region. The second rotated PCA mode accounted for 11.6%, while the third and fourth rotated modes accounted for 9.6% and 7.5% of the spatial rainfall variance respectively. All the four rotated PCA modes accounted for only up to 43% of the total MAM rainfall. Similar results have been observed from previous studies (Ogallo 1989; Indeje *et al.*, 2000; Schreck and Semazzi 2004; Omondi *et al.*, 2012).

During the OND season, Figure 9b, the first rotated PCA modes accounted for 51.7% of the spatial rainfall variance over the region, with large positive loadings over the whole region. The maximum loadings were concentrated over the Equatorial parts of the Great Rift Valley. The second PCA mode accounted for 10.8% of the spatial rainfall variance over the region.

The spatial patterns for the second PCA mode displayed a dipole pattern (positive and negative loadings over the northern and southern parts of the Equator). The sum total variance of the third and fourth PCA modes accounted for only 8.3% of spatial rainfall variance.

The first two modes were the most dominant accounting for about 62% of the total spatial rainfall variance. The first two PCA modes can adequately represent temporal and spatial rainfall variance of the rainfall during the OND season in the region. However, the first two PCA modes during MAM season cannot adequately be used to represent the rainfall variability since their sum total variance were only 28%.

The patterns of the first PCA mode during OND season may be representative of mean rainfall variability of the region. The configurations of the second PCA mode reflected the commonly observed ENSO region signals and migration of the meridional arm of the ITCZ (Ogallo *et al.*, 1988; Indeje 2000; Indeje *et al.,* 2006).

The PCA T-mode solutions were used to isolate the years with similar spatial patterns. The T-mode PCA loadings were classified into large positive and negative loadings. Figures 10 and 11 show the T-PCA modes during the MAM and OND seasons respectively. Only the first two PCA T-modes were used to delineate the wet and dry years. The time coefficients of the dominant PCA modes represent the dry and wet rainfall years in areas where the specific mode has high variances and coefficients for the S-mode solutions. Thus, the first two MAM and OND PCA modes are able to provide more representative characteristics of rainfall during their respective seasons.

According to PC1 during MAM (Figure 10), the average cold ENSO events were pronounced in the decades 1980–1990 resulting to depressed rainfall in the region. The PC2 during the MAM season represented a dipole spatial pattern over the region. The third mode could be related to the inter-annual trend mode and variability (Bowden and Semazzi 2007). The MAM T-mode results were integrated with care since their variance was very low. It was clear that the representation of

the MAM rainfall using the T-mode is very challenging since all dominant PCA modes accounted for only 43% of the variance.

Figure 11 represented the T-mode characteristics during the OND season. The PC1 and PC2 during OND season showed large positive and negative loading patterns spread throughout the time slice period. Table 5 summarizes the wet and dry years from PCA analyses mainly from the first and second PC modes. The time series from PC1 and 2 modes during OND season indicated some consistence with ENSO variability (Ogallo 1988; Indeje *et al.,* 2000). Previous studies based on the PCA analyses to characterize wet and dry years, associated these positive and negative loading patterns with the wet and dry rainfall signals (North *et al.,* 1982; Ogallo 1989; Okoola 1996; Camberlin and Philipon 2002; Omondi *et al.,* 2013).

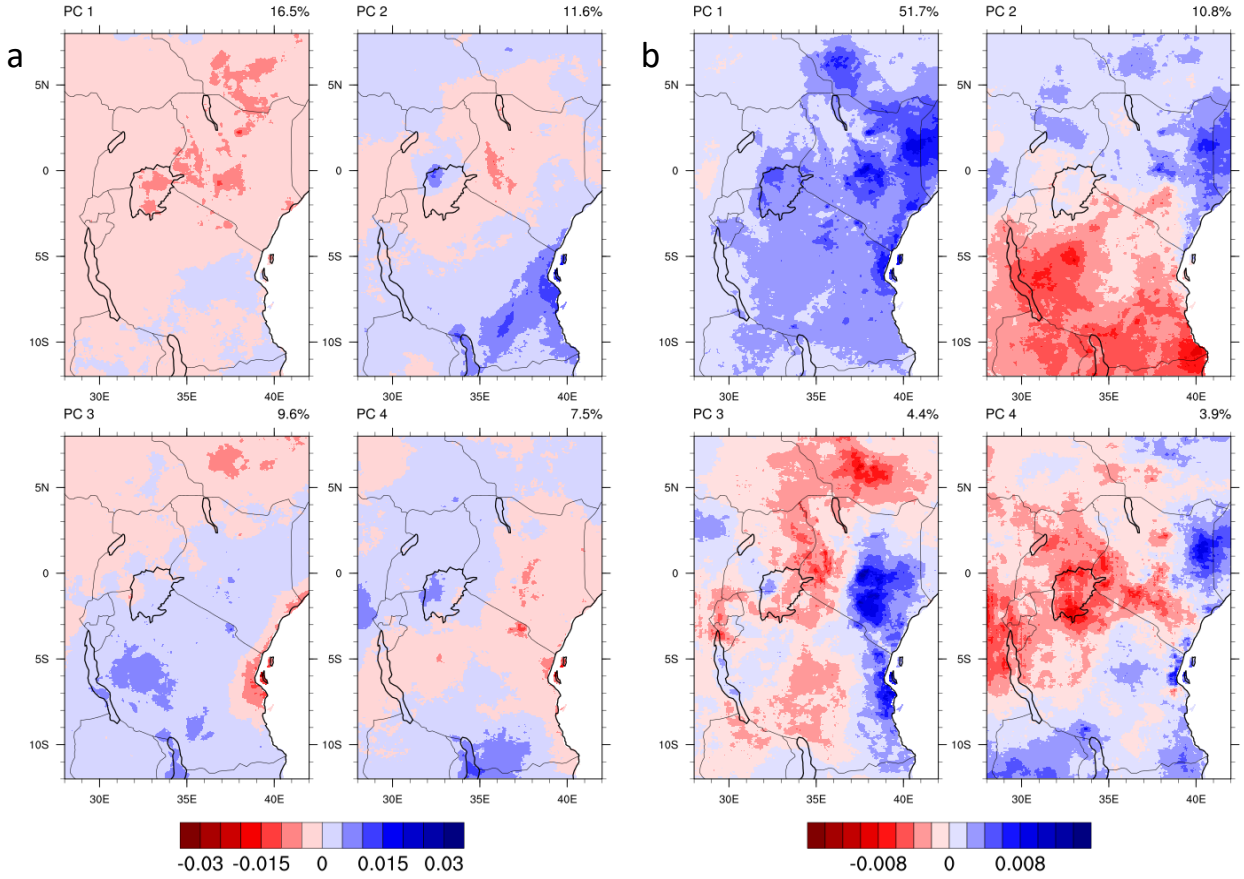

Figure 9: The S-mode for (a) MAM and (b) OND) loading patterns for the Varimax rotated EOFs over East Africa. The blue (red) shadings denote areas with wet (dry) rainfall anomalies over the period 1981-2016. The first four PC modes accounted for 45% and 70% of the total rainfall variance during MAM and OND seasons respectively.

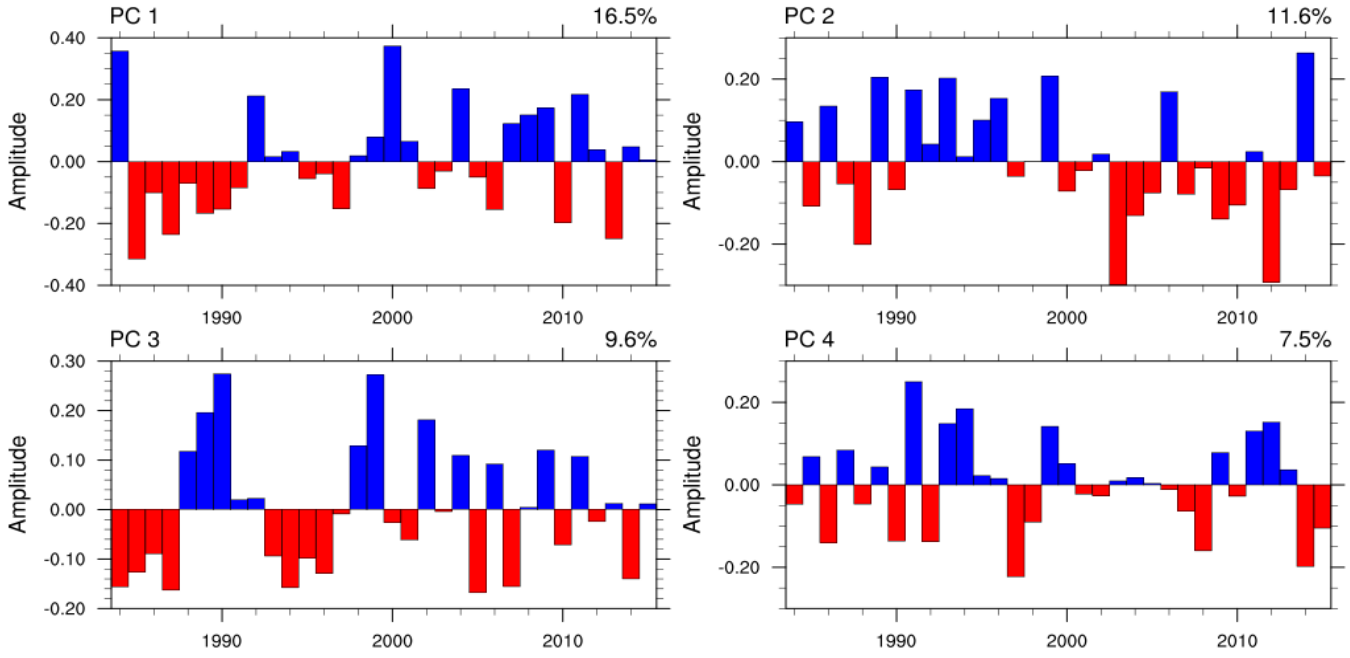

Figure 10: The T-mode Varimax rotated PCA modes during the MAM season loading patterns over East Africa region between 1981 to 2016. The blue (red) bars represent positive (negative) loading patterns.

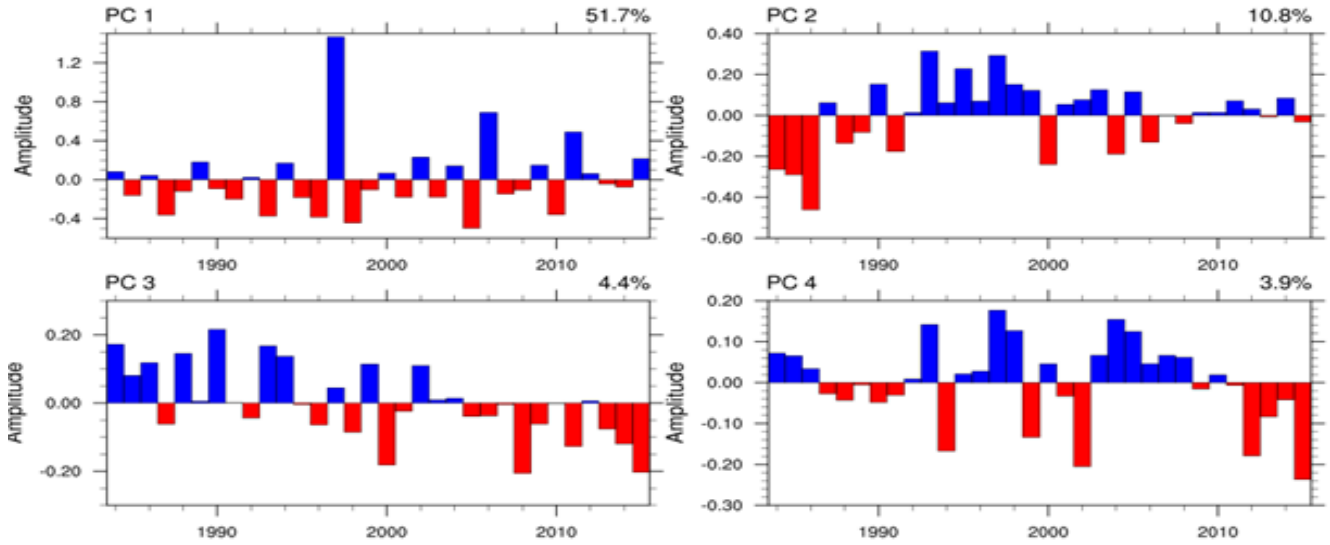

Figure 11: The T-mode Varimax rotated PCA for the OND season loading patterns over East Africa region between 1981 to 2016. The blue (red) bars represent positive (negative) loading patterns.

Table 5: The Wet and Dry Years from PCA analyses between 1981to 2016 during MAM and OND seasons over East Africa

MAM season		
	Positive loadings	**Negative loadings**
PC1	1984, 1992, 2000, 2004, 2007, 2008, 2010, 2011, 2014	1985, 1986, 1987, 1988, 1989, 1990, 1992
PC2	1986, 1989, 1991, 1992, 1993, 1995, 1996, 1998, 1999, 2002, 2006, 2011, 2014	1985, 1987, 1988, 1990, 1997, 2003, 2004, 2005, 2007, 2009, 2010, 2012, 2013
OND season		
	Positive loadings	**Negative loadings**
PC1	1997, 2002, 2006, 2011, 2015	1984, 1985, 1986, 1998, 1999, 2005, 2010
PC2	1985, 1986, 1988, 1989, 1991, 2000, 2004, 2006, 2008, 2012	1987, 1990, 1993, 1994, 1995, 1996, 1997, 1998, 1999, 2001, 2002, 2003, 2005, 2010, 2011, 2014

The results from SRI and PCA analyses isolated the widespread wettest (driest) years of 1989,1997, 1998, 2006, 2012, 2015 (1984, 1988, 2000, 2007, 2008, 2010). All these years except 2012 and 2007 had previously been isolated as dry and wet by Okoola (1999), Owiti *et al.* (2008) and Philipon *et al.* (2015). These years were therefore subjected to composite analyses.

5.2.4 Composite Analyses

Figures 12 and 13 show rainfall anomalies of individual years and their corresponding wet and dry composites during MAM and OND seasons respectively. During the MAM season, the wet and dry rainfall anomalies were not as strong as was observed during OND season (Figures 12 and 13). This is due to both local and large-scale mixed rainfall drivers that are not very easy to isolate. There was a strong signal of wet and dry rainfall anomalies during OND season in each case (Figures 12 and 13), a characteristic of the large-scale systems that dominate the season which was easily isolated by the first PC modes. These common characteristics of wet and dry conditions during OND season had been associated with El Niño (La Niña) years over Equatorial East Africa (Ogallo 1988, 1989; Owiti *et al.,* 2008; Ogwang *et al.,* 2015a). Therefore, all the analyses were based on the wet and dry composites during MAM and OND rainfall seasons.

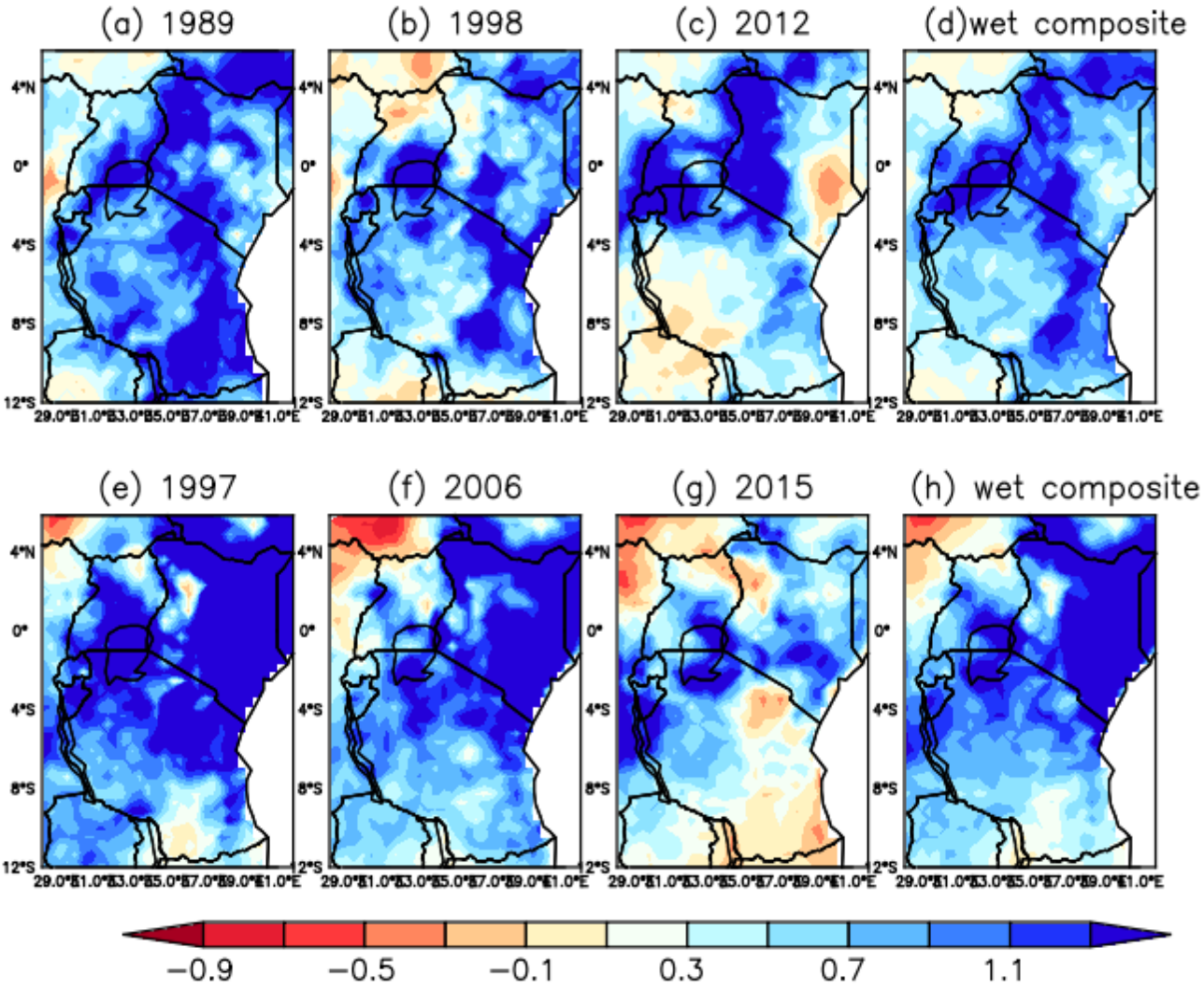

Figure 12: The rainfall anomalies (mm/day) for the wet years during MAM (top: 1989, 1998 and 2012) and OND (bottom: 1997, 2006 and 2015) rainfall seasons. The corresponding composites are placed to the right of the individual years. The blue and red shadings denote areas with positive and negative rainfall anomalies respectively. The anomalies are calculated from a base period of 1981-2016.

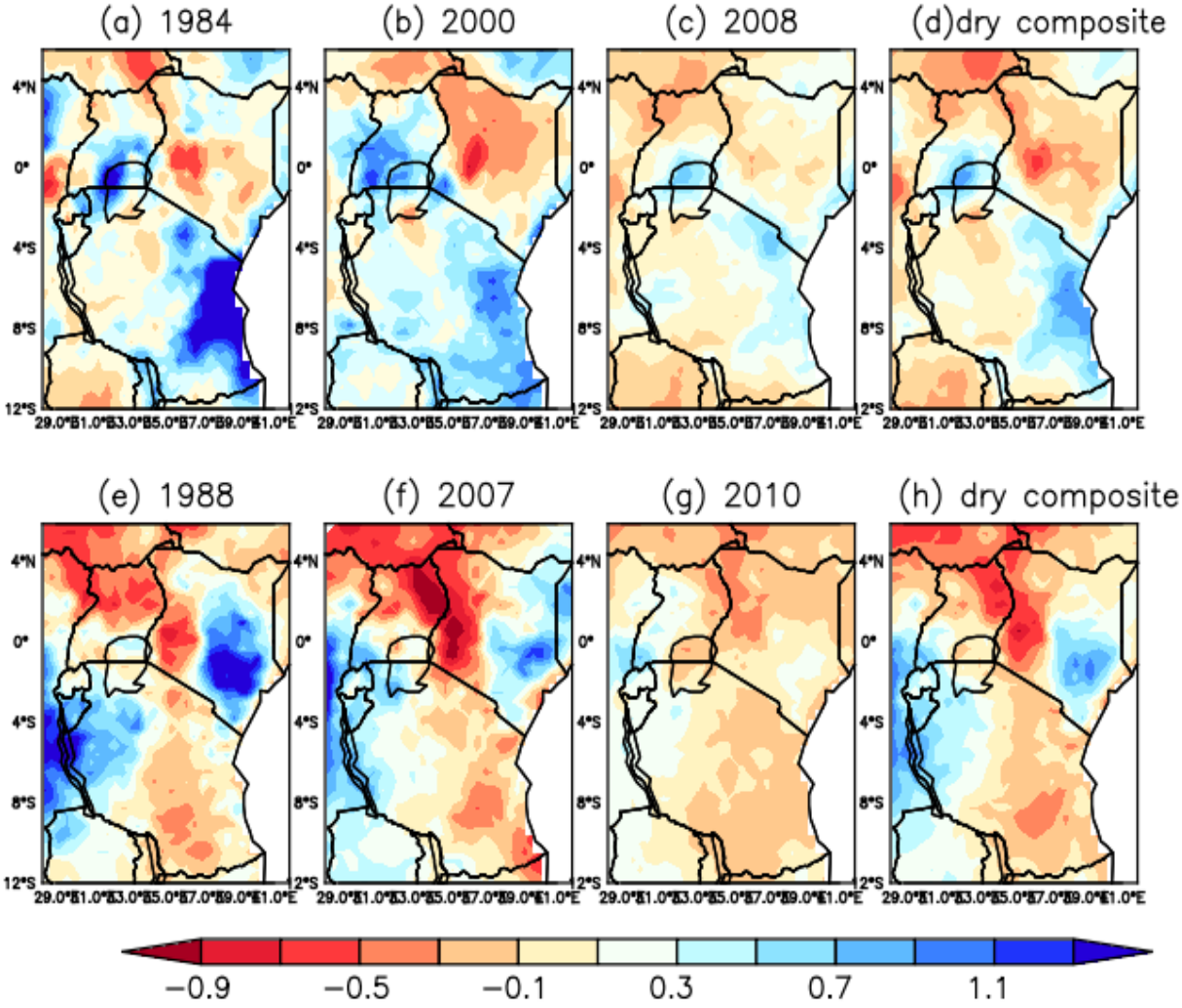

Figure 13: The rainfall anomalies (mm/day) for the dry years during MAM (top: 1984, 2000 and 2008) and OND (bottom: 1988, 2007 and 2010) rainfall seasons. The corresponding composites are placed to the right of the individual years. The blue and red shadings denote areas with positive and negative rainfall anomalies respectively. The anomalies are calculated from a base period of 1981 to 2016.

In summary, this study found that the first few eigenvectors (modes) are useful in explaining the rainfall variability over East Africa. The coherence between the rainfall and its variability in the dataset was higher during OND season than MAM season. Studies by North *et al.* (1982), and Richman *et al*. (1986) found that cutting the eigenvectors to about 3 to 4 factors usually generate robust results useful for explaining the variability. The time coefficients of the dominant PCA modes give a better representative of the dry and wet rainfall variability.

This study for the first time demonstrated that the rainfall drivers for the wet and dry years can actually be isolated through the rotated EOFs. The interpretation of the PCA modes to delineate

wet and dry signals however needs to be done with care. This is because the interaction of local and large-scale makes the variability very low during the MAM season.

5.3 The Determination of the skill of four cumulus parameterization schemes in simulating intrinsic rainfall characteristics during the wettest and driest years

The first objective of the study sought to assess the reproducibility of the cumulus parameterization schemes (CPSs) on mean rainfall patterns, number of rainy days (NRD), Intensity of rainy days (IRD) and frequency of rainfall intensity (FRI) (Table 2)**.**

5.3.1 The Spatial and Temporal Daily Rainfall Distribution and the associated model Biases

This section presented results from mean rainfall both spatially and temporally, model biases and associated error metrics.

5.3.1.1 Spatial Mean Rainfall Distribution

Figures 14 and 15 show daily rainfall patterns for wettest and driest years during the MAM and OND seasons.

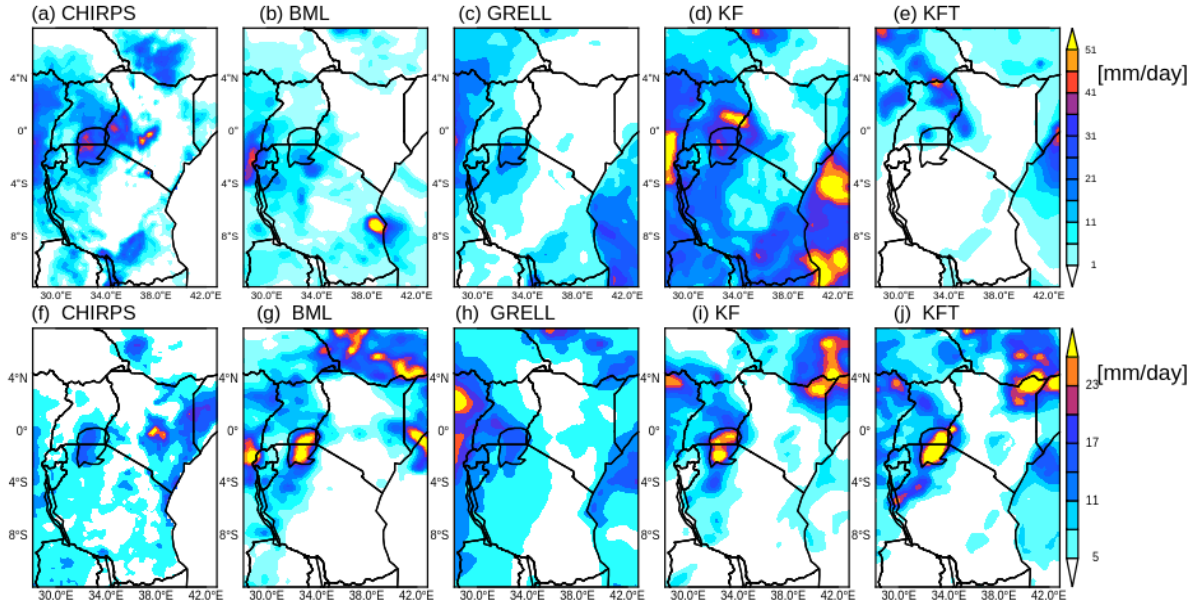

Figure 14: The mean daily rainfall (mm/day) for CHIRPS, BML, GRELL, KF and KFT schemes for the wet composites for the MAM (top) and the OND (bottom) seasons

During MAM season (Figure 14), rainfall was observed to be concentrated on the western Equatorial belt of the region according to CHIRPS (Figure 14a). Rainfall above 25 $mmday^{-1}$ was observed over the western parts of Kenya, much of the central parts of Uganda, the shores of Lake Victoria and the western parts of southern Tanzania. Much of the eastern parts of Kenya and central parts of Tanzania recorded depressed rainfall of less than 5mm/day. The maximum rainfall of above 35 $mmday^{-1}$ was received over the slopes of Mount Kenya. The maximum rainfall was over the equatorial and northern parts of the region.

The KF and KFT schemes simulations were closer to the observations over the western parts of the EA region (Figure 14d, e). The KF schemes fairly simulated the observed rainfall over the northern and western parts of Tanzania. Comparatively, the simulations by KFT scheme were much better (Figure 14e). The BML and GRELL CPS presented low rainfall amount over much of Kenya and correctly simulated rainfall over the western equatorial including northern parts of Tanzania, Burundi and Rwanda (Figure 14b, c). The KF and KFT schemes on the other hand correctly reproduced rainfall location and intensity in some instances.

During the OND season for wet years (Figure 14f-j), rainfall was confined to the western parts of the equator and the central and eastern parts of Kenya (Figure 14f). The BML and GRELL CPS correctly simulated rainfall over the western parts of the Equator but overestimated their intensities (Figure 14f, g, h), however the CPS simulated a drier condition over Kenya and Tanzania (Figure 14g, h).

The schemes can be viewed as either simulating excess rainfall (i.e KF and KFT schemes) resulting to wetter rainfall biases or simulate fewer rainfall resulting to drier rainfall biases (i.e. GRELL and BML schemes). For example, rainfall amount of about 25mm/day was observed to the northern parts, and southern parts of Tanzania (Figure 14a). In the BML and GRELL CPSs (Figure 14b, c), rainfall over the same locations were depressed or misplaced. On the other hand, KF and KFT schemes correctly simulated rainfall over the western parts of the equator, but overestimated their intensity. The Figure 15 shows rainfall simulations for the dry composites during MAM and OND rainfall seasons.

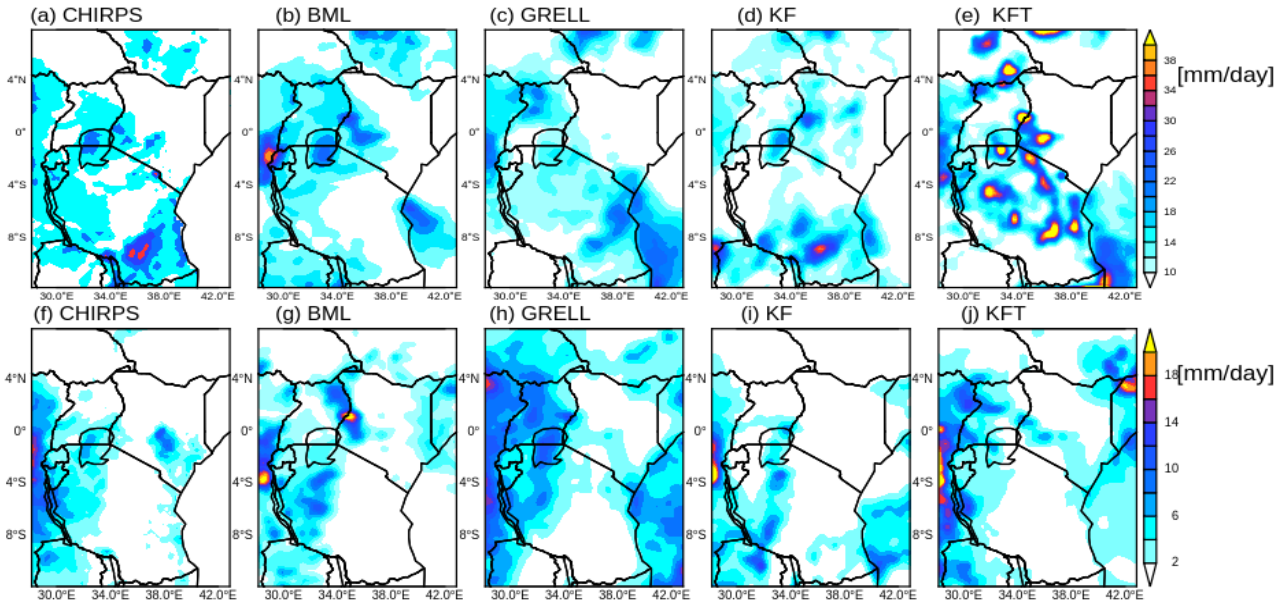

Figure 15: The mean daily Rainfall (mm/day) for CHIRPS, BML, GRELL, KF and KFT schemes during dry years for the MAM (top) and OND (bottom) seasons.

The rainfall of the range 10 to 20 mm/day was observed over the western parts of the Equator and the lower southern parts of Tanzania during the MAM season (Figure 15a). The central Tanzania region and the North Eastern and Eastern parts of Kenya witnessed drier rainfall condition (Figure 15a). For the OND season, rainfall was further depressed with average rainfall of below 10mm/day simulated over the north western parts of Tanzania, the Equator, coastal and central parts of Kenya (Figure 15f).

The CPSs reasonably reproduced much better rainfall during the OND than the MAM seasons. Specifically, BML and GRELL CPS correctly simulated the rainfall location but under-estimated the rainfall amount (Figure 15b, c). The KF and KFT CPSs, on the other hand, correctly reproduced the rainfall location but over-estimated the rainfall amount (Figure 15d, e). During the OND season, the GRELL and BML schemes simulated rainfall correctly over western parts of the region but failed to reproduce rainfall over mountainous area of Kenya (Figure 15f, g, h). The KF scheme simulated convincing results albeit weakly simulating rainfall over the Kenyan highlands and mountainous area (Figure 15i, j). Better rainfall produced in KFT scheme over Tanzania and Kenya (Figure 15j) is an indication of the additive effects of moisture-based trigger function in KF scheme.

Figure 16 demonstrate the clear differences between KF and GRELL schemes through the wet minus dry analyses. The results revealed that the GRELL scheme is a drier scheme and KF is a wetter scheme during MAM season. The BML reproduced both dry and wet rainfall conditions alternately. The OND season was quite closer to the observations. All the CPSs reproduced the East-west rainfall gradient.

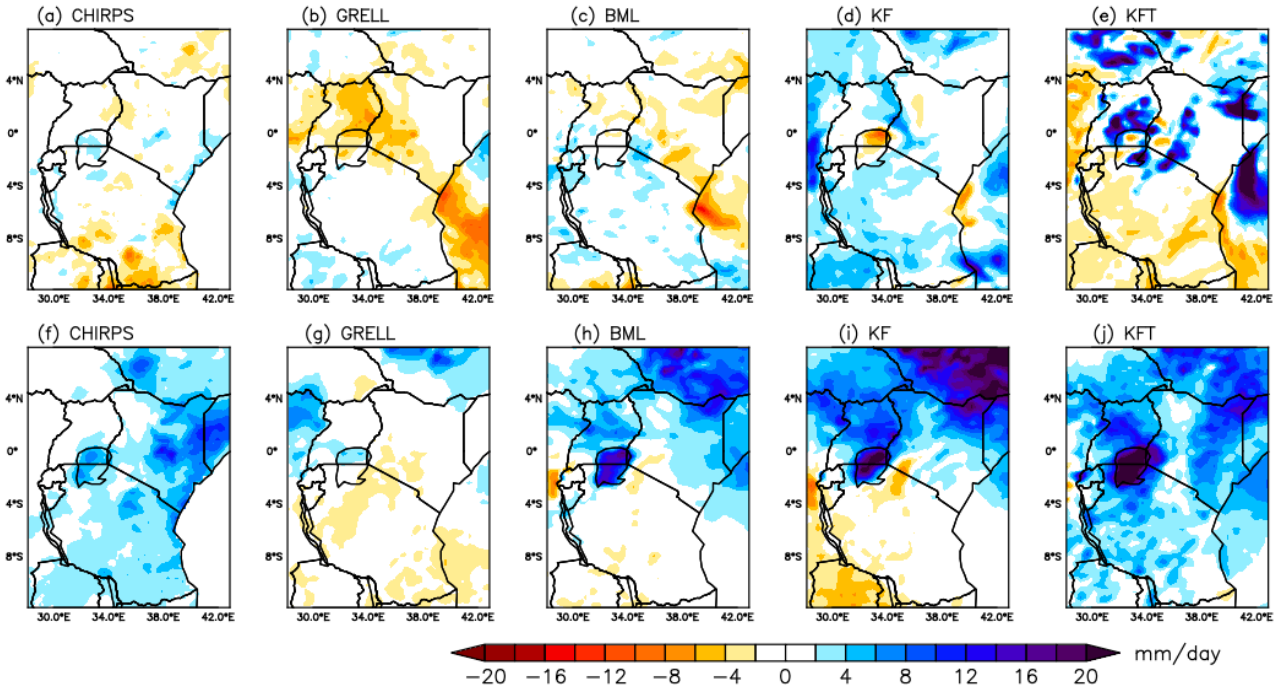

Figure 16: The observed and simulated wet minus dry rainfall (mm/day) for CHIRPS, GRELL, BML, KF and KFT CPS. The top (MAM) and bottom (OND) seasons. The blue (orange) shadings denote areas with enhanced wetness (dryness).

The rainfall simulations were more skillful during the drier years than wetter years. The OND rainfall season is easily simulated by the schemes than the MAM season for both cases (Figures 14 and 15). The skillful rainfall simulation during the OND season is due to the strong spatial coherence that has been partially associated with the ENSO signals and stronger during the OND season. This is not the case for the MAM season, where rainfall is majorly driven by the complex interaction of both local and large-scale systems (Ogallo 1989).

The location of maximum rainfall to the equator and the northern parts and minimum rainfall to the southern and eastern parts of EA region during the MAM and OND seasons was consistent with the rainfall climatology. The climatology mainly depends on the location and migratory arm

of the ITCZ (Ogallo 1989; Nicholson 1996; Okoola 1998, 1999). The reduction in rainfall amount in the KFT scheme was due to the introduction of cloud feedback mechanism to the radiation in the scheme. The feedback mechanism reduces the passivity of cloud to the shortwave radiation so that the surface evaporation due to heating is minimized (Alarparty *et al.,* 2009).

The observed rainfall differences in the GRELL and KF schemes could be attributed to the variations in their closure assumptions schemes. The KF is a low-level control cumulus scheme based on a mass flux approach. It considers the Langragian parcel theory to determine the level at which convection is activated. The GRELL scheme treats cloud as a one-dimensional system with downdraft and updraft branches at the top and bottom of the cloud. Both dynamic and trigger moisture controls are assumed to be a combination of closure assumption based on CAPE, low-level vertical velocity or moisture convergence.

The BML scheme on the other hand, is a convection inhibitor. It is a deep-layer control convective scheme, and assumes that the energy to raise the air parcel depends on the size of the environment. In the absence of buoyant air at any level, convection will not be activated. The scheme design favors the activation of convection within the vicinity of significant moisture at low and middle level between 300-500hPa (Wang and Seaman 1997).

The EA region is characterized by the moisture convergence, emanating from the Indian Ocean and the Congo Basin at lower levels. Both GRELL and KF schemes are associated with sinking and rising of air which makes them suitable for process studies over the region (Pohl *et al.,* 2011). From the analyses, it may be concluded that, GRELL, KFT and KF schemes are suitable in simulating mean rainfall patterns over the East Africa region. The GRELL scheme, however, was better for drier years only.

5.3.1.2 Temporal Rainfall Distribution

The variability and the spread in the model schemes were assessed based on the box and whisker plots over NEA, SEA, CEA and LVB sub-domains. Figures 17 and 18 show the box-plots for the simulated rainfall distribution during wettest composites for MAM and OND seasons respectively.

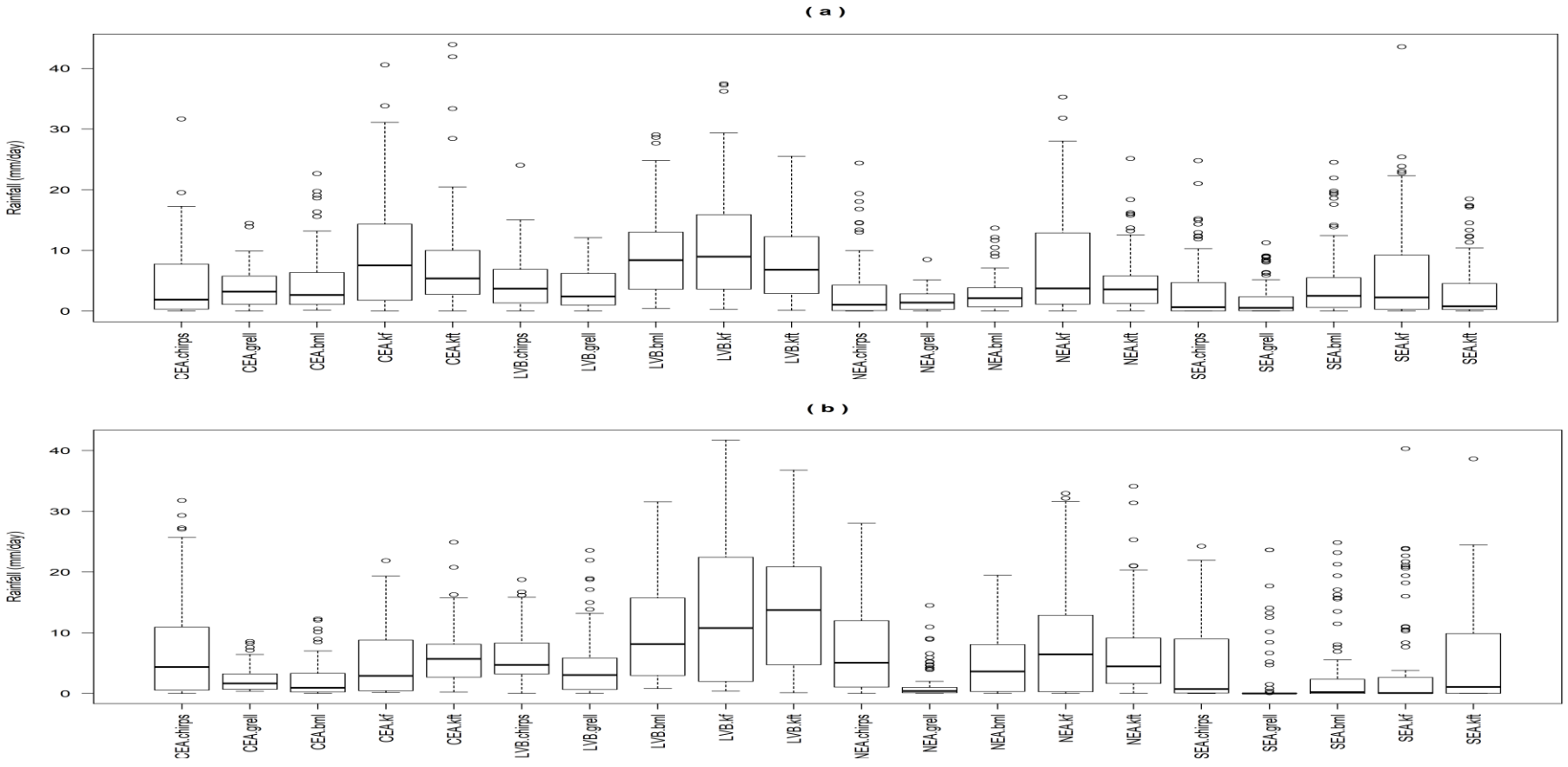

Figure 17: The boxplot for daily rainfall distribution from CHIRPS, GRELL, BML, KF and KFT CPS during wet composites for (a) MAM and (b) OND seasons over NEA, SEA, LVB and CEA sub-domains. The boxes have lines at the lower, median, and upper quartile values. The whiskers are lines extending from each end of the box to 1.5 inter-quartile ranges.

Over the CEA region for MAM season (Figure 17a), only BML scheme was closest to the observation in terms of mean values. The rest of the CPSs either underestimated or overestimated the mean values. Similar observations were replicated over LVB sub-domain. The BML and GRELL CPSs were closest to the observation over NEA region. Better distribution was found over SEA region in GRELL and KFT schemes. During the OND season (Figure 17b), the KF and KFT schemes mean values and rainfall distribution pattern were closer to the observation, the GRELL and BML CPSs underestimated the mean values over CEA region. Over LVB, only the GRELL scheme mean values were closest to the observation. Over NEA only KFT scheme was most skillful with most of the CPSs being skillful over SEA region except the KFT scheme. Fewer extreme rainfall values above 30mm/day were recorded in most of the CPSs.

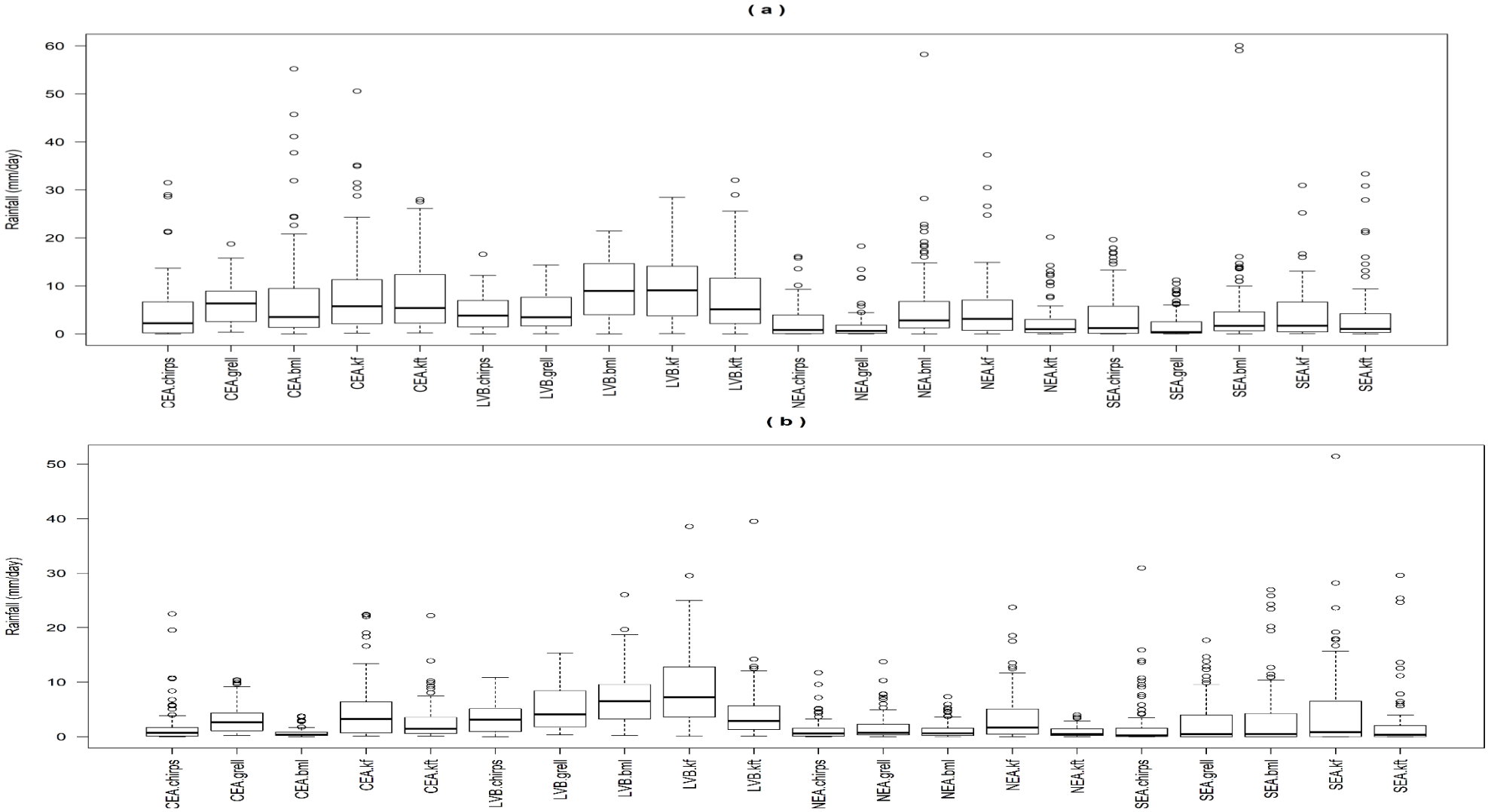

Figure 18: The box-plots for daily rainfall distribution from CHIRPS, GRELL, BML, KF and KFT CPS during dry composites for (a) MAM and (b) OND seasons over NEA, SEA, LVB and CEA sub-domains. The boxes have lines at the lower, median, and upper quartile values. The whiskers are lines extending from each end of the box to 1.5 inter-quartile ranges.

Figure 18 shows the simulated rainfall distribution and the observation during drier years over CEA, LVB, NEA and SEA regions. Most of the CPSs mean values were in close agreement with the observations over most of the regions. The temporal mean rainfall distribution showed that the simulations of KFT and BML tended to be closer to the observations in terms of median and mean values during both MAM and OND seasons as shown in Figures 18a and b. The GRELL scheme mean values were in most cases closer to the observations than KF and KFT CPSs.

The reproducibility of the mean rainfall pattern by the CPSs was evident in the rainfall gradient as a result of the large-scale systems like the ITCZ. Although, the temporal variability was not quite well reproduced in all the CPS, the KF and KFT simulations were consistently closer to the observed values. The OND season was better reproduced than the MAM season. In terms of temporal rainfall distribution, the KF was the best, while GRELL CPS was the best during dry years only.

5.3.2 Model Bias Analysis

In order to understand the variation between the model estimate and observation, the differences between model schemes and rainfall were analyzed and their associated RMSE and SC calculated per grid point over the EA region.

5.3.2.1 Spatial Model Biases

Figures 19-20 show seasonal rainfall amounts and associated biases against CHIRPS over EA domain during MAM and OND for wet and dry years respectively. The model biases strongly varied from one scheme to another. A recurrent spatial structure was however observed over central parts of Kenyan Coastal region during MAM and the western parts of the equatorial region during the OND season. The BML and GRELL CPSs simulated a drier bias over most parts of Kenya and weak wetter bias over the southern and western parts of the EA region. The KF scheme reproduced a stronger wetter bias over the western parts of EA and a drier bias to the south. The reverse situation occurred in the KFT scheme where a wetter bias dominated southern and western parts of EA during the MAM season (Figures 19a, b, c, d).

The spatial rainfall structures in the BML, KF and KFT schemes were common across each during the OND season. For example, all the schemes except GRELL simulated strong north-south rainfall gradient, where wetter biases confined to the North and dry bias to the south of the EA region (Figure 19e, g, h). A similar rainfall structure was observed during the MAM season where

the northern parts of the EA recorded drier bias while the southern parts of the region recorded a wetter bias (Figure 19a, b, d). This spatial structure was enhanced in the KF and BML schemes (Figure 19e and g).

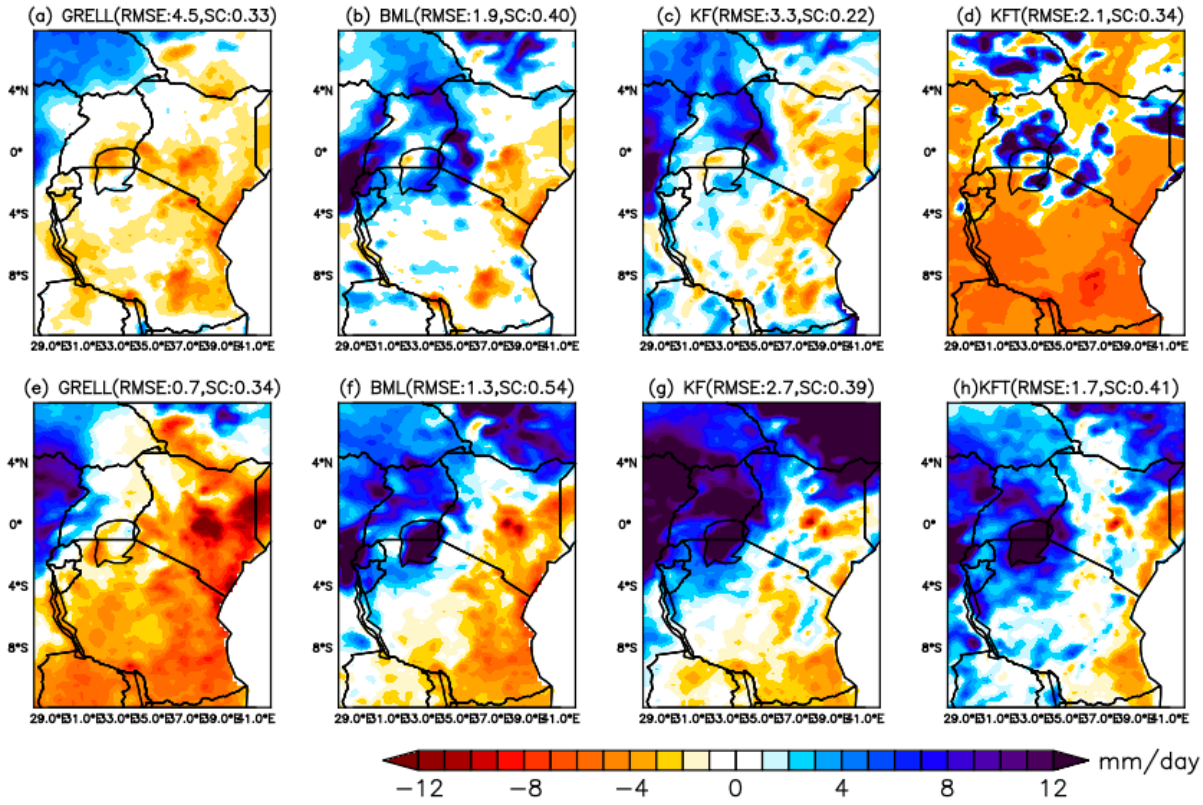

Figure 19: The differences between simulated and observed rainfall (mm/day) for the composite of wet years. The top panel is for the MAM season and the bottom panel is for the OND season. The blue (orange) shadings denote positive (positive) rainfall differences over the region.

In all the schemes, a dry bias was found around the central parts of Kenya especially the areas of Mount Kenya during MAM and OND seasons. The western parts of EA region presented a consistent wetter bias irrespective of the season and the CPS used. Although all the CPSs presented different rainfall spatial biases, the KF scheme reproduced a dry or wet bias comparatively during MAM and OND seasons.

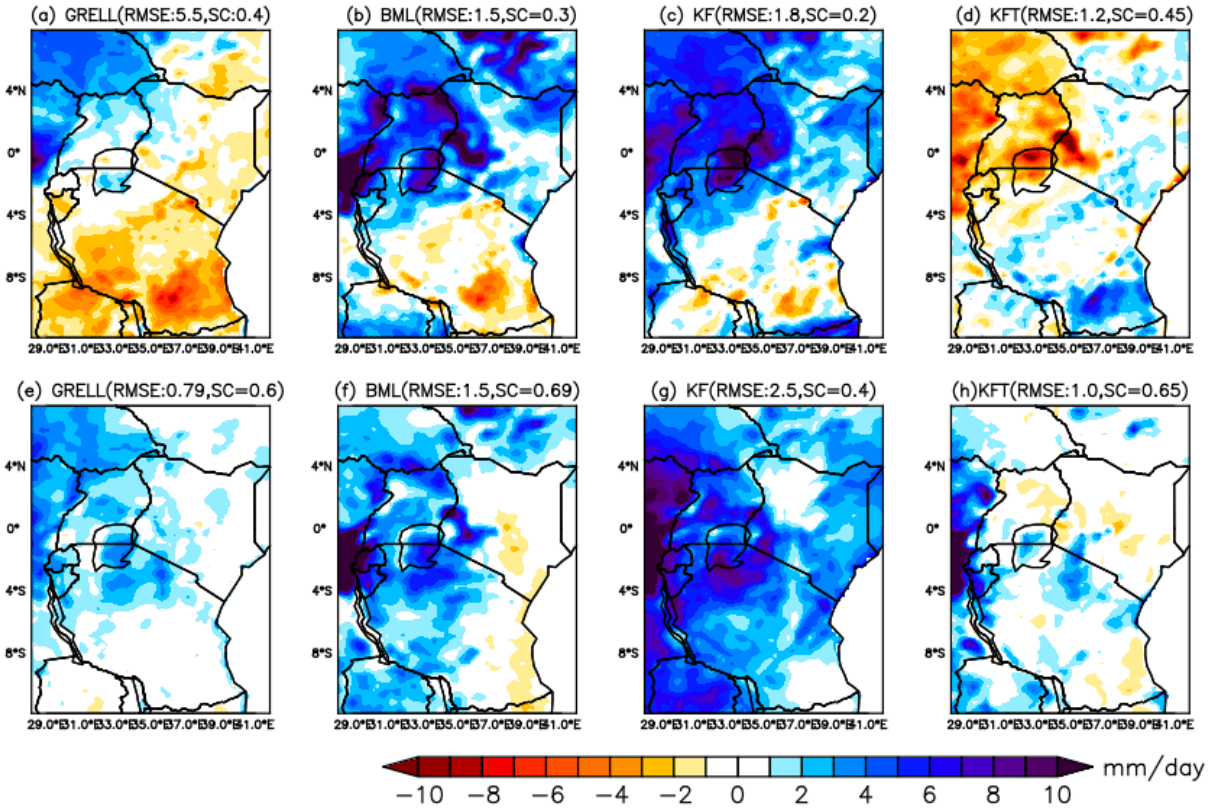

Figure 20: The differences between simulated and observed mean rainfall (mm/day) for the composite of dry years. The top panel is the MAM season and bottom panel is the OND season. The blue (orange) shadings denote positive (negative) differences over the region.

A similar observation was made for the case of the drier years as was depicted in Figure 20. The biases varied from one scheme to another. The KFT and KF CPSs had wetter biases around Tanzania and central parts of north eastern Kenya in KFT schemes during MAM season (Figure 20d). The GRELL and BML simulated a strong dry bias to the East and wet bias to the western parts of EA region (Figures 20a and b). There were smaller biases around the central Kenya and south eastern parts of Tanzania in GRELL and KF schemes (Figures 20f and g). A strong-weak dry bias was evident in the KFT and GRELL schemes over mountainous areas of Kenya (Figures 20f, h).

These dry biases over mountainous areas could be as a result of poor simulation of the orographic effect in the schemes. Also, the localized rainfall driving systems over these areas are poorly simulated. The study hypothesized that the resolution used in the simulation could in part contribute to the observed biases. The rainfall biases were clearly depended on the scheme used. There were fewer biases in the KFT and the GRELL CPSs during the OND season than the MAM

season (Figures 19 and 20). The KF scheme was associated with wet biases, with a greatest reduction of the same in the KFT CPS, attributed to the moisture-based trigger function introduced in the scheme.

The CPSs simulated successfully the north-south rainfall gradient which could be as a result of the meridionally oriented the ITCZ arms. During the MAM and OND seasons, the ITCZ migrates from the south to the north, and vice versa. As it moves, both its zonal and meridional alignment produces rainfall within its vicinity (McHugh, 2006). It could be deduced that the schemes do not properly capture the rainfall over these locations hence the observed biases especially during MAM season.

Studies by Separovic *et al.* (2008) and Sanchez-Gomez *et al.* (2009) pointed out that RCM models traditionally produce the largest uncertainties at the central parts of their domain or near the outflow boundary. Such rainfall patterns are believed to be related to the uncertainties in the latitudinal variation of the ITCZ, a basic morphological feature of rain-bearing system over the EA region. Similar rainfall biases have been found by (Cretat *et al.*, 2012; Marteua *et al.*, 2015).

The reduced rainfall biases in the model over the western Equatorial parts and central Kenya have also been reported by Njeri (2012). The study documented that a well-defined structure of the ITCZ produces less noise. These large rainfall biases imputed the observed wetter rainfall conditions generated by the KF and KFT schemes. The drier biases further explained the observed drier rainfall conditions associated with the GRELL scheme (Figures 14 and 15).

The large and small values of RMSE in KF and KFT schemes signified the relative differences in the simulated rainfall between the two CPSs. The larger (smaller) RMSE values represented how far (close) the model simulations become closer to the observation. Based on this, the GRELL and BML schemes succeeded in getting smaller RMSE values during the drier years than wetter years. The large biases in the KF scheme during the wettest and driest years were greatly reduced in the KFT schemes giving RMSE values closer to the observation. Tables 6 and 7 shows a summary of RMSE values computed over SEA, NEA, CEA and LVB sub-domains.

Table 6: The RMSE (mm/day) computed between the observation and GRELL, BML, KF and KFT schemes during MAM and OND seasons for the composite of wet years. The average was done over the NEA, SEA, CEA and LVB sub-domains.

Scheme/Region	NEA (MAM)	SEA (MAM)	CEA(MAM)	LVB(MAM)
GRELL	0.9	0.9	0.3	0.6
BML	0.2	0.6	0.4	2.8
KFT	4.3	1.8	3.6	4.6
KF	1.2	1.5	3.9	3.5
	NEA (OND)	**SEA (OND)**	**CEA(OND)**	**LVB(OND)**
GRELL	3.0	2.1	2.4	0.7
BML	1.3	1.3	2.5	2.6
KFT	0.2	0.5	0.4	4.5
KF	0.9	0.8	1.5	4.2

The GRELL and BML CPSs simulated relatively low RMSE across all the sub-domains. The KFT CPSs had the highest RMSE followed by KF scheme during MAM season. The errors were least over NEA and largest over LVB sub-domains. During the OND season, KFT and KF cumulus schemes reproduced the least errors. Comparatively, the RMSE were smaller during the OND season than the MAM season as shown in Table 6.

The analyses for the composite of dry years showed BML scheme simulated the smallest RMSE values comparatively as shown in Table 7 during MAM and OND seasons. The KFT scheme similarly simulated fairly low RMSE values. Comparatively, the RMSE values during OND season were lower. Over the NEA sub-domain, the KFT, BML and KF schemes simulated low RMSE values, over SEA and CEA domains, GRELL and BML schemes were most skillful during MAM season. For OND season, KFT and GRELL schemes were most skillful over NEA, CEA and SEA regions. It was evident from these analyses that the four CPSs skill drastically vary based on the sub-domain and the season. The CPSs consistently simulated larger RMSE values over LVB and CEA sub-domains than over SEA and NEA sub-domains. This perhaps signifies a weakness in the schemes to reproduce the cloud processes and the associated local scale dynamics.

Table 7: The RMSE (mm/day) computed between the observation and GRELL, BML, KF and KFT schemes during MAM and OND seasons for the composite of dry years. The average was done over the NEA, SEA, CEA and LVB sub-domains.

Scheme/Region	NEA (MAM)	SEA (MAM)	CEA(MAM)	LVB(MAM)
GRELL	2.3	1.3	0.9	1.1
BML	1.2	0.5	0.8	2.4
KFT	0.3	2.3	1.6	1.6
KF	1.5	1.7	2.4	3.1
	NEA (OND)	**SEA (OND)**	**CEA(OND)**	**LVB(OND)**
GRELL	1.2	1.4	1.7	1.0
BML	1.8	1.3	0.8	2.1
KFT	0.9	2.2	2.8	4.6
KF	1.3	1.4	1.2	3.2

The relatively higher skill (low RMSE) over NEA and SEA domains during the OND season had been reported by Ogallo (1989) to be due to the well prescribed and aligned Indo-pacific SST influence. Owing to the known nature of the region, where the land areas and water bodies constitute key physical features, the KF and GRELL CPSs become better options for studying rainfall characteristics over the East Africa region.

5.3.2.2 Temporal Model Biases

The study also assessed how the model biases evolved with time over the four sub-domains. Figures 21-22 showed rainfall biases at daily timescale during MAM and OND seasons for the wet composites. For MAM season, the variability with respect to amplitude in the rainfall biases was low and reduced during over the NEA and SEA regions (Figure 21a and b). The errors were larger over LVB and CEA regions. The KF and KFT schemes were consistent in simulating the negative and positive peaks low rainfall peaks. The GRELL and BML simulations were inadequate. During the OND season, the errors were relatively smaller within the first 20days of the season and became very “noisy” as the season progressed over all the sub-domains. Comparatively SEA and CEA regions had smallest error values within the first 15days (Figure 22b and d). The GRELL and KF schemes consistently simulated low rainfall biases and less variability across all the domains.

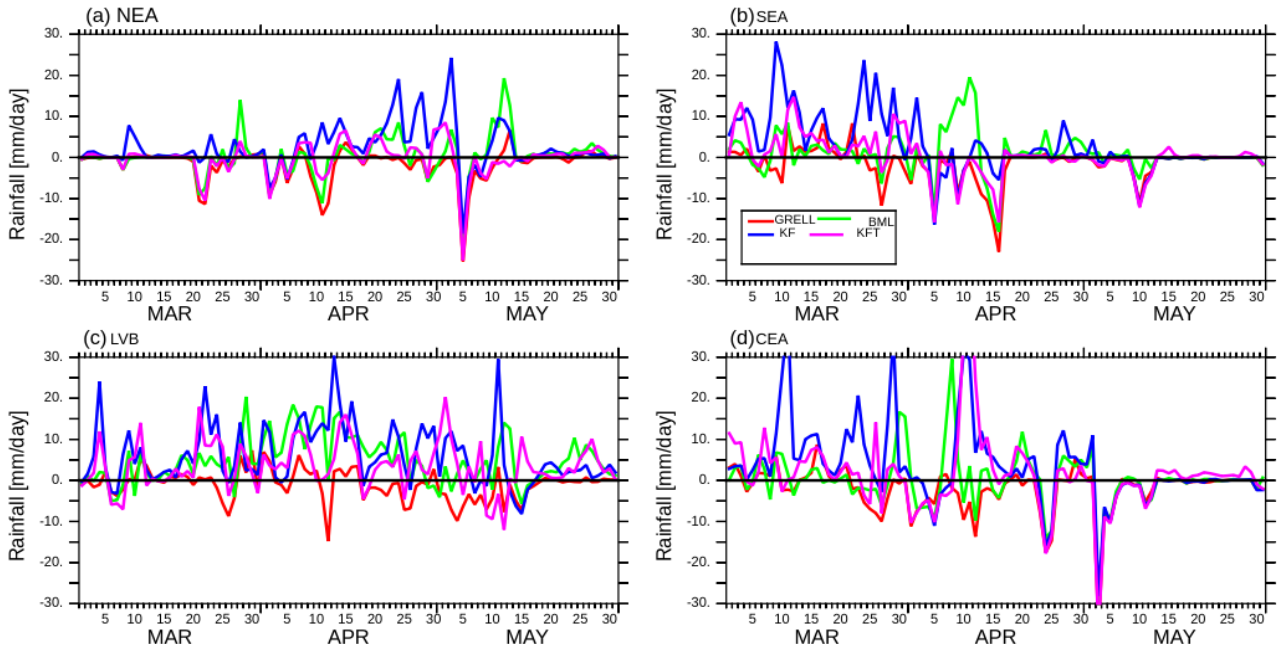

Figure 21: Spatially averaged rainfall biases (mm/day) for the BML, GRELL, KF and KFT schemes over the NEA, SEA, CEA and LVB domains for the composite of wet years during MAM season. The model biases were calculated with reference to CHIRPS

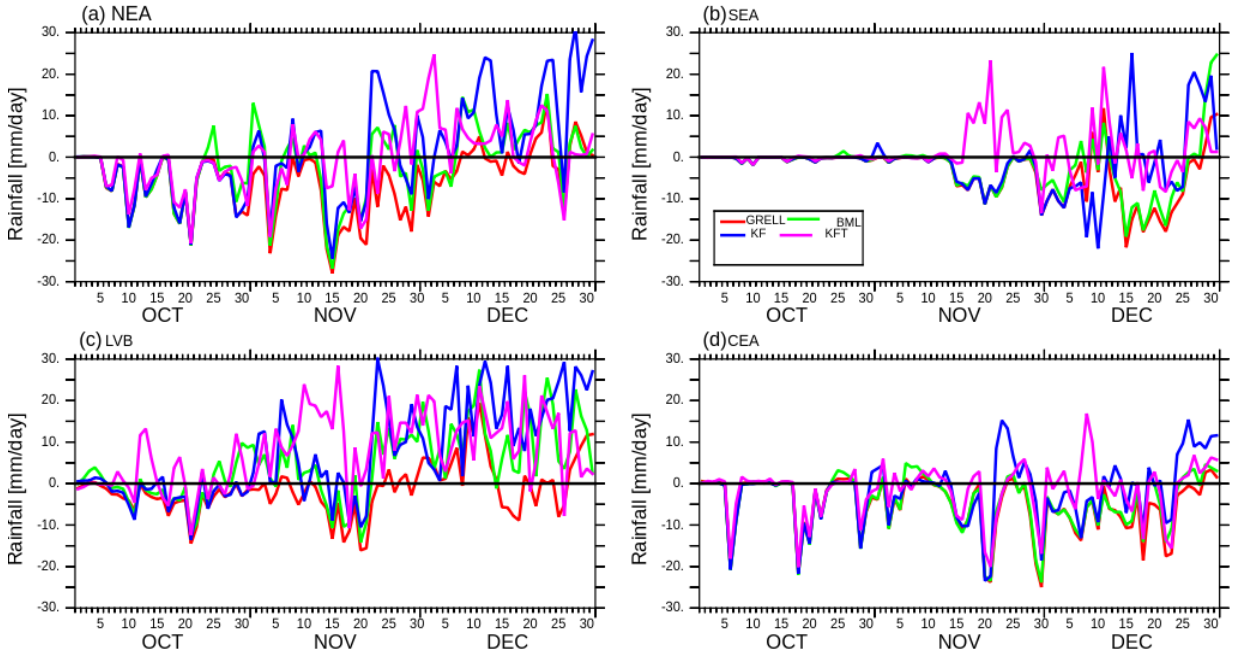

Figure 22: Spatially averaged rainfall biases (mm/day) for the BML, GRELL, KF and KFT schemes over the NEA, SEA, CEA and LVB domains for composite of wet years during OND season. The model biases were calculated with reference to CHIRPS

Similar analyses were applied for dry composites as shown in Figures 23 and 24 during MAM and OND seasons respectively. The errors were relatively smaller for BML and KFT schemes during MAM season but progressively became larger as the season progressed. The last 5 days of the season also registered a reduction in the error amplitude (Figure 23). The OND season on the other hand simulated even further low amplitude (Figure 24). This was expected since the composited dry years signal is stronger during the OND season than MAM season. All the CPSs simulated low biases except KF CPS over LVB and CEA domains (Figure 24c and d).

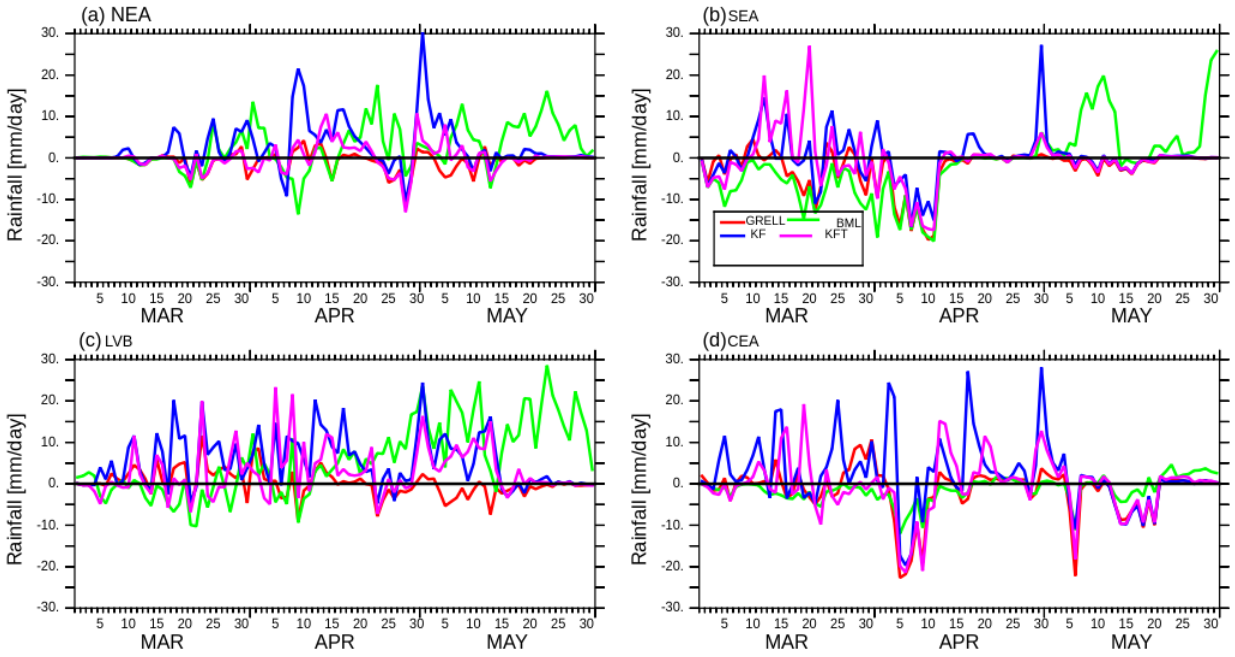

Figure 23: Spatially averaged rainfall biases (mm/day) for the BML, GRELL, KF and KFT schemes over the NEA, SEA, CEA and LVB domains for composite of dry years during MAM season. The model biases were calculated with reference to CHIRPS

The CPSs were skillful in simulating the alternating dry and wet rainfall peaks especially during the wettest years (Figure 23 and 24). The GRELL and KFT CPSs on average simulated weak positive and negative biases during the OND and MAM seasons. The overestimation of rainfall in the KF scheme was evident in the larger biases during the wet rainfall season. One of the possible explanations for the variability in the rainfall biases could emanate from the uncertainties in the observational dataset. A study by Sylla *et al.* (2013) found that uncertainty in the observational dataset is a one of the factors limiting a rigorous evaluation of climate models over Africa.

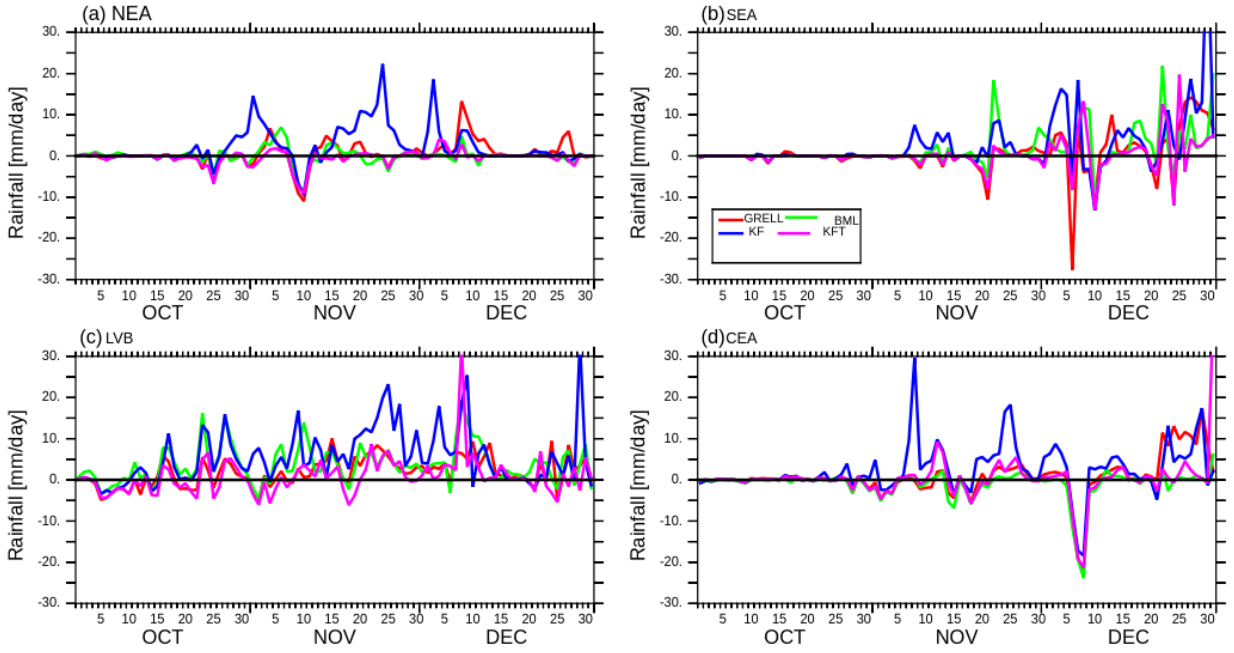

Figure 24: Spatially averaged rainfall biases (mm/day) for the BML, GRELL, KF and KFT schemes over the NEA, SEA, CEA and LVB domains for composite of dry years during OND season. The model biases were calculated with reference to CHIRPS

Based on the above analysis, we conclude that KF simulates wetter biases associated with large rainfall amount over the western parts of the region. The BML and GRELL schemes performed well during drier years than wet years. The trigger function reduces these biases in the KFT scheme. One important observation here is the error growth as the season progresses in the schemes. This signifies the importance of the reduced time-slice for better rainfall reproducibility for the convective rainfall processes over the region.

One of the issues that lowers the quality of the NWP solutions is exponential error growth. The error growth emanates from the baroclinic and conditional instability associated with unstable vertical distribution of energy (Selz and Craig 2015). According to Zhang *et al.* (2007), the error growth has three unique phases. The first phase consists of fast small-scale error growth caused by the convective instability and moist convective processes. These errors rapidly dissipate into individual convective cells. At time-scale level, this could be within the first 10-15 days of the model integration. For the second phase, the convective cells slowly adjust to the balanced motions of the baroclinic instability; which is up-scaled into the third phase beyond the 20th day of the model integrations. In terms of the model physics and dynamics, the inaccurate forcing and

parameterizations used to represent the sub-grid scale processes are ingredients for the model deficiency and error growth (Danforth *et al.,* 2007). Based on this explanation, the deterioration of the CPSs skill beyond the 15th day could emanate from the parameterization schemes used in the simulations.

A consistent pattern in the simulations revealed that the WRF model schemes simulate rainfall features better during the dry years than the wet years. This is due to the fact that whenever the moisture criteria in the scheme is not reached, the scheme is not activated so that the difference between observed and simulated rainfall remains smaller. These findings were in close agreement with those from Marteau *et al.* (2015). In their study they found that, WRF model is skillful in reproducing dry rainfall conditions than wet conditions.

The studies by Flaounas *et al.* (2011), Pohl *et al.* (2011) and Cre´tat *et al.* (2012) found out that the rainfall biases in the climate models are related to too many rainy days with high rainfall intensity. The smaller errors and rainfall underestimation in GRELL and BML schemes could be related to few summation rainy days and their intensity. The seasonal dependency of the CPSs in rainfall simulations as was depicted in Figures 21, 22, 23 and 24 suggest that the choice of a physical package of the model is partly responsible for the accuracy of the rainfall forecasts over the EA region where convective activities are prevalent. From these analyses, it may be concluded that the KFT and GRELL schemes were therefore suitable in reproducing the temporal rainfall biases.

5.3.2.3 Seasonal Rainfall Migration

In this section we examine how the various CPSs simulations represent the seasonal rainfall over the regions of maximum rainfall. Figures 25-26 show the latitude-time variations of the observed and simulated daily rainfall during for MAM and OND seasons for wet and dry years.

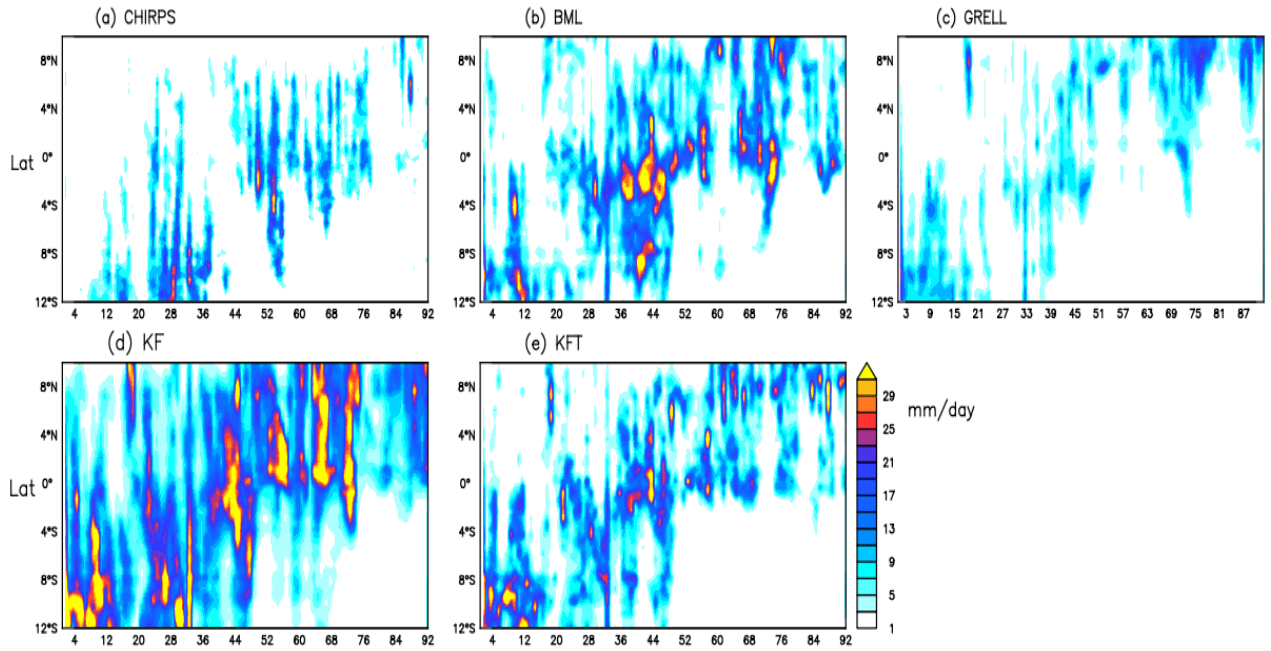

Figure 25: The space-time cross-section of rainfall (mm/day) averaged over longitude 29°E and 36°E for (a) CHIRPS (b) BML (c) GRELL (d) KF (e) KFT during MAM season for the composite of wet years.

The start of the season was marked by rainfall occurring from the 20th day in the south, and then a rainfall break occurred from 35th day as it shifts to the north. A weakening rainfall situation sets in that persisted towards the end of the season (Figure 25a). All the schemes succeeded in reproducing rainfall band from south-north as the season progressed. The KFT scheme reasonably simulated the rainfall amount and the location but failed to reproduce the rainfall timing. The BML and KF schemes overestimated the rainfall amount, while GRELL underestimated rainfall intensity (Figures 25b, c, d, and e). During the OND season (Figure 26), rainfall band was to the north and shifted to the south as the season progressed. High rainfall amount were confined towards the end season. All the schemes reproduced the rainfall band but overestimated the rainfall amount. The GRELL scheme underestimated the rainfall amount (Figure 26c).

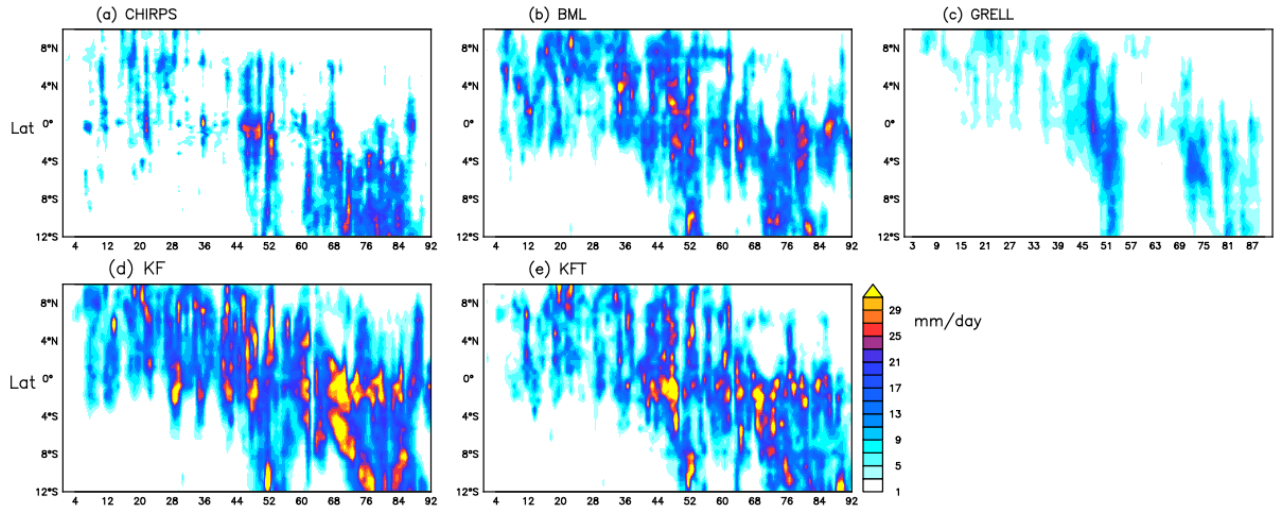

Figure 26: The space-time cross-section of rainfall (mm/day) averaged over longitude 29°E and 36°E for (a) CHIRPS (b) BML (c) GRELL (d) KF (e) KFT during OND season for the composite wet years.

The simulation for dry years (Figure 27) also revealed the same rainfall pattern as for the wet years but clearly and distinctively was characterized by two distinct features. The first one is the persistence of enhanced rainfall within the equatorial belt, between 2 °S and 2 °N, throughout the season. The second feature is an apparent retreat in observed rainfall amount in the middle of the season, which was weakly reproduced in the simulations. The rainfall break was reflected in the quantity of the observed rainfall whereby relatively more rainfall occurred at the beginning of the season. This was common in the KFT and KF schemes (Figure 27b, d, e).

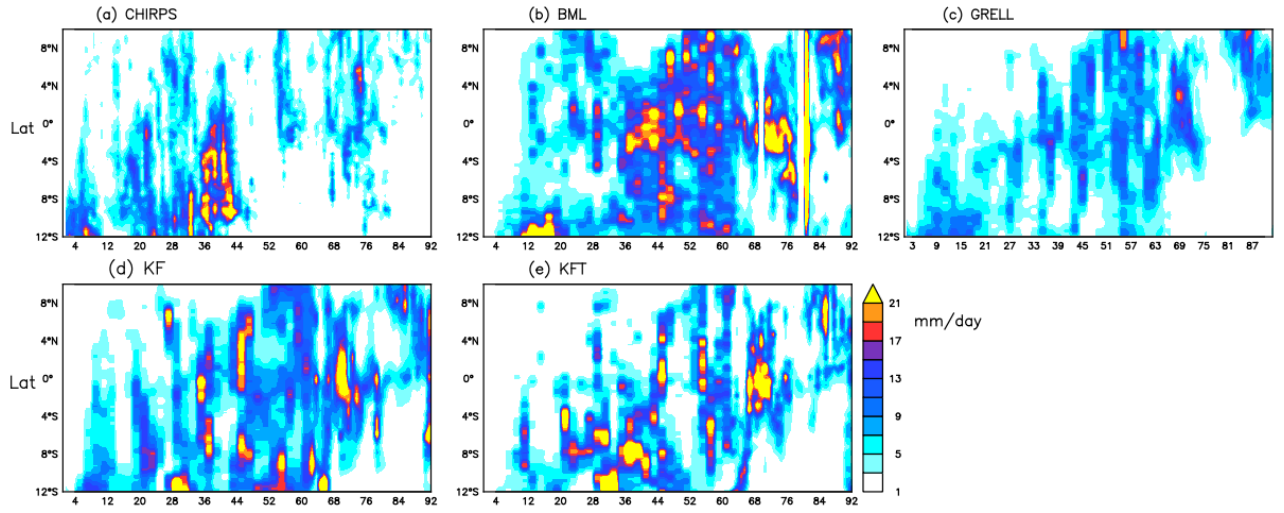

Figure 27: The space-time cross-section of rainfall (mm/day) averaged over longitude 29°E and 36°E for (a) CHIRPS (b) BML (c) GRELL (d) KF (e) KFT during MAM season for the composite dry years.

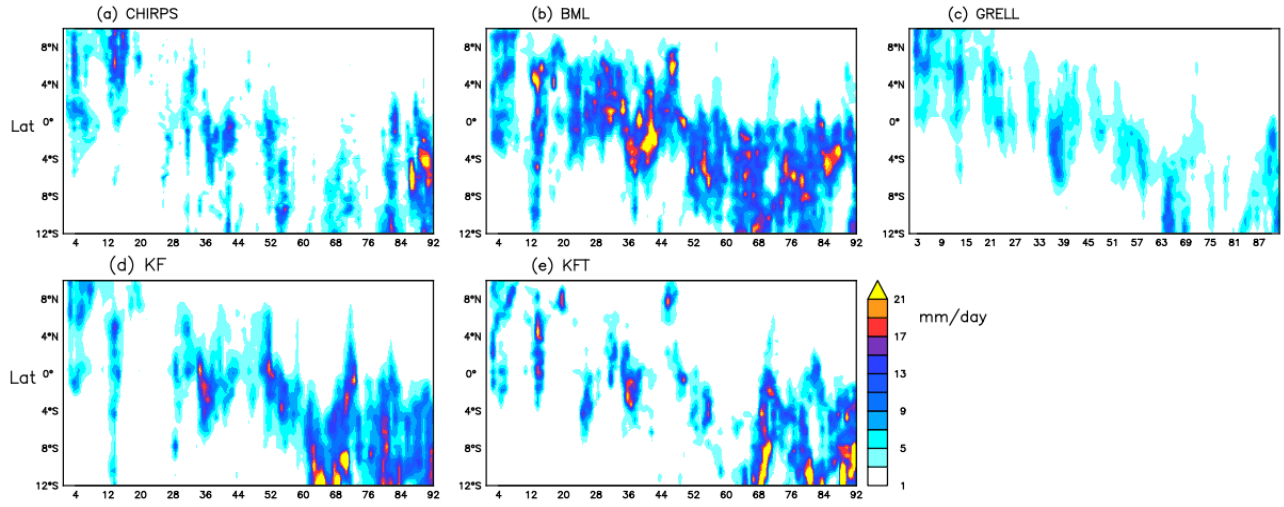

Figure 28: The space-time cross-section of rainfall (mm/day) averaged over longitude 29°E and 36°E for (a) CHIRPS (b) BML (c) GRELL (d) KF (e) KFT during the OND season for the composite of dry years.

This feature was even better reproduced during the OND season than the MAM season (Figure 28e). The wet rainfall conditions simulated over the Equatorial region could be as a result of the sustained strong convective activities confined within the latitude 2°S -2°N and longitude 20°E - 30°E (Figures 27-28); a likely manifestation of the WRF model's ability to capture localized convection (Anyah and Semmazi 2007). The time-latitude evolution of the simulated seasonal

rainfall exhibited a quasi-stationary mode associated with high rainfall throughout the season within the equatorial belt and a feature associated with the movement of the ITCZ driven southward-northward regions of rainfall maximum.

The results from the time-latitude confirmed the fact that, strong sustained convection within the equatorial region (2 °S-2 °N and 20°E-30°E) induces wetter conditions in the KF scheme. This wetter rainfall condition was reduced in the KFT scheme. Such wetter conditions is a likely manifestation of the WRF model ability to capture localized convection (Anyah and Semmazi 2007) within the equatorial strip. Anyah *et al*. (2006) found that over the equatorial region the enhanced rainfall is induced by local topography and inland lakes. The orientation of the lakes astride to the equator sandwiched on both sides by high mountains, oriented in the north–south direction on both sides provides an enabling environment for frequent development of active convection and precipitation throughout the season (Waliser and Gautier 1993).

Although out of the scope for the current study, other physical dynamical processes that plays role in determining the simulation of rainfall characteristics in terms of rainfall location, intensity and timing and the associated equatorial rainfall maximum include solar radiation, topography, SST forcing, and remote teleconnections to the western parts of Africa and Indian monsoon systems (Cook and Vizy 2013). Furthermore, the rainfall maximum shift is associated with the meridional movement of the African Easterly Jet (AEJ), a feature more dominant over West Africa.

The Kain-Fritsch and Grell-Devenyi schemes are far separated by their rainfall amount and simulated rainfall biases. The GRELL CPS favors a drier rainfall pattern associated with drier biases, while the KF CPS favors a wetter rainfall pattern associated with its wetter biases. The KFT scheme potentially minimized the wet rainfall biases in the KF scheme by lowering the passivity of the long and short-wave radiation. The simulations by the BML scheme was associated with mixed rainfall signal. On the basis of this, the KF scheme outperformed all the other CPSs, and therefore was the most suitable for the EA region. Similar findings had been reported by Pohl *et al.* (2011) over the region but did not clearly separate these schemes in terms of the wet and dry years.

It can be concluded that the KFT and KF schemes are suitable in separating the wet and dry rainfall characteristics over the region. The GRELL scheme only reproduced drier rainfall patterns better.

5.3.3 Intra-seasonal Rainfall Characteristics

This section presents results from the analyses of various intra-seasonal rainfall characteristics including number of rainy days (NRD), intensity of rainy days (IRD) and frequency of rainfall intensity (FRI).

5.3.3.1 Number of Rainy Days

Figures 29 and 30 show the biases in the simulated NRD for wet and dry years respectively. There were more NRD above 40 days simulated over the northern parts of the Equatorial region in all the schemes as was illustrated in the Figures 29a, b and c except in the KFT scheme shown in Figure 29d where it underestimated the NRD by above 30 days over most parts of the region during the MAM season. The KFT scheme, however, had minimum biases in the NRD between (5-10days) over the western Equatorial region. These biases in the NRD were underestimated during OND over the southern parts of the region in the GRELL, BML and KF schemes (Figures 29e, f, g). The KFT scheme simulated the minimum NRD over the same locations and few NRD over the Equatorial and Eastern parts of the domain (Figures 29h).

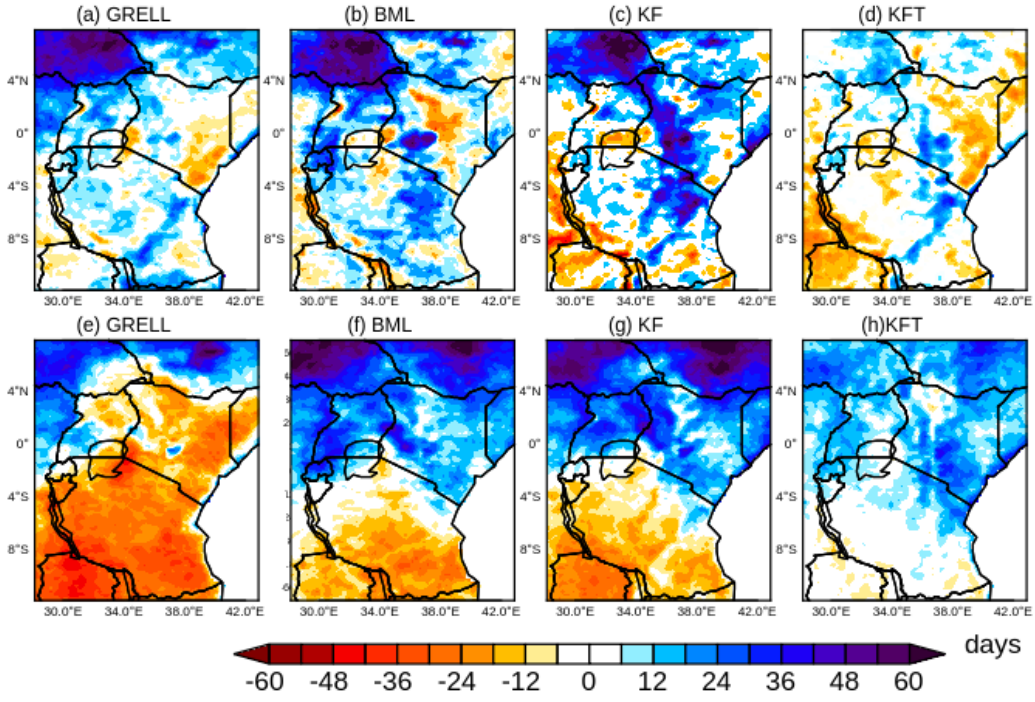

Figure 29: The differences between simulated and observed NRD (days) by (a) GRELL (b) BML (c) KF and (d) KFT CPSs for the composite of wet years during MAM season and (e) GRELL (f) BML (g) KF (h) KFT during OND season. The blue (orange) shadings denote areas with positive (negative) differences in the NRD.

For the dry years, the CPSs simulated fewer NRD between 15 to 30 days to the southern and overestimated by over 20 days over the Equatorial and Northern sector of the region during MAM season as was depicted in Figures 30a, b and c. The biases in the KFT CPS were reduced by between 8 to 12 days over the equatorial region. During the OND season, there were fewer NRD simulated over the southern parts of the region in all the CPSs except for the KFT scheme shown in Figures 30e, f and g. The KFT scheme simulated between 5 to 20 days more over the northern parts of Tanzania and above 10 days over the northern equatorial region (Figure 30h). In general, the OND season was relatively better simulated with reduced biases than during the MAM season. Reduced biases in NRD were mostly confined over the northern part of the Equatorial region and the northern parts of Tanzania. The simulated biases in the NRD were relatively smaller during drier years than wetter years. The GRELL scheme simulated fewer NRD and KF simulated more NRD.

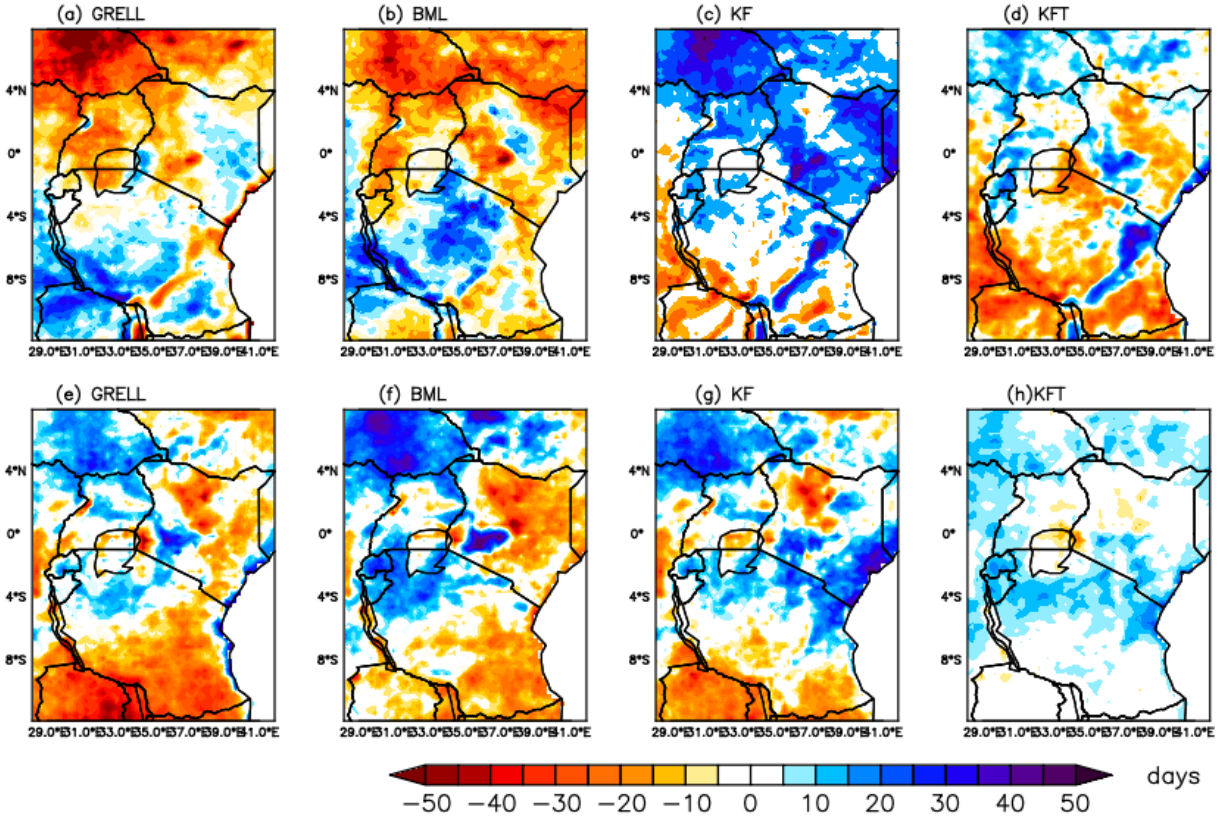

Figure 30: The differences between simulated and observed NRD (days) by (a) GRELL (b) BML (c) KF and (d) KFT CPSs for the composite of dry years during MAM season and (e) GRELL (f) BML (g) KF (h) KFT during OND season. The blue (orange) shadings denote areas with positive (negative) differences in the NRD.

These analyses revealed that the regions with EA domain with more (less) rainfall (Figures 14 and 15), coincided with the areas under more (fewer) NRD (Figures 29 and 30). All the CPSs captured the area of maximum NRD (northern and western parts of Equatorial region). All the schemes overestimated the NRD over these locations. The over-estimation of the NRD was common over the highland areas and lake regions. As Ratna *et al.* (2013) reported, most RCMs have bias in generating orography-induced rainfall.

In terms of the number of rainy days, it can be concluded that, large rainfall amounts over the equatorial northern part of the domain are associated with more NRD while the underestimation of rainfall over southern parts and eastern regions results from fewer NRD. The GRELL and KF schemes succeeded in reproducing these rainfall patterns. This study is the first in the region to demonstrate the separation of rainfall activities by the KF and GRELL schemes.

5.3.3.2 Rainfall Intensities

In order to investigate rainfall intensity, three rainfall categories (i) 1-10mm/day (ii) 11-20mm/day (iii) >20mm/day were defined based on the WMO rainfall indices (Ongoma *et al.*,2018). These categories were referred to as light, moderate and heavy rainfall categories respectively in this text. The spatial distribution of the wettest and driest rainfall years for the NRD was analyzed based on these three categories.

Figures 31 and 32 show the biases in the simulated rainfall intensities of the NRD for light, moderate, and heavy rainfall categories during wet years for the MAM and OND seasons. The NRD under the light categories were overestimated between 4 to 12 days over the western Equatorial region, central parts of Kenya and Tanzania in the GRELL, BML and KFT schemes as shown in Figures 31a, b and d. The KF scheme underestimated the intensity of rainy days by 1-5days (Figure 31c). For the moderate intensities, the GRELL, BML and KFT schemes (Figures 31e, f, and h) weakly underestimated rainfall biases from 1 to 4 days. The KF scheme overestimated the NRD between 4 to 8 days as shown in Figure 31g.

For heavy rainfall intensities, the schemes performed with reduced biases in the intensities. For example, over the central parts of Kenya, Tanzania and the coastal strips of Kenya the biases in the rainfall intensities were between 1 to 4 days. The KF and KFT schemes overestimated the NRD over the equatorial region under this category (Figures 31k, l) but correctly simulated the NRD over the eastern, central and southern parts of the region.

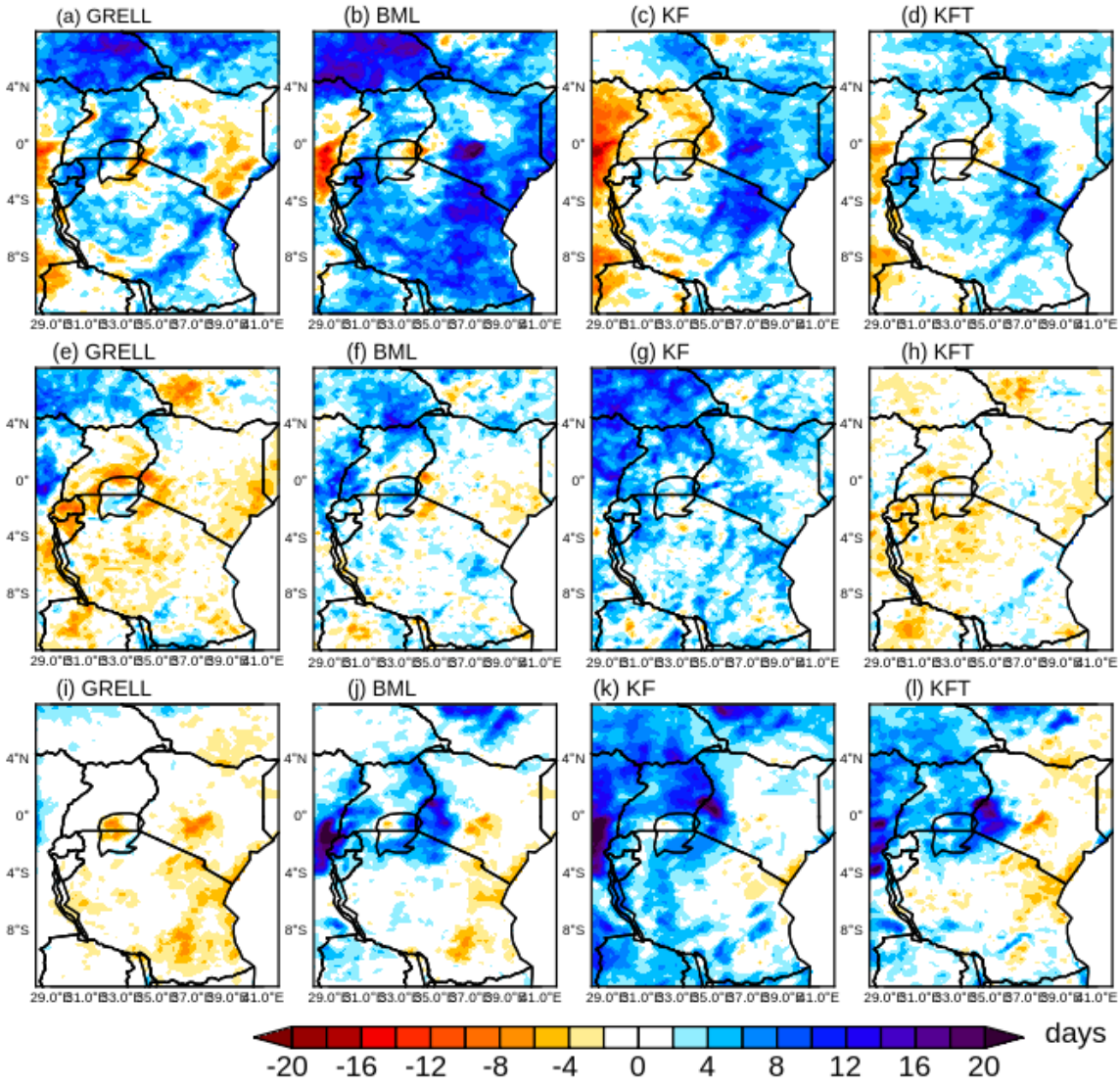

Figure 31: The differences between simulated and observed rainfall Intensities of the NRD for composite of wet years (1992, 1998 and 2007) during MAM season. The top, middle and bottom panels represents the light (1-10mm/day), moderate (11-20mm/day) and heavy (>20mm/day) rainfall intensities respectively over East Africa region. The blue (dark orange) shadings denote areas with negative (positive) differences.

During the OND season for wet years, parts of the western equatorial region received minimum number of rainy days associated with light rainfall categories (Figures 32a, b, c, d). There was underestimation of the NRD under light categories, overestimation of NRD under moderate and heavy rainfall intensities. Over the eastern, north eastern, coastal parts of Kenya and Tanzania, rainfall under light category were overestimated, and underestimated under heavy rainfall intensities. The spatial distribution of different rainfall intensities were well captured by the CPSs

under heavy rainfall intensities over the western parts of Tanzania and Kenya. The KF scheme consistently overestimated the NRD under moderate and heavy rainfall intensities, and under-estimated the light rainfall categories. Comparatively, the overestimation of NRD in KF was reduced in KFT. The GRELL scheme generated fewer NRD under both rainfall categories.

The GRELL and KFT schemes indicated better simulation under heavy rainfall categories (simulated minimum biases of 1 to 5 days). The KF scheme was not any better under any rainfall category since it consistently underestimated or overestimated the NRD. These analyses indicate that over the western parts of the equatorial region, the areas that predominantly receive high rainfall are also associated with many NRD.

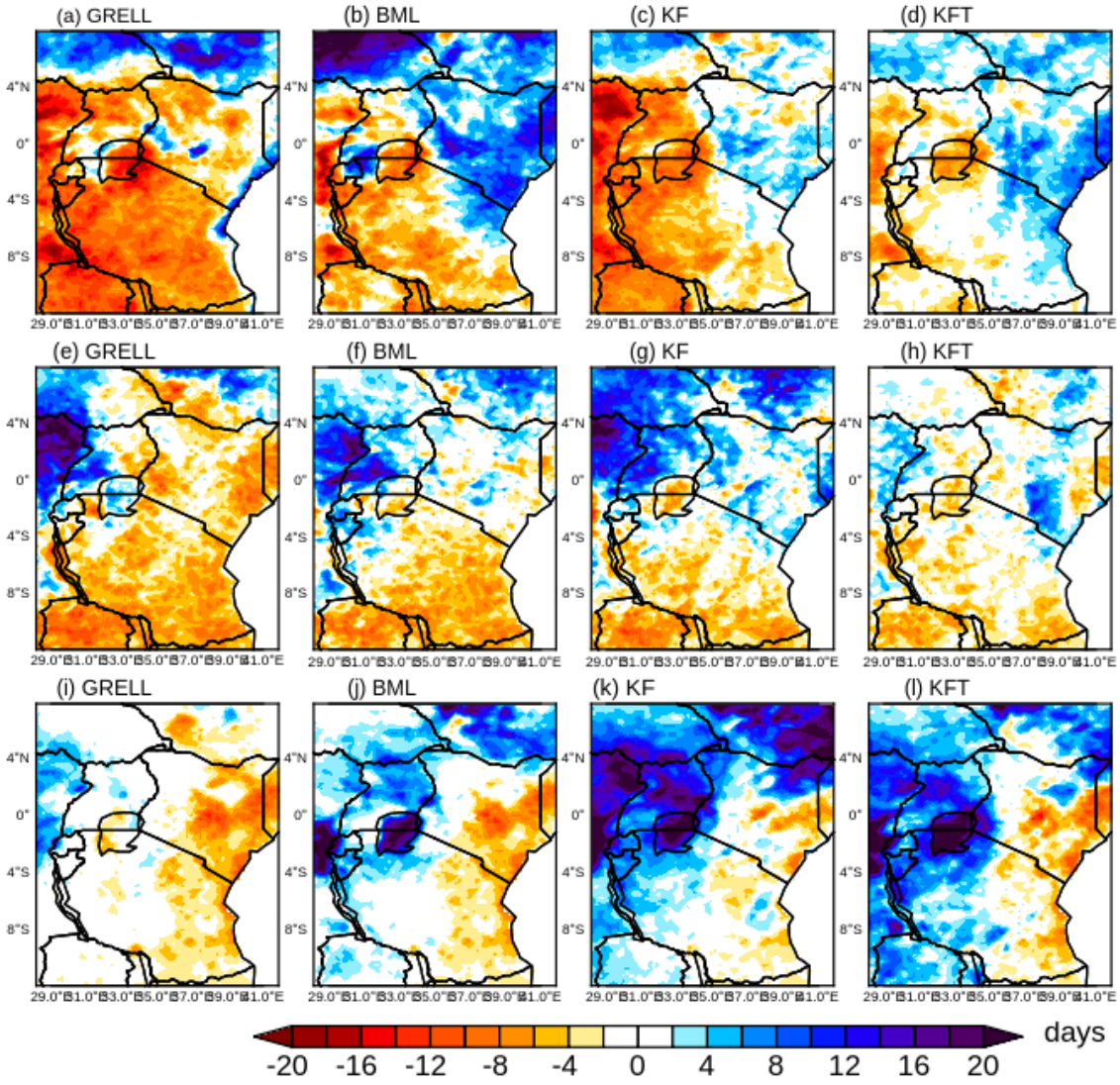

Figure 32: The differences between simulated and observed rainfall intensities of NRD for the composite of wet years during the OND season. The top, middle and bottom panels represents the light (1-10mm/day), moderate (11-20mm/day) and heavy (>20m/day) rainfall intensities respectively over East Africa region. The blue (orange) shadings denote areas with positive (negative) differences.

For dry years during MAM season (Figure 33), light rainfall intensity was mostly underestimated over western Equatorial parts by about 8 days. The underestimation was pronounced in GRELL scheme while the BML simulated a west-east rainfall gradient (Figures 33a and b). The overestimation of NRD in the KF scheme (Figures 33c) was clearly reduced in KFT scheme (Figures 33d) by about 10 days. The moderate rainfall intensities were mostly underestimated in

GRELL and BML schemes as shown in Figures 33e, f and h by about 10 days. Under heavy rainfall intensity, the biases were smaller. The GRELL simulated these intensities better (Figures 33i); the BML, KF and KFT schemes (Figures 33j, k, l) overestimated the NRD under heavy rainfall intensity over the equatorial region by about 8 days. Better results and simulations were found over the southern parts of Tanzania and the central parts of Kenya.

For the dry years during the OND season (Figure 34), the biases were relatively smaller, the rainfall intensity under light rainfall were clearly overestimated (Figure 34a, b ,c and d) and reasonably simulated with low biases between 1 to 3 days as was illustrated in Figures 34i,j,k and l. The KFT scheme had smaller biases compared to the KF schemes (Figures 34k). Throughout the analyses, the study revealed that the areas with the maximum NRD (Western Equatorial region, Figures 14 and 15) are predominantly associated with light rainfall categories while the areas with minimum NRD (Eastern, central, and coastal parts of the region) are associated with heavy rainfall intensities over the EA region during the MAM and OND seasons.

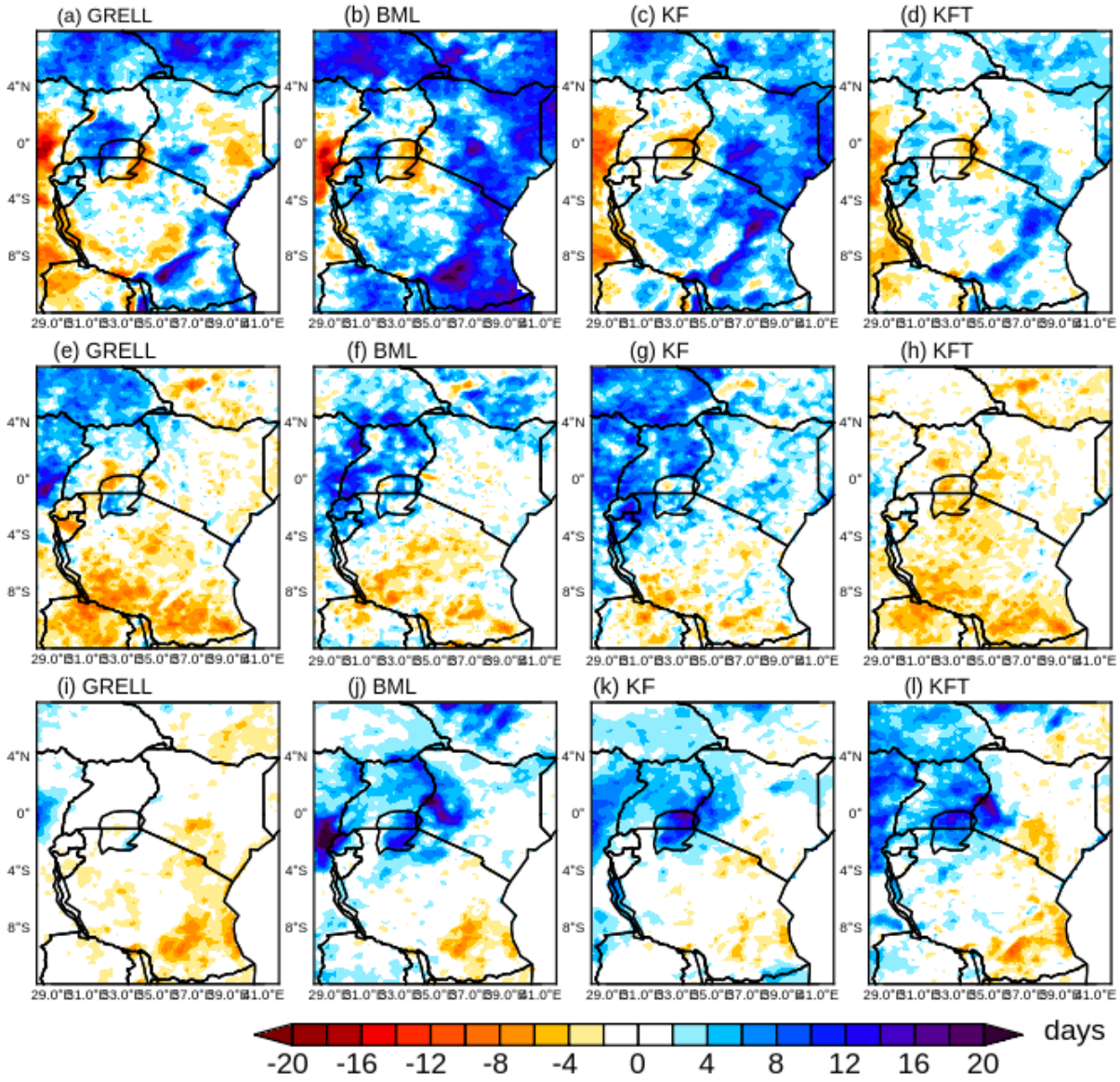

Figure 33: The Spatial patterns of the average NRD according to three rainfall intensity categories for the composite of dry years during the MAM season. The (a), (b), (c), (d) denote light rainfall category, (e), (f), (g), (h) denote moderate category and (i), (j), (k), (l) denote heavy rainfall intensities simulated by the BML, GRELL, KF and KFT schemes over EA region.

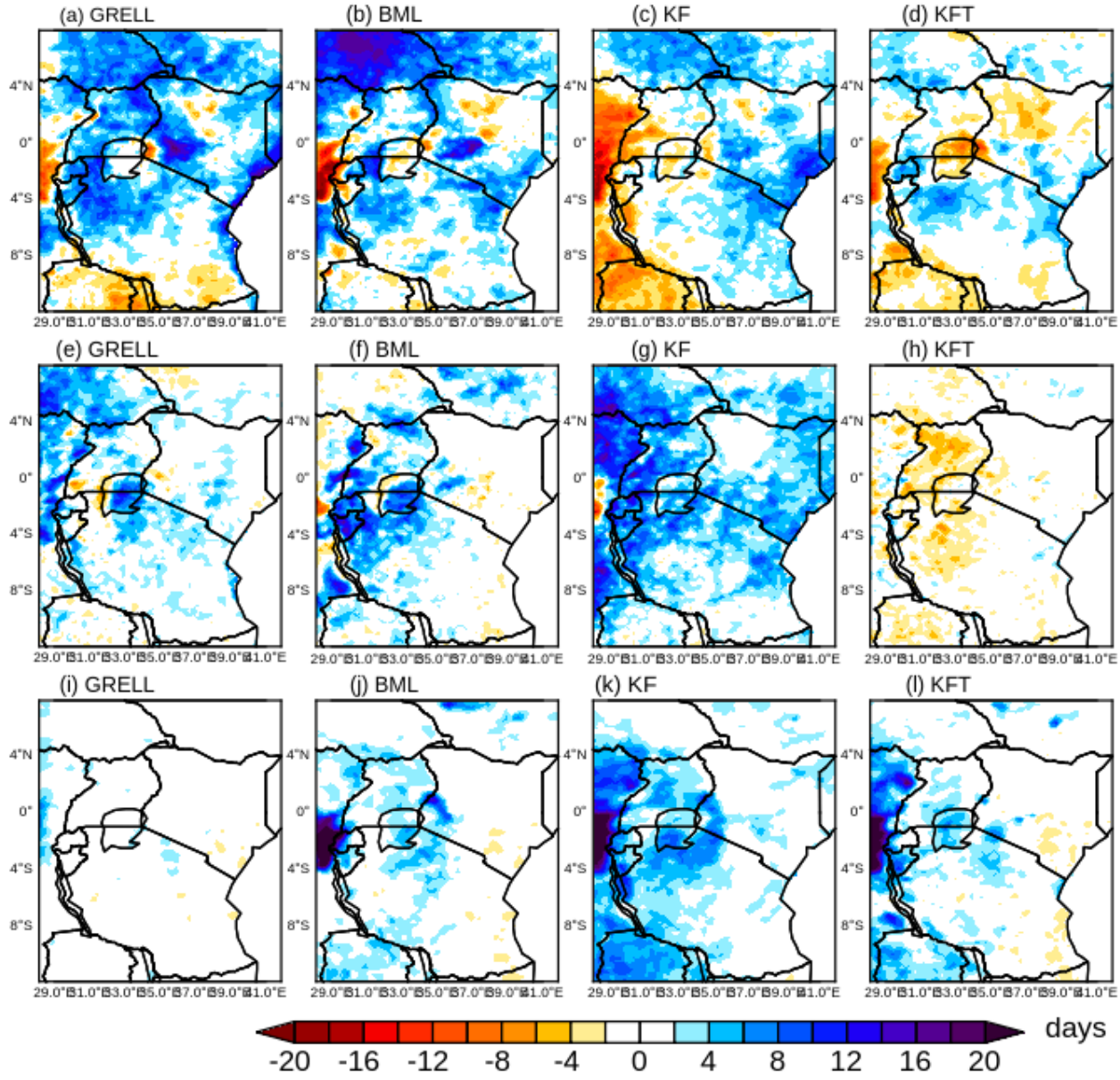

Figure 34: The Spatial patterns of the average NRD according to three rainfall intensity categories for the composite of dry years during the OND season. The (a), (b), (c), (d) denote light rainfall category, (e), (f), (g), (h) denote moderate category and (i), (j), (k), (l) denote heavy rainfall intensities simulated by the BML, GRELL, KF and KFT schemes over EA region.

From the above analyses, it can be concluded that high rainfall amount reproduced by the KF scheme was as a result of too many rainy days under the light intensities. Similarly, the drier rainfall patterns in the GRELL CPS emanated from fewer NRD. The over-estimation was higher in KF and reduced in KFT schemes. The western equatorial region received rainfall of above

20mm/day, and moderate rainfall over eastern parts of the region. In most cases, the KF and GRELL had closer rainfall agreement over southern parts of the region and coastal cities of the study domain. The moderate rainfall category was poorly simulated by the schemes. The CPSs generated more rainy days under the light rainfall category; compensated by fewer rainy days under heavy-moderate rainfall intensities. Similar findings had been reported by Cretat *et al.* (2011). From the analyses of the rainfall intensities, the GRELL and KFT schemes were most skillful in reproducing heavy-moderate rainfall intensities.

5.3.3.3 The Relative Frequency of the Rainfall Intensities

In this section, the study analyzed how often the rainfall intensities occur. This was done by dividing the NRD for any given category by the total NRD and expressed in percentage points to give relative rainfall frequency. Figure 35 shows the relative frequencies of the various rainfall intensities during the wet years of the MAM season. Light rainfall occurred more frequently and was overestimated by over 40% over Eastern, Central and Southern parts of the region by GRELL, BML, KF and KFT schemes (Figure 35a, b, c and d). Similarly, over the western parts of the equatorial region, rainfall occurred less frequent and were mostly underestimated by about 20%. The heavy rainfall intensity was less frequent and in certain instances underestimated by about 20% over the central parts of Kenya, eastern parts of Tanzania and northern parts of Kenya.

The simulations were better over the western parts of the Equatorial region (Figure 35i, j, k, and l). All the CPSs considerably overestimated the rainfall frequency during the MAM season but with differing magnitude of light precipitation over the central parts of Kenya, and southern parts of Tanzania. The KFT scheme generated fewer biases under light rainfall intensity over the western and central parts of Tanzania. The biases under the heavy rainfall category were reduced relatively by about 20%. This probably implied that the cumulus schemes reasonably reproduce the rainfall amount under the heavy rainfall intensity. In the KF and KFT schemes, the rainfall intensities were slightly over-estimated by about 10-20% compared to about 20-50% under light intensities (Figures 35a, b, c, d).

The simulations for moderate frequency were not so distinct and as such clear differences in the frequency biases could not be noticed. During the OND season (Figure 36), the GRELL and BML cumulus schemes (Figures 36a and b) overestimated the frequency of light rainfall intensity (40-60%) over the coastal parts of Tanzania and Kenya, central and eastern parts of Kenya. Over the

western parts of the equatorial region, the light rains were less frequent and in certain cases underestimated by the cumulus schemes. Under heavy rainfall intensity, there was reasonable agreement between the schemes and observation in GRELL and BML (Figures 36i, j) over the western equatorial parts of the region. The KF scheme overestimated the frequencies over these regions whilst the KFT scheme reasonably reproduced the frequency over southern and western parts of Kenya (Figures 36k, l).

Most of the CPSs simulated the heavy rainfall frequency better than the light rainfall frequency (Figures 35 and 36) over the western parts of equatorial region; and generally reproduced the large-scale pattern probably due to the ITCZ. Although there was general overestimation and underestimation of the frequencies of heavy and light rainfall, the results suggest that the climate models experience too many rainy days with light rainfall, but perform rather well in simulating the heavy rainfall frequency (Sun *et al.,* 2006).

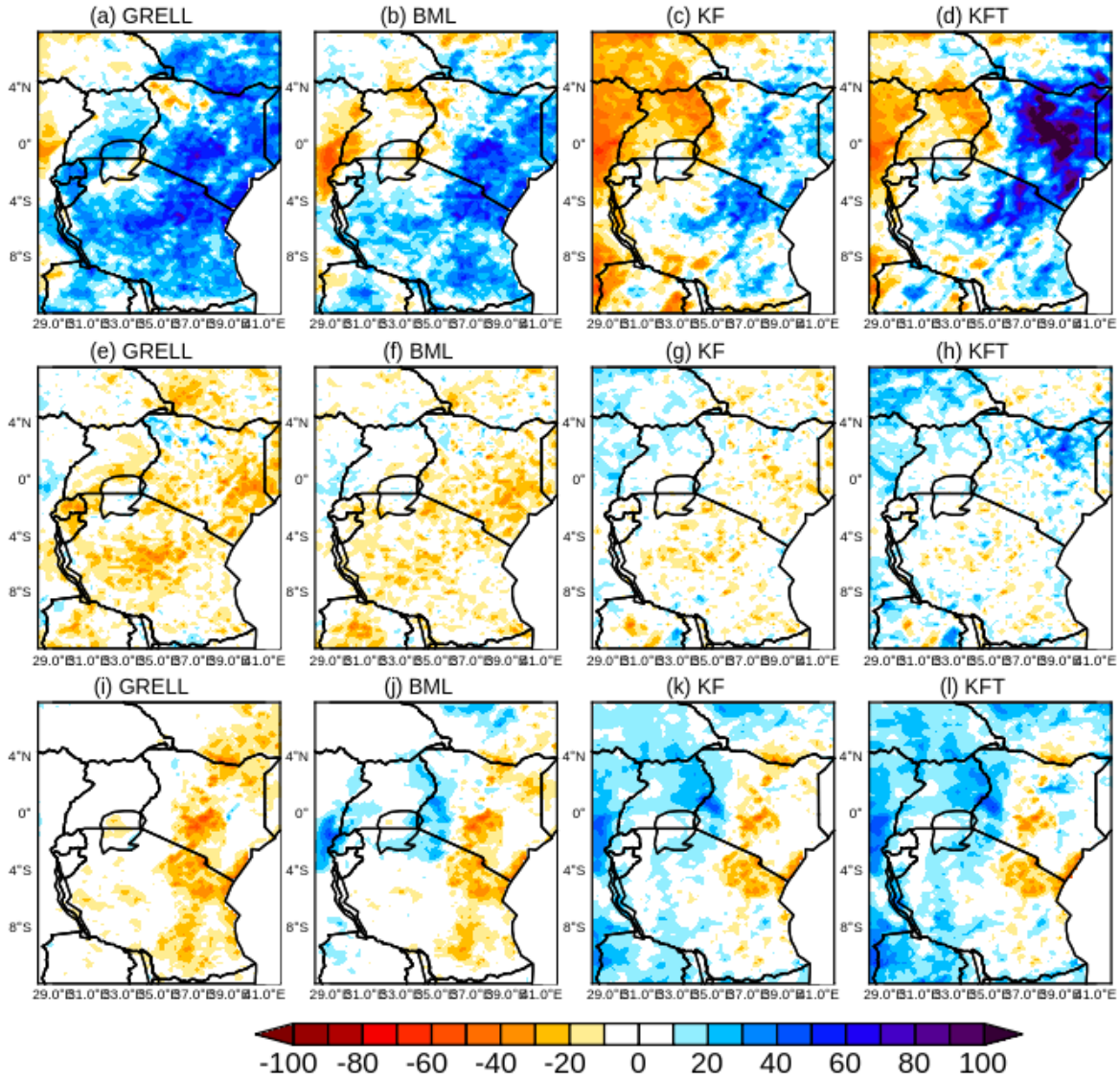

Figure 35: The differences between simulated and observed rainfall frequencies (%) for the wet composite during the MAM season. The (a), (b), (c), (d) denote light rainfall category, (e), (f), (g), (h) denote moderate category and (i), (j), (k), (l) denote heavy rainfall intensities simulated by the BML, GRELL, KF and KFT schemes over EA region. The difference was taken with respect to CHIRPS data. The blue (dark orange) shadings denote areas with positive (negative) differences.

The overestimation of rainfall and the biases in KF and subsequent reduction of the same in KFT scheme; and the underestimation of the same by GRELL cumulus scheme was mostly generated due to higher or fewer NRD in the light rainfall intensity concentrated over western equatorial parts of the region. For the heavy rainfall category, most of the schemes reproduced both their intensity and frequency reasonably. It is inferable that light rains are more frequent while heavy rains are less frequent.

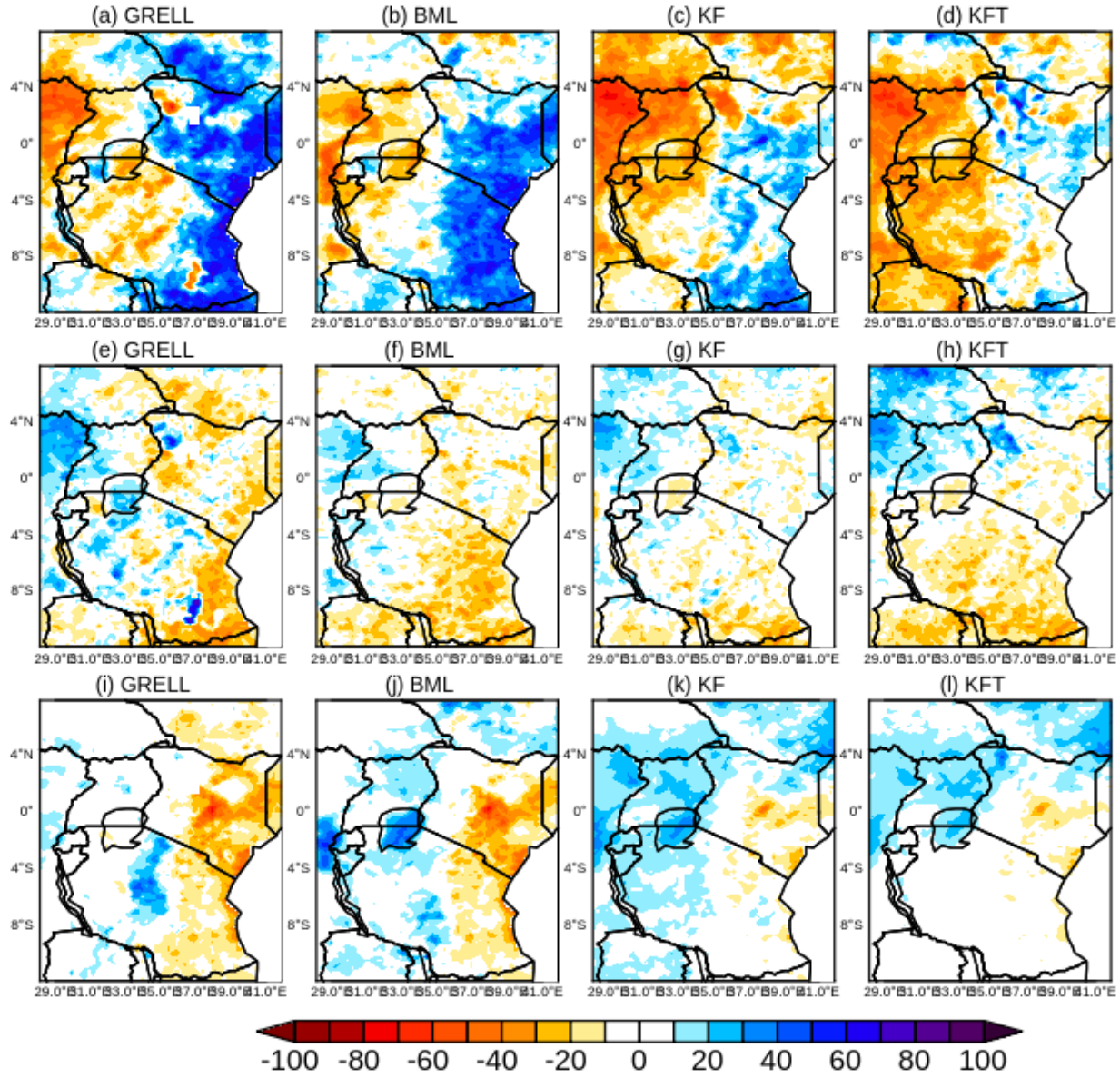

Figure 36: The differences between simulated and observed rainfall frequencies (%) for the wet composite during the OND season. The (a), (b), (c), (d) denote light rainfall category, (e), (f), (g), (h) denote moderate category and (i), (j), (k), (l) denote heavy rainfall intensities simulated by the BML, GRELL, KF and KFT schemes over EA region. The difference was taken with respect to CHIRPS data. The blue (dark orange) shadings denote areas with positive (negative) differences.

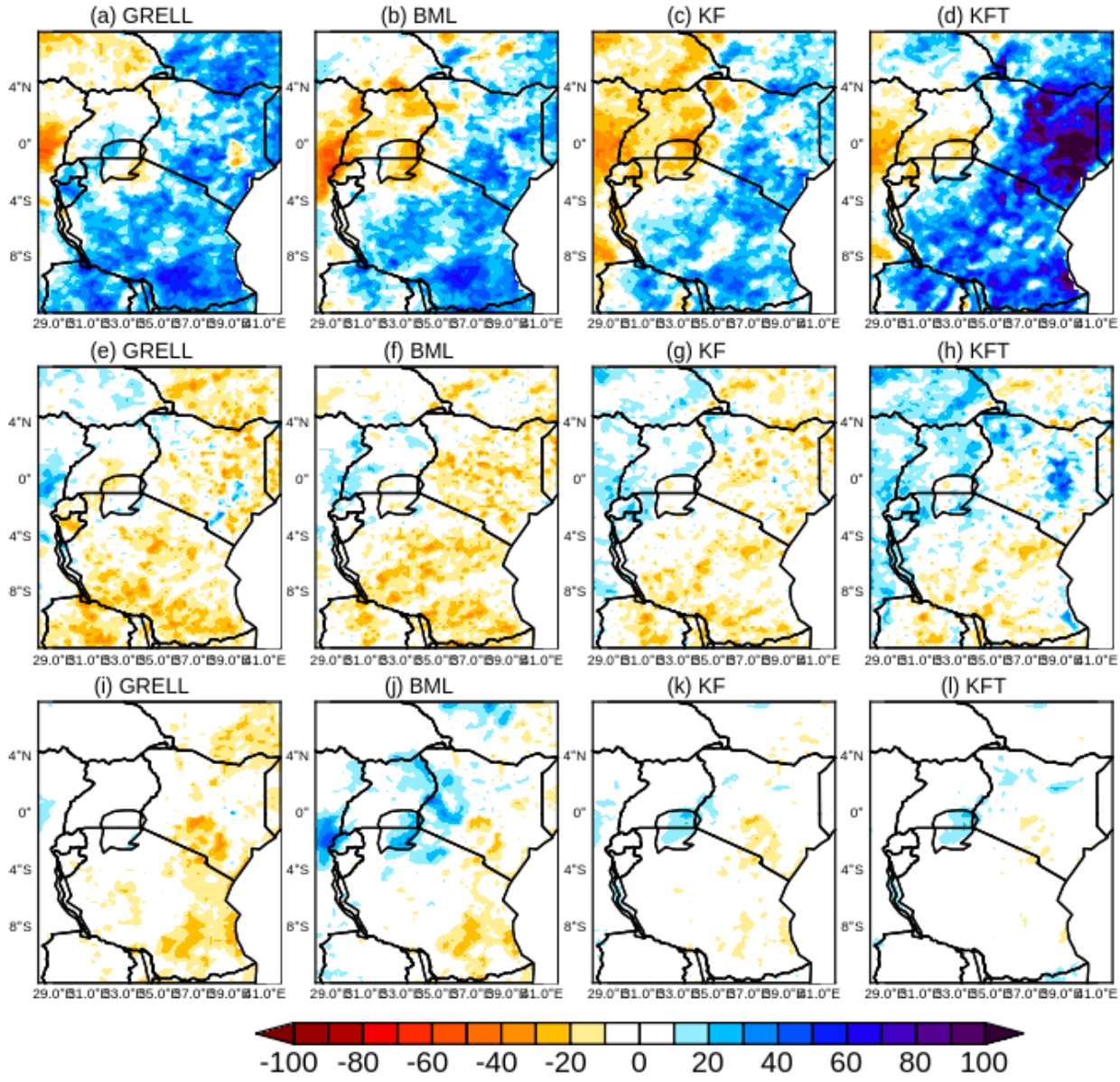

Figure 37: The differences between simulated and observed rainfall frequencies (%) for the dry composite during the MAM season. The (a), (b), (c), (d) denote light rainfall category, (e), (f), (g), (h) denote moderate category and (i), (j), (k), (l) denote heavy rainfall intensities simulated by the BML, GRELL, KF and KFT schemes over EA region. The difference was taken with respect to CHIRPS data. The blue (orange) shadings denote areas with positive (negative) differences

For the dry MAM season (Figure 37), the frequency of light rainfall intensities was overestimated by the CPSs over the eastern, central, southern and northern parts of the region by between 20 and 60 %. Over the western equatorial part, there was a consistent underestimation of the rainfall

frequency by about 30%. The biases in the heavy rainfall frequency were smaller. All the CPS reproduced heavy rainfall frequency over the equatorial region (Figures 37a, b, c, i, j, k, l). The moderate rainfall (11-20mm/day) were not skillfully resolved like for the light and heavy rainfall events. The biases during the OND season for dry years (Figure 38) showed better simulations of heavy rainfall frequency, with larger biases observed under light rainfall intensity especially in KFT and KF schemes (Figure 38c and d).

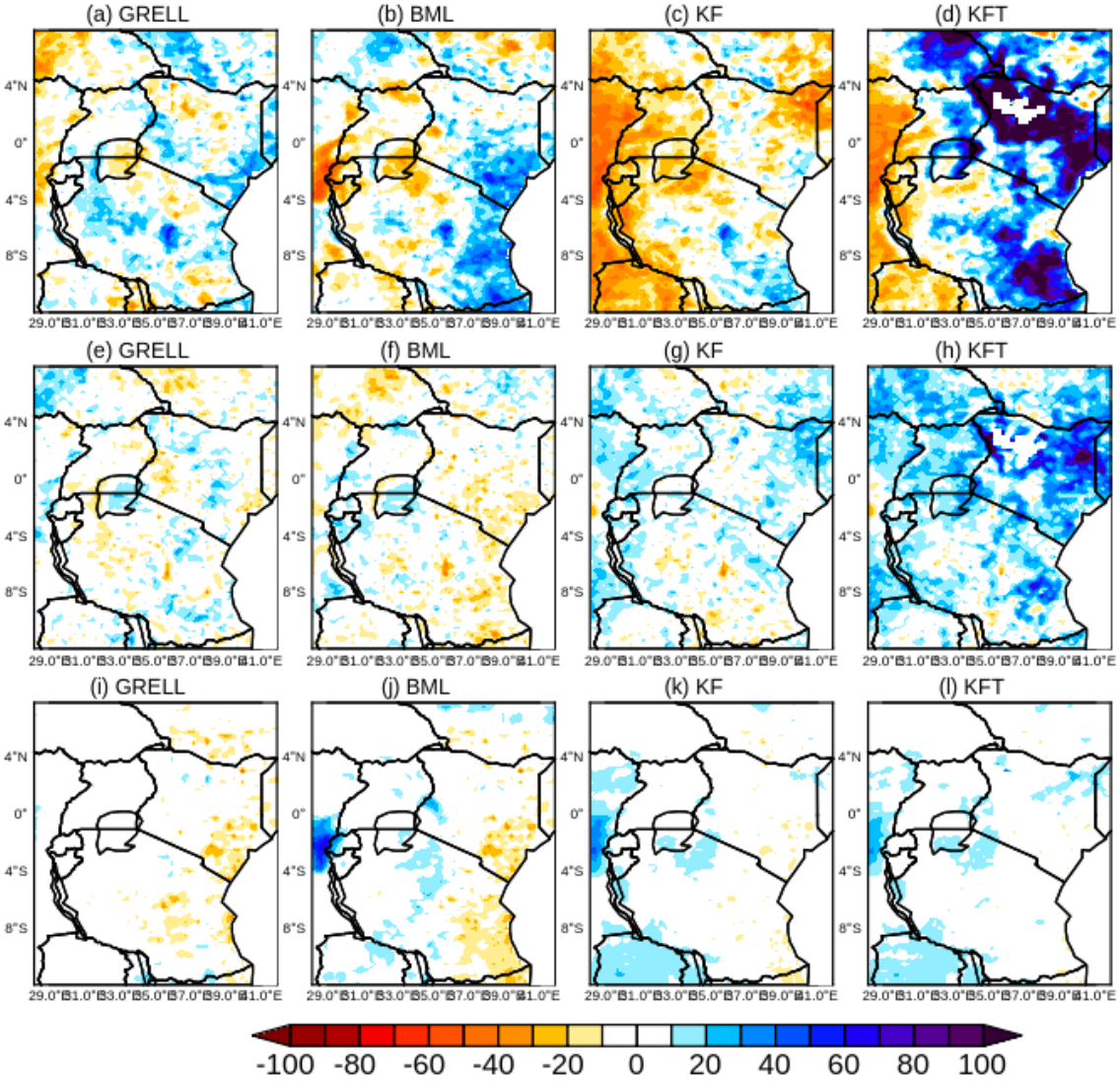

Figure 38: The differences between simulated and observed rainfall frequencies (%) for the dry composite during the OND season. The (a), (b), (c), (d) denote light rainfall category, (e), (f), (g), (h) denote moderate category and (i), (j), (k), (l) denote heavy rainfall intensities simulated by the BML, GRELL, KF and KFT schemes over the EA region. The difference was taken with respect to CHIRPS data. The blue (orange) shadings denote areas with positive (negative) differences

From the analyses, it can be deduced that the regions with more NRD predominantly receive high amount rainfall seasonally, whilst the regions with fewer NRD predominantly receive low rainfall. Over the region, light rainfall intensity (1-10mm/day) occur more often which was consistently overestimated by the CPSs. All the CPSs simulated well the rainfall intensity under heavy rainfall (>20mm/day), as well as their frequencies. The analyses for the frequency of rainfall intensity revealed a consistent pattern in the KFT and GRELL simulations.

5.3.4 Ranking the Schemes based on Taylor Diagram

The study summarized the skill of the CPSs based on their rainfall pattern and their amplitude of the observed rainfall in a Taylor diagram. Figures 39 and 40 show the spatial pattern correlation (r), root mean square difference, and the amplitude of variation (standard deviation) of seasonal mean rainfall for CHIRPS, GRELL, BML, KF and KFT CPSs during the MAM and OND seasons for wet and dry composites over NEA, SEA, CEA and LVB sub-domains, respectively.

During the wet years (Figure 39), the CPSs were most skillful over SEA and LVB sub-domains with correlation coefficients ranging between 0.4-0.6. The KF, KFT and GRELL schemes simulated correlation values of about 0.5 during the MAM season as shown in Figure 39. The OND season was poorly replicated in all the domains except over SEA and LVB where KFT scheme simulated correlation values of 0.65 and 0.4 respectively.

For the dry composites (Figure 40), the GRELL and KFT CPSs were most skillful with mean correlation values of 0.8 and 0.6 respectively over NEA region during the MAM season. The GRELL and BML CPSs simulated correlation of 0.5 and 0.4 respectively. Over SEA and CEA sub-domains the correlation values for all the CPSs were about 0.5 except for the BML scheme that had poor relationship with the rainfall mechanism here. Similar correlation coefficients were recorded during the OND season (Figures 40e-h). During this season, the KFT and BML schemes simulated correlation values of 0.6 and 0.4 respectively over NEA and SEA sub-domains. The simulations over LVB and CEA domains were poor. Smaller RMSD of about 2.3 mm/day was simulated by the KF and BML schemes over NEA and SEA sub-domains. The KF, KFT and GRELL schemes in most cases had RMSD ranging between 1.5 to 6mm/day with standard deviation of 1.5. From the above analyses, the KF and KFT were most skillful; the GRELL was most skillful during drier years.

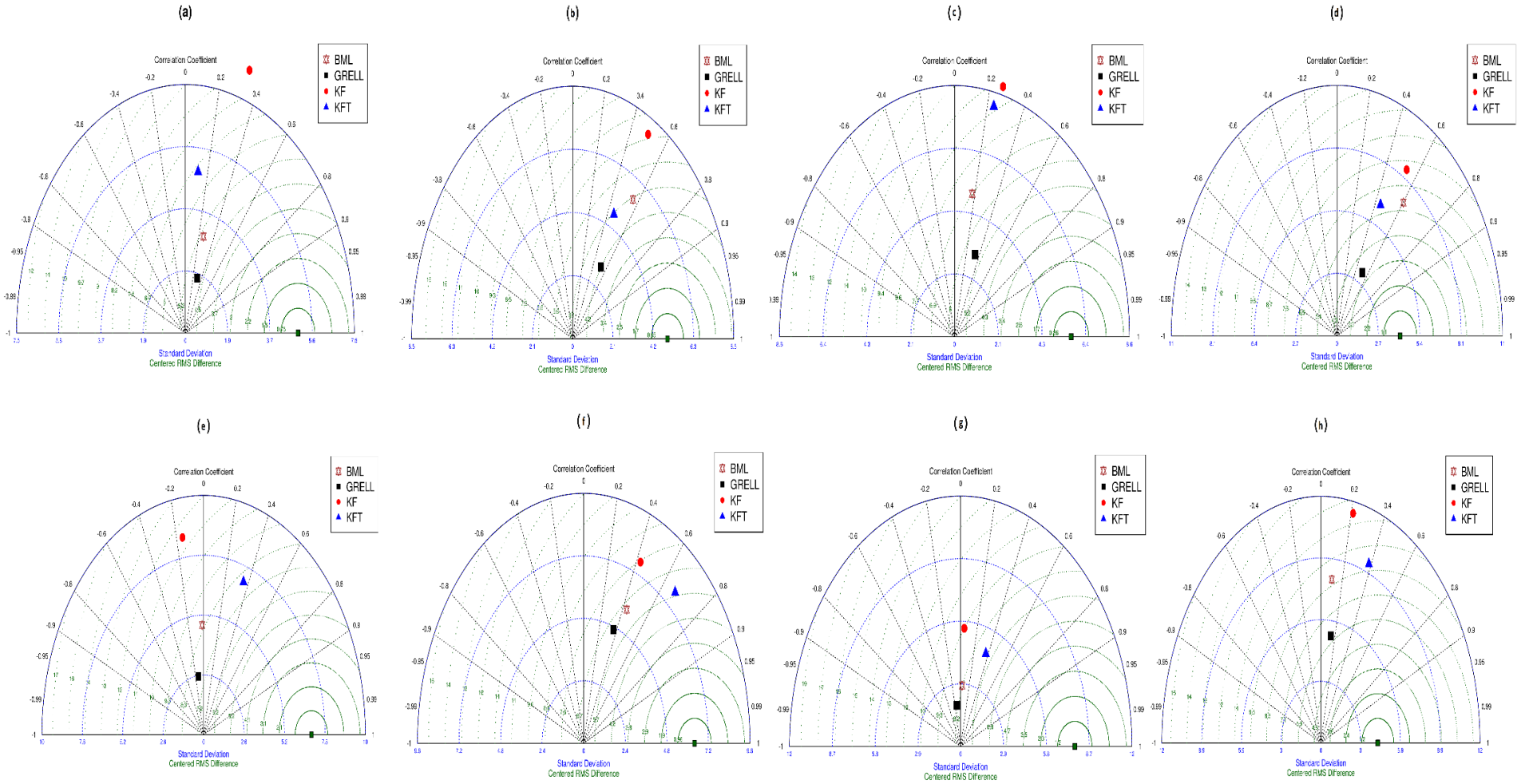

Figure 39: Taylor diagram displaying statistical comparison of seasonal mean rainfall for BML (brown), GRELL (black), KF(red) and KFT(blue) with observations over (a) NEA (b) SEA (c) CEA (d) LVB sub-domains during the MAM season and (e) NEA (f) SEA (g) CEA and (h) LVB sub-domains during the OND season. The blue and green curves represent standard deviation (SD) and root mean square differences (RMSD) respectively for the composite of wet years

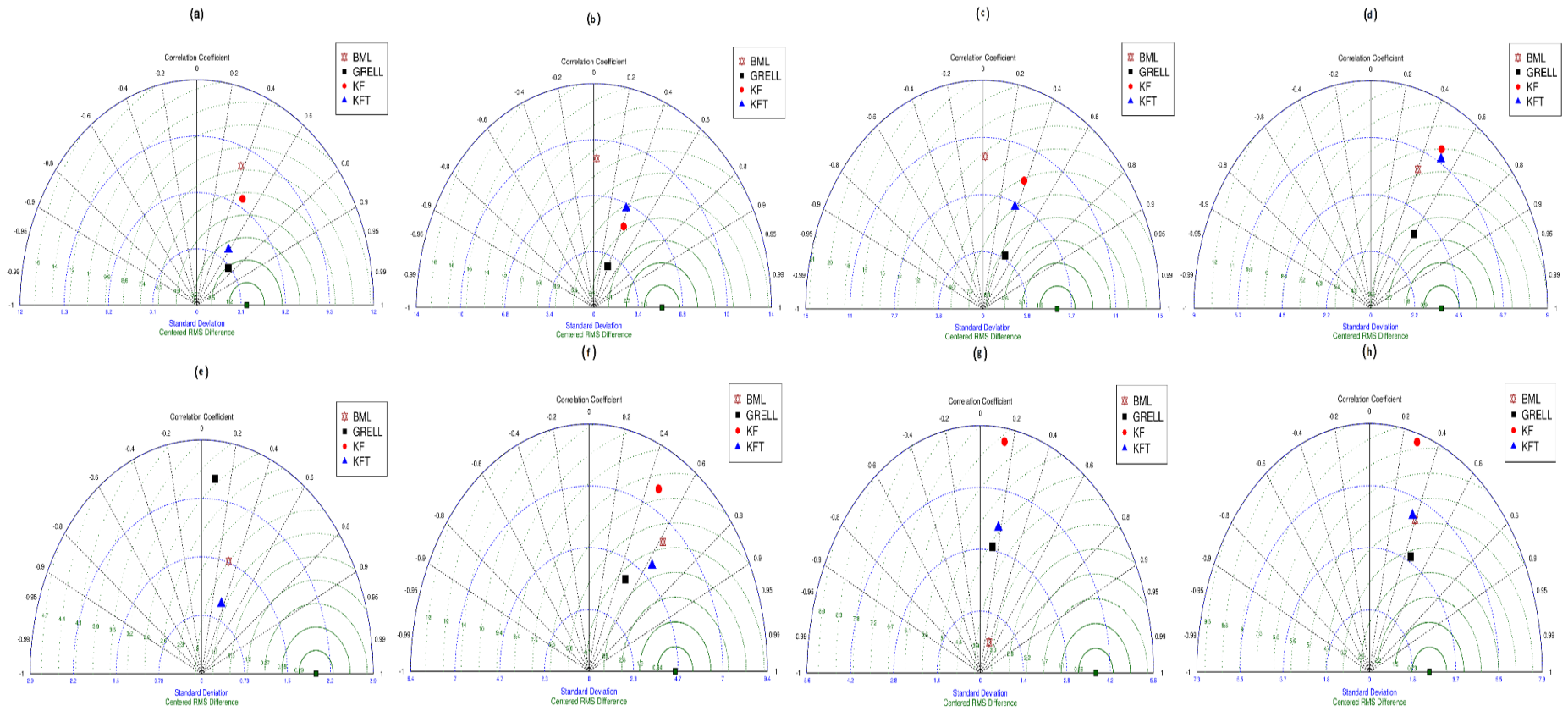

Figure 40: Taylor diagram displaying statistical comparison of seasonal mean rainfall for BML (brown), GRELL (black), KF(red) and KFT(blue) with observations over (a) NEA (b) SEA (c) CEA (d) LVB sub-domains during the MAM season and (e) NEA (f) SEA (g) CEA and (h) LVB sub-domains during the OND season. The blue and green curves represent standard deviation (SD) and root mean square differences (RMSD) respectively for the composite of dry years

The KF and GRELL schemes are known to have a dipole effect, where KF is associated with wetness and GRELL is associated with dryness, the BML having compensating effect between the KF and GRELL (Pohl *et al.,* 2011). The GRELL and KF schemes are suitable for use over the EA region due to moisture convergence emanating from the Indian Ocean and the Congo basin at lower levels. To this extent, the simulation using the KF scheme were satisfactory for studying the rainfall characteristics over the region; with additive effects found when trigger function is used. The suitability of the GRELL scheme was clearly manifested during dry years. Again the study found the KF scheme to outscore all the rest of the CPS.

From the above analyses, the CPSs can be classified into two main categories. The first category as those favoring wetter rainfall conditions, more NRD, light intensity and less frequency. The second category is those favoring drier rainfall conditions, less NRD, heavy rainfall intensity. The KF and GRELL CPSs fall into the first and second category respectively. The BML simulations are between KF and GRELL CPSs.

The observed rainfall biases, NRD and the associated IRD in the CPSs result into a weaker reproducibility nature of seasonal rainfall characteristics around the mountainous areas and the vicinity of the ITCZ (Vanvyve *et al.,* 2008). The CPSs reproduced the east-west rainfall gradient driven by the large-scale systems like the ITCZ during both the MAM and OND seasons. The trigger function in the KFT scheme certainly brings in additive effects by lowering the biases in the KF scheme. The drier years were better simulated than wetter years. This is partly due to the sensitivity of the CPSs to the strong thermal forcing during drier years.

Rainfall characteristics including the spatio-temporal variability patterns of daily rainfall have been found to be better reproduced during drier years than wetter years (Crétat *et al.,* 2011; Crétat and Pohl 2012, 2015). These findings therefore agree with the previous researchers. The WRF model tends to simulate wetter (drier) conditions mostly related to more(less) rainfall frequent over the equatorial region. More rainfall of light category (1-10mm/day) frequented the region and was consistently overestimated in the CPSs. On the other hand, heavy rainfall exceeding 20mm/day frequented the region less and was well reproduced by the CPSs. It could be deduced that the rainfall intensity contributes less to the mean rainfall. Studies by Tennant and Hewitson (2002) over South Africa reported that a season with a high total rainfall generally has a higher number of heavy rain days and not necessarily an increase in light rain days.

The wettest biases and rainfall overestimation in the KF and the driest biases and underestimation of rainfall in the GRELL and BML schemes have been previously reported by (Ratna *et al.*, 2013; Pohl *et al.*, 2014). The biases were found to stem from atmospheric conditions that were too unstable and large moisture convergence advected from the tropics (Ratna *et al.*, 2013). Based on the analyses of mean rainfall patterns, the error analyses, and the analyses of rainfall characteristics, it was concluded with certainty that the KF scheme is suitable for reproducing rainfall characteristics over the equatorial region. The GRELL scheme is mostly suitable for studying rainfall characteristics during dry years.

5.4 Establishment of the circulation features associated with the various convective schemes

The second objective aimed at establishing the skill of the four CPSs in reproducing the circulation features and atmospheric dynamics. The quantities analyzed were; vertically inter-grated moisture flux (VIMF), upper level divergence/convergence, omega analyses and convective available potential energy (CAPE).

5.4.1 The Vertically Integrated Moisture Flux

The results for VIMF patterns observed during the wet and dry years were presented here for both the MAM and OND seasons. Figures 41 and 42 show the integrated moisture flux during the MAM and OND seasons for the wet and dry years, respectively.

During the MAM season, there was enhanced moisture transport into East Africa region from the southeast Indian Ocean in GRELL CPS as illustrated Figure 41a. For the BML, KF and KFT schemes, strong moisture transport was observed over the northeastern Indian Ocean and Arabian high regions as was illustrated in Figures 41c, 41e and 41g. Regions of moisture convergence were seen over parts of the Congo region, southern parts of the region and around the northern parts of Ethiopia in all the CPSs. Over the Indian Ocean, there was no convergence of moisture (divergence), a weak cyclonic circulation characterized the central parts of the Indian Ocean. In the KF and KFT CPSs, enhanced moisture convergence could be seen around the Congo region and the western parts of Ethiopia (Figure 41c and d). During the OND season (Figure 42), strong moisture transport was observed around Equatorial region from the Indian Ocean in all the CPSs (Figure 42a, b, c and d).

Although the CPS moisture flux and convergence were somehow similar, they showed quantitative differences in both the moisture flux, and convergence/divergence biases.

The regions that had positive biases in VIMF convergence and divergence coincided with regions of positive and negative rainfall biases (Figures 14,15,16 and 17) as was simulated by the KF scheme. The moisture flux bias showed enhanced VIMF being transported to the southern parts of the Indian Ocean and northern parts into western parts of the equatorial region. This has the potential to generate wetter rainfall conditions over the same areas.

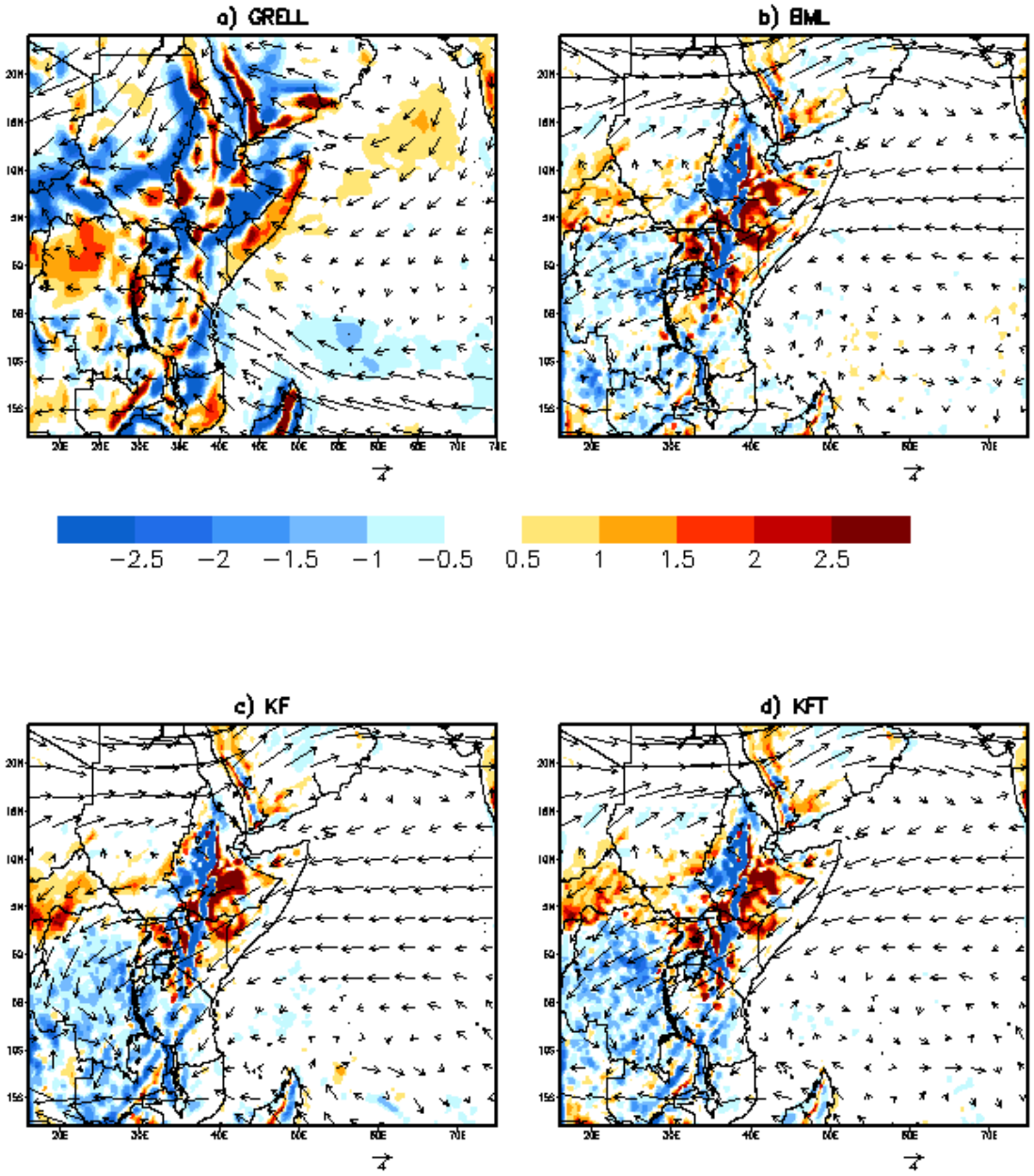

Figure 41: Spatial patterns of vertically Integrated moisture convergence and divergence (from 850 to 300 hPa) and the associated differences (x 10^3) (shaded) and moisture fluxes (arrows) from (a) GRELL (b) BML (c) KF and (d) KFT convective schemes for the composite of wet years(1989,1998 and 2012) during the MAM season. The differences were calculated with respect to ERA interim reanalysis. The orange and blue shading denotes positive and negative values representing areas of moisture divergence and convergence respectively.

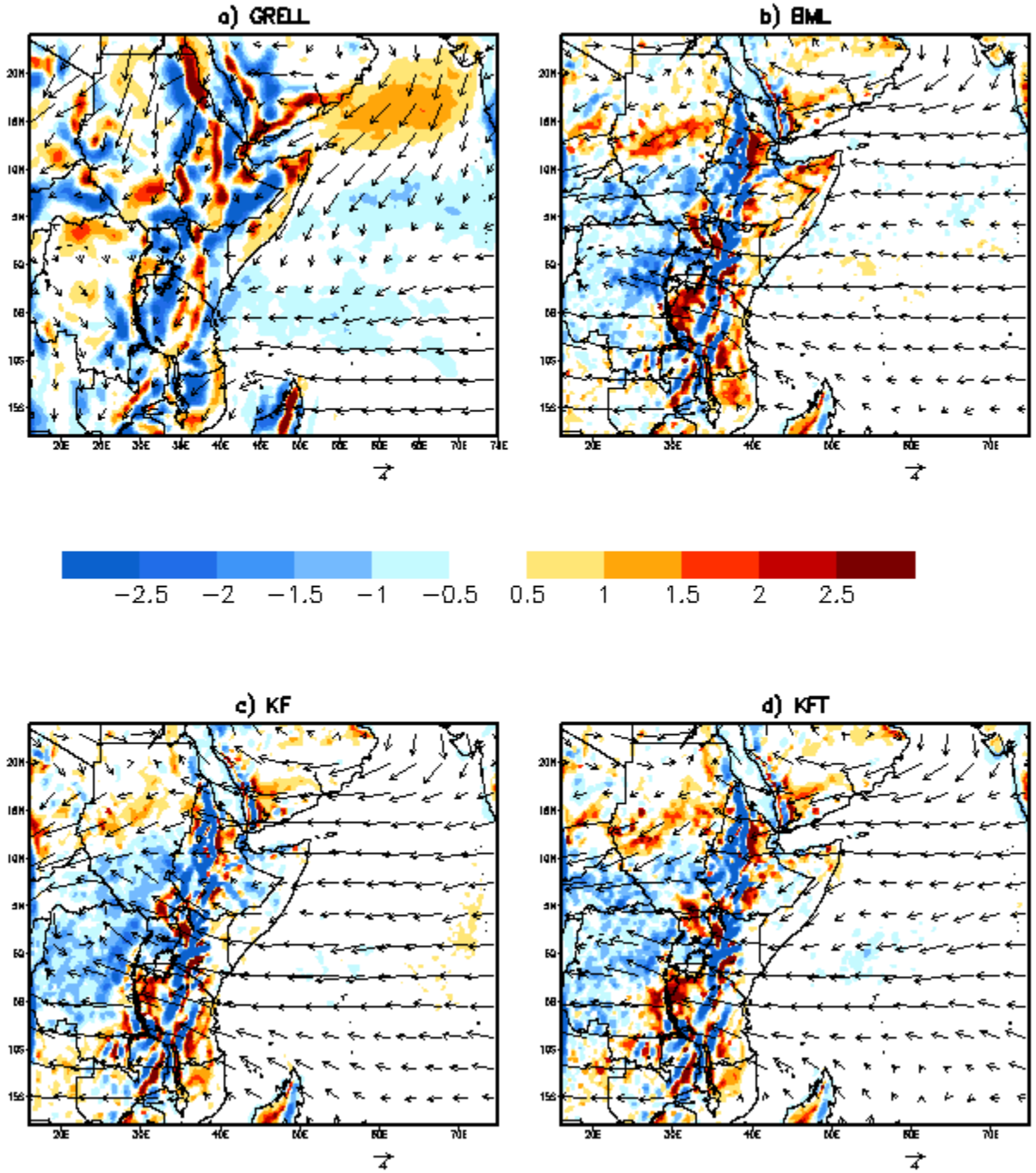

Figure 42: Spatial patterns of vertically Integrated moisture convergence and divergence (from 850 to 300 hPa) and the associated differences (x 10^3) (shaded) and moisture fluxes (arrows) from (a) GRELL (b) BML (c) KF and (d) KFT convective schemes for the composite of wet years(1997, 2006 and 2015) during the OND season. The differences were calculated with respect to ERA interim reanalysis. The orange and blue shading denotes positive and negative values representing areas of moisture divergence and convergence respectively.

The GRELL CPS moisture flux bias was found to have an outflow of moisture over the western parts of the region, resulting in a negative moisture flux convergence that generates less rainfall over the regions. The moisture transport during the OND season (Figure 41 and 42), was more enhanced around the Congo basin in nearly all the CPS. A weak cyclonic flow develops in GRELL scheme (Figure 40a) over Indian Ocean. A moderate easterly flow over the Indian Ocean were observed in the KFT scheme, while enhanced easterly moisture transport were common in the KF CPS (Figure 41 and 42c, d). For rainfall to be sustained, moisture transport has to be steady. The convergence was enhanced over the land than the ocean.

For the case of dry years, there was a weak moisture convergence over the entire region as was depicted in Figure 43 for both MAM and OND season. The KF and KFT schemes, however, experienced more enhanced moisture convergence around the Congo basin during OND season (Figure 44c and d). The GRELL and BML moisture transport were weaker. The seasons were riddled with weak moisture flows and convergence in GRELL and BML CPSs. To this extent, it could be deduced that part of the reason why KF and GRELL CPSs generated too many or fewer NRD was related to the enhanced moisture transport. The differences in the moisture convergence/divergence corresponded well with those from rainfall.

Over the Congo region, the moisture transport was away from the Equatorial region, cutting the supply of moisture into the region. As had earlier been reported by Segele *et al.* (2009) and Philipon and Camberlin (2002), near the tip of the Horn of Africa, north easterlies are enhanced in conjunction with anomalous high-pressure cells that develops over the Arabian Sea region. These northeasterly winds advect moist air toward the Ethiopian highlands and this by extension impact the East Africa rainfall regimes. From the analysis of moisture and circulation, it was evident that the rainfall biases employ a strong relationship with the moisture flux and the convergence and divergence. The inability of the WRF model using the CPSs to correctly simulate the large-scale flow patterns and or changes in the sea surface temperatures over the key moisture sources could have contributed to the simulated moisture flux biases. Such inadequacy in the RCMs had been earlier reported by Yang *et al.* (2015). Secondly, the domain not covering much of Indian Ocean to the west and Congo region could have contributed to the observed moisture flux biases.

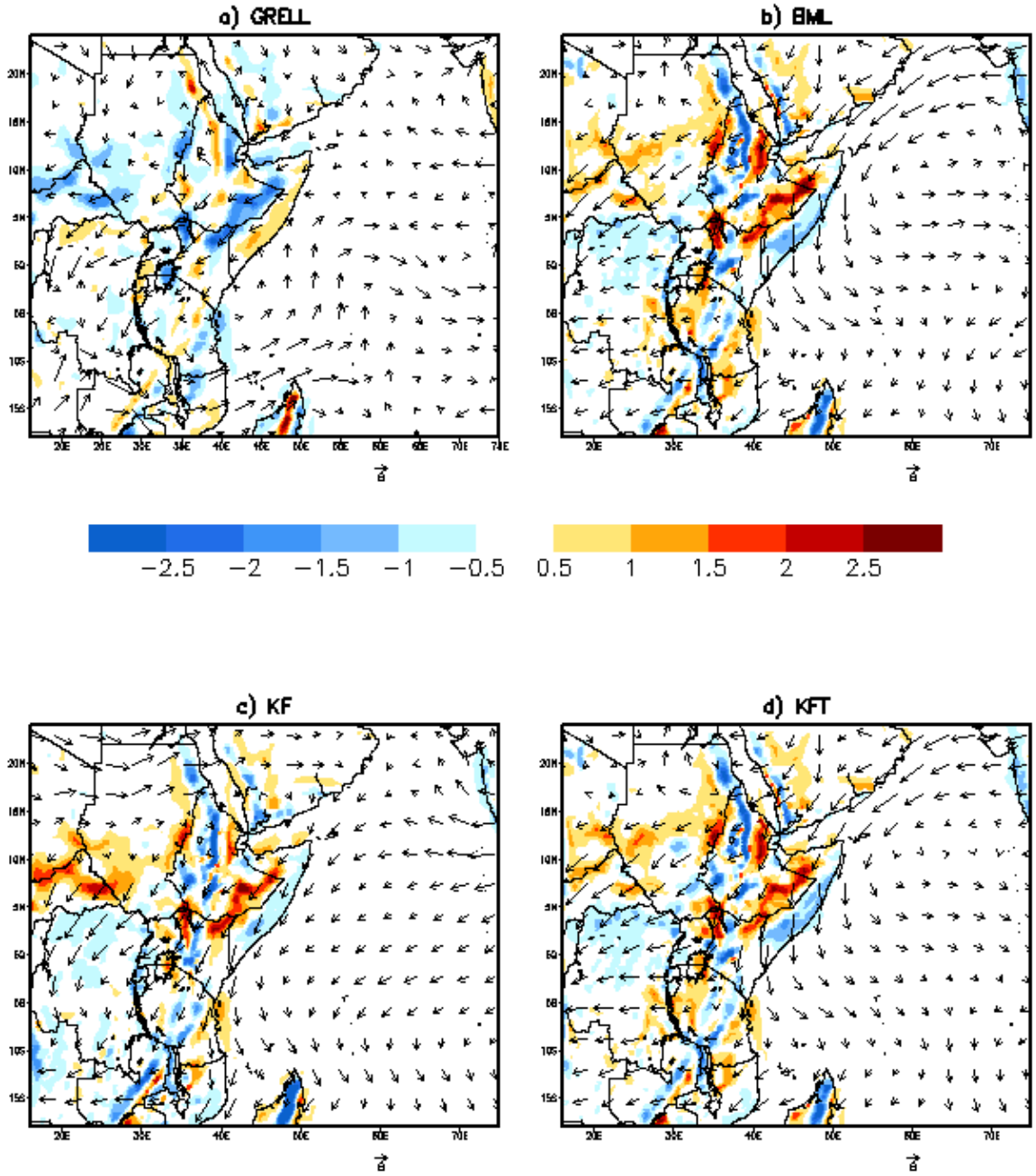

Figure 43: Spatial patterns of vertically Integrated moisture convergence and divergence (from 850 to 300 hPa) and the associated differences (x 10^3) (shaded) and moisture fluxes (arrows) from (a) GRELL (b) BML (c) KF and (d) KFT cumulus schemes for the composite of dry years(1984, 2000 and 2008) during the MAM season. The differences were calculated

with respect to ERA interim reanalysis. The orange and blue shading denotes positive and negative values representing areas of moisture divergence and convergence respectively.

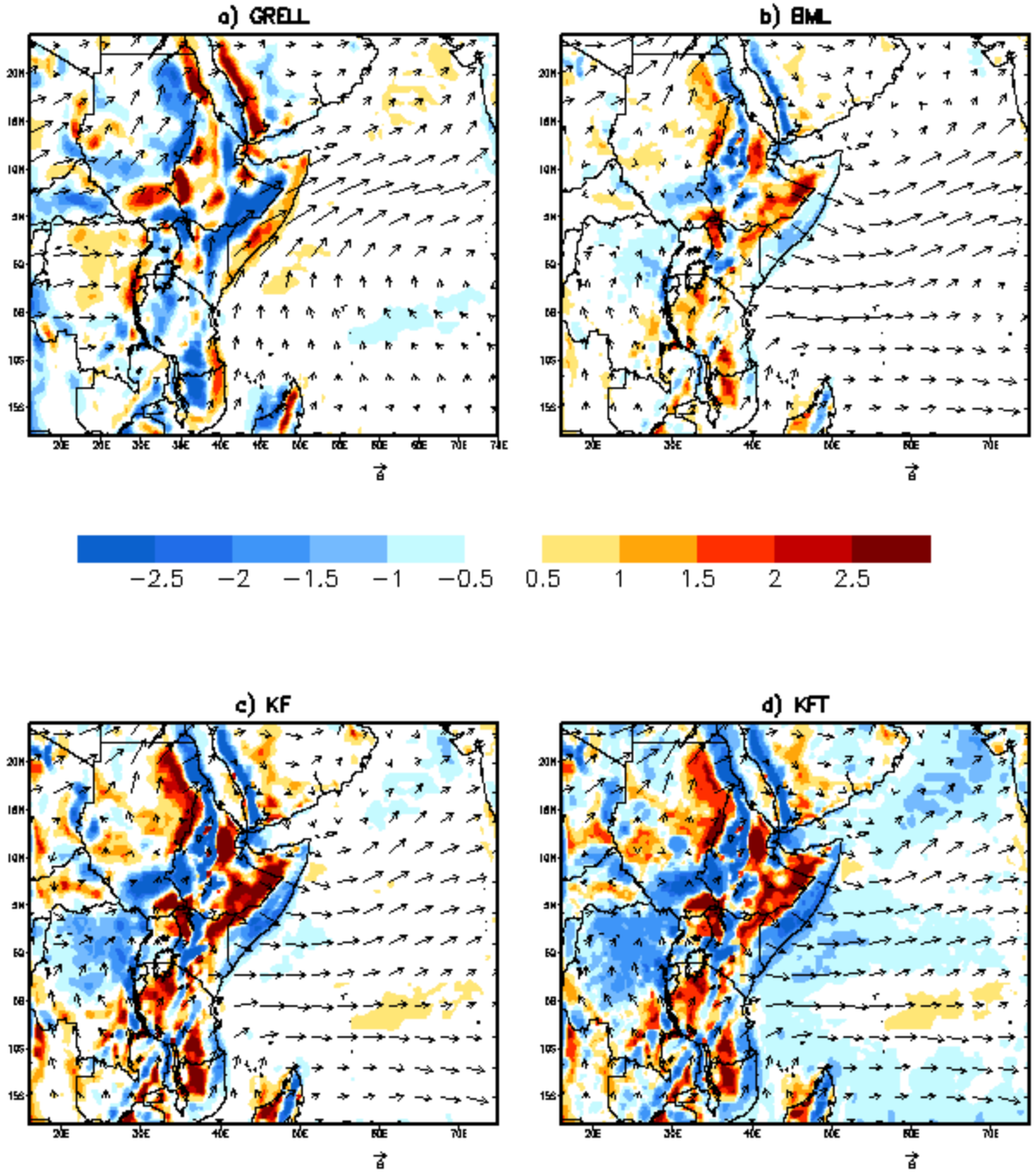

Figure 44: Spatial patterns of vertically Integrated moisture convergence and divergence (from 850 to 300 hPa) and the associated differences (x 10^3) (shaded) and moisture fluxes (arrows) from (a) GRELL (b) BML (c) KF and (d) KFT cumulus schemes for the composite of dry years(1988, 2007 and 2010) during the OND season. The differences were calculated with respect to ERA interim reanalysis. The orange and blue shading denotes positive and negative values representing areas of moisture divergence and convergence respectively.

It may be assumed that the deficiency in rainfall over EA can be as a result of lack/weak moisture transport agent, obstruction by the mountains within the region and also wrong alignment of circulation patterns. The study by Okoola (1999) reported that, the reduced frequency of lower tropospheric westerly winds is due to the barrier effect of the north–south mountain chains which allow only the most intense westerly winds to cross the mountains into the EA region.

The easterly moisture transport evidently contributes to the rainfall cycles of the EA region characterized by cyclonic activities over the highlands in the northern parts of Madagascar. This was corroborated by the steady easterly flow and development of cyclonic activity over northern Madagascar and along the EA coasts during the OND and MAM seasons. These were best replicated in the KF and GRELL schemes. Similar findings had been reported by Chen *et al.* (2010). The easterly moisture flux during wet years over the tropical Indian Ocean has been found to contribute to moisture advection towards EA and to favor moist convective processes (Cretat *et al.*, 2011). Although noisy, the moisture convergence biases were larger over landmass as well as over parts of the nearby Indian Ocean, corroborating the observed larger rainfall biases noted over many parts of East Africa. From the analyses of VIMF, it may be concluded that GRELL and KFT schemes reproduced moisture fluxes and circulations best during both wet and dry years.

5.4.2 Deep Convection associated with rainfall biases

The analyses were extended on the deep convection over the region during the widespread wet and dry years. As proxies to deep convection, we analyzed the horizontal mass fluxes (wind) at 200hPa, together with their divergence (interpreted as large-scale conditions favoring deep ascents), and omega at 500hPa (the mass center of the air column, in the free atmosphere above the PBL), Cook (1999). The horizontal wind fields and the divergence at the 200hpa pressure level were utilized. Figures 45 and 46 show the horizontal mass flux and divergence during the MAM and OND seasons for the composite of wet years.

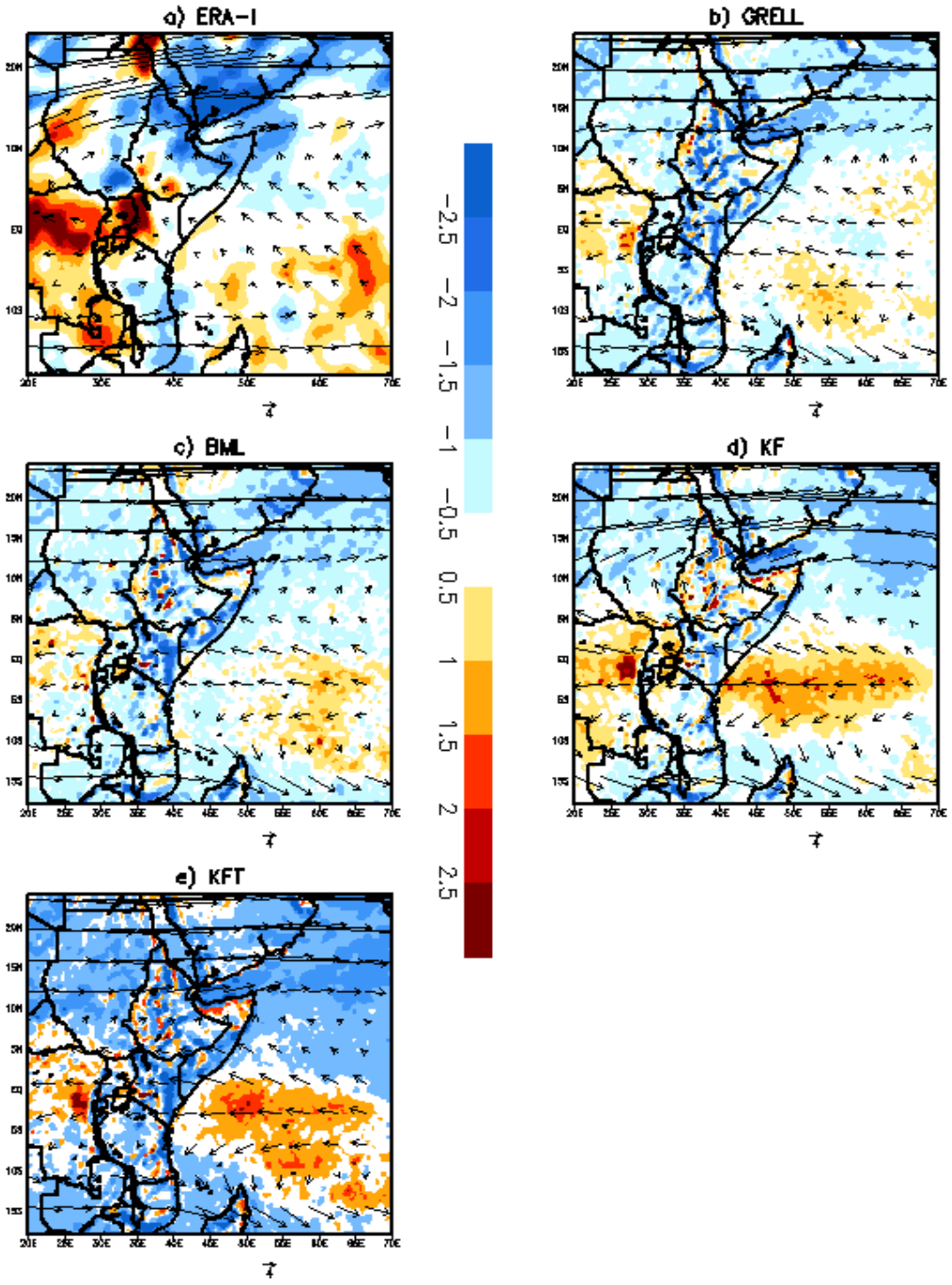

Figure 45: Horizontal mass fluxes (vectors) and upper level divergence (shaded, $\times 10^4\ s^{-1}$) at the 200hpa for the composite of wet years (1989, 1998 and 2012) during the MAM season. The orange and blue shadings denote positive and negative values representing areas of moisture divergence and convergence, respectively.

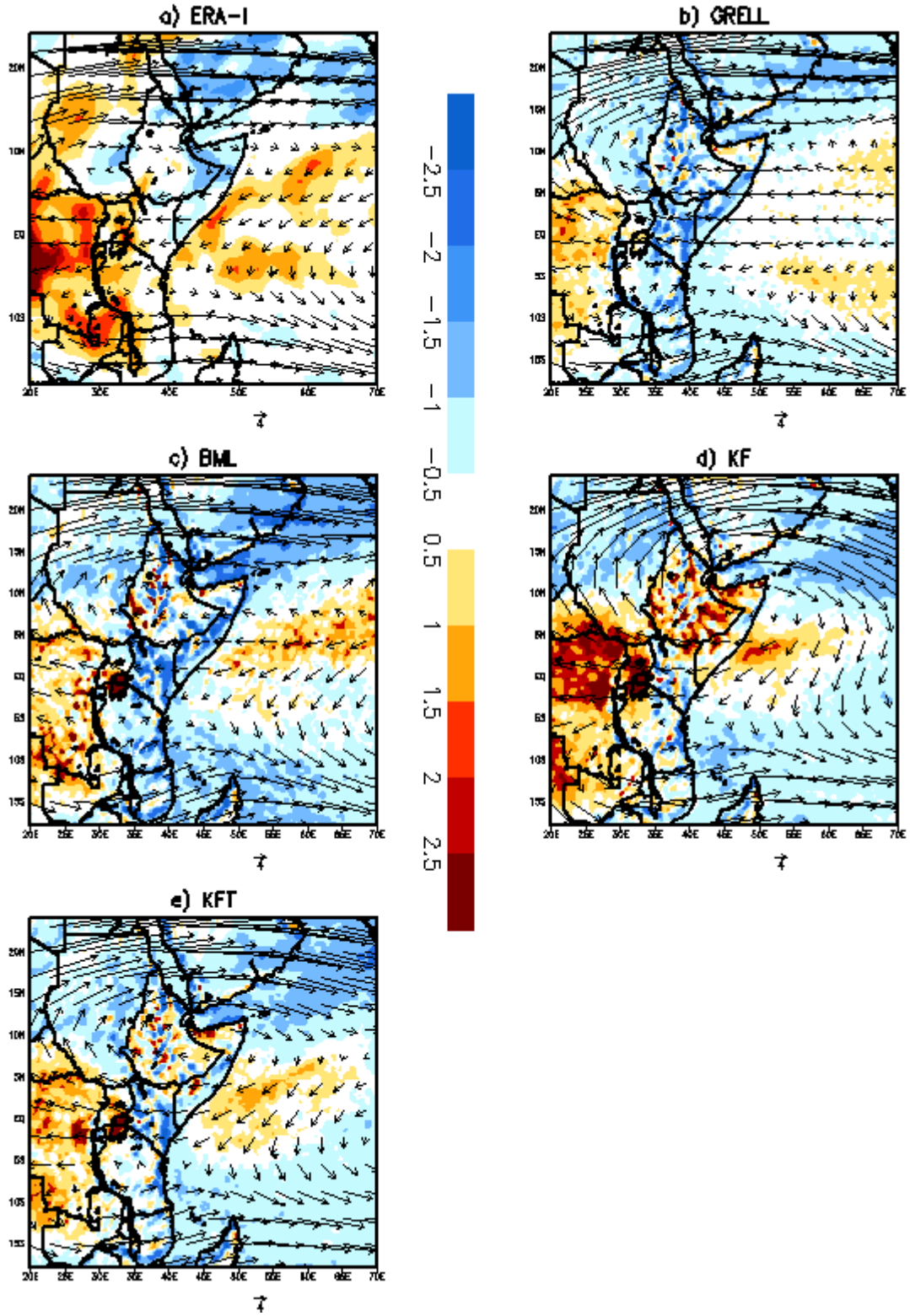

Figure 46: Horizontal mass fluxes (vectors) and upper level divergence (shaded, $\times 10^4\ s^{-1}$) at the 200hpa for the composite of wet years (1997, 2006 and 2015) during the OND season. The orange and blue shadings denote positive and negative values representing areas of moisture divergence and convergence, respectively.

During the wet years for the MAM season (Figure 45), the divergence was weaker in all the CPSs over the western parts of the region and the eastern parts of the Indian Ocean comparatively. The moisture convergence (negative divergence) was stronger over the northern parts of the region around the Arabian high. This suggests that the areas that experienced divergence at upper levels (200hPa), experienced low level (850hPa) convergence and vice-versa; this is referred to as dines compensation law (Wiin-Nielsen 1973). The GRELL and BML CPSs underestimated the divergence and convergence observed in the ERA-interim (Figures 45b and c) but reproduced fairly the circulation pattern. Although, the KF and KFT CPSs overestimated the magnitude of divergence/convergence, they fairly reproduced the regions of divergence/convergence as was illustrated in Figure 45d and 45e.

During the OND season, the divergence was more enhanced in ERA-interim reanalysis but weakly reproduced in all the CPSs except KF scheme, as was shown in Figures 46a, b, c and d. The CPSs reproduced the divergence/convergence patterns correctly, however, the wind flow and direction were poorly represented.

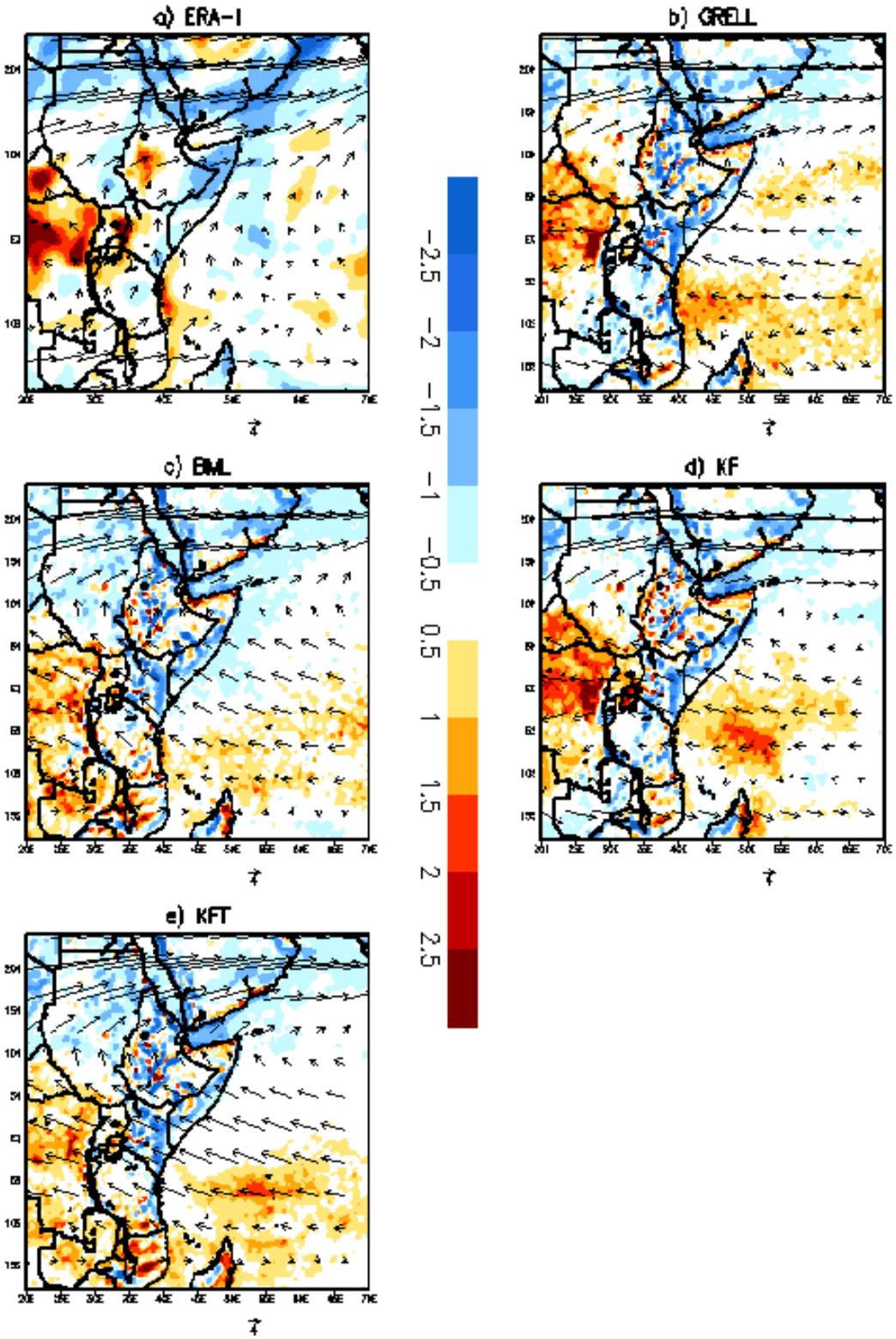

Figure 47: Horizontal mass fluxes (vectors) and upper level divergence (shaded, $\times 10^4\ s^{-1}$) at the 200hpa for the composite of dry years (1984, 2000 and 2008) during the MAM season. The orange and blue shadings denote positive and negative values representing areas of moisture divergence and convergence, respectively.

For the dry years during the MAM season (Figure 47), strong divergences over the western parts of the region and weak divergence over the Indian Ocean were observed in the ERA-Interim re-analysis and the CPSs (Figure 47a, b, c, d and e). However, the CPSs had a bias towards generating the divergences over the Indian Ocean.

The GRELL portrayed a weak easterly flow into the equatorial region (Figure 47b). The BML and KF schemes reasonably simulated the easterly wind patterns; the KFT scheme overestimated the wind speed but located the correct regions under divergence (Figures 47b, c, d, and e). The divergent of easterly flow along the equator was poorly developed.

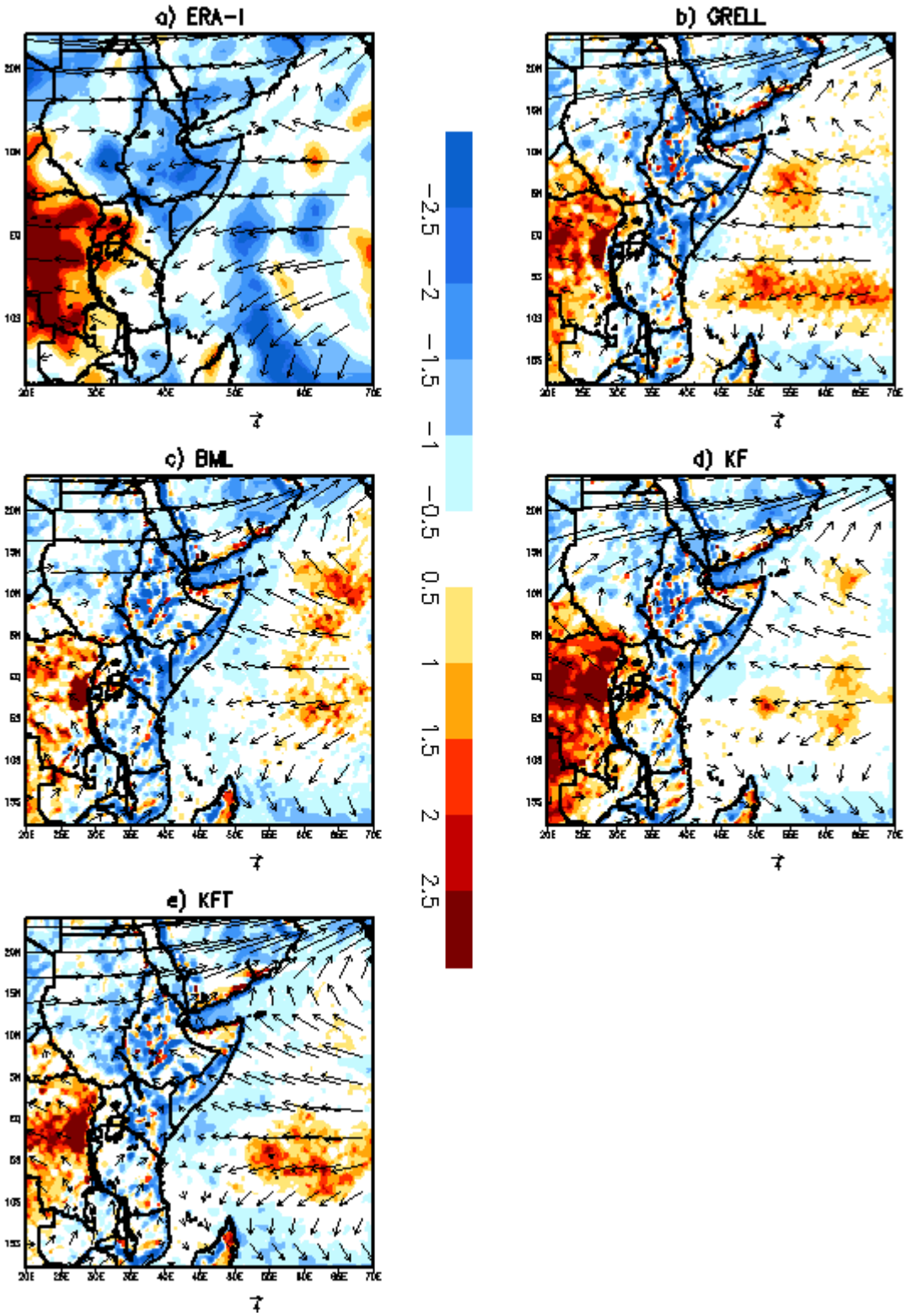

Figure 48: Horizontal mass fluxes (vectors) and upper level divergence (shaded, $\times 10^4\ s^{-1}$) at the 200hpa for the composite of dry years (1988, 2007 and 2010) during the OND season. The orange and blue shadings denote positive and negative values representing areas of moisture divergence and convergence, respectively

The results for the OND dry years (Figure 48) revealed similar divergent and convergent patterns. Generally, the wet years were found to be associated with intensification of the upper level divergence and strong easterlies flow into the equatorial region, while dry years were associated with weakening of the upper level divergence especially over the Indian Ocean and the Congo region.

The stronger westerly winds during the wet years were seen to promote the ascent of warm air by enhancing the circulation along the equatorial African coasts and surface convergence. The intensification of the westerly flow displaces the ITCZ northward and intensifies the convergence associated with it. The ascending motion associated with the ITCZ sinks into the tropical rain belt contributing to its intensification. The areas under divergence/convergence biases corresponded well with areas of low and high rainfall amount (Figures 14 and 15). From the analyses of horizontal mass fluxes and the associated divergence, it was evident that all the CPSs fairly reproduced the observed divergences/convergences and the associated circulation regimes.

5.4.3 Vertical Velocity in Pressure Coordinates

It was imperative to investigate how rainfall biases under various rainfall characteristics (Section 5.4.3) are associated with biases in vertical velocity (omega). The Figures 49 and 50 show omega differences between ERA-Interim and the CPSs during the MAM and OND seasons respectively for the composite of wet years. During the MAM season (Figure 49a and b), there was more sinking of air in the schemes compared to the re-analysis around the central and eastern parts of Kenya and Southern parts of Tanzania. Over the western parts of equatorial region and Congo region, there was stronger ascent in the schemes than in the reanalysis. The ascent over the Indian Ocean and Congo region was even enhanced during the OND season for the wet years (Figures 50).

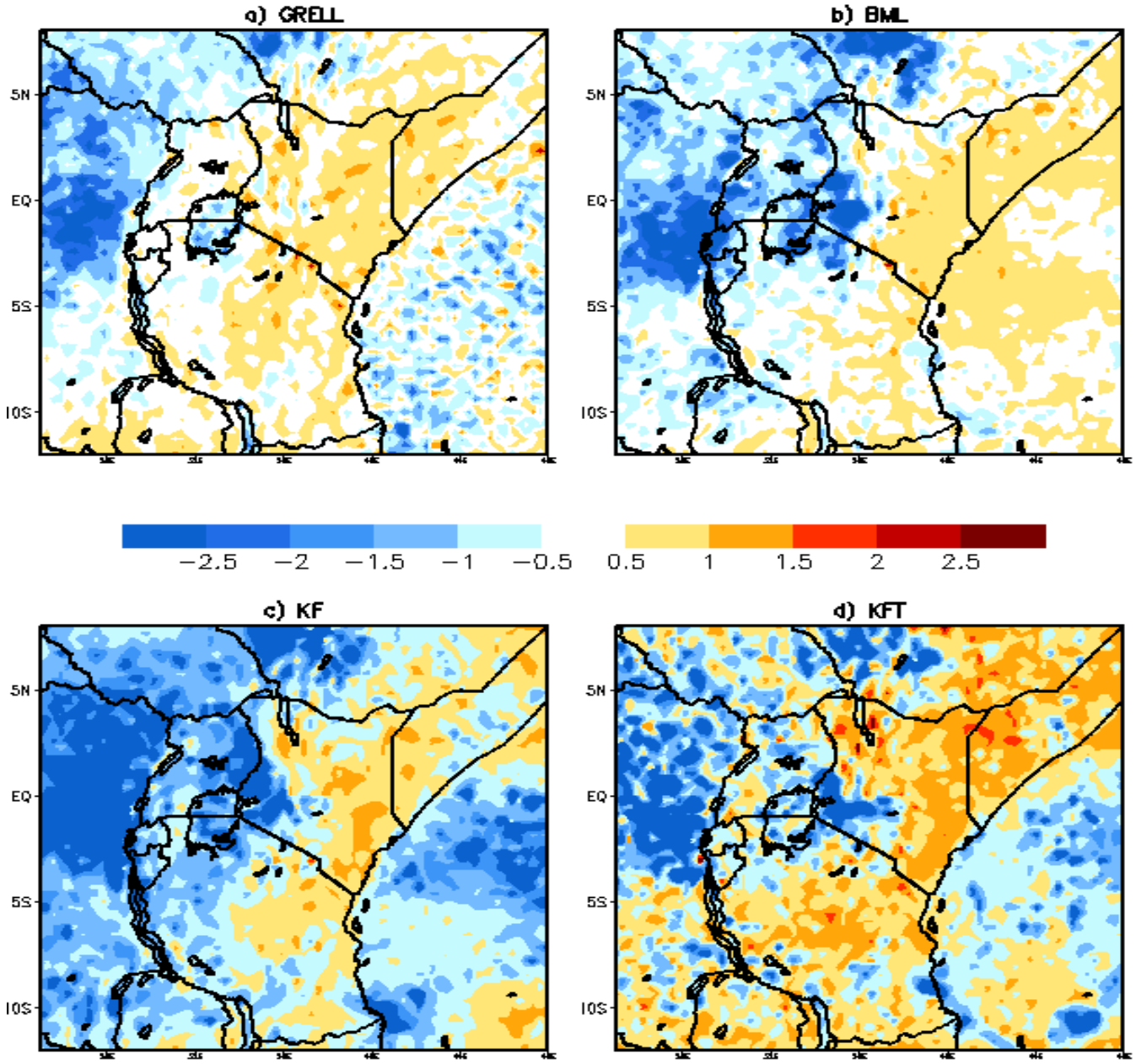

Figure 49: The omega (x10^2 Pa s^{-1}) differences between the cumulus schemes and ERA-I during MAM season (1989, 1998 and 2012) for composite of wet years. The negative (positive) values of ω are associated with upward (downward) motion. The orange shading indicates reduced uplift in the model compared with the reanalysis and blue enhanced uplift.

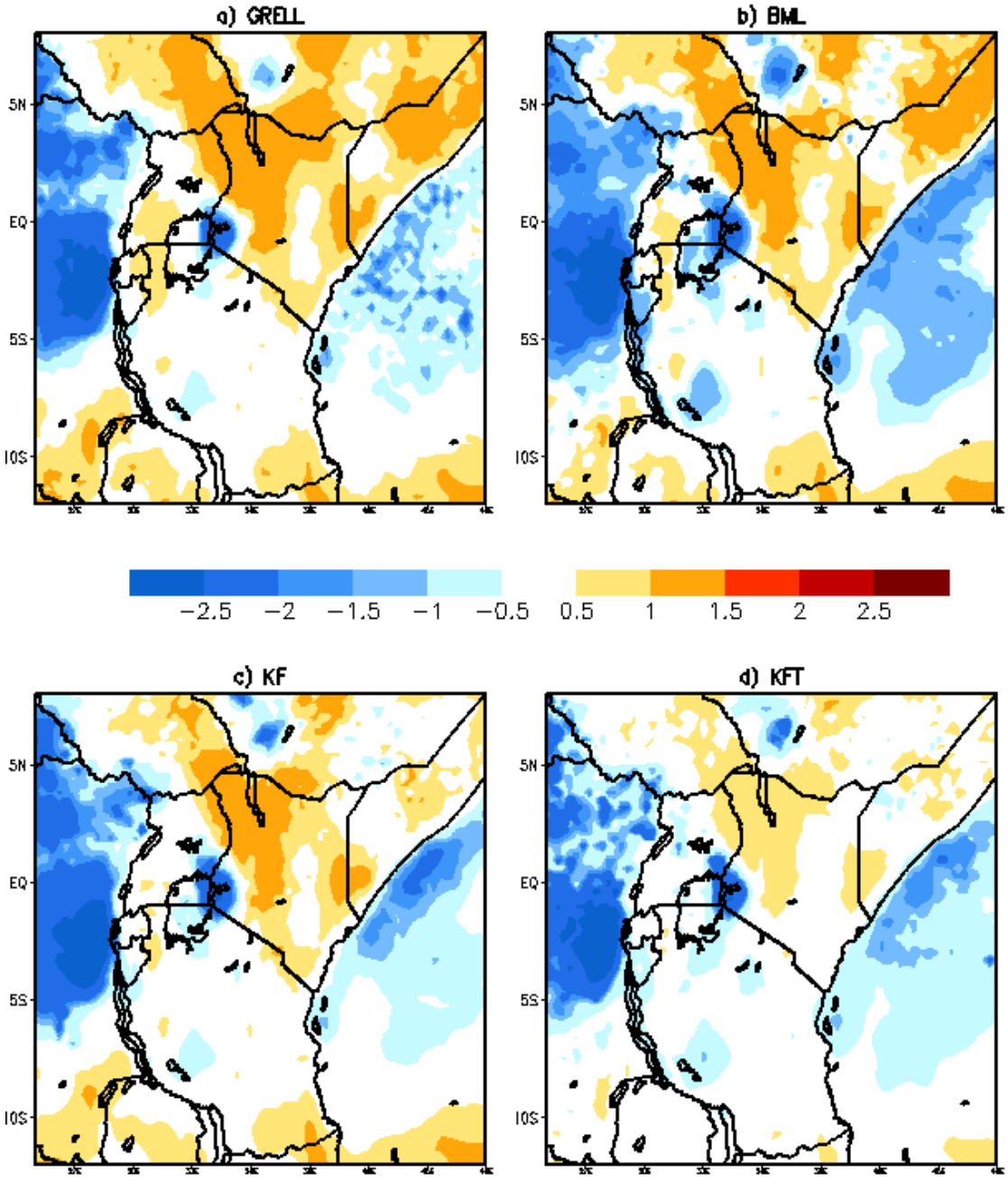

Figure 50: The omega (x10^2 Pa s^{-1}) differences between the cumulus schemes and ERA-I during the OND season (1997, 2006 and 2015) for composite of wet years. The negative (positive) values of ω are associated with upward (downward) motion. The orange shading indicates reduced uplift in the model compared with the reanalysis and blue indicates enhanced uplift.

For the dry years (Figures 51 and 52), there was more enhanced ascent over the western and Indian ocean in the CPSs than in the ERA-interim reanalysis.

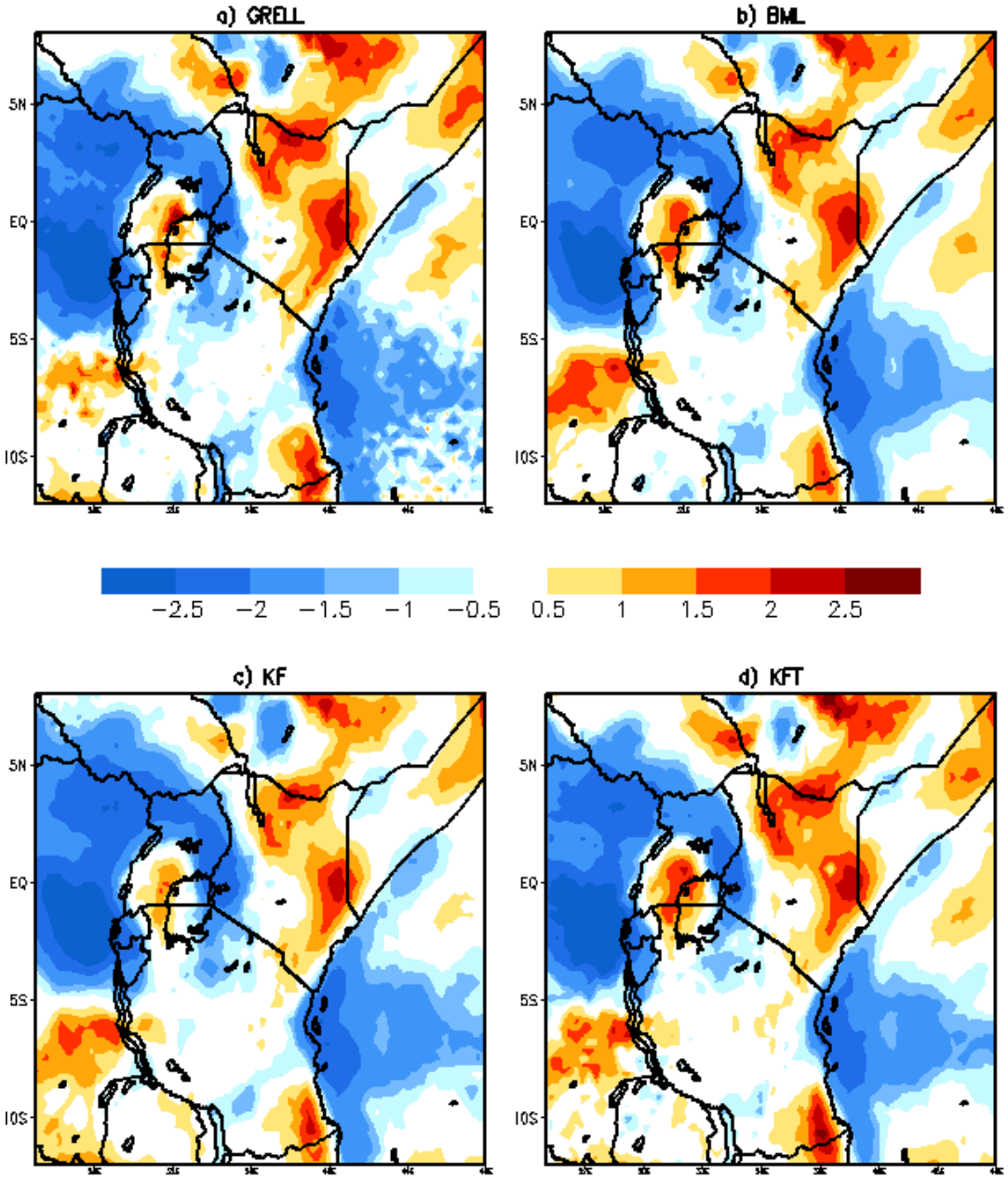

Figure 51: The omega (x10^2 Pa s^{-1}) differences between the cumulus schemes and ERA-I during the MAM season for the composite of dry years (1984, 2000 and 2008). The negative (positive) values of ω are associated with upward (downward) motion. The orange shading indicates reduced uplift in the model compared with the reanalysis and blue enhanced uplift.

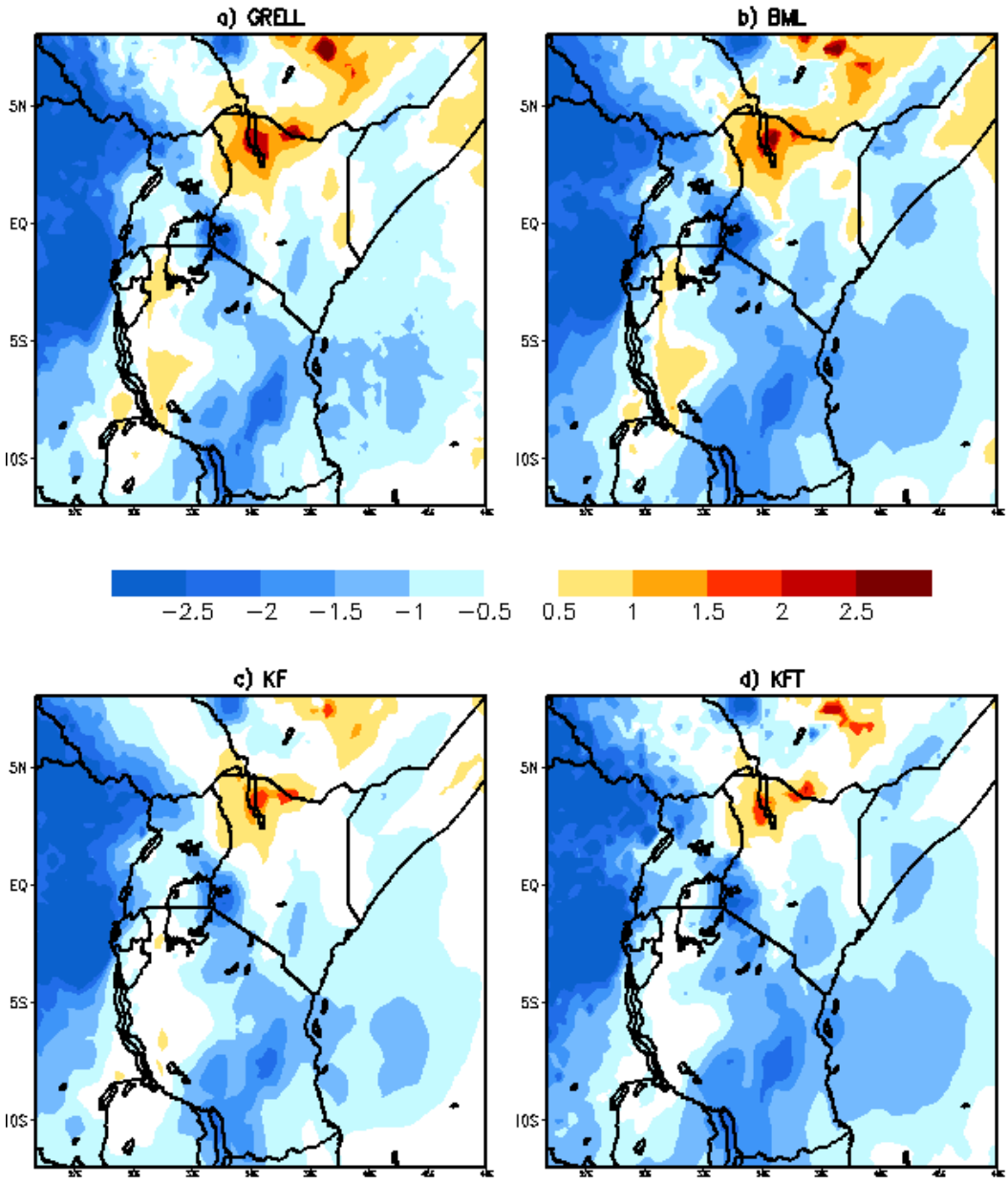

Figure 52: The omega (x10^2 Pa s^{-1}) differences between the cumulus schemes and ERA-I during the OND season for composite of dry years (1988, 2007 and 2010). The negative (positive) values of ω are associated with upward (downward) motion. The orange shading indicates reduced uplift in the model compared with the reanalysis and blue enhanced uplift.

The omega and rainfall biases did not match exactly but meaningful deductions could be drawn from the analyses. For example, in the previous section (Section 5.4.3), wet (dry) rainfall biases of rainfall were confined to the western (eastern) parts of equatorial region, over these locations

there were sinking (rising) of air. A salient feature of strong rising air was found over the Kenya highlands. The rising of air was pronounced over the western equatorial parts of the region and the Indian Ocean. For dry years, there were more sinking of air than rising over Indian Ocean, Congo and equatorial parts of the region. The southern parts of Tanzania were dominated by rising motion. This is true since the dry years were observed to be deficient of moisture and transport mechanism (Section 5.5.1).

The convective processes that results into rainfall activity are activated when there is uplift to create a region of low pressure. The CPSs largely were able to simulate the migration of tropical convection due to the ITCZ. The maximum uplift occurred over much of the eastern parts of equatorial region, and in the southern parts of equator. The chief moisture sources over the equator (Congo region and Indian Ocean) were riddled by the maximum ascent.

This suggests that WRF model generate overly strong convection overland and tropical oceans, a deviation from the recent work by Johnson *et al*. (2017) who reported that regional climate models generate strong convection over Indian Ocean than land although their studies used different RCMs from the one under the current study. The dry years were dominated by descent while the wet years were characterized by ascent. This could be associated with the complex topography over the region (Mutemi *et al.,* 2007; Ogwang *et al.,* 2015a).

It can be reported that the simulated rainfall biases were associated with low level divergence (sinking) and upper level convergence (rising of air), a finding that largely agreed with previous work by Ogwang *et al.* (2015b). The recent study by James *et al.* (2017) reported that over tropical Africa, the areas with too much or too little precipitation are related to the vertical rising/sinking of air. It may be concluded from the results of vertical velocity (omega) that KF and GRELL CPSs were more robust in representing the vertical circulations features and the associated divergence and convergences.

5.4.4 Atmospheric Convective Instability

To establish atmospheric convective stability, CAPE was used as a proxy to convection. The figures 53 and 54 show the analyses of CAPE for the composite of wet and dry years respectively. The estimated CAPE values from ERA-interim were above 100J/kg over the western parts of the region and below 40J/kg over the eastern parts of Kenya, central and southern parts of the region

during wet years. The MAM season had sustained large CAPE values above (100 J kg^{-1}) confined within the equatorial belt (5°S-5°N) throughout the season. During the OND season (Figure 53, bottom); convection was more intense and confined within the equatorial region in KF and KFT schemes and slightly weaker in GRELL and BML CPSs (Figure 53). |For the dry years, CAPE values were below 70 J kg^{-1} both for MAM and OND seasons as was displayed in Figure 54. The GRELL and KF scheme generated the highest level of instability (large and low CAPE values). This seemed to produce highly convective unstable atmosphere. This could have triggered the simulation of the wettest and driest rainfall biases over the EA region (Section 5.4.3).

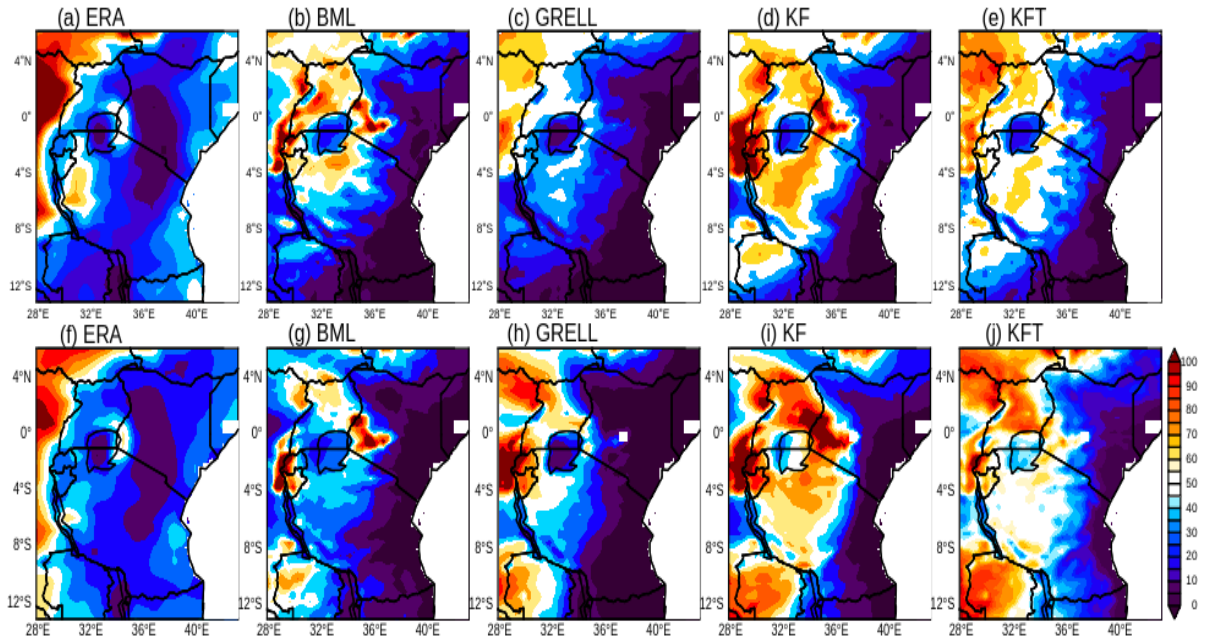

Figure 53: The estimated Available Potential Energy (CAPE) (J/kg), values from cumulus schemes and ERA interim during MAM (top) and OND (bottom) panels for composite of wet years.

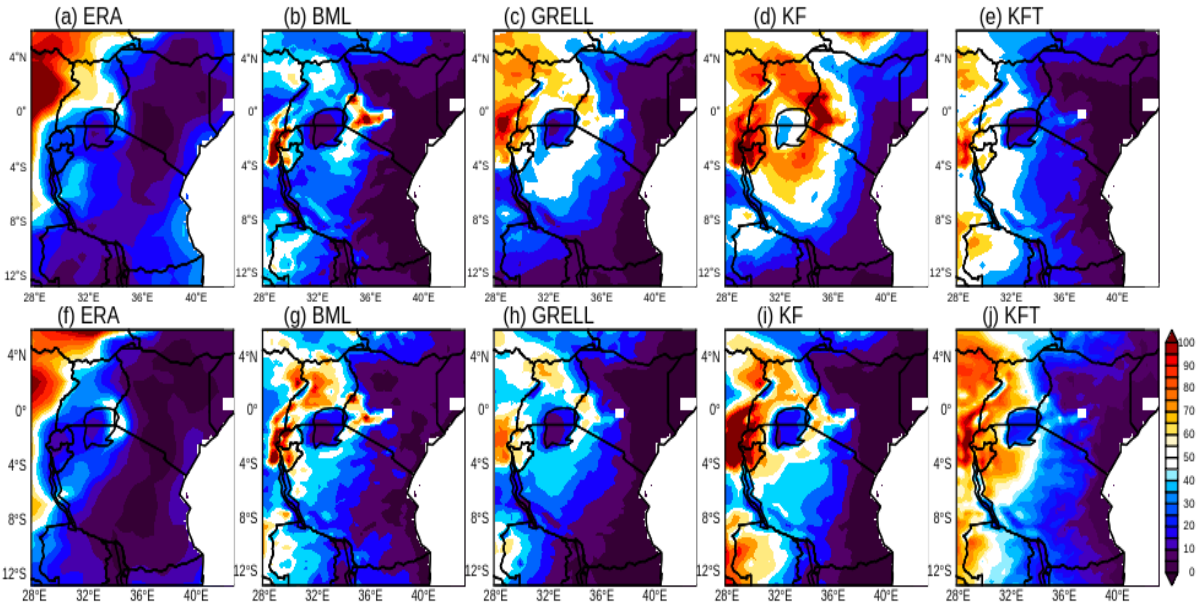

Figure 54: The estimated Available Potential Energy (CAPE) (J/kg), values from cumulus schemes and ERA interim during MAM (top) and OND (bottom) panels for composite of dry years.

The analyses of the CAPE have shown that due to strong instability, the model reproduces too many rainy days and wetter conditions. Although the differences between individual CPSs in terms of CAPE were not distinct, the KF and GRELL produced large and small values of CAPE resulting to wetter and drier conditions they simulated respectively. Based on the analyses of CAPE, the Kain-Fritsch scheme provided better characteristics of atmospheric convective stability.

The mean rainfall have a direct link to the atmospheric circulations and dynamics. The KF and GRELL CPSs were consistent in their atmospheric simulations and provided clear response to the rainfall conditions. The Betts Miller simulations were not quite consistent and were seen as convection inhibitor (Pohl *et al.,* 2011). The strong VIMF to the western sides of the domain corresponded well to the areas under high rainfall, high NRD and low Intensity. The upper level divergence which in turn induces low level convergence was consistent with the moisture fluxes over western equatorial and eastern parts of the region. The eastern parts of the region experienced less VIMF due to low level convergence.

From all the analyses done under this section, Kain-Fritsch cumulus scheme provided consistent and better simulations across the time periods. The GRELL scheme stood out to be better during

drier years only. The moisture fluxes, convergence and divergences therefore provide better convective signatures for rainfall over the region.

In the third and last objective, the study assessed three tunable parameters in Kain-Fritsch scheme. This was done to demonstrate the extent to which the scheme can be tuned for value addition in the forecasts and simulations. The tunable parameters of KF scheme were extensively described in section 2.3.1.

5.5 The Determination of the Specific Adjustable parameters within the cumulus schemes that can be customized to improve simulations of Extreme Rainfall characteristics

As described in the previous section, this section assessed the value addition derived in using Kain-Fritsch scheme for rainfall simulations and forecasting when its parameters are tuned. Here, the study assessed the impact of using old Kain-Fritsch (KF-old) and new Kain-Fritsch (KF-new) for the wet and normal years of 1997 and 1998 during MAM and OND seasons.

5.5.1 Mean Rainfall Pattern and associated Biases

Figures 55 and 56 show spatial mean rainfall for the KF-old and KF-new cumulus schemes. Also presented in Figure 57 is the rainfall biases for the years 1997 and 1998 respectively during the MAM and OND seasons.

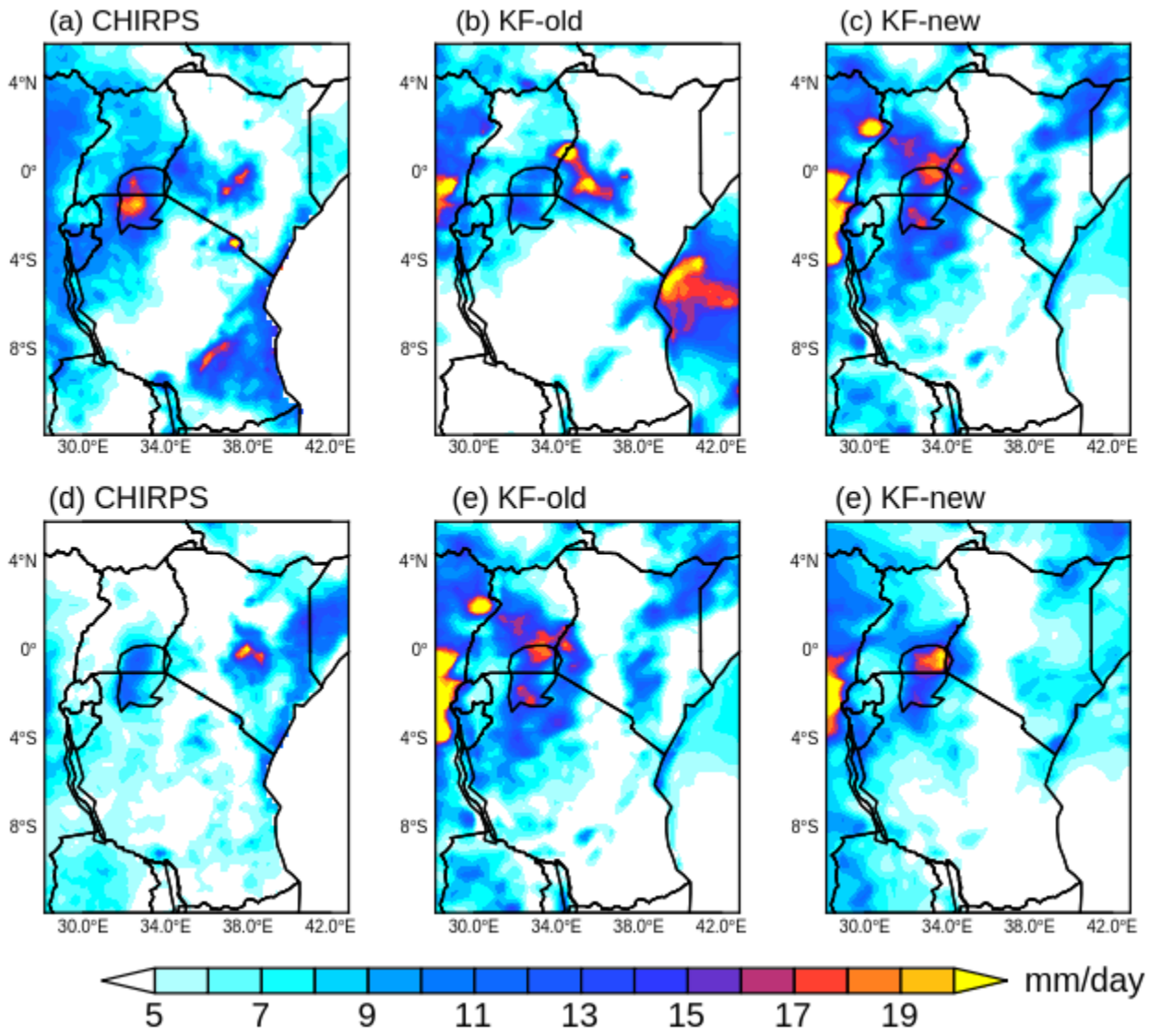

Figure 55: The daily mean rainfall (mm/day) for CHIRPS, KF-old, and KF-new during the MAM (top) and OND (bottom) seasons for the year 1997.

There were small differences between the KF-new and KF-old simulations, although KF-new simulations were conspicuously robust over the western equatorial sector as shown in Figures 55 and 56. The KF-new simulations were, however, the best in the simulating the observed rainfall distribution. This was evident from the simulations during the OND season of 1998 as depicted in Figures 56d and e.

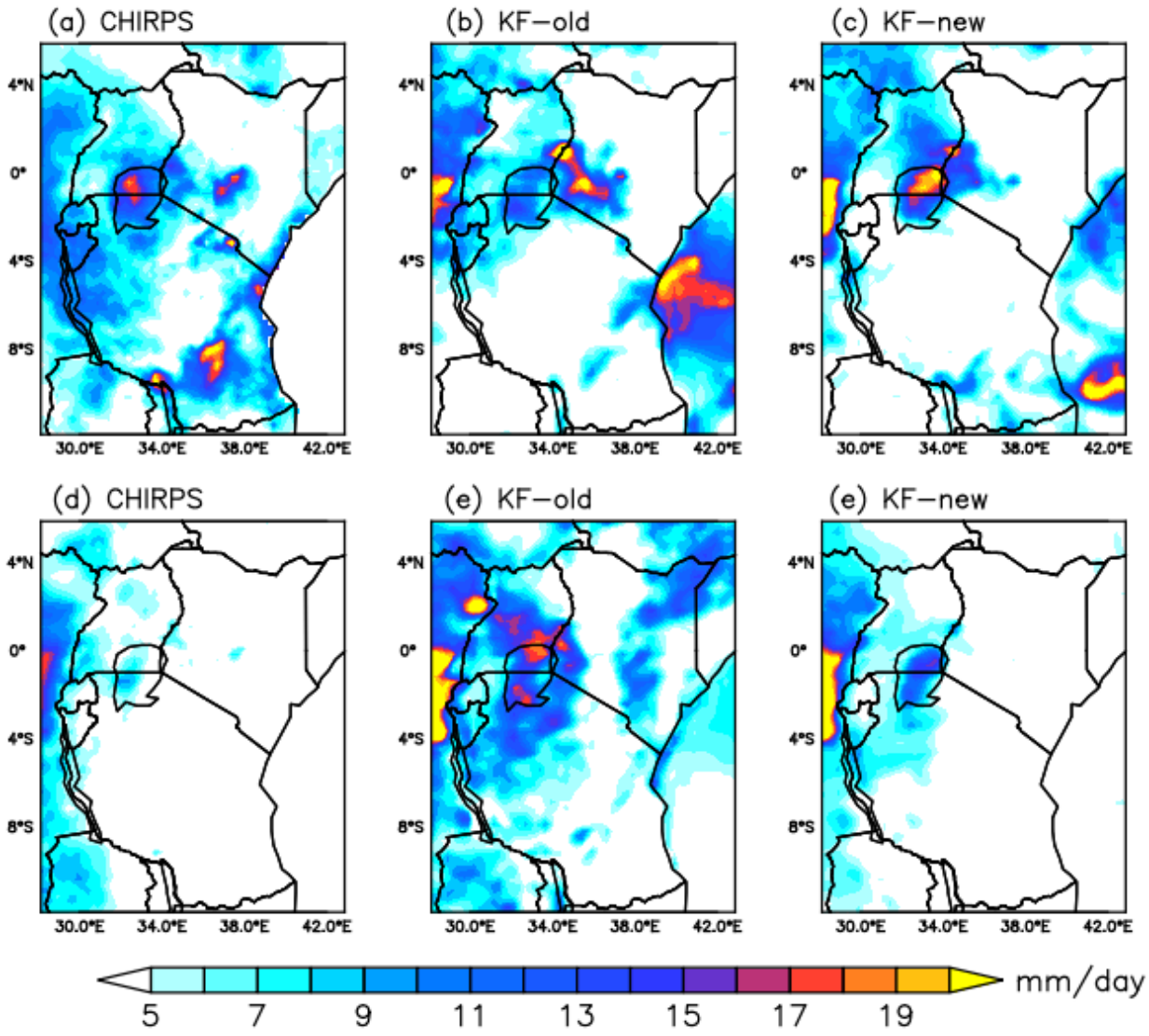

Figure 56: The daily mean rainfall (mm/day) for CHIRPS, KF-old, and KF-new during the MAM (top) and OND (bottom) seasons for the year 1998.

It was evident that rainfall biases were greatly reduced in the KF-new scheme compared to KF-old scheme, as shown in Figure 57. These biases were least in KF-new during OND rainfall seasons (Figure 57h), over the western equatorial parts of the region.

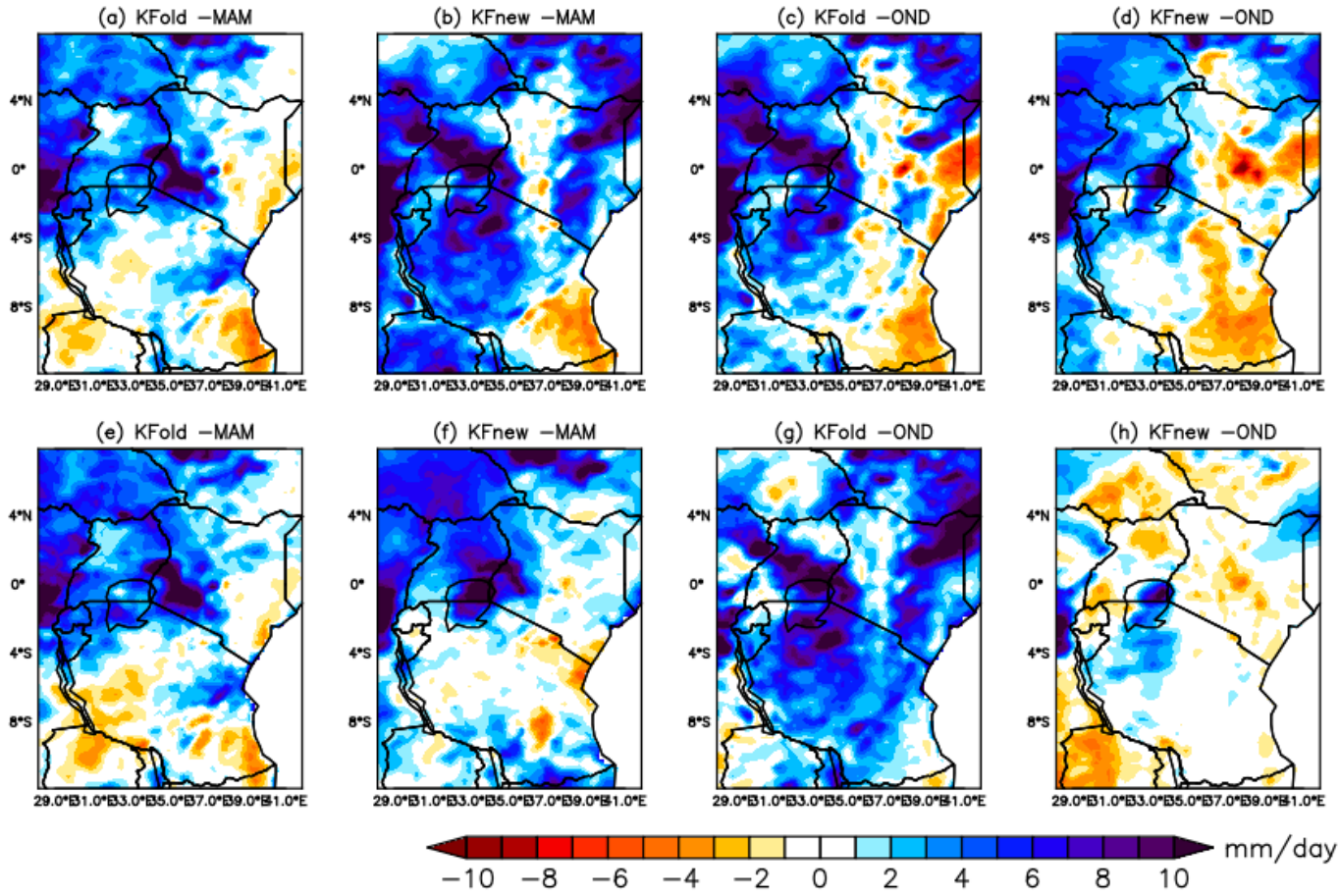

Figure 57: The rainfall biases (mm/day) for 1997 (top) and 1998 (bottom) during the MAM and OND seasons. The blue (orange) shadings denote areas where rainfall is overestimated (underestimated).

5.5.2 Seasonal Rainfall migration

The time-latitude (hovmöller) was analyzed to establish how the KF-new scheme reproduces rainfall migration due to the ITCZ over the region within the longitude 28°E to 42°E for the years 1997 and 1998. Figure 58 present a time-latitude of rainfall evolution with the longitude 28°E to 42°E.

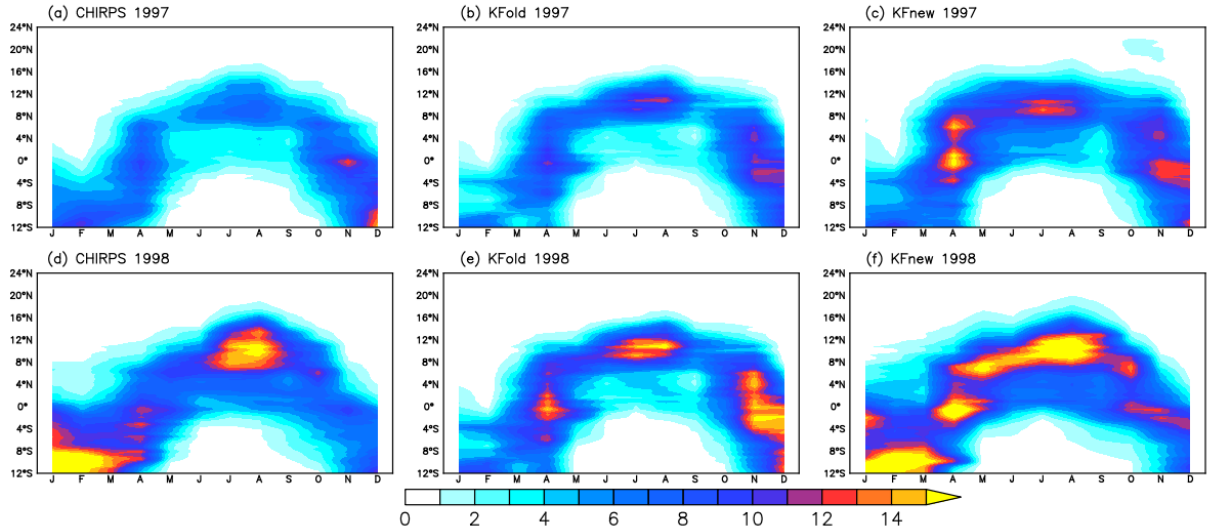

Figure 58: The rainfall (mm/day) time-latitude evolution averaged over longitude 29°E and 36°E for CHIRPS, KF-old and KF-new cumulus schemes. The top panel is for 1997 and the bottom panel is for 1998.

The rainfall reproducibility was high between the two cumulus schemes. High rainfall amount above 10 mm day^{-1} was confined to the southern parts of the equator during the start of the year and migrated to the north from March to May. The peak of the rainfall was attained during the month of April. The rain shifted further north from the month of July up to September with a small break during June (Figure 58a). This was correctly reproduced in KF-old and KF-new schemes (Figures 58b, c). The maximum rainfall band corresponded to the EEA short rainy seasons in the month of November.

It could be seen that the EA region experiences three distinct maximum rainfall bands in April, July-August and November. These maximum rainfall timings corresponded well with the peak rainfall seasons of MAM, June-July August (JJA) and OND seasons as was depicted in Figures 58d, e and f). Based on the analyses of mean rainfall, rainfall biases and evolution, the KF-new scheme was the best although smaller differences in the rainfall simulations between the two schemes existed.

5.5.3 Temporal Rainfall Evolution and distribution from KF-old and KF-new schemes

The Figures 59 and 60 show the results from the annual cycle for mean monthly rainfall over NEA, SEA and LVB regions for 1997 and 1998, respectively. The reproducibility of the distinct rainfall seasons over the four sub-domains in KF-new scheme was adequate as shown in Figure 59 for the

year 1997. The main rainfall season reproduced adequately was the MAM season, the OND season was only reproduced under NEA region. For the 1998 (Figure 60), the KF-old simulation of rainfall seasonality was not well defined, but the KF-new scheme succeeded in simulating the observed rainfall pattern. The KF-old scheme missed both the rainfall direction and its magnitude.

In terms of temporal rainfall distribution, the box and whisker plots were used to evaluate the variability and the spread in the model schemes over the NEA, SEA, CEA and LVB sub-domains. The figures 61 and 62 show rainfall distributions during the years 1997 and 1998, respectively. Over the NEA and SEA regions, the rainfall distribution in the KF-new CPS was closer to the observation than over other sub-domains for both 1997 and 1998 (Figures 61 and 62). In most cases, the median value of the KF-new was closest to the rainfall observations. The median values in the KF-old scheme were closer to the observations in certain instances, but generally the values deviated from the observed values. The analyses here for rainfall annual cycles and rainfall distribution clearly showed that, the new Kain-Fritsch scheme outperformed the KF-old scheme.

The KF-new scheme successfully reproduced peak rainfall months in April and July/August reasonably well. This notwithstanding the overly wet conditions generated during the retreat phase in August–September compared to observations. The extended wet rainfall conditions during the retreat phase of JJA season is believed to stem from persistent rainy days over the LVB region associated with the lake evaporation (Anyah and Semazzi 2007; Sylla *et al*., 2013).

These results showed that the KF-new scheme during the year 1998 was very skillful in reproducing the large-scale systems associated with the ITCZ and the SST. These systems are known to be dominant during the OND and MAM seasons over the EA region (Ogallo *et al.,* 1989; Segele *et al.,* 2009; Gitau *et al.,* 2013). The rainfall annual cycle over LVB revealed strong convective activity during the main rainfall seasons (MAM and OND). It can be concluded from these analyses that KF-new scheme was more skillful in reproducing the distribution and annual rainfall cycles associated with large-scale systems like the ITCZ. One important outcome here was the variability in the annual cycles across the four sub-domains.

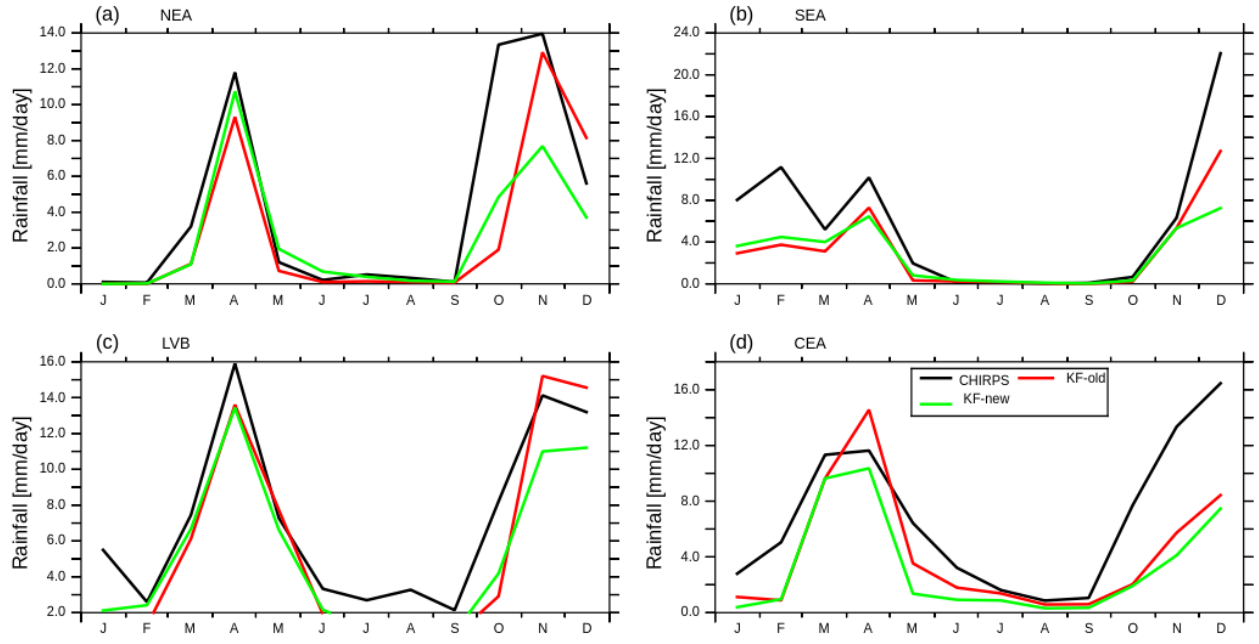

Figure 59: The rainfall annual cycles from the KF-new, KF-old and CHIRPS over NEA, SEA, CEA and LVB sub-domains of East Africa for the year 1997. The black, red and green colors represent CHIRPS, KF-old and KF-new schemes respectively.

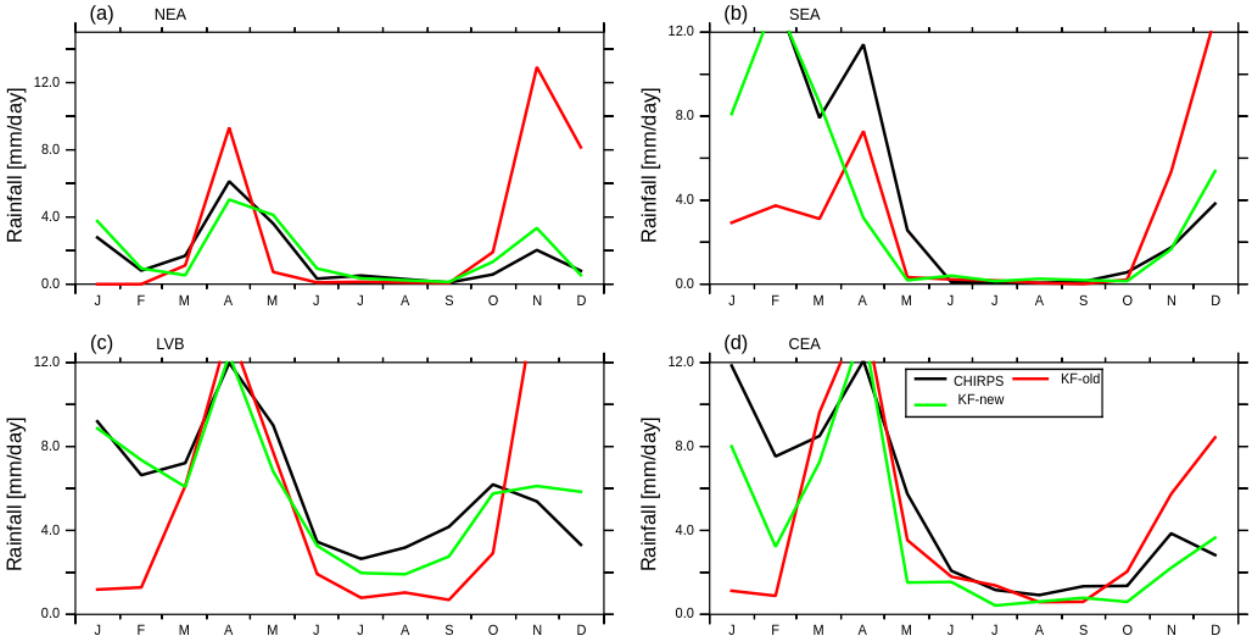

Figure 60: The rainfall annual cycles from the KF-new, KF-old and CHIRPS over NEA, SEA, CEA and LVB sub-domains of East Africa for the year 1998. The black, red and green colors represent CHIRPS, KF-old and KF-new schemes respectively.

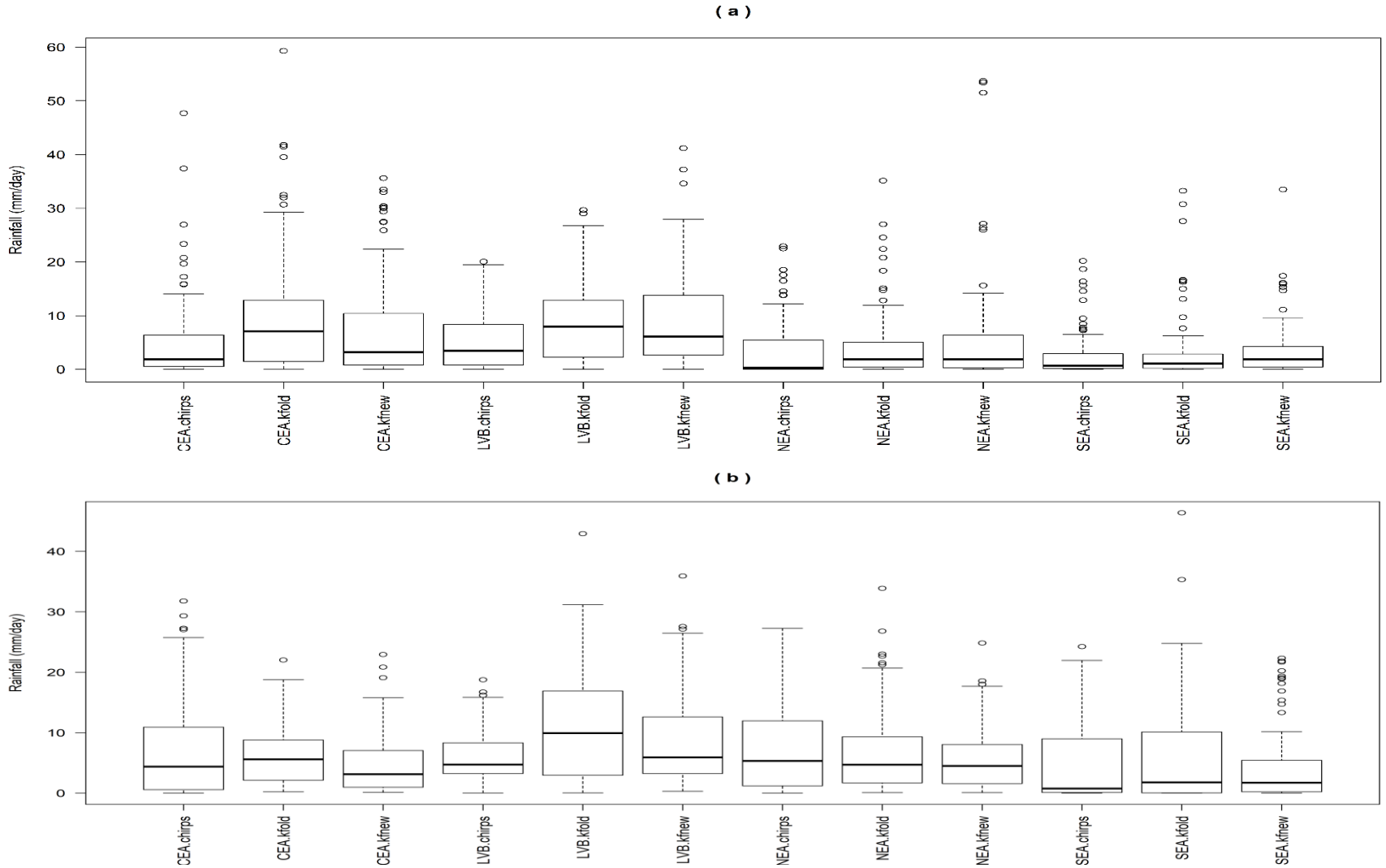

Figure 61: The boxes and whiskers for daily rainfall distribution from CHIRPS, KF-old and KF-new during (a) MAM and (b) OND seasons over NEA, SEA, CEA and LVB sub-domains for the year 1997.The boxes have lines at the lower, median, and upper quartile values.

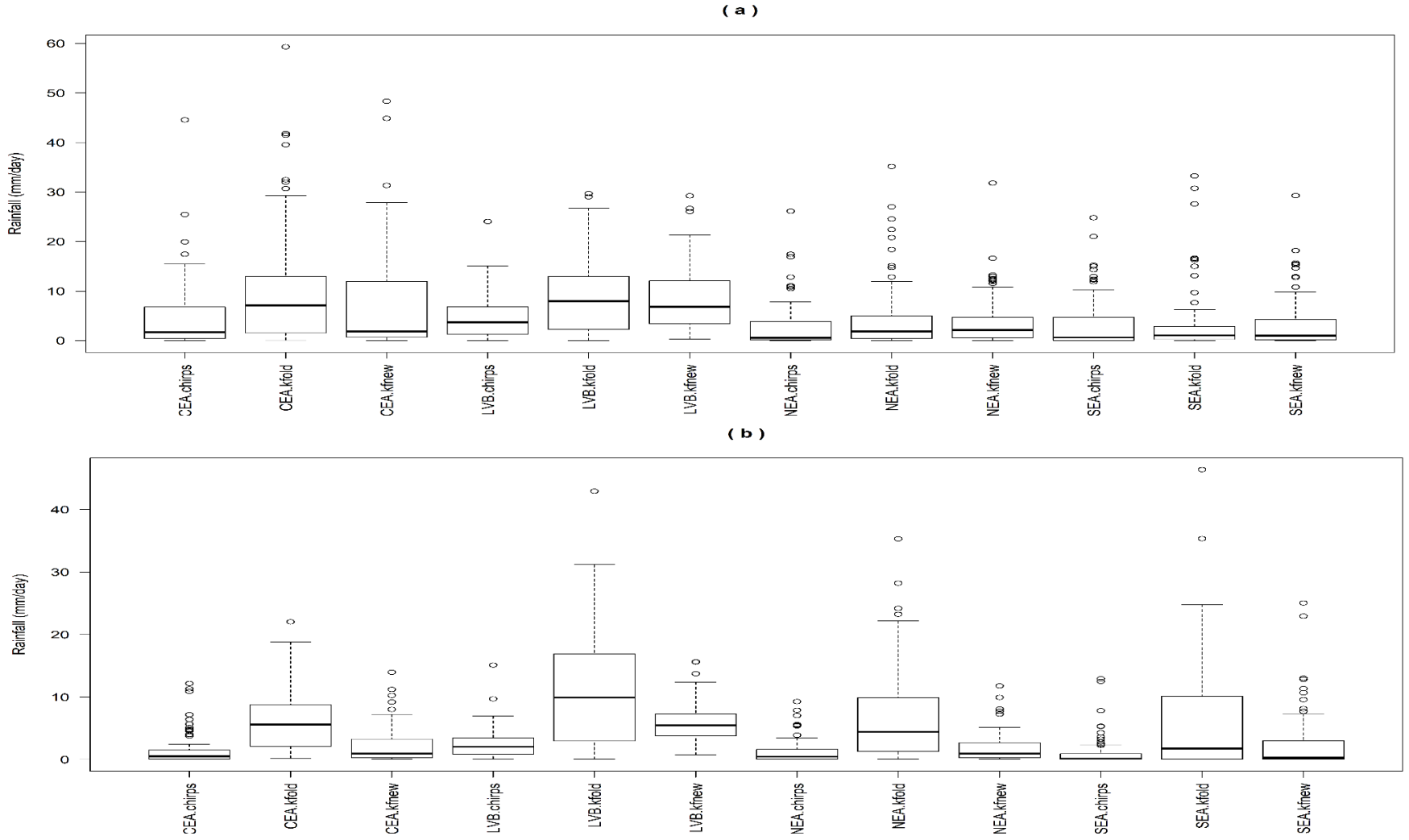

Figure 62: The boxes and whiskers for daily rainfall distribution from CHIRPS, KF-old and KF-new during (a) MAM and (b) OND seasons over NEA, SEA, CEA and LVB sub-domains for the year 1998.The boxes have lines at the lower, median, and upper quartile values.

The quantitative analyses for KF-new and KF-old schemes were done based on the correlation, standard deviation (SD) and root mean square differences (RMSD) and results summarized in a Taylor diagram. Figures 63 and 64 show Taylor diagrams for MAM and OND seasons during the year 1997. In most cases, the KF-new scheme simulated correlation mean value of 0.5 while KF-old correlation values were below 0.4. The corresponding RMSD differences in most cases were between 1.2 to 3.0 mm/day (Figures 63 and 64).

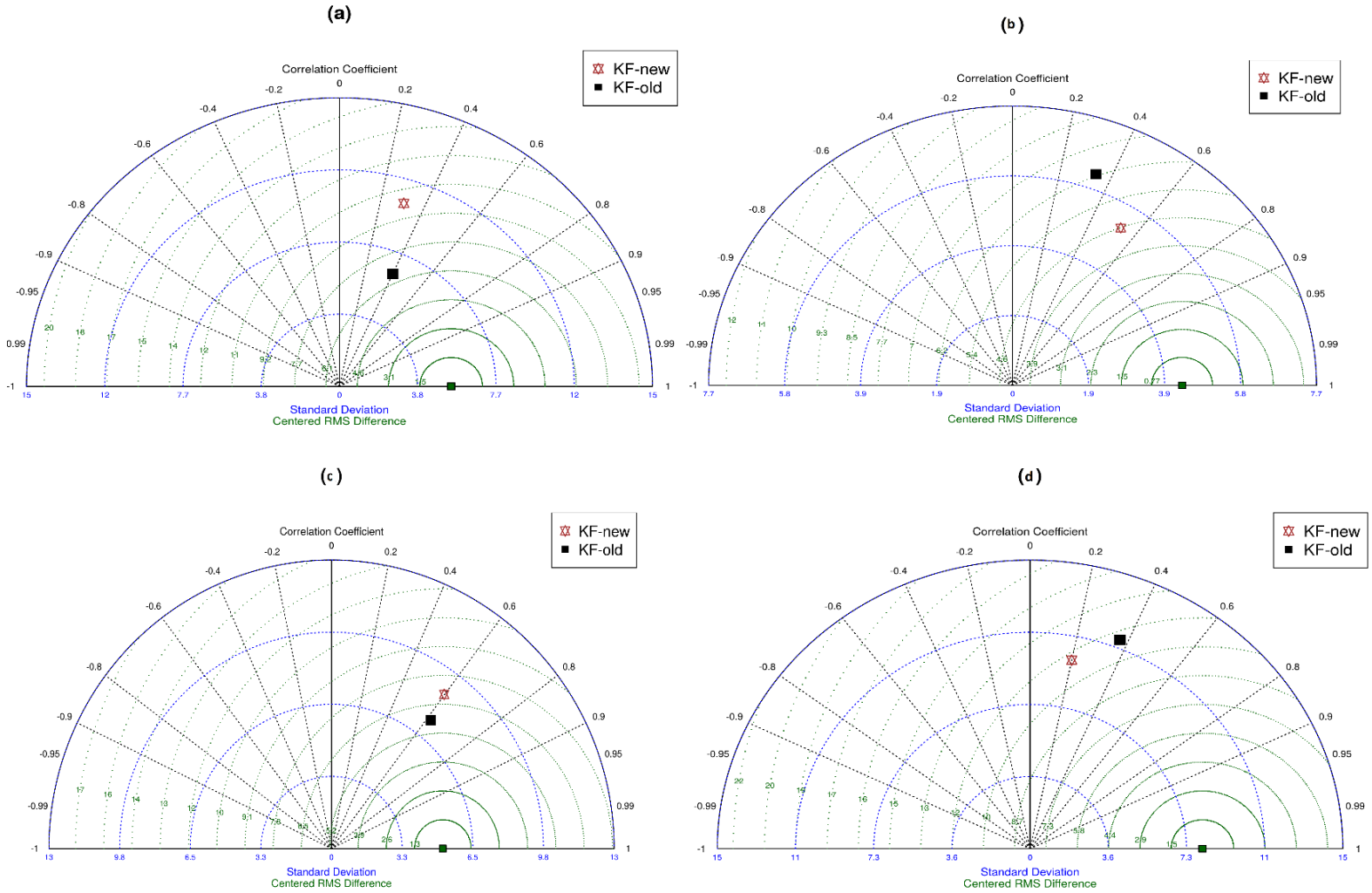

Figure 63: Taylor diagram displaying statistical comparison of seasonal mean rainfall for the KF-new (brown) and KF-old (black) schemes over (a) NEA (b) SEA (c) LVB (d) CEA sub-domains for the year 1997 MAM season. The blue and green curves represent standard deviation (SD) and root mean square differences (RMSD) respectively

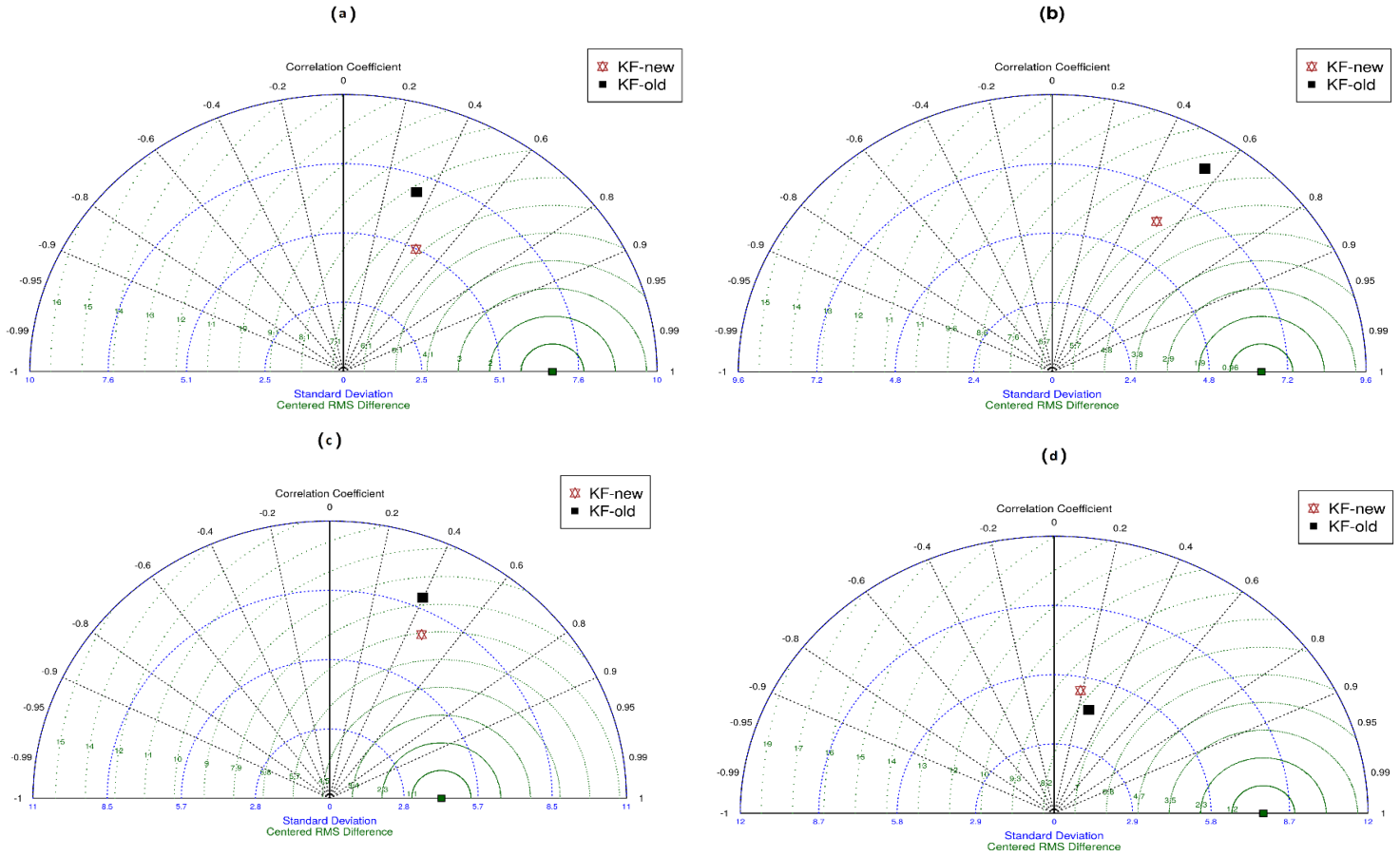

Figure 64: Taylor diagram displaying statistical comparison of seasonal mean rainfall for the KF-new (brown) and KF-old (black) schemes over (a) NEA (b) SEA (c) LVB (d) CEA sub-domains for the year 1997 OND season. The blue and green curves represent standard deviation (SD) and root mean square differences (RMSD) respectively

5.5.4 Intra-Seasonal Rainfall Characteristics

In this section, the performance of the KF-new scheme in simulating the number of rainy days (NRD), intensity of rainy days (IRD) and the frequency of rainy days (FRI) were further analyzed.

5.5.4.1 Number of Rainy Days

From Figure 65 for 1997 during the MAM season, the KF-old scheme simulated more NRD to the northern parts and fewer NRD to the southern parts of the region as shown in Figure 65a. Similarly, in the KF-new scheme (Figure 65b), more NRD over almost the entire region (positive biases) were simulated. The OND season was characterized by fewer NRD over the southern and equatorial parts of the region in both the CPSs (Figure 65d); this implied good agreement between the model and the observation over this region and season. The simulations during 1998 were relatively better for the OND than MAM season. The KF-new scheme simulated least biases especially for the OND season. For example, the KF-new scheme simulated biases of the range 0-4 mm/day over the western parts of the equatorial region (Figure 65d and h).

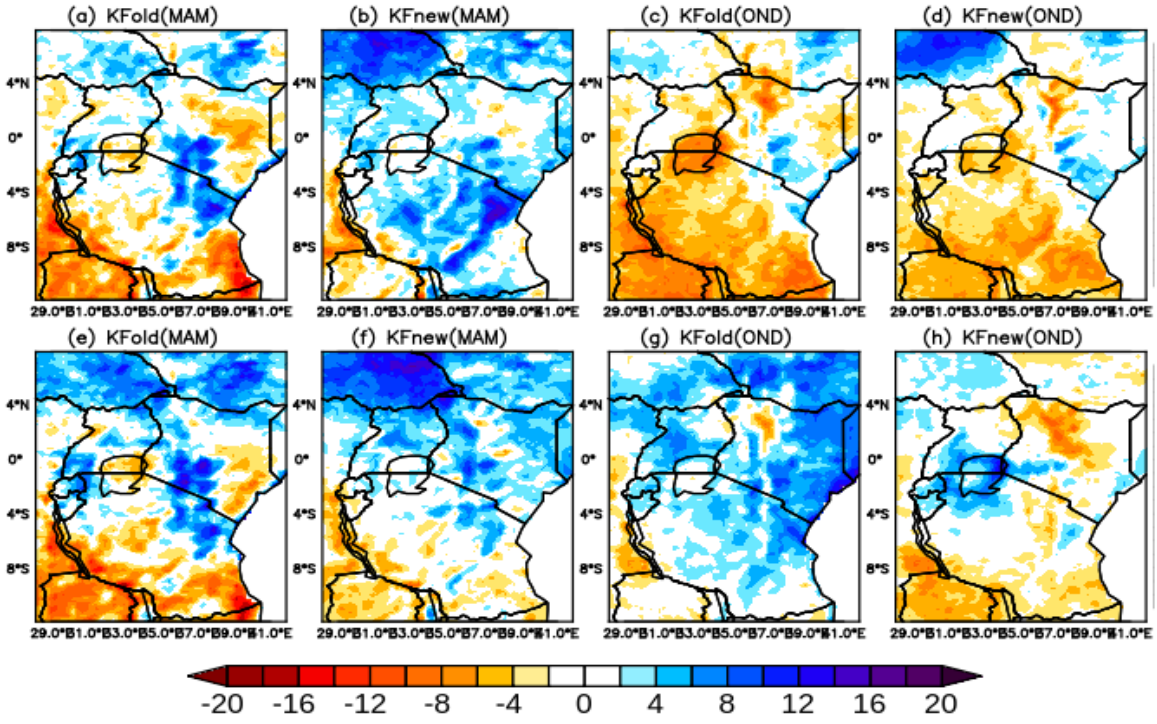

Figure 65: The differences between simulated and the observed NRD (days) for KF-old and KF-new cumulus schemes. The top panel is for the year 1997 for MAM and OND seasons. The bottom panel is for the year 1998 for the MAM and OND seasons. The dark blue (orange) shadings denote positive (negative) differences.

It is evident from these analyses that, the number of rainy days directly impact on the seasonal rainfall amount as had previously been reported. The inspection of KF-new and KF-old CPSs revealed that KF-new was better and more skillful in reproducing these rainfall characteristics.

5.5.4.2 Intensity of Rainy Days

Figures 66 and 67 show the biases in the intensities of the NRD for the light (1–10 mm/day), moderate (11-20 mm/day) and heavy rainfall intensities (>20 mm/day) for 1997 and 1998. The NRD under the light rainfall category was slightly overestimated by about 15days over the western equatorial region, central parts of Kenya and northern parts of Tanzania in KF-old during the MAM season (Figure 66a). The overestimation of light rainfall intensity was also evident over the southern and central parts of Tanzania in KF-new as shown in Figure 66b. During the OND season, the KF-old and KF-new schemes were in close agreement with the observations over the western part of the equatorial region (there were fewer days that were either over-(under)estimated).

Over the eastern parts of the region, slight overestimated of the light rainfall intensity was realized (Figure 66c, d). The moderate rainfall intensity was characterized by underestimation of NRD mostly over the entire region, with few pockets of more NRD over the northern parts of the region (middle panel).

For heavy rainfall intensity, the CPSs overestimated NRD by about 8 days to the western and southwestern parts of the region. The central parts had good agreement with the observations. The eastern parts and coastal regions of the domain experienced few NRD. This was pronounced in KF-new during OND season as was shown in Figure 66. Comparatively, there was a tendency by the CPSs to overestimate rainfall under light rainfall intensities, and simulated fairly the heavy rainfall intensity over the western parts of the equatorial region.

For the 1998 simulations (Figure 67), the observations were similar to the year 1997 except that both the KF-old and KF-new schemes overestimated the NRD during the MAM season over the entire domain. This was contrasted by the consistent simulation of fewer NRD with good agreement between the CPSs and the observation over the western parts of equatorial region and the western parts of Tanzania (Figures 67a, b, c and d). The biases in NRD during OND season were greatly reduced. The moderate rainfall intensity was characterized by fewer NRD over western and southern parts of domain and slightly more NRD to the northwestern parts of region.

Comparatively, the OND season had fewer NRD overestimated over the equatorial region. The eastern parts, experienced fewer NRD with the western parts of Kenya, central and southwestern parts of Tanzania simulated correct NRD (Figure 67k, l). In general, better simulations were realized over the southern parts and the coastal parts of the region under heavy rainfall intensity.

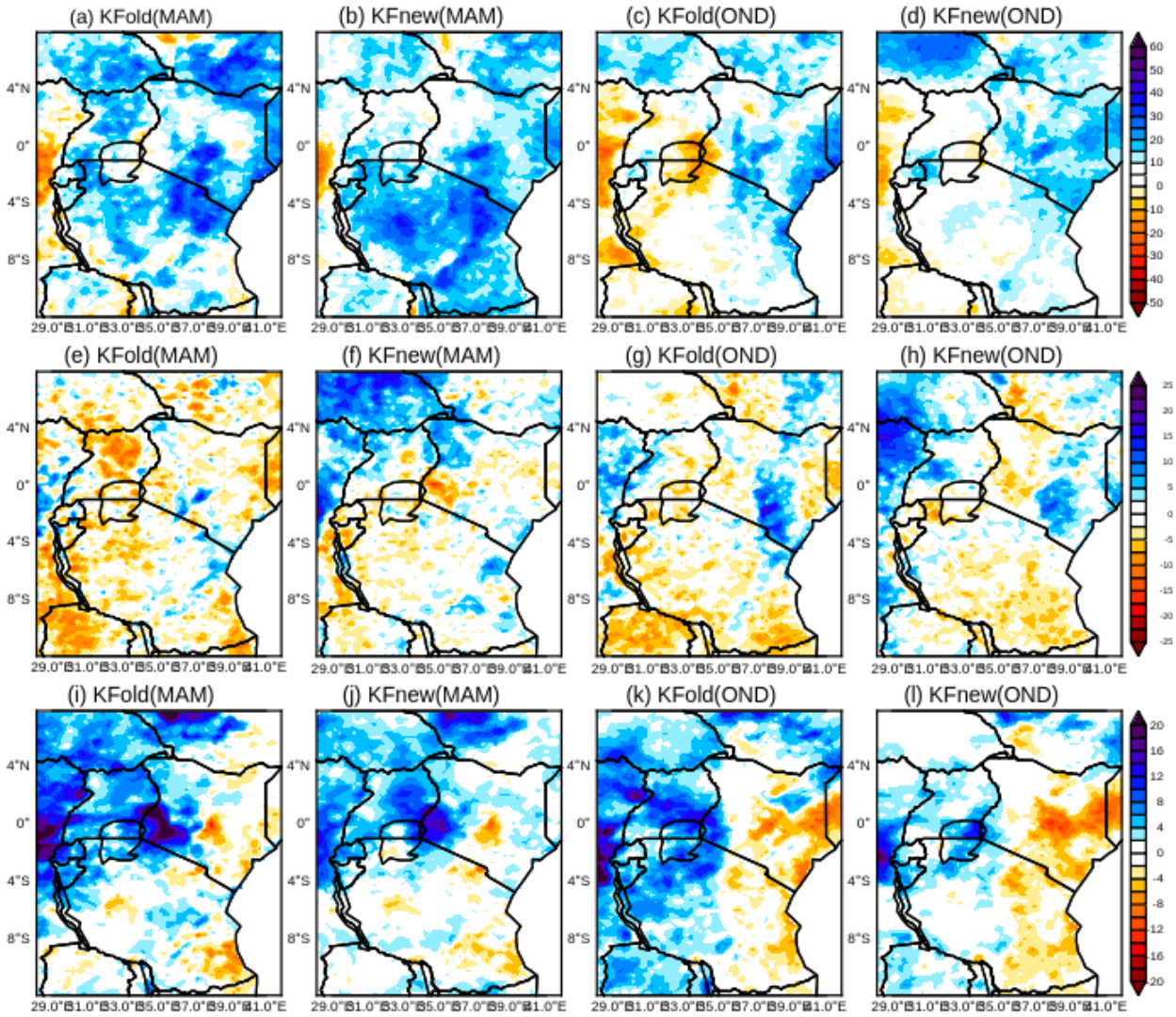

Figure 66: The differences between simulated and observed rainfall intensity (days) during the year 1997. The top, middle and bottom panels represent the light (1-10mm/day), moderate (11-20mm/day) and heavy (>20 mm/day) rainfall intensities respectively for both the MAM and OND seasons. The blue (orange) shadings denote positive (negative) differences.

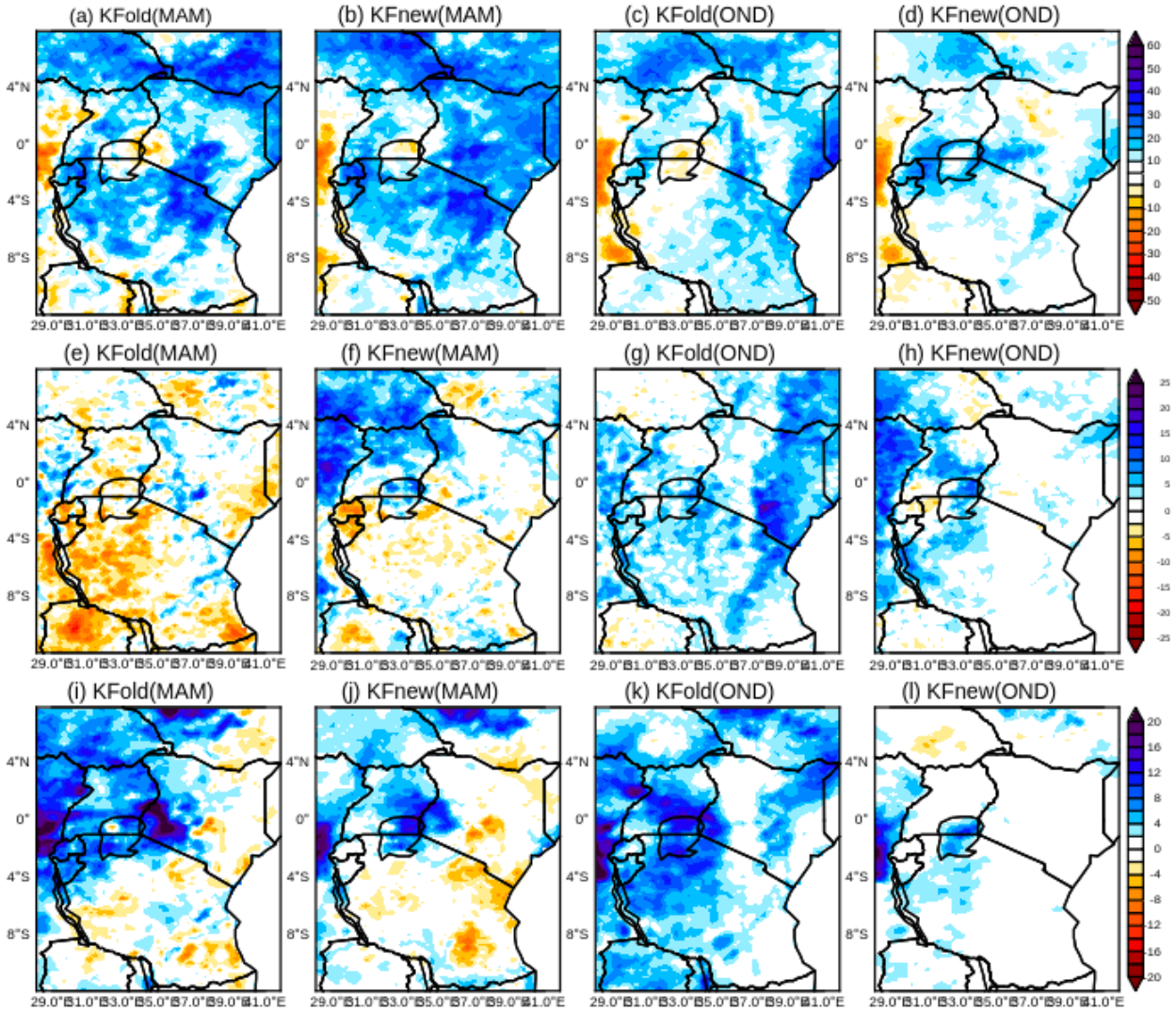

Figure 67: The differences between simulated and observed rainfall intensity (days) during the year 1998. The top, middle and bottom panels represent the light (1-10mm/day), moderate (11-20mm/day) and heavy (>20 mm/day) rainfall intensities respectively for both the MAM and OND seasons. The blue (orange) shadings denote areas of positive (negative) differences.

It was evident that, the rainfall biases from the WRF model is attributable to the many number of rainy days simulated by the model. The intensity of rainy days does not necessarily contribute to the mean rainfall. Using the KF-new CPS provided better and improved simulations than using KF-old scheme. We can conclude that there were slight improvements in the simulation rainfall intensity using KF-new scheme compared to the KF-old scheme.

5.5.4.3 Relative Frequency of Rainy Days

In the previous section, the study assessed the reproducibility of the mean rainfall, rainy days and their intensities. This section present results from simulated rainfall frequencies; this offered understanding how the WRF model reproduce such rainfall characteristics. Figures 68 and 69 show the biases in the simulated rainfall frequencies under the various rainfall intensities for the year 1997 and 1998, respectively, during the MAM and OND seasons.

It was observed that for 1997 (Figure 68), the light rainfall intensity occurred more frequently (overestimated by about 20%) over the eastern, central and southern parts of the region in all the schemes (Figures 68a, b, c, d). During the MAM season, the lowest biases in NRD for light rainfall intensity were observed over the northern parts of equatorial region. The KF-new biases were reduced greatly over the same regions (Figure 68b and d).

The heavy rainfall occurred less frequently (underestimated by about 15%) over the central parts of Kenya and eastern parts of Tanzania (Figures 68i, j, k, l). The equatorial parts and western parts of Tanzania reproduced rainfall closest to the observations (Figures 68i, j, k, and l). Similar observations were made for the year 1998 (Figure 69) with the exception of KF-old during OND season that presented rather fewer NRD over the entire domain (Figure 69c).

All the cumulus schemes considerably overestimated rainfall frequency during MAM season but with differing magnitude of light precipitation over the central parts of Kenya, and southern parts of Tanzania. The CPSs tended to reproduce heavy rainfall fairly well and overestimated the light rainfall intensity. The simulations for moderate frequency were not so distinct and as such clear differences in the cumulus frequency biases could not be noticed.

From these analyses, the region with wettest or driest rainfall biases was related to more or few NRD. The simulations of rainfall by KF-new CPS were better, with reduced biases in rainfall, rainfall intensity and frequency. The areas with the maximum NRD are predominantly associated with heavy rainfall categories while the areas with minimum NRD are associated with light rainfall intensities over the EA region. This observation implied that, rainfall over East Africa are always frequent but of light intensity. The seasonal rainfall pattern is least characterized by the heavy rainfall intensity, while the light rainfall intensity occurs most often.

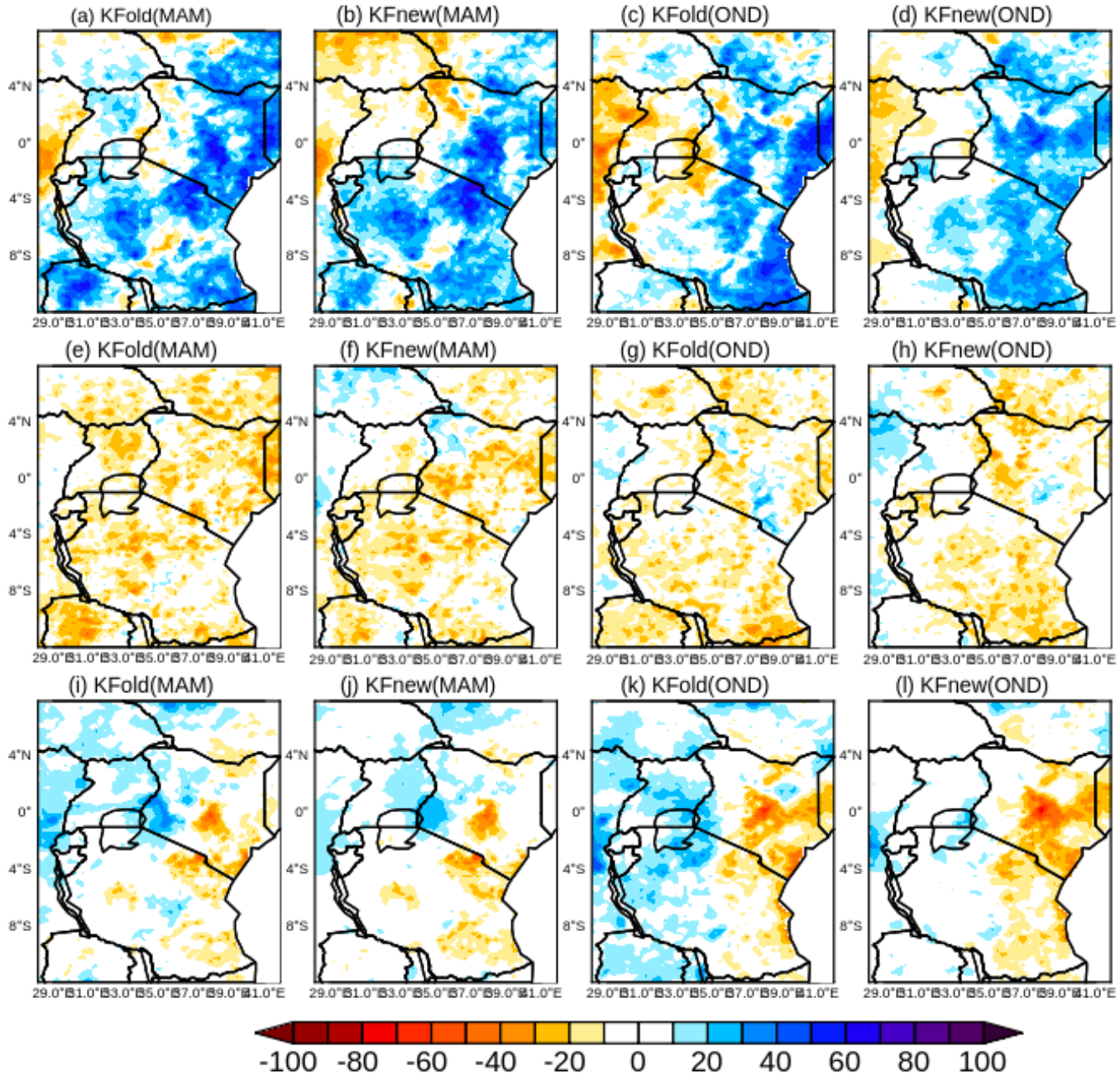

Figure 68: The differences between simulated and observed rainfall frequency (%) during the year 1997. The top, middle and bottom panels represent the light (1-10mm/day), moderate (11-20mm/day) and heavy (>20mm/day) rainfall intensities, respectively for the MAM and OND seasons. The blue (orange) shading represent positive (negative) differences implying areas that receive higher (low) rainfall under each category.

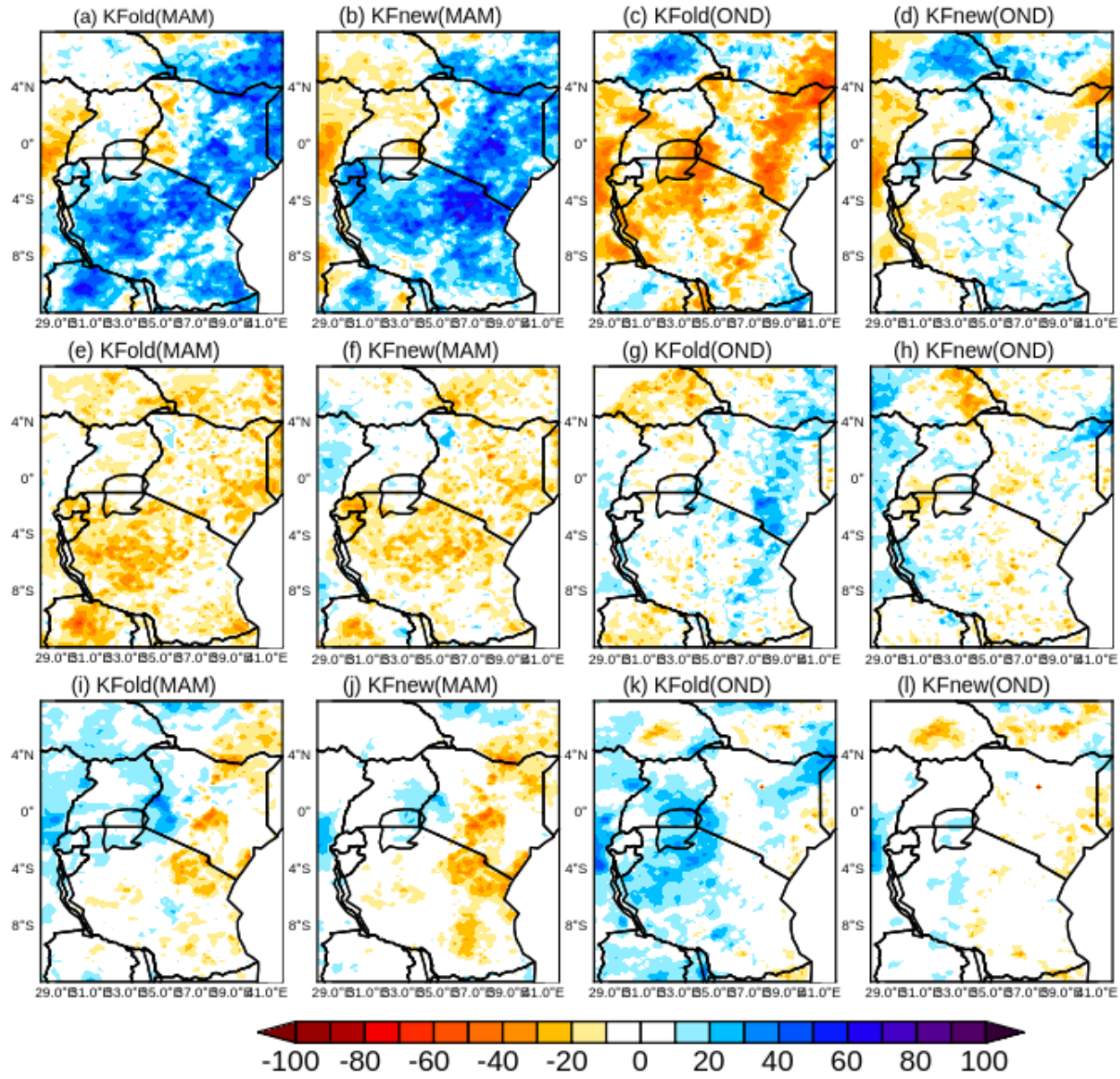

Figure 69: The differences between simulated and observed rainfall frequency (%) during the year 1998. The top, middle and bottom panels represent the light (1-10mm/day), moderate (11-20mm/day) and heavy (>20mm/day) rainfall intensities, respectively for the MAM and OND seasons. The blue (orange) shading represent positive (negative) differences implying areas that receive higher (low) rainfall under each category.

Although the KF-new and KF-old CPSs performed well in simulating heavy rainfall with reduced biases during the OND season and in some cases MAM season, they tended to overestimate the light rainfall intensities. The general overestimation and underestimation of the heavy and light rainfall, suggest that the climate models experience too many rainy days under light rainfall, but

perform rather well in simulating the heavy rainfall events (Sun *et al.,* 2006). Based on the analyses of rainfall frequency, the study found KF-new to be most accurate in simulating the rainfall characteristics.

5.5.5 Simulated Atmospheric Dynamics and circulations

The analyses were extended to establish whether the improvements in the KF-new simulations were related to better realignment of the atmospheric quantities. Specifically, the study analyzed the VIMF, upper level divergence and convective stability of the atmosphere.

5.5.5.1 Vertically Integrated Moisture Flux

The Figures 70 and 71 show the integrated moisture flux during MAM and OND seasons for the years 1997 and 1998, respectively. During the MAM and OND seasons for the 1997 (Figure 70), there were enhanced moisture convergence over the entire domain in the reanalysis (Figures 70a and b) and smaller areas under moisture divergence. The moisture transport was more southeasterly and westerly flows during the MAM season (Figure 70a). A reverse situation was seen during OND season (Figure 70b) where moisture transport was more of easterlies and north easterlies into the equatorial region.

Studies by Vizy and Cook (2003), reported that these moist southeasterly and easterlies flow from the Indian Ocean penetrates over eastern parts of Africa through a narrow break in the topography between the Ethiopian and east African Highlands. However, for the long-rains season westerly/easterly circulations occur in alternation over the region associated with either wet or dry rainfall conditions (Okoola 1999).

There was strong moisture convergence over western sector of East Africa region, and strong moisture divergence over the northern parts of Sudan, eastern and central parts of Ethiopia simulated by both the KF-new and KF-old CPSs as shown in Figure 70c and d. These same areas were under moisture convergence and divergences in the ERA-interim re-analysis. Over the Indian Ocean, the CPSs simulated a weaker convergence of moisture. The simulations for the moisture convergence/divergence were better during the OND than for MAM season in the KF-new scheme.

In general, the regions of strong moisture convergence were seen over parts of the Congo region, southern parts of the region and around the northern parts of Ethiopia in all the CPSs. There was a weak moisture convergence over the Indian Ocean. The northern parts of Sudan, Arabian high and

red sea regions were generally associated with moisture divergence; the moisture convergences were also seen along the Great Rift Valley channel in all the simulations.

For the 1998 simulations (Figure 71), the moisture transport was from northeasterly direction into the region through the eastern parts of the Ethiopian highlands (Figure 71a). Weak moisture convergence was observed over the Congo region and weak divergence generally dominated the equatorial region (Figure 71a). During the OND season (Figure 71b), the East Africa region and parts of the Ethiopian highlands were dominated by strong moisture divergence. There were however, pockets of moisture convergence to the southern parts of Sudan. The moisture transport was more of southeasterly to the south and easterly to the northern parts of the region. The KF-old scheme over-estimated the moisture convergence over the Congo region, and fairly reproduced the weak divergence over the Indian Ocean during MAM season (Figure 71c). During the OND season, KF-old poorly reproduced the areas under moisture convergence. The moisture divergences along the channels of the Great Rift Valley were, however, well simulated by the KF-old scheme (Figure 71d).

The KF-new scheme reasonably reproduced the moisture sources, fluxes and intensity especially during OND season (Figures 71e, f). The regions of positive biases in moisture convergence and divergence were found to coincide with regions of positive and negative rainfall biases, number of rainy days, intensity of rainy days and their frequency (sections 5.5.1, 5.5.3.1 and 5.5.3.3). The reproducibility of the VIMF was better during the OND season than MAM season. As had been found earlier, the areas of maximum rainfall biases were associated with either divergence or convergence.

The current study found that, the Arabian region that is least considered as moisture source for the region plays a significant role in the modulation of low-level convection through the entrance and exit of the jets at 200hPa (Segele *et al.,* 2009, 2015). The biases in the simulated rainfall over the western parts of equatorial region could be attributed to either moisture divergence or convergence biases between 850 to 300hPa. From the moisture flux analyses based on the VIMF, KF-new reproduced moisture convergence/divergence better compared to the KF-old cumulus scheme.

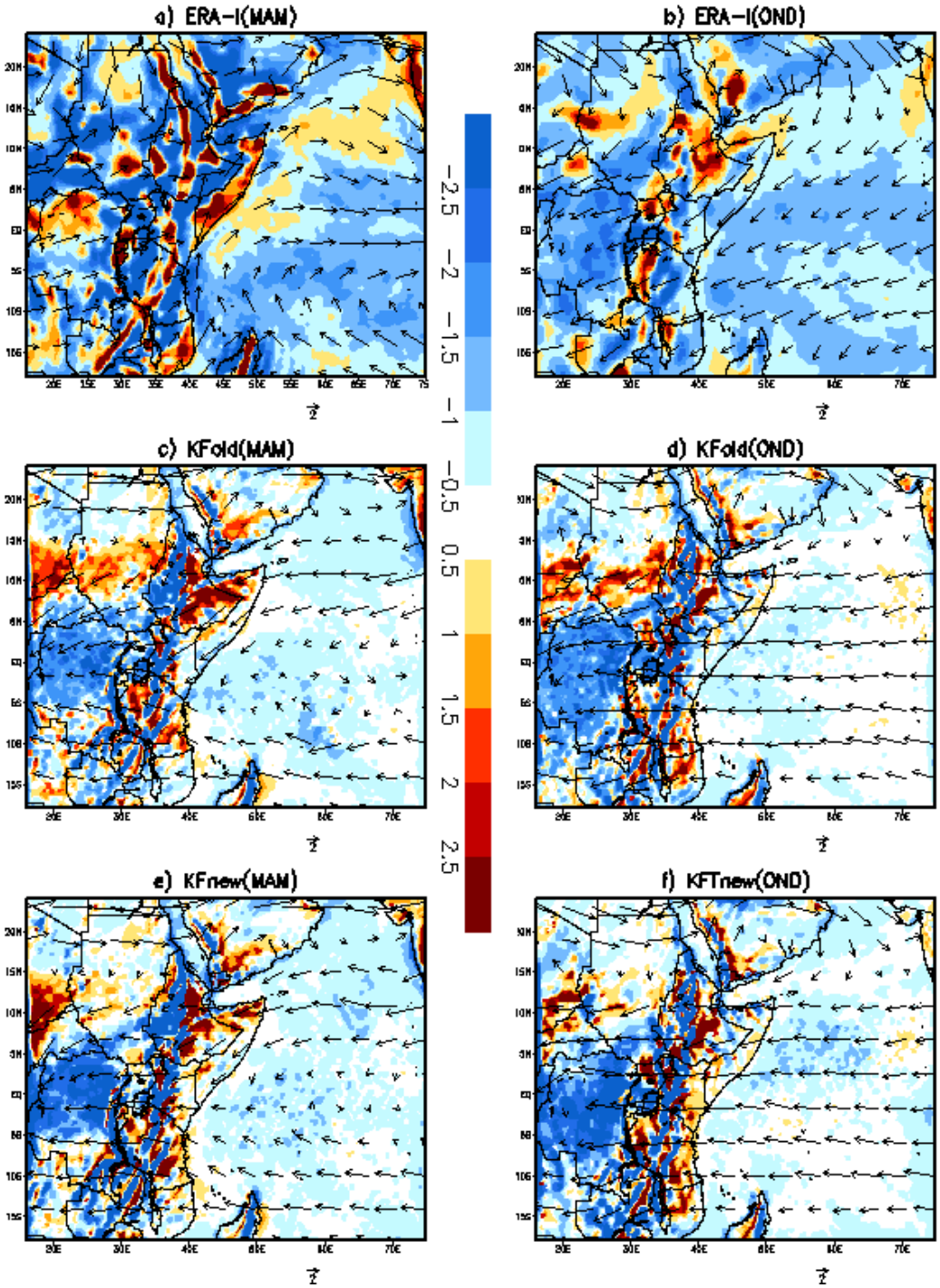

Figure 70:The spatial patterns of vertically integrated moisture fluxes (from 850 to 300 hPa) moisture convergence and divergence (x 10^3) (shaded) and moisture fluxes (arrows) from ERA-interim reanalysis, KF-old and KF-new cumulus schemes for MAM and OND seasons during the year 1997. The orange and blue shading denote positive and negative values representing areas of moisture divergence and convergence respectively.

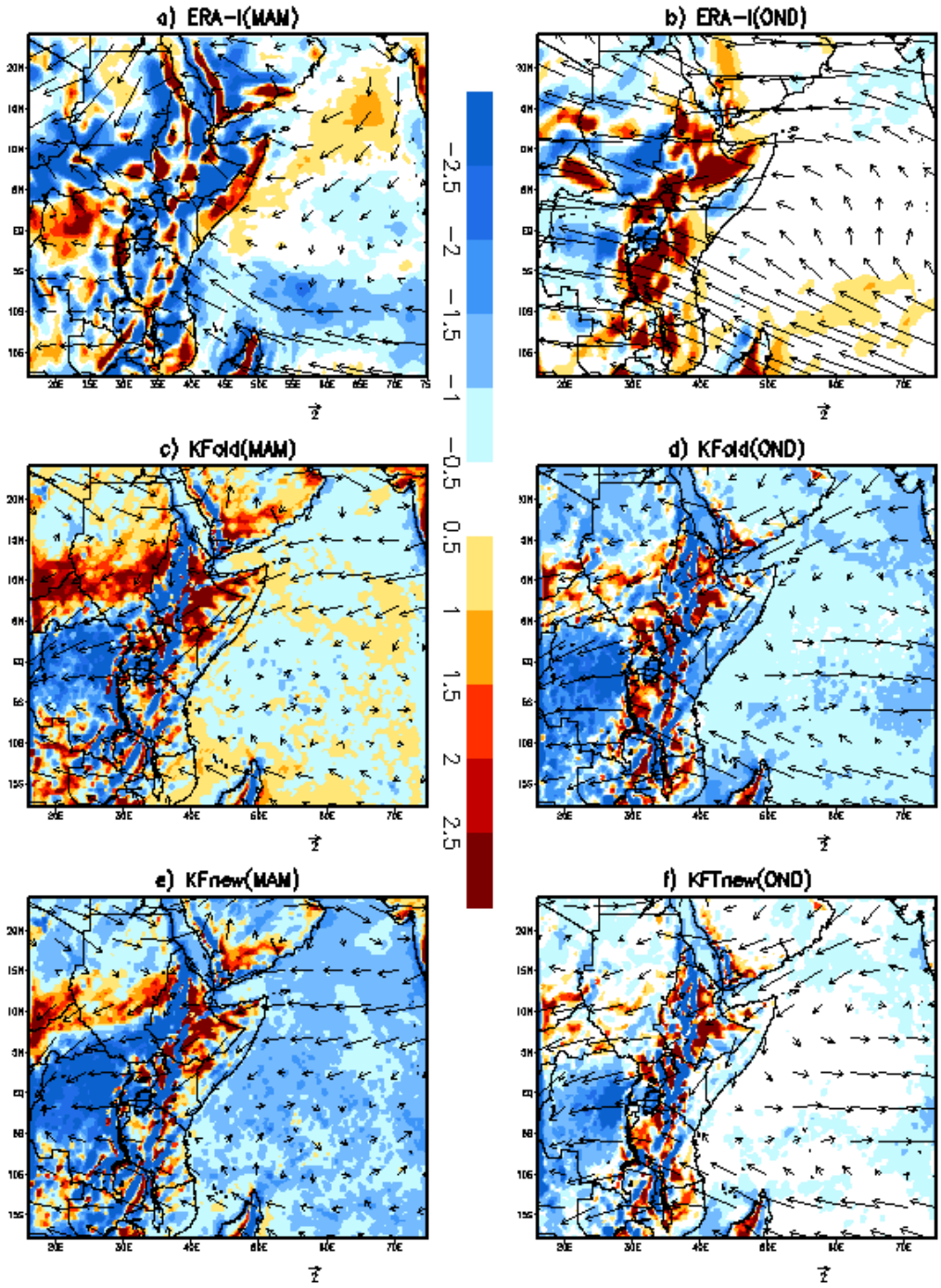

Figure 71:The spatial patterns of vertically integrated moisture fluxes (from 850 to 300 hPa) moisture convergence and divergence (x 10^3) (shaded) and moisture fluxes (arrows) from ERA-interim reanalysis, KF-old and KF-new cumulus schemes for MAM and OND seasons during the year 1998. The orange and blue shading denote positive and negative values representing areas of moisture divergence and convergence respectively

5.5.5.2 Deep Convection associated with rainfall biases

The analyses of the deep convection over the region during the 1997 and 1998 years were also done. As had been explained previously (Section 5.4.2), the upper level (300 hpa) divergence and omega at 500 hPa were used as proxies to the deep ascent. Figures 72 and 73 show the horizontal mass flux and divergence during the MAM and OND seasons for the years 1997 and 1998 respectively.

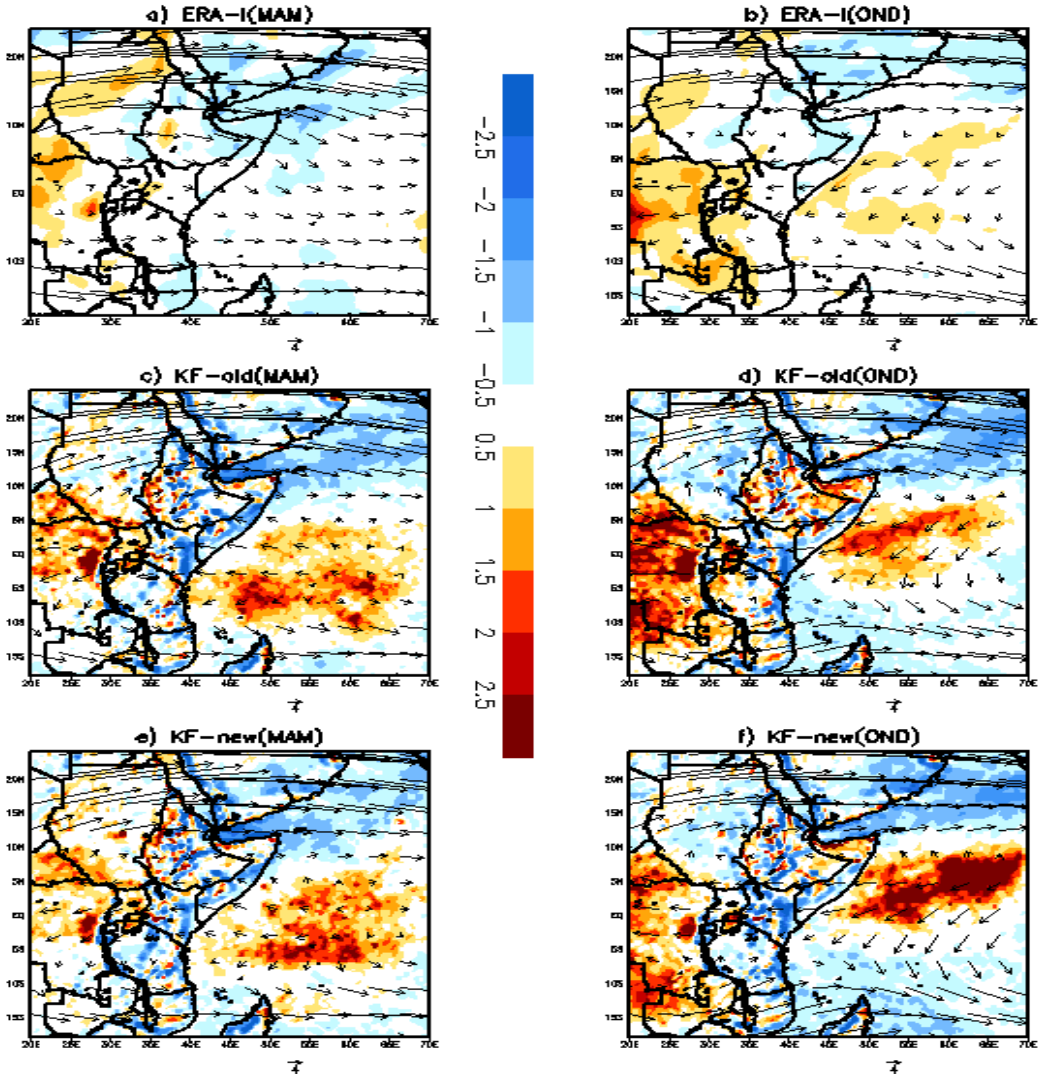

Figure 72: Horizontal mass fluxes (vectors) and upper level divergence (shaded, $\times 10^4$ s^{-1}) at the 200hPa for MAM and OND season during 1997. The orange and blue shading denotes positive and negative values representing areas of moisture convergence and divergence respectively.

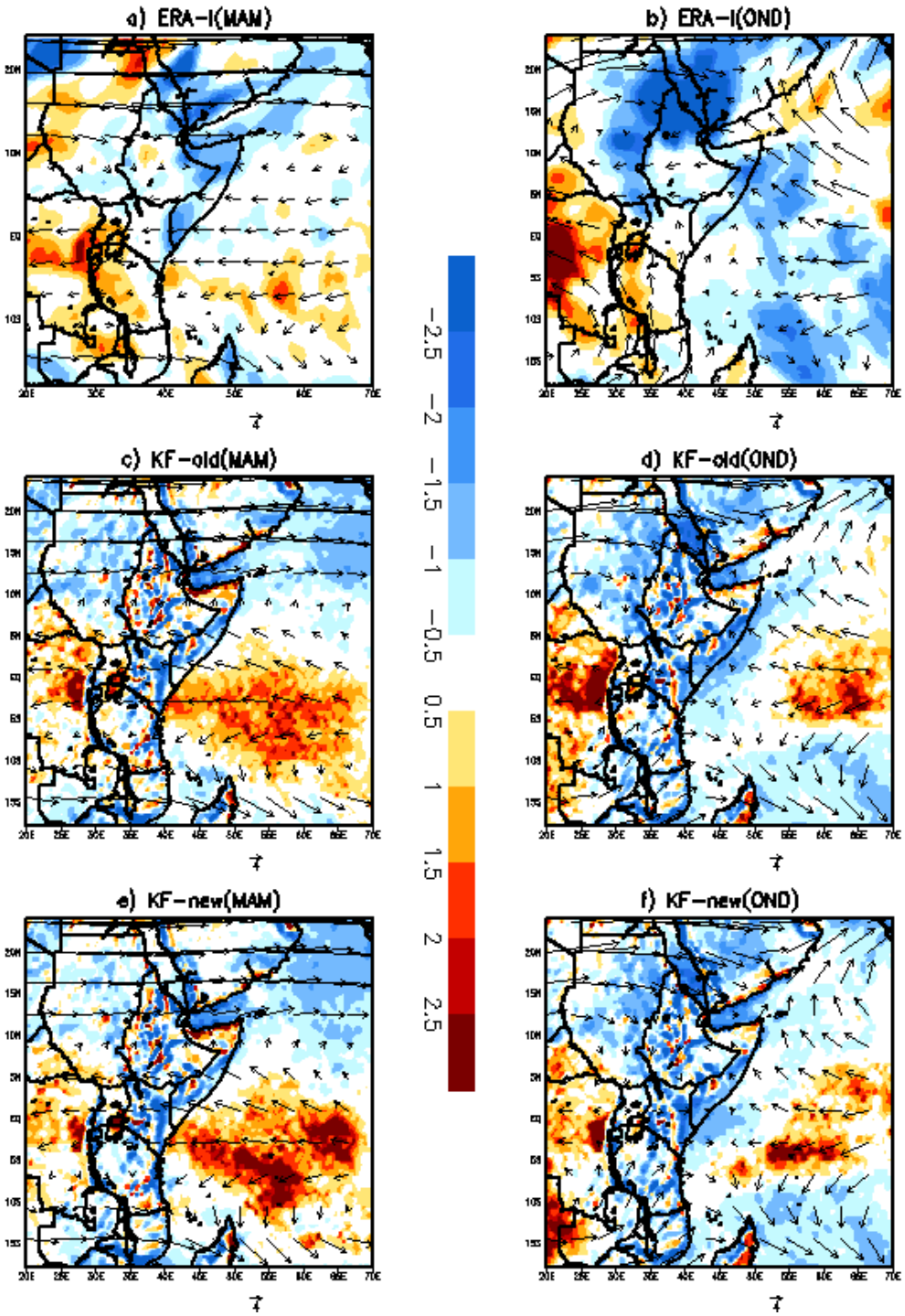

Figure 73: Horizontal mass fluxes (vectors) and upper level divergence (shaded, $\times 10^4\ s^{-1}$) at the 200hPa for the MAM and OND seasons during 1998. The orange and blue shading denotes positive and negative values representing areas of moisture convergence and divergence respectively.

During 1997 MAM and OND seasons (Figure 72a and b), the divergence was weaker over the entire region. The circulations were more of westerly over the Indian Ocean, strong upper level jets to the northern and southern parts of the region during the MAM season. During the OND season, the flow was more of easterly with westerly jets around the northern and southern parts of the region. All the CPSs correctly simulated the regions of convergence and divergence but greatly overestimated their magnitude. The flow in the KF-old and the KF-new CPSs during MAM season was reversed (more of easterly) instead of westerly. The simulated divergences during the OND season for both the CPSs were closer to the observation. The overestimation of the convergence and divergence and generation of strong westerly winds could explain why the CPSs tended to be wetter and favored heavy rainfall intensity especially for the KF and KFT cumulus schemes.

During the year 1998, the circulation in the ERA-interim for the MAM season (Figure 73a), were more of strong easterly over the Indian Ocean into the equatorial region. The convergence was enhanced over the northern parts of region around Arabian high, and red sea. The divergence was stronger over the Congo region (Figure 73a). The same was observed during the OND season, strong divergence to the west and strong convergence to the northern parts around the Arabian high region (Figure 73b). This suggests that areas under divergence at upper levels (300hPa), experienced low level (850hPa) convergence and vice-versa. A weak cyclonic flow around the Mozambique Channel and strong southerly winds, weak easterly winds were evident during the OND season.

All the CPSs reproduced the observed circulation patterns during the OND season in the KF-new cumulus scheme. Noticeably, the CPSs replaced the convergence observed in ERA-interim during the OND season with strong divergence over the Indian Ocean. This has an effect of introducing low level convergence over the same area to produce biases in the model as was earlier observed with the other CPSs.

The analyses here further confirmed that rainfall biases in the model could be associated with realignment of the circulations and divergence/convergence patterns. Comparatively, the KF-new simulations were quite consistent with the observations. The simulations between KF-old and KF-new were quite distinct in terms of their reproducibility of the surface and atmospheric variables. The KF-new was therefore a robust a scheme in reproducing the divergence and convergences for both 1997 and 1998.

5.5.5.3 Vertical Velocity in Pressure Coordinates

The vertical velocity (omega) was analyzed to establish if there exist any relationship between the vertical motion and the surface variables like precipitation. Figures 74-75 show omega differences between ERA-interim and KF-new and KF-old cumulus schemes during the MAM and OND seasons for 1997 and 1998, respectively.

During the year 1997, there were more descent simulated by the CPSs over the northern and along the coastal parts of Kenya than in the observation for MAM season, as was illustrated in Figure 74a and b. The descent in the KF-new scheme was more than in the ERA-interim (Figure 74b). Over the chief moisture sources of the Indian Ocean and Congo region, the CPSs experienced weaker ascent motion than in the reanalysis. The ascent was more enhanced during the OND season than MAM season (Figure 74c and d) in the schemes than in the reanalysis. For the year 1998, during the MAM season the schemes simulated stronger sinking motion over most of the domain, especially over the northern parts of the region, as shown in Figure 75a and 75b. Over the Indian Ocean and Congo region, the schemes simulated more ascent motion than in the observation during the OND season (Figure 75c and d).

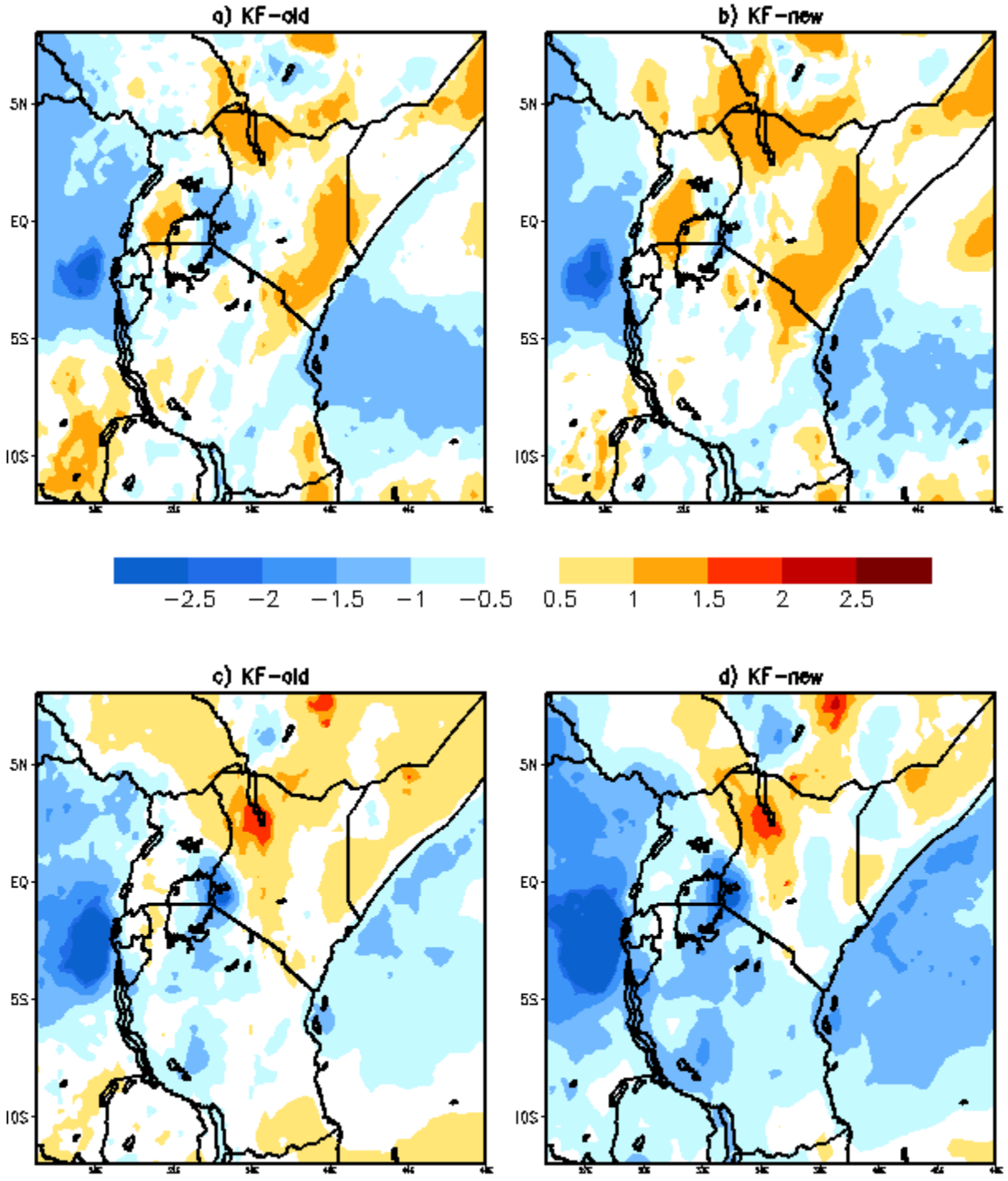

Figure 74: The omega (x10^2 Pa s^{-1}) differences between the cumulus schemes and ERA-I during MAM (a,b) and OND (c, d) seasons for the year 1997. The negative (positive) values of ω are associated with rising (sinking) motion. The blue shading indicates rising and orange shading denotes sinking motion.

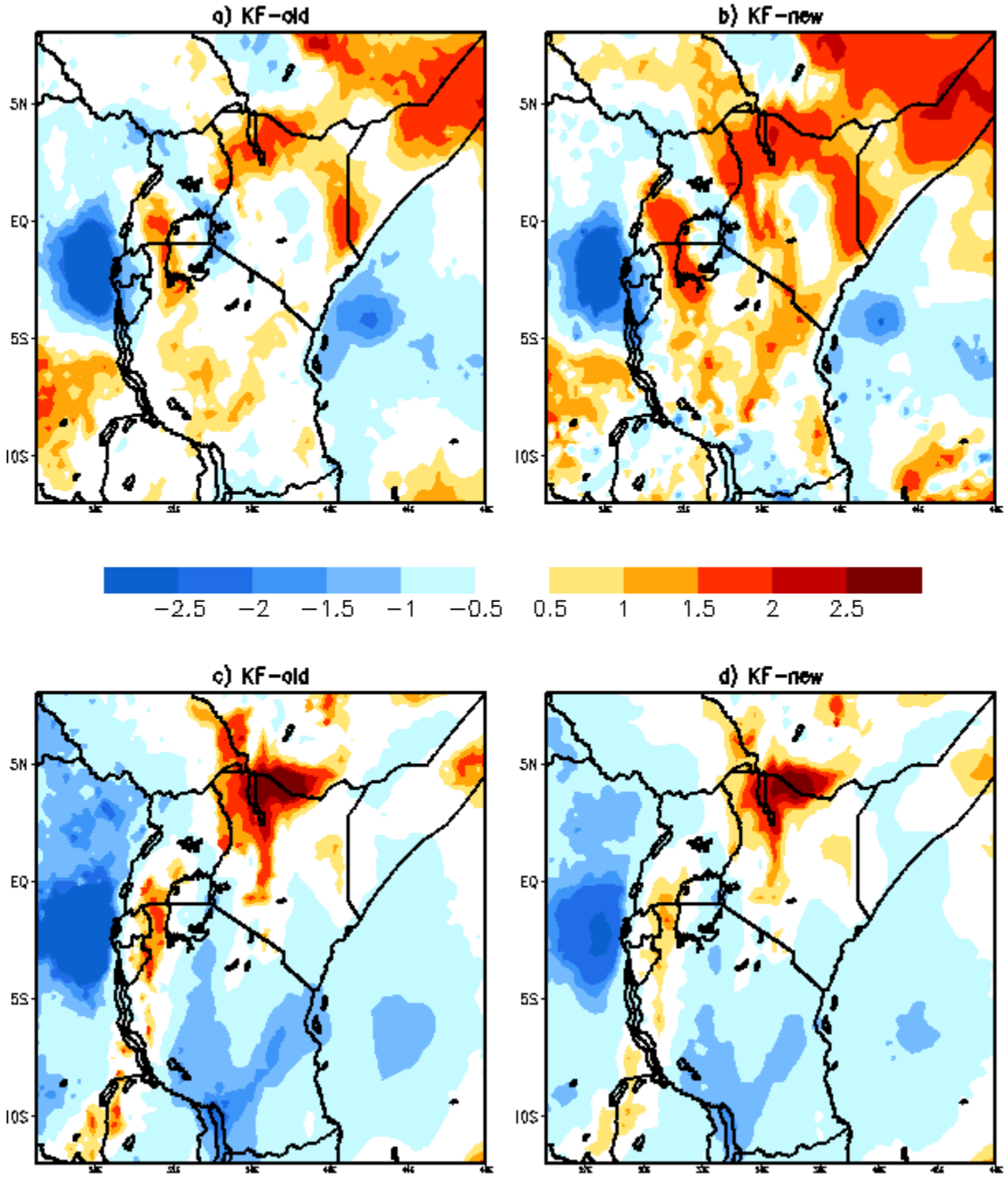

Figure 75: The omega (x10^2 Pa s^{-1}) differences between the cumulus schemes and ERA-I during MAM (a,b) and OND (c, d) season for the year 1998. The negative (positive) values of ω are associated with rising (sinking) motion. The blue shading indicates rising and orange shading denotes sinking motion.

It is clear from these analyses that the CPSs tended to simulate wetter rainfall conditions as a result of stronger ascent compared to the weaker ascent in the reanalysis, notably over the Congo region and Indian Ocean. The regions that were too dry were associated with descent notably over the northern parts of the domain where large ω500mb bias relative to the ERA-interim reanalysis were observed. Similar findings had been reported by James *et al.* (2017) over the East Africa and West Africa regions.

This denotes that WRF model generate overly strong convection overland and tropical oceans. It can be concluded here that model generate rainfall biases due to the influence of divergence/convergence motion. This was true for the cases of large omega biases relative to ERA-interim. At the 500hPa, the divergence at low level results into vertical sinking and suppresses convection due to subsidence (Ogwang *et al.*, 2015a).

Studies by Hastenrath (1999) and Hastenrath *et al*. (2007) pointed out that the vertical motion, together with the fast surface westerly and enhanced subsidence results to the deficient rainfall at the coast of East Africa. Similar findings were highlighted by Ongoma *et al.* (2015). Their studies reported that, the low-level convergence during the MAM season must be coupled with slow moving south easterlies that partly transport moisture from the Indian Ocean to the equatorial region. In the presence of enhanced easterlies, moisture supply is cut short over to the equatorial East Africa region. This tends to create a regime of slowly moving equatorial westerly and decreased subsidence which results to the abundance rainfall over equatorial East Africa.

The KFT scheme alleviated the wet rainfall biases in the KF scheme due to the moisture advection function introduced. The moist advection causes the delays in the initiation of convection; thus increasing the non-convective precipitation. Furthermore, the low temperature perturbation in the KFT scheme lowers the rate of solar heating at the surface (Choi *et al.*, 2015).

The moisture deficiency in the GRELL scheme is related to the cloud formulation structures in the scheme. The convective clouds in the scheme act to stabilize the environment as soon as the large-scale processes destabilize it. Both entrainment and detrainment along the cloud edges are not allowed only at the top and bottom of the circulations (Gianotti *et al.*, 2012). This assumption in the scheme inhibits the rapid generation of convective precipitation over East Africa characterized by very strong convection and fast moving westward projections (Laing *et al.*, 2011).

Owing to the low level moisture and highly unstable atmosphere within the equatorial East Africa, the KF scheme generates too much rainfall to lower the instability (Kim *et al.,* 2010). The BML scheme on the other hand, alternately over/under-estimate rainfall as a result of less latent heat released from simulated moisture amount in the scheme. The more frequent rainy days simulated under the heavy rainfall and light rainfall category in the KF and GRELL schemes could be attributed to phase errors of rainfall amount, and the peak time of the simulated rainfall intensity (Choi *et al.,* 2015). The over-estimation of light rainfall intensity is a common problem in most of the numerical climate models (Salih *et al.,* 2018). A study by Brisson *et al.* (2016) suggested that using convective permitting model would lower the biases associated with light rainfall intensities. This alleviates too much precipitation due to their conventional nature of being designed for deep clouds and not shallow clouds (Prein *et al.,* 2015).

CHAPTER SIX

6 Summary, Conclusion and the Recommendation of the study

This chapter provides a summary of the study, key results and major conclusions drawn from the results. It also provides some recommendations for applications of the study findings and suggestions for future studies.

6.1 Summary

The main objective of the study was to identify the most suitable cumulus parameterization scheme (CPS) in the WRF model that provides more accurate results when used for simulating the extreme East Africa rainfall characteristics. The four CPSs used for the sensitivity experiments were; Kain-Fritsch (KF), Kain-Fritsch with a moisture-advection based trigger function (KFT), Grell Dévényi (GRELL) and Betts Miller Janjic (BML). The simulated analyzed rainfall characteristics included number of rainy days (NRD), intensity of rainy days (IRD) and the frequency of rainfall intensity (FRI) and the associated atmospheric dynamics.

The seasons considered were March-April-May (MAM) and October- November-December (OND). The methodologies adopted in the study were the standardized rainfall index (SRI), principal component analyses (PCA) and composite analyses to delineate the wet and dry years used in the study. The skill of the four CPSs were examined based on root mean square error (RMSE), mean bias error, spatial correlation (SC), coefficient of variation (CV), Taylor diagram and Box and whisker plots. The atmospheric dynamics calculated included the divergence analyses, vertically inter-grated moisture fluxes (VIMF) and vertical velocity.

The value addition derived from the best scheme in simulating rainfall characteristics was achieved through the optimum configurations of its tunable parameters. These configurations were; adjustment time scale (ATS), cloud-radiation coupling and entrainment based on lifting condensation level (LCL). The Climate Hazards Group Infrared Precipitation with Station data (CHIRPS) and ERA-Interim reanalysis were the main dataset used for the model evaluation.

The study identified the KF and the GRELL schemes as the most suitable CPSs for rainfall simulations that can provide better and more accurate forecasts. Higher skill and accuracy in the simulations was obtained with KF-new scheme when KF scheme was further tuned using the tunable parameters. The GRELL scheme, however, provided better forecast during the drier years

only. The BML CPS simulations were not consistent and skillful in most cases. There were however notable variations in simulating individual rainfall characteristics by the CPSs.

The simulations of mean rainfall showed that the BML and KFT schemes simulated correctly the rainfall location but missed rainfall amount and timing in most cases. In terms of spatial correlation, KFT reproduced highest correlation value of 0.67 followed by GRELL 0.4 during the OND season. Relatively low correlation values (r=0.2) were noted during the MAM season. This clearly showed weak reproducibility of MAM rainfall systems by the CPSs.

The BML scheme also provided realistic simulations of the NRD. The simulation of the IRD based on the light (1-10mm/day), moderate (11-20mm/day) and heavy (>20 mm/day) rainfall categories showed that all the CPSs fairly reproduced these rainfall characteristics. However, the KF CPS greatly over-estimated the light rainfall intensity, while the KFT scheme was the best in reproducing heavy-moderate rainfall intensities. The analyses for VIMF showed the KF scheme most skillful in reproducing the main easterly moisture transport characterized by cyclonic activities over northern Madagascar highlands. The overall analyses showed the KF scheme as the best, with GRELL having better skill during drier years only. Therefore, the KF scheme was further subjected to higher skill and accuracy analyses through tuning its parameters.

The overall observations showed the superiority of KF-new simulations over KF-old scheme in-terms of reproducing the rainfall characteristics. Closer inspection of the individual rainfall aspects and characteristics revealed some noticeable differences between the old and new KF scheme. The correlation coefficients improved from 0.36 to 0.52 for MAM and 0.38 to 0.54 for OND seasons during the year 1997 and slightly improved for the year 1998. In terms of the error analyses, the RMSE reduced from 3.1mm/day to 1.6mm/day for MAM and 2.2mm/day to 0.9mm/day during the OND seasons.

Similarly, the RMSE values reduced in the year 1998 between the CPSs, from 3.2mm/day to 2.9mm/day during MAM and 4.1mm/day to 1.4mm/day during OND seasons. The analyses were also done for the various rainfall characteristics like in the case of objective one. The KF-new scheme outperformed the KF-old scheme in simulating these three rainfall descriptive properties. The variations between the CPS were noted in simulations of individual rainfall properties.

During the OND season, correct number of NRD was simulated over southern and Equatorial parts of the region in both the CPSs. There was a slight improvement in simulation rainfall intensity using KF-new scheme over the western parts of equatorial region. In determining how often these rainfall events occur, rainfall frequency for each particular event was computed. The KF-new simulations were better compared to KF-old scheme in simulating rainfall frequency. Both the CPS however, tended to reproduce heavy rainfall fairly well and overestimated the light rainfall intensity. The simulations for moderate frequency were not satisfactory. Most of the CPSs are designed for deep clouds hence their observed simulation characteristics.

The regions with wettest or driest rainfall biases were related to more or fewer NRD. The areas predominantly associated with heavy rainfall categories were associated with the maximum NRD, while the areas with light rainfall were associated with minimum NRD. This suggests that, light rainfall (1-10mm/day) occurred more frequently over the region but is poorly reproduced by the model. On the other hand, heavy rainfall events (>20mm/day) occurred less frequent and was correctly simulated by the WRF model

6.2 Major Conclusions

The representation of MAM rainfall using the T-mode is still challenging since the dominant PCA modes could only account for 43% of the variance. The first three modes of EOF during the OND season accounted for more than 70% of the total variance. This implies that the rainfall variability during the OND season can actually be isolated by the PCA analyses.

The moisture-based advection trigger function when applied to Kain-Fritsch scheme drastically minimizes the wet rainfall biases and consequently improve on rainfall simulation skill. The KF scheme also provides better skill for simulating heavy rainfall events (>20mm/day). This implies that the KF scheme can be applied to provide realistic forecasts for weather systems occurring at meso-micro scales.

The GRELL scheme is better for forecasting drier rainfall conditions. Thus, the scheme can provide useful information for drought forecasting and drier rainfall episodes. The similarity in the closure assumptions schemes for KF and GRELL is attributed to their adequate performance in rainfall simulations. Both schemes are based on the Langragian parcel method and thermal forcing. Applying this analogy, the current NWP formulation and dynamical processes needs to be based

upon the closure schemes similar to Kain-Fritsch and Grell Devenyi schemes so as to improve on the simulations of the East Africa rainfall characteristics and their spatial details.

The KF and GRELL CPSs skillful rainfall simulations arise from their well-defined atmospheric simulations. The enhanced moisture transport from the Indian Ocean to the continental parts of the equatorial region is responsible for most of the observed and simulated rainfall characteristics. Over the western parts of the equatorial region, the enhanced vertical moisture transport corresponds well to the areas under high rainfall and too many rainy days. The eastern parts of the region predominantly receive depressed rainfall due to weak vertical moisture transport inland and weak low-level convergence.

The observed biases in the simulated moisture flux by WRF model could be attributed to the model inability to correctly simulate the large-scale flow patterns and or changes in the sea surface temperatures over the key moisture sources. Secondly, the constrain on the domain extent towards the western Indian Ocean and Congo region could have contributed to the observed moisture flux biases.

The study provided a unique way of isolating the deficiencies and limitations of four cumulus parameterization schemes used in the WRF model in simulating extreme East Africa rainfall. The study carried out robust analyses and evaluation of suite of model simulations to identify the modified Kain-Fritsch scheme (KF-new) as the most suitable for application in WRF model in order to improve simulations of rainy days, rainfall intensity and other spatio-temporal features of East Africa rainfall.

Additionally, the study has also identified and tested three specific adjustable parameters within the cumulus schemes that can be customized to improve and optimize WRF model simulations of extreme rainfall. In many previous modeling studies, the treatment of cumulus parameterization schemes in NWP have not been subjected to extensive evaluation as provided in the current study. Such comprehensive evaluation is critical since most RCMs are developed and tested over mid-latitude regions and therefore not accustomed to the tropical regions. The tropics have unique convective rainfall characteristics and thus require that models are uniquely customized to reproduce weather and climate simulations dominated by regional and mesoscale convective systems. This has led to identification of the best cumulus scheme that can be used in the WRF model to improve the simulations of different rainfall characteristics.

The study adopted a more robust user relevant metrics to evaluate the performance/skill of WRF model simulations of East Africa rainfall. This makes the findings more useful and relevant in improving numerical weather forecasting/tools for East Africa to generate more user-relevant climate information.

The value of the ATS in the KF-new scheme can provide crucial information in determining how long it takes for multi-cell clouds (i.e tropical storms) to reach its maturity development stage. This can facilitate the tracking and monitoring of such severe weather systems for preparedness and reduced impact on the socio-economic sectors of the region. The cumulus parameterization schemes play crucial role in numerical modeling and rainfall space-time characteristics. The results from the current study are therefore very fundamental for the improvement of NWP tools and cumulus modifications processes over the region.

6.3 Recommendations

The recommendations were categorized under Researchers/Scientists, Users of climate services and policy makers.

6.3.1 Researchers/Scientists

The study recommends the use of new modified scheme (KF-new) by the various scientists and researchers from National Meteorological and Hydrological Services (NHMs), regional climate centers like ICPAC and institutions of higher learning. The current study tested only four cumulus parameterizations from WRF model due to computational limitations. In future and as a way of filling the research gap, investment on the high-performance computing capability at various research centers needs to be prioritized to provide a robust and extensive sensitivity analysis of the various physics options available in the regional climate models. This is very fundamental to the regional weather and climate downscaling of regional and local systems. This would enhance improved modeling, prediction and early warning. Further investigation on the ATS values needs to be explored to determine the optimum time for multi-cell development and tracking of storms development.

6.3.2 Users of Climate Information

The climate users should have confidence in the forecast's information from the new modified Kain-Fritsch scheme for disaster risk reduction. The drought and flood sectors should consider

using the new modified Kain-Fritsch and GRELL cumulus schemes for their sectorial impact analyses.

6.3.3 Policy Makers

Although the current study provided key informative findings, they may not be fully recommended for specific policy intervention. The results from the study are useful in the integration for further development and customization of NWP to improve simulations of salient characteristics and patterns of East Africa rainfall.

6.3.4 Further Research Work

The convective rainfall over East Africa in NWP is significantly influenced by other factors including radiation transfer, land-atmosphere coupling influenced by land use and land cover. The current study flagged out these processes as important research topics for further studies over the region.

7 REFERENCES

Adler, R. F., Huffman, G. J., Chang, A., Ferraro, R., Xie, P. P., Janowiak, J., and Gruber, A. (2003). The version-2 global precipitation climatology project (GPCP) monthly precipitation analysis (1979–present). *J hydrom.* ***4,*** *1147-1167.*

Alapaty, K., Herwehe, J. A., Otte, T. L., Nolte, C. G., Bullock, O. R., Mallard, M. S.,and Dudhia, J. (2012).Introducing subgrid-scale cloud feedbacks to radiation for regional meteorological and climate modeling. *Geophys Res. Lett, 39(24).*

Anyah, R. O., and Qiu, W. (2012). Characteristic 20th and 21st century precipitation and temperature patterns and changes over the Greater Horn of Africa. *Int. J. Clim.* ***32:*** *347–363.*

Anyah, R. O., and Semazzi, F. H. (2007). Variability of East African rainfall based on multiyear RegCM3 simulations. *Int.J. Clim.* ***27,*** *357-371.*

Anyah, R. O., Semazzi, F. H. M., and Xie, L. (2006). Simulated physical mechanisms associated with climate variability over Lake Victoria basin in East Africa. *Mon Wea Rev* ***134****:3588–3609.*

Anyah, R., and Semazzi, F. H. M. (2006). Climate Variability over the Greater Horn of Africa based on NCAR AGCM Ensemble. *Theor. Appl. Clim.* ***86,*** *39–62.*

Appelhans, T., and Nauss, T. (2016). Spatial patterns of sea surface temperature influences on East African precipitation as revealed by empirical orthogonal teleconnections. *J. Frontiers. In Earth Science****, 4,*** *3.*

Arakawa, A. (2004). The cumulus parameterization problem: Past, present, and future. *J. Clim. 17(13), 2493-2525.*

Arakawa, A., and Schubert, W. H. (1974). Interaction of a cumulus cloud ensemble with the large-scale environment, Part I. *J. Atm Sci, 31(3), 674-701.*

Argent, R., Sun, X.L., and Liu, B. (2015). The Development of a customization framework for the WRF Model over the Lake Victoria Basin, eastern Africa on seasonal timescales. *Adv in Met (2015).*

Batté, L., and Déqué, M. (2010). Seasonal Predictions of Precipitation over Africa using coupled ocean-Atmosphere General Circulation Models: Skill of the ENSEMBLES project multimodal Ensemble forecasts. *Tellus A,* ***63****, 283–299.*

Bechtold, P., Bazile, E., Guichard, F., Mascart, P., and Richard, E. (2001). A mass-flux convection scheme for regional and global models. *Quart J. of the RMS, **127**, 869-886.*

Bechtold, P., M. Köhler, T. Jung, F. Doblas-Reyes, M. Leutbecher,M. J. Rodwell, F. Vitart, and G. Balsamo.(2008). Advances in simulating atmospheric variability with the ECMWF model:From synoptic to decadal time-scales. *Quart. J. RMS, **134**, 1337–1351.*

Behera, S.K., Luo, J-J., and Masson, S. (2005). Paramount Impact of the Indian Ocean Dipole on the East African short rains: ACGCM Study**.** *J. Clim **18**, 4514-4530.*

Bergant, K., Belda, M., and Halenka, T. (2007). Systematic errors in the simulation of European climate (1961–2000) with RegCM3 driven by NCEP/NCAR reanalysis. *Int. J. Clim. **27**: 455–472.*

Berhane, F., and Zaitchik, B. (2014). Modulation of daily precipitation over East Africa by the Madden–Julian Oscillation. *J clim, **27**, 6016-6034.*

Betts, A. K. (1986). A new convective adjustment scheme. Part I: Observational and theoretical basis. *Quart. RMS, **112**, 677-691.*

Betts, A. K., Miller, M. J. (1986). A new convective adjustment scheme. Part II: single column tests using GATE wave, BOMEX, ATEX and arctic air-mass data sets. *Quart Meteorol Soc, **112**:693–709.*

Bony, S., Dufresne, J. L., Le Treut, H., Morcrette, J. J., and Senior, C. (2004). On dynamic and thermodynamic components of cloud changes. *J Clim Dynam**, 22,** 71-86.*

Bowden, J., and Semazzi, F.H.M. (2007). Empirical analysis of intraseasonal climate variability over the Greater Horn of Africa. *J. Clim. **20**, 5715–5731.*

Brisson E, Van W K, Demuzere M, Devis A, Saeed S, Stengel M, and van L N P (2016). How well can a convection-permitting climate model reproduce decadal statistics of precipitation, temperature and cloud characteristics? *Clim Dynam, **47,** 3043-3061.*

Brown, C., Arthur, G., Block, P., Alessandra, G. (2008). Review of Downscaling methodologies for Africa Climate Applications. Int Res Instit for Clim and Soc. IRI Technical Report 08-05: IRI Downscaling Report.

Bullock, O. R., Jr., K. Alapaty, J. A. Herwehe, and J. S. Kain. (2015). A dynamically computed convective time scale for the Kain–Fritsch convective parameterization scheme. *Mon. Wea. Rev., **143**, 2105–2120.*

Camberlin, P., and Okoola, R. E. (2003). The onset and cessation of the 'long rains' in Eastern Africa and their interannual variability. *Theor Appl Climatol **75**: 43-54.*

Camberlin, P., and Philippon, N. (2002). The East African March–May Rainy Season: Associated Atmospheric Dynamics and Predictability over the 1968–97 Period. *Clim, **15**, 1002-1019.*

Camberlin, P., Moron, V., Okoola, R., Philippon, N., and Gitau, W. (2009). Components of Rainy season's variability in Equatorial East Africa: onset, cessation, rainfall frequency and intensity. *Theor and Appl Clim, **98**, 237-249.*

Chen, F.,and Dudhia, J. (2001). Coupling an advanced land surface–hydrology model with the Penn State–NCAR MM5 modeling system. Part II: Preliminary model validation. Mon *Wea Rev, **129,** 587-604.*

Chen, L., Fan, X., and Ma, Z. (2010). Approaches for assessing dynamically downscale climate. AGU Fall Meeting, Dec. 13-17, 2010, San Francisco, CA, paper A21G-0181.

Chen, M., Dickinson, R. E., Zeng, X., and Hahmann, A. N. (1996). Comparison of precipitation observed over the continental United States to that simulated by a climate model. *J Clim **9,** 2223–2249.*

Choi, I. J., Jin, E. K., Han, J. Y., Kim, S. Y., and Kwon, Y. (2015). Sensitivity of diurnal variation in simulated precipitation during East Asian summer monsoon to cumulus parameterization schemes. *Geophys Res Atmos, **120,** 11-971.*

Cook, K. H. (1999). Generation of the African easterly jet and its role in determining West African precipitation. *J Clim, **12,** 1165-1184.*

Cook, K. H., and Vizy, E. K. (2013). Projected changes in East African rainy seasons. *J Climate, **26**, 5931-5948.*

Cook, K. H., and Vizy, E. K. (2013). Projected changes in East African rainy seasons. *Int J Clim **26,** 5931-5948.*

Costello, A. B., and Osborne, J. W. (2005). Best practices in exploratory factor analysis: Four recommendations for getting the most from your analysis. *Practical assessment, research & evaluation, **10,*** 1-9.

Cre´tat, J., and Pohl, B. (2012). How physical parameterizations can modulate internal variability in a regional climate model. *J Atmos Sci, **69**:714–724.*

Crétat, J., Pohl, B., Carmela, C.S., Vigaudd, N., and Yves, R. (2015). An original way to evaluate daily rainfall variability simulated by a regional climate model: the case of South African austral summer rainfall***,*** *Int. J. Clim.* ***35****: 2485–2502.*

Crétat, J., Pohl, B., Richard, Y., and Drobinski, P. (2012). Uncertainties in simulating regional climate of Southern Africa: sensitivity to physical parameterizations using WRF. *J Clim dyn,* ***38****, 613-634.*

Cristiano, E., Veldhuis, M. C. T., and Giesen, N. V. D. (2017). Spatial and temporal variability of rainfall and their effects on hydrological response in urban areas–a review. *Hydro and Earth Syst Sci,* ***21,*** *3859-3878.*

Dai, A. (2006). Precipitation characteristics in eighteen coupled climate models, *J. Clim.*, ***19****, 4605-4630.*

Dai, A., and Deser, C. (1999). Diurnal and semidiurnal variations in global surface wind and divergence fields. *J Geophys Res,* ***104****:31109– 31125.*

Dai, A., Lamb, P. J., Trenberth, K. E., Hulme, M., Jones, P. D., and Xie, P. (2004). The recent Sahel drought is real. *Int. J. Climatol.* ***24****, 1323–1331.*

Danforth, C. M., Kalnay, E., and Miyoshi, T. (2007). Estimating and correcting global weather model error. *Mon wea Rev,* ***135****, 281-299.*

Davis, N., Bowden,J., Semazzi, F.H.M., Xie, L., and Önol, B. (2009). Customization of RegCM3 Regional Climate Model for Eastern Africa and a tropical Indian Ocean domain. *J. Climate,* ***22,*** *3595–3616.*

Deardorff, J. W. (1972). Parameterization of the planetary boundary layer for use in general circulation models. *Mon Wea Rev,* ***100,*** *93-106.*

Dee, D. P., Uppala, S. M., Simmons, A. J., Berrisford, P., Poli, P., Kobayashi, S., and Bechtold, P. (2011). The ERA-Interim reanalysis: Configurations and performance of the data assimilation system. *Quart J RMS,* ***137****, 553-597.*

Denis, B., Laprise, D. R., Caya, J. (2002). Downscaling ability of one-way nested regional climate models. The Big-Brother Experiment. *Clim. Dyn.,* ***18****, 627-646.*

Diaconescu, E. P., Laprise, R., and Sushama, L. (2007). The impact of lateral boundary data errors on the simulated climate of a nested regional climate model. *J Clim dynam,* ***28,*** *333-350.*

Diro, G. T., Tompkins, A. M., and Bi, X. (2012). Dynamical downscaling of ECMWF Ensemble seasonal forecasts over East Africa with RegCM3. *Geophys Res: Atmos*, *117*(D16).

Dommenget, D. (2007). Evaluating EOF modes against a stochastic null hypothesis. *J. Clim Dyn, **28**:517–531.*

Done, J. M., Craig, G. C., Gray, S. L., and Clark, P. A. (2012). Case-to-case variability of predictability of deep convection in a mesoscale model. *Quart.J. RMS, 1**38**, 638-648.*

Done, J. M., Craig, G. C., Gray, S. L., Clark, P. A., and Gray, M. E. B. (2006). Mesoscale simulations of organized convection: Importance of convective equilibrium. *Quart J RMS, **132**, 737-756.*

Donner, L. J. (1993). A cumulus parameterization including mass fluxes, vertical momentum dynamics, and mesoscale effects. *J.Atmos sci, **50,** 889-906.*

Dunning, C. M., Black, E. C.,and Allan, R. P. (2016). The onset and cessation of seasonal rainfall over Africa. *J. Geophys Res. Atmos, 121(19).*

Dunning, C.M., Allan, R.P. and Black, E. (2017). Identification of deficiencies in seasonal rainfall simulated by CMIP5 climate models. *Environ Res Lett, **12**, p.114001.*

Endris, H. S., Lennard, C., and Hewitson, B. (2017). Teleconnection responses in multi-GCM driven CORDEX RCMs over Eastern Africa**.** *Clim Dyn, **46:** 2821-2837.*

Endris, H. S., Omondi, P., Jain, S., Lennard, C., Hewitson, B., Chang'a, L., and Panitz, H. J. (2013). Assessment of the performance of CORDEX regional climate models in simulating East African rainfall. *J of Clim , **26**, 8453-8475.*

Ferrier S, B. (1994). A double-moment multiple-phase four-class bulk ice scheme. Part I: Description. *J of Atmos Sci, **51,** 249-280.*

Flaounas, E., Bastin, S., Janicot, S. (2011). Regional climate modelling of the 2006 West African monsoon: sensitivity to convection and planetary boundary layer parameterization using WRF. *Clim Dyn **36,** 1083–1105.*

Fritsch, J. M., and Chappell, C. F. (1980). Numerical prediction of convectively driven mesoscale pressure systems. Part II. Mesoscale model. *J Atmos Sci, **37**, 1734-1762.*

Funk, C., Hoell, A., Shukla, S., Husak, G., and Michaelsen, J. (2016). The east african monsoon system: Seasonal climatologies and recent variations. In *The Monsoons and Climate Change* (pp. 163-185). Springer, Cham.

Funk, C., Verdin, A., Michaelsen, J., Peterson, P., Pedreros, D., and Husak, G. (2015). A global satellite assisted precipitation climatology. *Earth Syst. Sci. Data Discus., **8**, 401-426.*

Funk, C.,and Verdin, J. P. (2010). Real-time decision support systems: the famine early warning system network. In *Satellite rainfall applications for surface hydrology* (pp. 295-320). Springer, Dordrecht.

Gianotti, R. L., Zhang, D., and Eltahir, E. A. (2012). Assessment of the regional climate model version 3 over the maritime continent using different cumulus parameterization and land surface schemes. *J Clim, **25,*** 638-656.

Gichira, D.K. (2011). Predictability of weather on extended NWP Time Scales over Kenya using the NCEP GFS Model. *MSc Dissertation. University of Nairobi*

Giorgi, F., and Marinucci, M. R. (1996). An investigation of the sensitivity of simulated precipitation to model resolution and its implications for climate studies. *Mon Wea Rev, **124,** 148-166.*

Giorgi, F., and Mearns, L. O. (1999). Introduction to special section: Regional climate modelling revisited, *J. Geophys. Res., **104**, 6335–6352.*

Giorgi, F., and Shields, C. (1999). Tests of precipitation parameterizations available in latest version of NCAR regional climate model (RegCM) over continental United States. *J. Geophys. Res., **104,** 6353–6375.*

Giorgi, F., Coppola, E., Solmon, F., Mariotti, L., Sylla, M.B., Bi,X., Diro, G.T., Nair,V., Giulia,G.,Turuncoglu,U.U.,Cozzini,S.,O'Brien,T.A.,Tawfik,A.B.,Shalaby, A., Zakey, A.S., Elguind, N., Güttler, I., Steiner, A.L., Stordal,F., Sloan,L.C., and Brankovic,C. (2012): RegCM4 model description and preliminary tests over multiple CORDEX domains. *J. Clim Res, **52,** 7–29.*

Gitau, W. (2011). Diagnosis and Predictability of Intra-seasonal characteristics of wet and dry spells over Equatorial East Africa. *PhD Thesis, University of Nairobi.*

Gitau, W., Camberlin, P., Ogallo, L. and Okoola, R. (2015). Oceanic and atmospheric linkages with short rainfall season intraseasonal statistics over Equatorial Eastern Africa and their predictive potential. *Int J of Clim, **35**, 2382-2399.*

Gitau, W., Ogallo, L., Camberlin, P. and Okoola, R. (2013). Spatial coherence and potential predictability assessment of intra-seasonal statistics of wet and dry spells over Equatorial Eastern Africa. *Int J of Clim, **33,** 2690-2705.*

Grell, G. A., and Dévényi, D. (2002). A generalized approach to parameterizing convection combining ensemble and data assimilation techniques. *Geophys Res Lett, **29,** 38-1.*

Grell, G.A. (1993). Prognostic evaluation of assumptions used by cumulus parameterizations. *Mon Wea Rev. **121**:764–787.*

Gudoshava, M. (2016). An Investigation of the Sensitivity of East African Climate Variability to Urbanization. *PhD Thesis, North Carolina State University, USA.*

Harou, A. P., Lajoie, R., Dominic, R., and Michael, R. (2006). The Influence of the Indian Ocean Dipole Mode on Precipitation over the Seychelles, *J Clim. **26,** 45–54.*

Hastenrath S. (1999). Zonal circulations over the equatorial Indian Ocean. *J Climate, **13**, 2746-2756.*

Hastenrath, S., Polzin, D.,and Mutai, C. (2007). Diagnosing the 2005 drought in equatorial East Africa. *Clim, **20**, 4628-4637.*

Herwehe, J. A., Alapaty, K., Spero, T. L., and Nolte, C. G. (2014). Increasing the credibility of regional climate simulations by introducing subgrid-scale cloud-radiation interactions. *Geophy Res Atmos, **119**, 5317-5330.*

Himeidan, Y. E. S., and Kweka, E. (2012). Malaria in East African highlands during the past 30 years: impact of environmental changes. *Frontiers in physiology, 3, 315.*

Hoell, A., Hoerling, M., Eischeid, J., Quan, X. W., and Liebmann, B. (2017). Reconciling theories for human and natural attribution of recent East Africa drying. *J Climate, **30,** 1939-1957.*

Hogan, E., Shelly, A., and Xavier, P. (2015). The observed and modelled influence of the Madden–Julian Oscillation on East African rainfall. *Met Appl, **22**, 459-469.*

Hong, S. Y., and Lim, J. O. J. (2006). The WRF single-moment 6-class microphysics scheme (WSM6). *J. Korean Meteor. Soc, **42**, 129-151.*

Hong, S. Y., Noh, Y., and Dudhia, J. (2006). A new vertical diffusion package with an explicit treatment of entrainment processes. *Mon. Wea Rev.**34**, 318–2341.*

Huang, D., and Gao, S. (2017). Impact of different cumulus convective parameterization schemes on the simulation of precipitation over China. *Tellus A: Dyn Met and Ocean, **69,** 1406264.*

Hudson, D. A., and Jones, R. G. (2002). Regional climate model simulations of present-day and future climates of southern Africa. Hadley Centre Technical Note, 39, 41.

Huffman, G. J., Adler, R. F., Bolvin, D. T., and Gu, G. (2009). Improving the global precipitation record: GPCP version 2.1. *Geophys Res Lett, 36(17).*

Indeje, M., and Semazzi, F. H. M. (2000). Relationships between QBO in the lower equatorial stratospheric zonal winds and East African seasonal rainfall. *Meteorol and Atmos Phys, **73**, 227-244.*

Indeje, M., Neil, W., Ogallo,L.A., Glyn, D., Maxx, D., nd Anyamba, A.(2006). Predictability of the normalized difference vegetation Index in Kenya and potential applications as an Indicator of Rift Valley Fever Outbreaks in the Greater Horn of Africa. *J. Climate, **19,** 1673–1687.*

Indeje, M., Semazzi, F. H., and Ogallo, L. J. (2000). ENSO signals in East African rainfall seasons. *Int J of Climatol, **20**, 19-46.*

Ininda, J.M., Athumani, C., and Mutemi, J.N. (2008). Towards improvement of seasonal rainfall forecasting through model output statistics (MOS) downscaling of Echam forecasts over Tanzania. *J of the KMS, **2,** 99-108.*

James, R., Washington, R., Abiodun, B., Kay, G., Mutemi, J., Pokam, W., and Senior, C. (2018). Evaluating climate models with an African lens. *Bull Americ Meteor Soc*, ***99,*** 313-336.

Janjić, Z. I. (1994). The step-mountain eta coordinate model: Further developments of the convection, viscous sublayer, and turbulence closure schemes. *Mon Wea Rev, **122,** 927-945.*

Jankov, I., Grasso, L. D., Sengupta, M., Neiman, P. J., Zupanski, D., Zupanski, M and Yuan, H. (2011). An evaluation of five ARW-WRF microphysics schemes using synthetic GOES imagery for an atmospheric river event affecting the California coast. *J of Hydrom, **12,** 618-633.*

Johnson, S. J., Turner, A., Woolnough, S., Martin, G., and MacLachlan, C. (2017). An assessment of Indian monsoon seasonal forecasts and mechanisms underlying monsoon interannual variability in the Met Office GloSea5-GC2 system. *Clim Dyn, **48,** 1447-1465.*

Kain, J .S. and Fritsch, J. M. (1992). Role of convective trigger functions in Numerical forecasts of mesoscale convective systems. *Meteor Atmos Phys, **49,** 93-106*

Kain, J. S. (2004). The Kain–Fritsch convective parameterization: An update. *J. Appl. Meteor., **43,** 170–181.*

Kain, J. S., and Fritsch, J. M. (1990). A one-dimensional entraining/detraining plume model and its application in convective parameterization. *J of the Atmos Scie, **47**, 2784-2802.*

Kain, J. S., and Fritsch, J. M. (1993). Convective parameterization for mesoscale models: The Kain-Fritsch scheme. In *The representation of cumulus convection in numerical models* (pp. 165-170). American Meteorological Society, Boston, MA.

Keil, C., Heinlein, F., and Craig, G. C. (2014). The convective adjustment time-scale as indicator of predictability of convective precipitation. *Quart. J. RMS, **140,** 480-490.*

Kerandi, N. M., Laux. P., Arnault, J., and Kunstmann, H. (2017). Performance of the WRF model to simulate the seasonal and interannual variability of hydrometeorological variables in East Africa: a case study for the Tana River basin in Kenya. *Theor and Appl Climatol. **130**, 401-418.*

Kessler, E. (1969). On the distribution and continuity of water substance in atmospheric circulations. In On the distribution and continuity of water substance in atmospheric circulations. American Meteorological Society, Boston, MA.

Kijazi, A. L., and Reason, C. J. C. (2005). Relationships between intra-seasonal rainfall variability of coastal Tanzania and ENSO. *Theor Appl Climatol. **82,** 153–176.*

Kijazi, A. L., and Reason, C.J.C. (2009). Analysis of the 1998 to 2005 drought over the northeastern highlands of Tanzania. *Clim Res. **38,** 209–223.*

Kim, H. M., Webster, P. J., and Curry, J. A. (2012). Seasonal prediction skill of ECMWF System 4 and NCEP CFSv2 retrospective forecast for the Northern Hemisphere Winter. *J of Clim Dynam, **39**, 2957-2973.*

Kim, I. W., Oh, J., Woo, S.,and Kripalani, R. H. (2018). Evaluation of precipitation extremes over the Asian domain: observation and modeling studies. *J Clim Dynam, 1-26.*

Kim, K., Eom, D. Y., Lee, D. K., and Kuo, Y. H. (2010). Diurnal variation of simulated 2007 summertime precipitation over South Korea in a real-time forecast model system. *Asia-Pac J Atmos Scie, **46***, 505-512.

Kipkogei, O., Bhardwaj, A., Kumar, V.,Ogallo, L.A., Opijah, F. J., Mutemi, J. N., Krishnamurti, T. N.(2016). Improving multi model medium range forecasts over the Greater Horn of Africa using the FSU super ensemble. *J Meteorol Atmos Phys, **128,** 441–451.*

Kipkogei, O., Mwanthi, A. M., Mwesigwa, J. B., Atheru, Z. K. K., Wanzala, M. A., and Artan, G. (2017). Improved seasonal prediction of rainfall over East Africa for application in Agriculture: statistical Downscaling of CFSv2 and GFDL-FLOR. *J Applied Meteor and Climatol, **56**, 3229-3243.*

Kisaka, M. O., Mucheru-Muna, M., Ngetich, F. K., Mugwe, J. N., Mugendi, D., and Mairura, F. (2015). Rainfall variability, drought characterization, and efficacy of rainfall data reconstruction: case of Eastern Kenya. *Adv in Meteor, 2015.*

Koech E (2014) Investigating the Global Climate Systems that cause wet spells over Kenya during December- February, *Msc. Thesis,University of Nairobi.*

Korecha, D. D. (2014). Characterizing the Predictability of seasonal climate in Ethiopia. *PhD. Thesis, University of Bergen, Norway.*

Krishnamurti, T. N. (1968). A calculation of percentage area covered by convective clouds from moisture convergence. *J Appl Meteor,* ***7,*** *184-195.*

Kuo, H. L. (1974). Further studies of the parameterization of the influence of cumulus convection on large-scale flow. *J Atmos Sci,* ***31,*** *1232-1240.*

Laing, A. G., Carbone, R. E., and Levizzani, V. (2011). Cycles and propagation of deep convection over equatorial Africa. *Mon Wea Rev,* ***139,*** *2832-2853.*

Leduc, M., and Laprise, R. (2009). Regional climate model sensitivity to domain size. *J Clim Dynam,* ***32****, 833-854.*

Lin, Y. L., Farley, R. D., and Orville, H. D. (1983). Bulk parameterization of the snow field in a cloud model. *J Clim and Appl Meteor,* ***22,*** *1065-1092.*

Lin, Y., Zhao, M., Ming, Y., Golaz, J. C., Donner, L. J., Klein, S. A., and Xie, S. (2013). Precipitation partitioning, tropical clouds, and intraseasonal variability in GFDL AM2. *J Clim,* ***26****, 5453-5466.*

Liu, P., Tsimpidi, A.P., Hu,Y., Stone, B., and Russell, A.G.(2012).Differences between downscaling with spectral and grid nudging using WRF. *Atmos Chem Phys.,* ***12,*** *3601–3610.*

Luhunga, P. M., and Djolov, G. (2017). Evaluation of the use of moist potential vorticity and moist potential vorticity vector in describing annual cycles of rainfall over different regions in Tanzania. *Front in Earth Sci, 5, 7.*

Lyon, B., and DeWitt, D. G. (2012). A recent and abrupt decline in the East African long rains. *Geophys. Res. Lett., 39 (2).*

Mapande, A. T., and Reason, C. J. C. (2005). Interannual rainfall variability over western Tanzania. *Int J Clim.* ***25****, 1355-1368.*

Marengo, J. A., Cavalcanti, I. F. A., Satyamurty, P., Trosnikov, I., Nobre, C. A., Bonatti, J. P., and Castro, C. A. C. (2003). Assessment of regional seasonal rainfall predictability using the CPTEC/COLA atmospheric GCM. *Clim Dynam, **21**, 459-475.*

Mariotti, L., Coppola, E., Sylla, M. B., Giorgi, F.,and Piani, C. (2011). Regional climate model simulation of projected 21st century climate change over an all-Africa domain: comparison analysis of nested and driving model results. *Geophy Res: Atmos, 116(D15).*

Marteau, R., Richard, Y., Pohl, B., Smith, C. C., and Castel, T. (2015). High-resolution rainfall variability simulated by the WRF RCM: application to eastern France. *Clim dynam, **44,** 1093-1107.*

Mchugh, M. J. (2006). Impact of South Pacific circulation variability on east African rainfall. *Int J Climatol, **26,** 505-521.*

Miguez-Macho, G., Stenchikov, G.L., and Robock, A. (2004). Spectral nudging to eliminate the effects of domain position and geometry in regional climate model simulations. G*eophys Res **109,** D13104.*

Mistry, V.V., and Conway, D. (2003). Remote forcing of east african rainfall and relationships with fluctuations in levels of Lake Victoria. *Int. J. Climatol. **23,** 67–89.*

Mlawer, E., Taubman, S., Brown, P., Iacono, M., and Clough, S. (1997). Radiative transfer for inhomogeneous atmosphere: RRTM, a validated correlated-k model for the long-wave. *Geophys. Res. **102**,16663–16682.*

Molini, L., Parodi, A., Rebora, N., and Craig, G. C. (2011). Classifying severe rainfall events over Italy by hydrometeorological and dynamical criteria. *Quart J RMS, **137**, 148-154.*

Moron, V., Camberlin, P., and Robertson, A. W. (2013). Extracting subseasonal scenarios: an alternative method to analyze seasonal predictability of regional-scale tropical rainfall. *Clim, **26,** 2580-2600.*

Moufouma-Okia, W., and Jones, R. (2015). Resolution dependence in simulating the African hydroclimate with the HadGEM3-RA regional climate model. *Clim dynam, **44**, 609-632.*

Mukabana, J. R.,and Piekle, R. A. (1996). Investigating the influence of synoptic-scale monsoonal winds and mesoscale circulations on diurnal weather patterns over Kenya using a mesoscale numerical model. *Mon Wea Rev, **124,** 224-244.*

Mutai, C. C., and Neil, M., W. (2000). East African rainfall and the tropical circulation convection on intra-seasonal to inter-annual time scales. *J. Clim, **3**, 3915–3939.*

Mutemi, J. N. (2003). Climate anomalies over eastern Africa associated with various ENSO evolution phases, *PhD thesis, University of Nairobi, Kenya.*

Mutemi, J. N., Ogallo, L. A., Krishnamurti, T. N., Mishra, A.K., and Kumar, T. S. V. (2007). Multimodel based superensemble forecasts for short and medium range NWP over various regions of Africa. *Meteorol Atmos Phys, **95,** 87–113.*

Mwangi, E., Wetterhall, F., Dutra, E., Di Giuseppe, F., and Pappenberge, F. (2014). Forecasting droughts in East Africa. *Syst. Sci. Discuss., **10,** 10209–10230.*

Newman, M., Kiladis, G. N., Weickmann, K. M., Ralph, F. M., and Sardeshmukh, P. D. (2012). Relative contributions of synoptic and low-frequency eddies to time-mean atmospheric moisture transport, including the role of atmospheric rivers. *J Clim, **25,** 7341-7361.*

Ngaina, J. N. (2015). Modelling aerosol-cloud-precipitation interactions for weather modification in East Africa, *PhD Thesis, and University of Nairobi, Kenya.*

Nguyen, M.T., Tran T.T., Pielke R.A.S., Castro C.L., and Giovanni L. (2008). Notes and Correspondence; A Modified Kain–Fritsch Scheme and Its Application for the Simulation of an Extreme Precipitation Event in Vietnam. *Mon.Wea, Rev, **137**,766-789.*

Nicholson, E. S. (2014). The Predictability of Rainfall over the Greater Horn of Africa. Part I: Prediction of Seasonal Rainfall. *J. Hydromet, **15**, 1011–1027.*

Nicholson, S. E. (1996). A review of climate dynamics and climate variability in Eastern Africa. *The limnology, climatology and paleoclimatology of the East African lakes,* 25-56.

Nicholson, S. E. (2017). Climate and climatic variability of rainfall over eastern Africa. *Rev of Geophys, **55,*** 590-635.

Nicholson, S.E., and Kim, J. (1997). The relationship of the El Niño-Southern Oscillation to African Rainfall. *Int J Climatol, **17**, 17–135.*

Nikulin, G., Colin, J.,Filippo, G., EAssem, A., Matthias, B.,Ruth, C.,and Andreas H. (2012). Precipitation Climatology in an Ensemble of CORDEX-Africa Regional Climate Simulations. *J Clim, **25**, 6057–6078.*

Njau, L.N. (2010). Seasonal-to-Interannual Climate variability in the context of Development and Delivery of science-based climate prediction and information services worldwide for the benefit of society, *Proc. Env. Sci, 411–420*

Njeri, J. K. (2012). *The potential predictability of March-April-May rainfall over East Africa using ITCZ indices, Masters Dissertation, University of Nairobi, Kenya.*

North, G. R., Bell, T. L., Cahalan, R. F., and Moeng, F. J. (1982). Sampling errors in the estimation of empirical orthogonal functions. *Mon Wea Rev, **110,** 699-706.*

Ntale, H. K., Gan, T. Y., and Mwale, D. (2003). Prediction of East African seasonal rainfall using simplex canonical correlation analysis. *Clim, **16,** 2105-2112.*

Ntwali, D., Ogwang, B. A., and Ongoma, V. (2016). The impacts of topography on spatial and temporal rainfall distribution over Rwanda based on WRF model. *Atmos and Clim Sci, **6**, 145.*

Nyakwada W, Ogallo L, and Okoola R. (2009). The Atlantic-Indian Ocean Dipole and Its Influence on East African Seasonal Rainfall, *J. Meteorol. Rel. Sci., **3**, 21–35.*

Oettli, P., and Camberlin, P. (2005). Influence of topography on monthly rainfall distribution over East Africa. *Clim Res, **28**, 199-212.*

Ogallo, L. A. (1989). The spatial and temporal patterns of East African- rainfall derived from principal component analysis; *Int. Climatol. **9,** 145–167.*

Ogallo, L., Bessemoulin, P., Ceron, J. P., Mason, S., and Connor, S. J. (2008). Adapting to climate variability and change: the Climate Outlook Forum process. *Bull WMO, **57***, 93-102.

Ogallo, L.J. (1988). Relationship between seasonal rainfall in East Africa and Southern Oscillation. *J Climatol. **8**, 34–43.*

Ogwang, B. A., Chen, H., Li, X., and Gao, C. (2014). The influence of topography on East African October to December climate: sensitivity experiments with RegCM4. *Adv in Meteor, 2014.*

Ogwang, B. A., Chen, H., Tan, G., Ongoma, V., and Ntwali, D. (2015a). Diagnosis of East African climate and the circulation mechanisms associated with extreme wet and dry events: a study based on RegCM4. *Arabian Geoscien, **8,*** 10255-10265.

Ogwang, B. A., Ongoma, V., Xing, L., Faustin, K. O. (2015b). Influence of Mascarene High and Indian Ocean Dipole on East African Extreme Weather Events. G*eographica Pannonica, **19,** 64-72.*

Okeyo, A. E. (1987). Towards the development of a forecasting numerical model for Kenya, *PhD Thesis, University of Nairobi, Kenya.*

Okoola, R. E. (1998). Characteristics of the Inter-Tropical Convergence Zone over Equatorial Eastern Africa based on station rainfall records. *J. Meteorol. Rel. Sci., **3,** 61-101*.

Okoola, R. E. A. (1996). Space-time characteristics of the ITCZ over equatorial Eastern Africa during anomalous rainfall years, *PhD Thesis, University of Nairobi, Kenya*.

Okoola, R., Camberlin, P., and Ininda, J. (2008). Wet periods along the East Africa Coast and the extreme wet spell event of October 1997. *J KMS, **2**, 67-83.*

Okoola, R.E. (1999). A diagnostic study of the eastern Africa monsoon circulation during the northern hemisphere spring season, *Int. J. Climatol, **19**,143–168.*

Omondi, A. P. (2010). The Teleconnections between decadal rainfall variability and global sea surface temperatures and simulation of future climate scenarios over East Africa. *PhD Thesis, University of Nairobi.*

Omondi, P., and Awange, J.L., Ogallo, L.A., Ininda, J., and Forootan, E. (2013). The influence of low frequency sea surface temperature modes on delineated decadal rainfall zones in Eastern Africa region. *Adv in Water Res, **54:** 161-180.*

Omondi, P., Awange, J. L., Ogallo, L. A., Okoola, R. A., and Forootan, E. (2012). Decadal rainfall variability modes in observed rainfall records over East Africa and their relations to historical sea surface temperature changes. *J of Hydro, **464,** 140–156.*

Omondi, P., Ogallo, L., and Okoola, R. (2009). Decadal Rainfall Variability Modes in observed Rainfall Records over East Africa and their Predictability using sea surface temperature. *J.Meteorol. Rel. Sci., **3,** 37–54.*

Ongoma, V., Chen, H., and Omony, G. W. (2018). Variability of extreme weather events over the equatorial East Africa, a case study of rainfall in Kenya and Uganda. *Theor and Appl Climatol, **131**, 295-308.*

Ongoma, V., Guirong, T., Ogwang, B. A., and Ngarukiyimana, J. P. (2015). Diagnosis of seasonal rainfall variability over East Africa: A Case study of 2010-2011 drought over Kenya. *Pak J of Meteorol, 11(22).*

Opijah, F. J. (2014). Application of the EMS-WRF Model in Dekadal Rainfall Prediction over the GHA region. *Africa J of Phys Scie, **1**, 2313-3317.*

Otieno, G. (2013). Assessing the skill of the seasonal rainfall prediction over the Greater Horn of Africa using global models as multimodel ensemble, *Msc. Dissertation, University of Nairobi, Kenya.*

Otieno, G. L., Opijah, F. J., Mutemi, J. N., Ogallo, L. A., Anyah, R. O., Ongoma, V., and Sabiiti, G. (2014). Seasonal rainfall forecasting using the Multi-Model Ensemble Technique over the Greater Horn of Africa. *Int. J. of Phys. Sci, **2**, 095-104.*

Otieno, G., Mutemi, J., Opijah, F., Ogallo, L., and Omondi, H. (2018). The Impact of Cumulus Parameterization on Rainfall Simulations over East Africa. *Atmos and Clim Sci, **8(03),** 355.*

Otieno, V. O., and Anyah, R. O. (2013b). CMIP5 simulated climate conditions of the Greater Horn of Africa (GHA). Part II: projected climate. *Clim dynm, **41**, 2099-2113.*

Otieno, V. O., Anyah, R. O. (2012). Effects of land use changes on climate in the Greater Horn of Africa. *Clim Res. **52**, 77–95.*

Otieno, V. O., Anyah, R. O. (2013a). CMIP5 Simulated Climate conditions of the Greater Horn of Africa (GHA). Part I: Contemporary Climate. *J. Clim Dyn, **41**:2081–2097.*

Oueslati, B., and Bellon, G. (2015). The double ITCZ bias in CMIP5 models: interaction between SST, large-scale circulation and precipitation. *Clim dyn, **44,** 585-607.*

Owiti, Z., and, Zhu, W. (2012). East African rainfall seasonality based on modulated annual cycle (MAC) *Int. Journal of Phys. Sci., **7**, 3050-3061.*

Owiti, Z., Ogallo, L. A., Mutemi, J. N. (2008). Linkages between the Indian Ocean Dipole and East African Seasonal Rainfall Anomalies. *J. Meteorol and Rel Sci., **2**, 3-17.*

Paeth, H., Born, K., Ralf, P.,and Daniela, J.(2005). Regional dynamical downscaling over West Africa: model evaluation and comparison of wet and dry years, *Meteorologische Zeitschrift, **14**,349-367.*

Pal, J. S., Giorgi, F., Bi, X., Elguindi, N., Solmon, F., Gao, X., and Ashfaq, M. (2007). Regional climate modeling for the developing world: the ICTP RegCM3 and RegCNET. *Bull. AMS, **88**, 1395-1410.*

Perkey, D. J. (1986). Formulation of mesoscale numerical models. In Mesoscale Meteorology and Forecasting (pp. 573-596). American Meteorological Society, Boston, MA.

Petters, M. D., and Kreidenweis, S. M. (2007). A single parameter representation of hygroscopic growth and cloud condensation nucleus activity. *Atmos Chem and Phys, **7,** 1961-1971.*

Philippon, N., Camberlin, P., and Fauchereau, N. (2002). Empirical predictability study of October–December east African rainfall. *J Atmos Sci and Applied meteor and Physical Ocean, **128,*** 2239-2256.

Philippon, N., Camberlin, P., Moron, V., and Boyard-Michea, J. (2015). Anomalously wet and dry rainy seasons in Equatorial East Africa and associated differences in intra-seasonal characteristics, *Clim Dyn, **45**, 1819–1840.*

Pohl, B., and Camberlin, P. (2006a). Influence of the Madden–Julian oscillation on East African rainfall: II. March–May season extremes and inter-annual variability. *Quart Royal Met Soc, **132**, 2541-2558.*

Pohl, B., and Camberlin, P. (2006b). Influence of the Madden–Julian oscillation on East African rainfall. I: Intra-seasonal variability and regional dependency. *Quart. J. RMS, **132,** 2521-2539.*

Pohl, B., and Cretat, J. (2014). On the use of nudging techniques for regional climate modeling: application for tropical convection, *Clim Dyn, **43,**1693–1714.*

Pohl, B., Cre´tat, J., Camberlin, P.(2011).Testing WRF capability in simulating the atmospheric water cycle over Equatorial East Africa. *Clim Dyn **37**:1357–1379.*

Pohl, B., Macron, C., and Monerie, P. A. (2017). Fewer rainy days and more extreme rainfall by the end of the century in Southern Africa. *Scientific Reports, 7, 46466.*

Prein A F, Langhans W, Fosser G, Ferrone A, Ban N, Goergen K, and Brisson E (2015) A review on regional convection-permitting climate modeling: Demonstrations, prospects, and challenges. *Rev of Geophys, **53**, 323-361.*

Ratna, S. B., Ratnam, J. V., Behera, S.K., Ratnam, J. V. de C J., Rautenbach, C .W., Lennard ,J.-J. Luo, Y. Masumoto, K., and Yamagata, T. (2013). Performance assessment of three convective parameterization schemes in WRF for downscaling summer rainfall over South Africa, *Clim, Dyn, **26**, 6015–6032.*

Ratnam, J.V., Behera, S.K., Ratna, S.B., C. J. de W Rautenbach, C., Lennard, J.-J., Luo, Y., Masumoto, K. Takahashi, and Yamagata, T. (2013). Dynamical Downscaling of Austral Summer Climate Forecasts over Southern Africa Using a Regional Coupled Model. *Climat, **26**, 6015–6032.*

Rauscher, S. A., Coppola, E., Piani, C., and Giorgi, F. (2010). Resolution effects on regional climate model simulations of seasonal precipitation over Europe. *Clim Dyn, **35,** 685-711.*

Richman, M.B. (1986). Review article. Rotation of principal components. *J Climat.* ***6,*** *293–335.*

Rowell, D. P., Booth, B. B., Nicholson, S. E., and Good, P. (2015). Reconciling past and future rainfall trends over East Africa. *J Clim,* ***28****, 9768-9788.*

Sagero, P. O. (2012). Numerical Simulation of Weather over Kenya using the Weather Research and forecasting environmental Modelling System. *Msc Dissertation University of Nairobi, Kenya.*

Saji, N. H., Goswami, B. N., Vinayachandran, P. N., and Yamagata, T. (1999). A dipole mode in the tropical Indian Ocean. *Nature,* ***401(****6751), 360.*

Salih, A. A., Elagib, N. A., Tjernström, M., and Zhang, Q. (2018). Characterization of the Sahelian-Sudan rainfall based on observations and regional climate models. *Atmos Res,* ***202,*** *205-218.*

Sanchez-Gomez, E., Somot, S., and Déqué, M. (2009). Ability of an ensemble of regional climate models to reproduce weather regimes over Europe-Atlantic during the period 1961–2000. *Clim Dyn,* ***33****, 723-736.*

Schneider, T., Smith, K. L., O'Gorman, P. A., and Walker, C. C. (2006). A climatology of tropospheric zonal-mean water vapor fields and fluxes in isentropic coordinates. *Clim,* ***19****, 5918-5933.*

Schreck, C. J., and Semazzi, F. H. M. (2004). Variability of the Recent Climate of Eastern Africa. *Int. J. Climatol.* ***24****, 681-701.*

Schwendike, J., Govekar, P., Reeder, M. J., Wardle, R., Berry, G. J., and Jakob, C. (2014). Local partitioning of the overturning circulation in the tropics and the connection to the Hadley and Walker circulations. *Geophys Res Atmos,* ***119,*** *1322-1339.*

Segele, Z. T., Lance, M. L., and Lamba, P J. (2009). Evaluation and adaptation of a regional climate model for the Horn of Africa: rainfall climatology and inter-annual variability. *Int. J. Climatol.* ***29****, 47–65.*

Segele, Z. T., Leslie, L. M., and Tarhule, A. A. (2015). Sensitivity of horn of Africa rainfall to regional sea surface temperature forcing. *J Climat,* ***3,*** *365-390.*

Selz, T., and Craig, G. C. (2015). Upscale error growth in a high-resolution simulation of a summertime weather event over Europe. *Mon Wea Rev,* ***143,*** *813-827.*

Separovic, L., De Elia, R., and Laprise, R. (2008). Reproducible and irreproducible components in ensemble simulations with a regional climate model. *Mon Wea Rev,* ***136****, 4942-4961.*

Seth, A., and Giorgi, F. (1998). The effects of domain choice on summer precipitation simulation and sensitivity in a regional climate model. *J Clim, **11,** 2698-2712.*

Shongwe, M. E., Geert, J. O., Bart, H., Maarten, A. (2011).Projected changes in mean and extreme precipitation in Africa under global warming. Part II: East Africa. *J. Clim, **24,** 3718–3733.*

Shukla, S., Funk, C., and Hoell, A. (2014). Using constructed analogs to improve the skill of National Multi-Model Ensemble March–April–May precipitation forecasts in equatorial East Africa. *Environ Res Lett, **9**, 094009.*

Skamarock, W. C. (2008). A description of the advanced research WRF version 3. Tech. Note, 1-96.

Skamarock, W. C., Klemp, J. B., Dudhia, J., Gill, D. O., Barker, D. M., Wang, W., and Powers, J. G. (2005). A description of the advanced research WRF version 2 (No. NCAR/TN-468+ STR). National Center for Atmospheric Research Boulder Co Mesoscale and Microscale Meteorology Div.

Small, E. E., Giorgi, F., and Sloan, L. C. (1999). Regional climate model simulation of precipitation in central Asia: Mean and interannual variability. G*eophys Res: Atmos, **104**, 6563-6582.*

Souverijns, N., Thiery, W., Demuzere, M., and Van Lipzig, N. P. (2016). Drivers of future changes in East African precipitation. *Environ Res Lett, **11,** 114011.*

Stensrud, D. J. (2007). *Parameterization schemes: keys to understanding numerical weather prediction models*. Cambridge University Press.

Stephens, G. L. (2005). Cloud feedbacks in the climate system: A critical review. *J Clim, **18,** 237-273.*

Sun, X., Xie, L., Semazzi, F. H., and Liu, B. (2014). A numerical investigation of the precipitation over Lake Victoria basin using a coupled atmosphere-lake limited-area model. *Adv in Meteorol, 2014.*

Sun, Y., Dair, A., and Solomon, S. (2006). How often does it rain? *J. of clim, **19**, 916-934.*

Sylla, M. B., Gaye, A. T., Pal, J. S., Jenkins, G. S., and Bi, X. Q. (2009). High-resolution simulations of West African climate using regional climate model (RegCM3) with different lateral boundary conditions. *Theor and Appl Climatol, **98,** 293–314.*

Sylla, M. B., Giorgi, F., Coppola, E., and Mariotti, L. (2013). Uncertainties in daily rainfall over Africa: assessment of gridded observation products and evaluation of a regional climate model simulation. *Int J. Clim, **33**, 1805-1817.*

Tang, J., Niu, X., Wang, S., Gao, H., Wang, X., and Wu, J. (2016). Statistical downscaling and dynamical downscaling of regional climate in China: Present climate evaluations and future climate projections. *Geophys Res Atmos, **121**, 2110-2129.*

Taylor, K. E., Stouffer, R. J., and Meehl, G. A. (2012). An overview of CMIP5 and the experiment design. *BAMS **93**, 485-498.*

Temesgen, G. (2011). Improved Convective Parameterization for Precipitation modeling over the Greater Horn of Africa. *Msc Thesis, Addis Ababa University, Ethiopia.*

Tennant, W. J., and Hewitson, B. C. (2002). Intra-seasonal rainfall characteristics and their importance to the seasonal prediction problem. *Int J Climatol, **22,** 1033-1048.*

Tiedtke, M. I. C. H. A. E. L. (1989). A comprehensive mass flux scheme for cumulus parameterization in large-scale models. *Mon Wea Rev, **117**, 1779-1800.*

Tokioka, T., Yamazaki, K., Kitoh, A., and Ose, T. (1988). The equatorial 30-60 day oscillation and the Arakawa-Schubert penetrative cumulus parameterization. *J Met Soc of Japan. II , **66** , 883-901.*

Trenberth, K.E., Fasullo, J.T, Mackaro, J. (2011). Atmospheric moisture transports from ocean to land and global energy flows in reanalyses. *J Clim **24**:4907–4924.*

Uhe, P., Philip, S., Kew, S., Shah, K., Kimutai, J., Mwangi, E. and Cullen, H. (2018). Attributing drivers of the 2016 Kenyan drought. *Int J Climatol, **38**, 554-568.*

Ummenhofer, C. C., England, M. H., McIntosh, P. C., Meyers, G. A., Pook, M. J., Risbey, J. S., and Taschetto, A. S. (2009). What causes southeast Australia's worst droughts? *Geophys Res Lett, 36*(4).

Vanvyve, E., Hall, N., Messager, C., Leroux, S., and Van, Y. J.P. (2008). Internal variability in a regional climate model over West Africa. *Clim Dynam, **30,**:191–202.*

Vellinga, M., and Milton, S. F. (2018). Drivers of interannual variability of the East African “L ong Rains”. *Quart J. Royal Meteor Soc, **144**, 861-876.*

Vizy, E. K., and Cook, K. H. (2003). Connections between the summer East African and Indian rainfall regimes. *Geophys Res: Atmos, 108(D16).*

Von, S., Langenberg, H. H., and Feser, F. (2000). A Spectral Nudging Technique for Dynamical Downscaling Purposes, *Mon Wea Rev, **128,** 3664-3673.*

Waliser, D. E., and Gautier, C. (1993). A satellite-derived climatology of the ITCZ. *J Clim.* ***6,*** *2162-2174.*

Wang, W., and Seaman, N. L. (1997). A comparison study of convective parameterization schemes in a mesoscale model. *Mon Wea Rev,* ***125****, 252-278.*

Wiin-Nielsen A. (1973). Compendium of Meteorology: Dynamic meteorology. WMO, No. 364.

Wilks, D.S. (1995). Statistical Methods in the Atmospheric Sciences. Academic press, 399-402.

Wilks, D.S. (2006). Statistical methods in Atmospheric Sciences. 2nd Ed. International Geophysics Series, 91. Academic Press, 592.

Xue, Y., Vasic, R., Janjic, Z., Mesinger, F., and Mitchell, K. E. (2007). Assessment of dynamic downscaling of the continental US regional climate using the Eta/SSiB regional climate model. *J Clim,* ***20,*** *4172-4193.*

Yang, W., Seager, R., Cane, M. A., and Lyon, B. (2014). The East African long rains in observations and models. *J Clim,* ***27****, 7185-7202.*

Yang, W., Seager, R., Cane, M. A., and Lyon, B. (2015). The rainfall annual cycle bias over East Africa in CMIP5 coupled climate models. *J Climate,* ***28,*** *9789-9802.*

Zaroug, M. A. H., Giorgi, F., Coppola, E., Abdo, G. M., and Eltahir, E. A. B. (2014). Simulating the connections of ENSO and the rainfall regime of East Africa and the upper Blue Nile region using a climate model of the Tropics. *Hydrol. Earth Syst. Sci.,* ***18,*** *4311–4323.*

Zhang, F., Bei, N., Rotunno, R., Snyder, C., and Epifanio, C. C. (2007). Mesoscale predictability of moist baroclinic waves: Convection-permitting experiments and multistage error growth dynamics. *J Atmos Sci,* ***64,*** *3579-3594.*

Zhang, G. J., and McFarlane, N. A. (1995). Sensitivity of climate simulations to the parameterization of cumulus convection in the Canadian Climate Centre general circulation model. *Atmos-Ocean,* ***33****, 407-446.*

Zheng, Y., Alapaty, K., Herwehe, J. A., Del Genio, A. D., and Niyogi, D. (2016). Improving high-resolution weather forecasts using the Weather Research and Forecasting (WRF) Model with an updated Kain–Fritsch scheme. *Mon Wea Rev,* ***144****, 833-860.*

APPENDICES

Appendix 1

Table 8: The coefficient of variation (CV, %) for CHIRPS, GRELL, BML, KF and KFT cumulus schemes over the NEA, SEA, CEA and LVB sub-domains. The computations was done during the MAM and OND seasons for the composite of wet years over EA region

Scheme/Region	NEA (MAM)	SEA (MAM)	CEA(MAM)	LVB(MAM)
CHIRPS	22.9	19.4	21.9	20.4
GRELL	21.3	12.4	13.2	11.8
BML	22.4	13.1	25.8	13.8
KFT	29.2	48.7	20.7	23.6
KF	36.9	12.0	21.9	14.1
	NEA (OND)	**SEA (OND)**	**CEA(OND)**	**LVB(OND)**
CHIRPS	58.6	98.9	17.9	10.0
GRELL	19.2	19.5	15.6	97.3
BML	14.6	37.5	22.2	11.6
KFT	49.9	17.7	13.5	14.8
KF	69.3	58.8	57.5	18.8

Table 9: The coefficient of variation (CV, %) for CHIRPS, GRELL, BML, KF and KFT cumulus schemes over the NEA, SEA, CEA and LVB sub-domains. The computations were done during the MAM and OND seasons for the composite of dry years over EA region

Scheme/Region	NEA (MAM)	SEA (MAM)	CEA(MAM)	LVB(MAM)
CHIRPS	21.0	13.9	16.7	11.8
GRELL	19.4	12.7	11.1	20.6
BML	28.9	16.8	50.1.	13.2
KFT	25.5	19.9	18.4.	17.0
KF	13.5	10.9	20.1	10.4
	NEA (OND)	**SEA (OND)**	**CEA(OND)**	**LVB(OND)**
CHIRPS	32.8	15.5	27.9	12.6
GRELL	15.7	12.5	43.0	85.19
BML	25.1	17.5	28.0	10.4
KFT	28.7	23.6	31.0	19.5
KF	13.7	13.8	18.7	10.2

Table 10: The coefficient of variation (CV, %) for the CHIRPS, KF-old and KF-new cumulus schemes over the NEA, SEA, CEA and LVB sub-domains. The computations was done during the MAM and OND seasons for the year 1997over EA region

Scheme/Region	NEA (MAM)	SEA (MAM)	CEA(MAM)	LVB(MAM)
CHIRPS	**17.4**	**20.4**	**20.9**	**10.3**
KF-old	16.5	16.1	16.1	12.6
KF-new	36.1	72.0	43.0	38.1
	NEA (OND)	**SEA (OND)**	**CEA(OND)**	**LVB(OND)**
CHIRPS	**15.6**	**98.9**	**16.9**	**10.2**
KF-old	16.0	20.9	11.4	13.4
KF-new	10.2	20.0	18.6	11.5

Table 11: The coefficient of variation (CV, %) for the CHIRPS, KF-old and KF-new cumulus schemes over the NEA, SEA, CEA and LVB sub-domains. The computations were done during the MAM and OND seasons for the year 1998 over EA region

Scheme/Region	NEA (MAM)	SEA (MAM)	CEA(MAM)	LVB(MAM)
CHIRPS	22.9	19.4	21.9	12.4
KF-old	16.5	16.1	16.1	12.6
KF-new	15.8	14.2	26.1	15.5
	NEA (OND)	**SEA (OND)**	**CEA(OND)**	**LVB(OND)**
CHIRPS	38.4	26.8	42.2	16.3
KF-old	16.0	20.9	23.0	13.4
KF-new	11.4	17.4	18.5	12.2